DOC.20070301.0001

QA: QA

ANL-MGR-GS-000002 REV 03

February 2007

Characterize Eruptive Processes at Yucca Mountain, Nevada

Prepared for:
U.S. Department of Energy
Office of Civilian Radioactive Waste Management
Office of Repository Development
1551 Hillshire Drive
Las Vegas, Nevada 89134-6321

Prepared by:
Sandia National Laboratories
OCRWM Lead Laboratory for Repository Systems
1180 Town Center Drive
Las Vegas, Nevada 89144

Under Contract Number
DE-AC04-94AL85000

DISCLAIMER

This report was prepared as an account of work sponsored by an agency of the United States Government. Neither the United States Government nor any agency thereof, nor any of their employees, nor any of their contractors, subcontractors or their employees, makes any warranty, express or implied, or assumes any legal liability or responsibility for the accuracy, completeness, or any third party's use or the results of such use of any information, apparatus, product, or process disclosed, or represents that its use would not infringe privately owned rights. Reference herein to any specific commercial product, process, or service by trade name, trademark, manufacturer, or otherwise, does not necessarily constitute or imply its endorsement, recommendation, or favoring by the United States Government or any agency thereof or its contractors or subcontractors. The views and opinions of authors expressed herein do not necessarily state or reflect those of the United States Government or any agency thereof.

QA: QA

Characterize Eruptive Processes at Yucca Mountain, Nevada

ANL-MGR-GS-000002 REV 03

February 2007

Sandia National Laboratories

Scientific Analysis/Calculation Signature Page/Change History

Complete only applicable items.

2. Document Title
Characterize Eruptive Processes at Yucca Mountain, Nevada

3. DI (Including Rev. No.)
ANL-MGR-GS-000002 REV 03

	Printed Name	Signature	Date
4. Originator	D. Krier	Jonathan Krier	2/26/07
5. Checker	J. McCleary	Tom W. Pfeifle for J. McCleary	2/26/07
5. QCS	S. Kassabian-Darnell	Sonnila K Darnell	02/26/07
7. Responsible Manager/Lead	G. Valentine	G Valentine	2/26/07
8. Responsible Manager	T. Pfeifle	Tom W. Pfeifle	2/26/07

9. Remarks

Change History

10. Revision No.	11. Description of Change
01/00	REV 01 of this report is a complete revision of REV 00 ICN 01 with both major and minor changes; therefore, changes to text are not highlighted with change bars. *The following sections have been added and/or expanded.* Section 4.2, Criteria: Discussion added relating criteria described in the *Yucca Mountain Review Plan, Final Report (NUREG-1804)* (NRC 2003) to discussions in this revision. Section 6.3.1, Characteristics of Eruptive Conduits, Dike Widths, and Dike Swarms: Expansion of text on processes of conduit formation and growth. Conduits and their depths are the subject of Part 6.18.2 Geometry of Volcanic Feeder System Model (R.2) of the *Model Validation Status Report* (ANL-WIS-MD-000005 REV 00). No additional information related to potential conduit depths is added to this analysis due to absence of YMP focused investigations or other relevant studies in the open literature since REV 00 ICN 01. The inherent assumption that conduit depth extends to greater than repository depth is continued in the current revision. The consequences of conduit depth and diameter on waste packages are discussed in *Number of Waste Packages Hit by Igneous Intrusion* (ANL-MGR-GS-000003), and explored further in *Atmospheric Dispersal and Deposition of Tephra from a Potential Volcanic Eruption at Yucca Mountain, Nevada* (MDL-MGR-GS-000002 REV 00). Section 6.4, Physical Volcanology of the Lathrop Wells Cone: Includes results of field studies on physical attributes of the Lathrop Wells Cone, tephra fall, xenolith incorporation, and volumes of volcanic products (cone, lava, and tephra). Section 6.5, Redistribution Processes of Basaltic Ash and Waste Particles: Discussion of sedimentary processes resulting in erosion, secondary transport, and deposition of

	volcanic ash and waste particles affecting the Reasonably Maximally Exposed Individual. Ash redistribution is the subject of Part 6.21.2 Soil Removal Model for Volcanic Disruption (U.1-2) of ANL-WIS-MD-000005 REV 00 (*Model Validation Status Report*). Information is included, which addresses soil removal in the context of redistribution and mixing/dilution of volcanic tephra near Lathrop Wells Cone, and which reports results of an investigation, using ^{137}Cs, of erosion and deposition on various landforms on the Fortymile Wash alluvial fan. Section 6.6: Potential eruption scenario at Yucca Mountain: Discussion based on volcanological characteristics of Lathrop Wells Cone deposits. Section 7.2, Output Parameters and Uncertainties: Addition of several volcanological parameters including number of dikes associated with formation of a new volcano, dike spacing, and duration of a single explosive phase constituting a violent Strombolian phase.
02/00	Rev. 02 of this analysis report is a complete revision of Rev. 01 with both major and minor changes; therefore, changes to text are not highlighted with change bars. *The following sections have been added and/or expanded* Rev. 02 of this analysis report includes text, in pertinent sections, that responds to Condition Reports (CR) 79B, 136C, 2714, 2839B, and 2843B. Section 4.2 is streamlined by listing individual criteria from the *Yucca Mountain Review Plan, Final Report (NUREG-1804*) (NRC 2003*),* which are addressed within this analysis report. Appendix B has been added to include the acceptance criteria and how and where each criterion is addressed within this analysis report. Additional subsections have been added to Section 6 to better delineate individual concepts. Section 6.3.1.3 is added to include consideration of earthquakes caused by the injection of magmatic dikes into the crust. Output data from this section is included in DTN: LA0407DK831811.001, which lists the Technical Product Output (TPO) of this analysis report. Section 6.3.3.5 includes consideration of entrainment of wall rock in ascending magma, and an expansion on the topic of entrainment of repository (waste) materials in the magma. Figure 6-13 includes a discussion of the thickness of eroded material from interchannel divide areas of the Fortymile Wash alluvial fan obtained from evaluation of ^{137}Cs in shallow sediment profiles.
02/00	Appendix A is added to include qualification of input data that strengthens the technical basis of TPO from this report. Appendix B is added to include both the acceptance criteria and how and where each criterion is addressed within this Analysis Report. Appendix C (Physical Volcanology of the Lathrop Wells Volcano) is added to include field and laboratory descriptions of the deposits of Lathrop Wells volcano. In REV 01, this discussion was in Section 6.
03/00	Rev. 03 of this analysis report is a complete revision, including renumbering of several sections, of Rev. 02 with both major and minor changes; therefore, changes to text are not highlighted with change bars. This revision focuses on the basaltic volcanism that characterizes the Yucca Mountain area and that drives the understanding of volcanic risk in the region.

	The following sections have been added and/or expanded: Rev. 03 Section 6.3.5.1 of this analysis report includes discussion that responds to Condition Report (CR) 5918. Section 6.3.1 summarizes the intrusive and eruptive phenomena associated with small-volume basaltic volcanoes in the Yucca Mountain region, which is detailed within appendices C through F. Section 6.3.3.1 summarizes the field characteristics of the magmatic dikes that feed regional basaltic volcanoes, including their attributes upon approach from repository levels to the surface eruptive vents. Section 6.3.3.3 synthesizes field observations of magmatic conduits as exposed in the set of regional analogue volcanoes. Section 7 tabulates output data from this analysis report that is developed within previous Section 6 subsections and the appendices. Many of the output distributions are better constrained than previous revisions, based on regional data derived from field studies on those volcanoes that define the volcanic hazard to the proposed repository. The output in Section 7 is also the subject of DTN: LA0612DK831811.001. Sections and comments related to post-eruptive volcanic ash redistribution by surface processes have been deleted in this revision and will be incorporated into revision of *Atmospheric Dispersal and Deposition of Tephra from a Potential Volcanic Eruption at Yucca Mountain, Nevada* (MDL-MGR-GS-000002), or a new analysis report. Appendices C through F are new or rewritten treatments of the physical volcanology of several basalt volcanoes within the Yucca Mountain region. Appendix C is completely rewritten to synthesize concepts, knowledge, and principles of the physical volcanology of Lathrop Wells volcano based on field studies and literature comparisons. Appendix D focuses on the five ~1 my basaltic volcanoes in Crater Flat and on the physical volcanology and evolution by surface processes of those scoria cones and lava fields. Appendix E reports on the two volcanic events at Sleeping Butte (Little Black Peak and Hidden Cone) and documents the processes and structural control that were active during emplacement of these volcanoes. Appendix F synthesizes knowledge of the shallow plumbing (shallow dikes, conduits, and vents) of the volcanism characteristic of the Crater Flat volcanoes and Basalt Ridge and east Basalt Ridge on northern Pahute Mesa.

INTENTIONALLY LEFT BLANK

CONTENTS

Page

CONTENTS (Continued)

Page

FIGURES

Page

FIGURES (Continued)

Page

FIGURES (Continued)

Page

INTENTIONALLY LEFT BLANK

TABLES

Page

INTENTIONALLY LEFT BLANK

ACRONYMS

DIRS	Document Input Reference System
FEPs	features, events, and processes
NRC	U.S. Nuclear Regulatory Commission
PVHA	probabilistic volcanic hazard analysis
RMEI	reasonably maximally exposed individual
TWP	technical work plan
TSPA	total system performance assessment
TSPA-LA	total system performance assessment for a license application
vol %	volume percent
wt %	weight percent
YMP	Yucca Mountain Project
YMRP	Yucca Mountain Review Plan

INTENTIONALLY LEFT BLANK

1. PURPOSE

The purpose of this scientific analysis report, *Characterize Eruptive Processes at Yucca Mountain, Nevada*, is to present information about natural volcanic systems and the parameters that can be used to model their behavior. This information is used to develop parameter-value distributions appropriate for analysis of the consequences of volcanic eruptions through a repository at Yucca Mountain. This is a revision and is conducted in accordance with *Technical Work Plan: Igneous Activity Assessment for Disruptive Events* (BSC 2006 [DIRS 178448], Sections 1.2.2 and 2.2.2).

This report provides information for revising the following reports: *Number of Waste Packages Hit by Igneous Intrusion*, (BSC 2005 [DIRS 174066]); *Atmospheric Dispersal and Deposition of Tephra from Potential Volcanic Eruption at Yucca Mountain, Nevada* (BSC 2005 [DIRS 174067]); *Dike/Drift Interactions* (BSC 2004 [DIRS 170028]); *Development of Earthquake Ground Motion Input for Preclosure Seismic Design and Postclosure Performance Assessment of a Geologic Repository at Yucca Mountain, NV* (BSC 2004 [DIRS 170027[1]]).

This report is organized into seven major sections. This section addresses the purpose of this document. Section 2 addresses quality assurance, Section 3 discusses the use of software, Section 4 identifies the requirements that constrain this work, and Section 5 lists assumptions and their rationale. Section 6 presents the details of the scientific analysis and Section 7 summarizes the conclusions reached.

Section 6, the scientific analysis, lists the parameters and values used to anticipate and model processes of shallow subsurface (less than about 350 m) and surface volcanic activity relevant to a repository at Yucca Mountain. Section 6.1 discusses the scientific approach, background, and data sources. The scientific approach includes the principle that the basaltic eruptive history of the Yucca Mountain region, in terms of analogue volcanoes, provides the best data to establish future volcanic scenarios. Section 6.2 lists the features, events, and processes (FEPs) supported by the analyses. Section 6.3 discusses the analyses of the eruptive processes, which include:

- Geometry of volcanic feeder systems (conduits and dikes) of small-volume basaltic volcanoes, which are of primary importance in modeling how much area and volume of the repository might be affected by an intrusion of a feeder system
- Description of the physical and chemical properties of the basaltic magma, which influence both eruptive styles and mechanisms for interaction with waste packages containing radioactive waste
- Characteristics of shallow intrusive features, including dikes and conduits

[1] The six-digit numerical identifier in brackets next to each reference is the Yucca Mountain Project (YMP) Document Input Reference System [DIRS] number, which is provided to assist the reader in locating a specific reference in the DIRS database. Within the reference list (Section 8), multiple sources by the same author and date (e.g., BSC 2002) are sorted alphabetically by title.

- Estimates of the maximum magnitude of dike-induced earthquakes
- Ascent velocity of magma at depth, onset of bubble nucleation and growth in the rising magmas, magma fragmentation, and velocity of the resulting gas-particle mixture
- Eruption volume, duration of eruptions, power output, and mass discharge rates.

Appendix A establishes the quality of the data used in this analysis, including the qualification of data obtained from external sources.

Appendix B identifies *Yucca Mountain Review Plan, Final Report* (YMRP) (NRC 2003 [DIRS 163274]) acceptance criteria applicable to this work, discusses how the criteria are addressed, and cites the relevant locations in this document for this information.

Appendix C provides results of field work and laboratory analyses and the interpretation of the eruptive history for Lathrop Wells volcano, which is a young cinder cone/tephra sheet/lava flow complex 18 km south of the repository site. Emphasis on the Lathrop Wells volcano is engendered by its young age and the cone's excellent state of preservation, combined with active quarrying operations that expose some of the cone interiors. *Final Report of the Igneous Consequences Peer Review Panel, with Appendices* (Detournay et al. 2003 [DIRS 169660], pp. 12 to 13) concurred with the conclusion by Perry et al. (1998 [DIRS 144335], p. vi) that the younger post-Timber Mountain caldera basalts (less than ~5 million years [Ma] old) provide the critical basis for forecasting the style of future possible magmatic activity in the Yucca Mountain region. The Lathrop Wells volcano retains many volcanic products and features of a young vent and, therefore, provides the best analogue of a potential eruptive center. It is the youngest example of the waning basaltic volcanism that characterizes the Yucca Mountain region.

Appendix D provides analysis of the analogue volcanoes in Crater Flat, which cluster in age at ~1 Ma. The volcanoes (Black Cone, Red Cone, Little Cones, and Makani volcano) preserve early histories of eruption and eruptive products that are similar to the younger Lathrop Wells volcano. The investigations described in Appendix D lay groundwork for interpreting eruptive history, and feeder dike number and geometry, and for applying the principles to potential eruptions in the Yucca Mountain region.

Appendix E concerns the physical volcanology of the Sleeping Butte area, known for two volcanoes, Little Black Peak and Hidden Cone. Sleeping Butte is within the Yucca Mountain region and provides additional technical basis for understanding the structural control on volcano location, as well as the types of eruption phenomenology expected during some future volcanic eruption.

Appendix F discusses the processes of volcanic conduit development and the characteristics of analogue conduits of the Yucca Mountain region, including dimensions, number, relation to feeder dikes, and spacings. These values provide technical basis for evaluating dimensions of potential conduits at the Yucca Mountain repository site.

2. QUALITY ASSURANCE

This work contributes to the analysis of data used to support performance assessment and is classified as important to waste isolation, as defined in LS-PRO-0203, *Q-List and Classification of Structures, Systems, and Components*. Consequently, importance to waste isolation aspects of this work are controlled via approved procedures. This analysis does not investigate potential impacts on any specific items or barriers, as listed in *Q-List* (BSC 2005 [DIRS 175539]).

This report was prepared under SCI-PRO-005, *Scientific Analyses and Calculations*. The revision to this scientific analysis report is conducted in accordance with *Technical Work Plan: Igneous Activity Assessment for Disruptive Events* (BSC 2006 [DIRS 178448], Sections 1.2.2 and 2.2.2). The following deviations have been made from the work scope as described in the TWP:

- YMRP Acceptance Criteria listed in Table 4-3 and described in Appendix B do not address model uncertainties or model abstraction outputs contained in other reports. This report provides output to model reports that support the total system performance assessment for license application (TSPA-LA).

- This report contains an update of FEPs from those listed in the technical work plan. The FEPs discussed in Section 6.2 are the FEPs being considered.

- Particle sizes of basaltic ash erupted from vents are discussed in Section 6.5 and given a size distribution.

In addition, the electronic management of data was accomplished in accordance with the controls specified in the TWP. Unqualified inputs from external sources are qualified for intended use in Appendix A using the criteria found in SCI-PRO-005, *Scientific Analyses and Calculations*. These criteria represent a subset of the methods and attributes required for qualification of data per SCI-PRO-001, *Qualification of Unqualified Data*.

INTENTIONALLY LEFT BLANK

3. USE OF SOFTWARE

Standard, built-in functions of Microsoft Excel, versions 8.0, 9.0, 10.0, and 11.0 (in Office '98, 2001, v.X, and Office 2004, respectively), for Apple Macintosh desktop computers operating in Classic and OS X environments were used to calculate the parameters reported here, including averages, medians, modes, and standard deviations. This software is exempt from the requirements of IM-PRO-003, *Software Management*. All other calculations were performed using hand-held calculators. The output was visually checked for correctness, and results were spot-checked for accuracy and reasonableness using hand-held calculators.

Input for these standard functions consisted of subsets of concentrations of volcanic gases, water content, sieve-fraction weight percent (wt %), microscope grain counts of pyroclast types in samples, and counts of xenolithic clasts quantities and sizes as measured in quarry exposures at Lathrop Wells volcano. Outputs consisted of averages, medians, modes, and standard deviations, depending on the type of statistical property required for sufficient description of the data distribution. Other inputs concerning physical properties of ascending magmas and eruptive jets are listed in Sections 6.3.2 and 6.3.4, including those parameters associated with equations 6-1, 6-2, 6-3, 6-4, and 6-7; outputs are shown in Tables 6-3, 6-4, and 6-5, and graphically in figures 6-5, 6-6, 6-7, and 6-8.

Conflow, version 1.0.0, is an open-source conduit flow code developed by Mastin and Ghiorso (2000 [DIRS 170144]) and further discussed by Mastin (2002 [DIRS 178163]). *Conflow* was run on a Windows-based desktop PC running Windows XP and was used within its range of validation. Use of this unqualified code in Appendix F is limited to providing context for characterizing the conduit flow conditions and final configuration of conduit profiles during the eruptions at the study areas. Actual eruptive conditions are inferred from the exposures of eruptive products and a few cases of subsurface conduits. *Conflow* is used, then, in a corroborative fashion to compare what is observed in the shallow subsurface with calculated conduit or vent configurations, given a small set of *Conflow* parameters. No numerical values or ranges are developed from the use of *Conflow*, and only profiles of conduit half-widths are generated for comparison with eroded volcanic analogues.

INTENTIONALLY LEFT BLANK

4. INPUTS

4.1 DIRECT INPUTS

In this scientific analysis report, relevant scientific literature and investigations of analogue volcanoes in the Yucca Mountain region are reviewed, and theoretical concepts, parameter values, and distributions are developed. This information is used to recommend parameter distributions for other models and analyses that inform the YMP total system performance assessment (TSPA) calculations. Parameter distributions are based on field-acquired data and data available in published sources. Brief descriptions of the data used as direct input are listed in Table 4-1. Data from external sources that are used as direct input are listed in Table 4-2. Data from these sources have been justified for intended use within this document per SCI-PRO-005 requirements and are considered qualified for intended use. These justifications are documented in Appendix A. Qualification status of the input data is indicated in the DIRS database.

Table 4-1. Data Used as Inputs for Calculations

Data Used	Application of Data	Data Sources (Data Tracking Number)
45 chemical analyses of products from Lathrop Wells volcano	Calculation of mean chemical composition of Lathrop Wells products	LA000000000099.002 [DIRS 147725]
Particle size data for tephra sheet from Lathrop Wells volcano	Development of particle size distribution for violent Strombolian eruption in the Yucca Mountain region	LA0302GH831811.002 [DIRS 162864]
Tephra thickness data for Lathrop Wells	Calculation of the eruption volumes of Yucca Mountain region volcanoes	LA0305DK831811.001 [DIRS 164026]
Lithic clasts measured at Lathrop Wells cone, Nevada	Illustration of decreasing xenolith content of Lathrop Wells cone during eruption; calculation of diameter of solid cylinder approximating diameter of conduit beneath Lathrop Wells volcano	LA0302GH831811.003 [DIRS 162865]
Volume estimates of tephra fallout, lavas, and cone at Lathrop Wells volcano	Relative volumes of eruptive products for potential eruptions	LA0609DK831811.001 [DIRS 178757]

Table 4-2. External Source Data Used as Inputs for Calculations in This Scientific Analysis Report

Data Used	Application of Data	Data Sources (Reference [DIRS Number])	Location in This Report
Dimensions of NE Little Cone	Calculation of eruption volume for Yucca Mountain region volcanoes	Stamatakos et al. (1997 [DIRS 138819], pp. 322 and 328)	Section 6.3.4.4
88 chemical analyses for the composition of volcanic gases	Calculation of percent concentration of volcanic gases	Symonds et al. (1994 [DIRS 101029], Tables 3 to 5)	Section 6.3.2.3 and Table 6-4
Equation relating water saturation to pressure in basaltic magmas	Calculation of saturation pressures, exsolution depths, and volume fraction of gas in magma as a function of pressure	Jaupart and Tait (1990 [DIRS 118292], p. 219)	Sections 6.3.2.4, and 6.3.4.2
Equation to estimate multiple phase-saturation (liquidus) temperatures in magma	Calculation of temperatures of magmas forming potential Yucca Mountain region volcanoes	Sisson and Grove (1993 [DIRS 122564], p. 178)	Section 6.3.2.4
Method for calculating magma viscosity as a function of composition	Calculation of viscosities of magmas forming potential Yucca Mountain region volcanoes	Shaw (1972 [DIRS 126270], pp. 873 to 878)	Section 6.3.2.4
Equation and H2O data to calculate density as function of composition, pressure and temperature	Calculation of magma density for potential Yucca Mountain region volcanoes	Lange and Carmichael (1990 [DIRS 147767], Table 3); Ochs and Lange (1999 [DIRS 144330], pp. 1,314 and 1,315, Eq. 2)	Section 6.3.2.4
Theoretical equations and results describing the ascent of basaltic magmas	Equation for velocity of magma below exsolution depths, relationship between magma-gas mixture density and water mass fraction, and plots of eruption velocity as a function of initial water content of magmas	Wilson and Head (1981 [DIRS 101034], pp. 2,974 and 2,983, Eqs. 16 to 18; Figure 7)	Sections 5, 6.3.4.1, 6.3.4.2, and 6.3.4.3, Equations 6-3 and 6-6, and Figures 6-6, 6-7, and 6-8
Duration for the formation of an entire volcano	Calculation of duration range for the formation of a volcano	Wood (1980 [DIRS 116536], p. 402, Figure 10)	Section 6.3.4.4
Durations of explosive eruptive phases, powers, and mass discharge rates for historic eruptions at Cerro Negro, Hekla, Tolbachik, Paricutin, and Heimaey volcanoes	Calculation of duration range and mass discharge rate range for explosive eruptive phases	Jarzemba (1997 [DIRS 100460], p. 136)	Section 6.3.4.4 and Table 6-9
Particle shape factor, F	Recommended shape factor	Jarzemba (1997 [DIRS 100460], p. 139)	Section 6.3.5.2
Estimated bulk density of pyroclastic fallout deposits	Recommendations for treatment of bulk deposit density in consequence analyses	Blong (1984 [DIRS 144263], p. 208); Sparks et al. (1997 [DIRS 144352], p. 366)	Section 6.3.4.6.3

4.2 CRITERIA

This scientific analysis report provides technical basis for parameters that will be used by the TSPA-LA related to the effects of a volcanic eruption within the Yucca Mountain region. The report provides discussion and summaries of uncertainties associated with inputs to the analysis and outputs from the analysis. The information and data in this report are based on literature values, direct and indirect field observations of analogue volcanoes and their feeder systems and supporting analyses (Appendices C, D, E, and F), and simple calculations as described in Section 6.

The following text identifies information in this report that addresses *Yucca Mountain Review Plan, Final Report* (YMRP) (NRC 2003 [DIRS 163274]) acceptance criteria and/or review methods related to descriptions of site characterization work, mechanical disruption of engineered barriers, volcanic disruption of waste packages, airborne transport of radionuclides, and the issues discussed in key technical agreement IA 1.02 regarding use of aeromagnetic data.

The general requirements to be satisfied by TSPA are listed in 10 CFR 63.114 [DIRS 176544] (*Requirements for Performance Assessment*). Technical requirements to be satisfied by TSPA are identified in the YMRP (NRC 2003 [DIRS 163274]). The acceptance criteria that will be used by the NRC to determine whether the technical requirements have been met are identified in the YMRP (NRC 2003 [DIRS 163274]). The pertinent requirements and YMRP acceptance criteria addressed by this report are listed in Table 4-3, and described in detail in Appendix B.

Table 4-3. Applicable Criteria

Integrated Subissue	10 CFR 63 Link	YMRP Acceptance Criteria[a]
Description of Site Characterization Work	10 CFR 63.21(b)(5)	1.5.3, criteria 1 (1) and 2 (1, 2)
Mechanical Disruption of Engineered Barriers	10 CFR 63.114(a)-(c) and (e)-(g)	2.2.1.3.2.3, criteria 1 (1, 2) and 2 (2, 3)
Volcanic Disruption of Waste Packages	10 CFR 63.114 (a)-(c) and (e)-(g)	2.2.1.3.10.3, criteria 1 (1, 2, 4) and 2 (1, 2, 3, 4)
Airborne Transport of Radionuclides	10 CFR 63. 114(a)-(c) and (e)-(g)	2.2.1.3.11.3, criteria 1 to 3

[a]NRC 2003 [DIRS 163274].

4.3 CODES, STANDARDS, AND REGULATIONS

No specific formally established codes (other than the CFR sections listed above), standards, or regulations have been identified as applying to this analysis and modeling activity.

INTENTIONALLY LEFT BLANK

5. ASSUMPTIONS

Analyses of eruptive processes are primarily based on the assumption that a plausible future volcanic eruption would have the same character as Quaternary basaltic eruptions in the Yucca Mountain region. Another overall assumption is that the event probabilities established in *Characterize Framework for Igneous Activity at Yucca Mountain, Nevada* (BSC 2004 [DIRS 169989]) pertain to the potential formation of a new volcano that would be accompanied by one or more dikes in the subsurface and some combination of scoria cone, spatter cones, ash and lapilli fall, and lava flows on the surface. Eruptive styles and magmatic composition recorded at the Lathrop Wells volcano, the most recent in the Yucca Mountain region, are emphasized. The following assumptions fall into two types: those that establish general equivalency of data (such as gas compositions), and those that support a reasonable technical approach to issue resolution. Assumptions specific to each report component are described in Section 6 and summarized below with corresponding section numbers.

1. *Assumption*: The most likely future eruptive event will have a magmatic chemical composition that is adequately represented by the mean composition of products of the Lathrop Wells volcano. This assumption is discussed in Section 6.3.2.1.

   Rationale: The Lathrop Wells volcano has geochemical, petrologic, and volcanological characteristics that are consistent with other Quaternary volcanoes of the Yucca Mountain region and provides the most detailed information on magma chemistry and eruptive processes because of its intensive study, relatively young age, and better preservation of deposits.

   Need for confirmation: Confirmation is not required because additional data should negligibly alter the mean composition values

2. *Assumption*: The most likely future eruptive event will exhibit eruptive styles that are adequately represented by nearby Quaternary basaltic volcanic cones in general and by the Lathrop Wells volcano, specifically. This assumption is discussed in Section 1 and forms the technical basis for the study of physical volcanology of Lathrop Wells volcano and other volcanoes in the Yucca Mountain region presented in Appendices C, D, E, and F.

   Rationale: Nearby Quaternary-age volcanoes are the best analogue for future eruptive styles in the Yucca Mountain region because they are representative of the same persistent eruption style, tectonic setting, magma type, and erupted volume. Also, the Lathrop Wells volcano, at about 80,000 years old, is the youngest eruptive center in the Yucca Mountain region and has the best-preserved geologic record of its eruptive processes.

   Need for confirmation: Confirmation is not needed because this assumption is based on the best available approach.

3. *Assumption*: Pressure in dikes and conduits during eruption is equal to lithostatic pressure. This assumption is discussed in Section 6.3.4.2.

   Rationale: Actual pressure is a complex function of the velocity, density, and composition of the magma as it rises, and of the strength of wall rocks. Because a general model for these effects (including the uncertainty associated with wall rock properties at depth) does not exist, lithostatic pressure is used as a first-order approximation. In addition, significant deviations from lithostatic pressure might result in partial failure of the dike walls or conduit walls such that the size of these features might adjust to maintain a fluid pressure that is near to lithostatic pressure.

   Need for confirmation: Confirmation is not needed because this assumption is based on the best available approach.

4. *Assumption*: Rising magma, composed of melt liquid and volatile gases and not undergoing fragmentation, can be considered homogeneous and characterized by equilibrium between melt and exsolved volatiles. This assumption is discussed in Section 6.3.4.2.

   Rationale: Actual ascent velocities of melt and bubbles are different (Wilson and Head 1981 [DIRS 101034]). During normal basaltic Strombolian activity (see Section 6.1.3.2), magma-ascent rates are low and large bubbles (to >1 m) can grow by gas diffusion and coalescence (Mastin and Ghiorso 2000 [DIRS 170144], p. 4), resulting in explosions of large bubbles of hot gases and clots of lava at the top of the magma column. However, for energetic lava fountains and violent Strombolian eruptions, ascending magma mixtures typically generate very small bubbles (0.1-mm to 1-mm diameter) whose rise velocity relative to the melt (10^{-7} m/s to 10^{-5} m/s; Mastin and Ghiorso 2000 [DIRS 170144], p. 4) is orders of magnitude less than the ascent velocity of the mixture (10^{-1} m/s to 10^{2} m/s), resulting in little or no coalescence and continuous streaming of the fragmented magma from the vent.

   Need for confirmation: Confirmation is not needed because this assumption is based on the best available approach, as discussed in Section 6.3.4.2.

6. DISCUSSION

6.1 INTRODUCTION

6.1.1 Scientific Approach and Technical Methods

This report is a compilation of values from literature sources and from field and laboratory studies of properties of magmatic/volcanic materials and processes. Magma properties (e.g., water content, viscosity) and characteristics of buoyant rise (e.g., velocity, volatile exsolution) that best reflect the basaltic magma characteristics of the Yucca Mountain region are taken from the literature, whereas the basaltic composition that might define the potential future volcanic event is derived from multiple chemical analyses from the nearby Lathrop Wells volcano. Because of its composition, relative youth, exposure, and position in the sequence of basaltic eruptive events in the Yucca Mountain region, the Quaternary Lathrop Wells volcano is an appropriate example of the type of eruptive event that could disrupt the proposed repository at Yucca Mountain. Eruptive processes are derived from observations and literature on eruptions of similar compositional type and from the eruptive sequences deduced from investigation of products deposited from the several basaltic volcanoes in the area, including Lathrop Wells volcano. Recommended values or distributions of values for key parameters, the methods for determining the values (e.g., literature research, field studies, or assumptions), and intended uses and uncertainties associated with the parameters, are provided throughout Section 6.3 and summarized in Section 7.

6.1.2 Units of Measurement

Measurement units employed in this analysis follow *System Internationale* standards except where English units are also used to help convey the scales of distance or volume.

6.1.3 Definition of Terms

6.1.3.1 Shallow Intrusive Features

Dike–A tabular, subplanar, magma-filled crack that cuts across the bedding of older rock. Length and width (or thickness) describe the size of a dike, although minor variations in width and strike direction can be expected along the length of any one dike.

Dike swarm–A group of one or more dikes resulting from the same magmatic event. The distance between two dikes is defined as dike spacing.

Conduit–A roughly cylindrical, vertically oriented, feature through which magma flows upward to a volcanic vent. The size of a conduit can be described by its diameter.

6.1.3.2 Eruption Mechanisms

Pyroclastic–Any eruption involving explosions and ejection of fragmented magma. Such eruptions might be driven by exsolution and expansion of magmatic volatiles (as in *Strombolian* and *violent Strombolian* eruptions described below) or by explosive interaction between rising magma and groundwater or surface waters (*hydrovolcanic* eruptions, described below).

Individual fragments produced by pyroclastic eruptions are termed *pyroclasts* (also simply as *clasts*), and accumulations of such fragments are termed *pyroclastic deposits* or *tephra*.

Strombolian–Eruptions typified by short (seconds to tens of seconds) bursts of gas and fluidal magma clots or fragments from a volcanic vent. Strombolian eruptions are driven by rise of large bubbles through a magma column and bursting of those bubbles when they reach the top of the column. Pyroclasts produced in these bursts are relatively coarse grained and follow ballistic paths to accumulate around the vent. Because of their relatively short residence time in the air, larger clasts do not cool very much before deposition and may weld to other clasts to form welded horizons (also referred to as agglutinate).

Violent Strombolian–Eruptions typified by sustained (tens of minutes to days) jets of gas and magma clots and fragments. Coarse clasts might follow ballistic paths, but most clasts are more finely fragmented (to lapilli and smaller sizes, see below) and are carried to heights of several hundred meters to a few kilometers as the eruptive jet becomes buoyant. Clasts tend to be cool and brittle upon deposition and fall out of the buoyant plume (eruption column) as it is transported by atmospheric winds.

Effusive–Eruptions that produce lava flows by the eruption of unfragmented magma. Eruption of lavas can occur simultaneously with Strombolian or violent Strombolian eruptions.

Hydrovolcanic–Explosive eruption driven by the interaction of rising magma with groundwater or surface waters. Eruption products tend to be relatively fine-grained and to be relatively rich in wall rock (lithic) fragments.

6.1.3.3 Eruptive Deposits and Features

Cone (or scoria cone or cinder cone)–A thick accumulation of pyroclastic deposits immediately surrounding a vent, usually forming a hill with the shape of an inverted cone that is truncated at the top by a crater. The outer slope of an uneroded scoria cone is close to the angle of repose of the deposits that make up the cone (typically 30 to 35 degrees).

Lava (or lava flow)–Cooled flows of unfragmented magma. At Quaternary basaltic centers of the Yucca Mountain region, lavas are typically a few meters to about 30-m thick, have natural levees along the insides and terminal ends of individual flows, and have brecciated tops and bottoms with massive, solid interiors. They typically extend up to about 1 km from their source vents (either main craters or flank vents on the cones).

Welded scoria (agglutinate)–Indurated deposits of mainly lapilli and bombs (see below) that were erupted sufficiently hot and plastic that they stuck together upon deposition. As accumulation rate and clast temperature increase during an eruption, degree of welding may increase up to an extreme case where clasts completely coalesce with each other and subsequently flow as a lava flow (termed *clastogenic flow*).

Tephra fall deposit (fallout deposit, tephra sheet, tephra blanket)–Well-sorted deposit of pyroclasts that blankets the terrain, gradually thinning with increasing distance from the source vent.

Pyroclastic surge deposit–Moderately sorted deposit of pyroclasts (typically ash to lapilli in size, see below) with evidence of deposition from a laterally-flowing density current (e.g., ripple marks, dune forms).

6.1.3.4 Pyroclast Characteristics

Bombs and Blocks (larger than 64 mm)–A volcanic bomb is a pyroclast "larger than 64 millimeters (mm) in diameter" that was "ejected while viscous [partly or completely fluid] and shaped while in flight" (Jackson 1997 [DIRS 109119], p. 75). Bombs are ballistically ejected from the crater and typically land around the vent, eventually accumulating to form a scoria cone. Depending upon the gas content, magma composition, and viscosity, basaltic bombs form a variety of shapes from spindles to "cowpies" that were deformed on impact with the ground surface. Bombs range in size from 64 mm to as much as several meters. Most are finely crystalline, with the quench-crystal, diktytaxitic textures (finely crystalline phases separated by open space and/or glass) found in most scoria of all clast sizes. Similarly, a volcanic block is a pyroclast larger than 64 mm in diameter but angular in shape, having been ejected in a solid state. Blocks also can contribute to formation of a scoria cone.

Lapilli (2 mm to 64 mm) **and ash** (< 2 mm)–Ash and lapilli are separated for the purpose of grain size analysis and characterization, but have the same variety of particle types:

- *Sideromelane droplets*–Clear brown basaltic glass is usually found as a product of energetic lava fountains where exsolving gases are released to form a "spray" of droplets and bombs ranging in size from only a few micrometers (μm) to decimeters. Many sideromelane pyroclasts are highly vesicular with low bulk densities. These are common in Hawaiian eruptions, but are also components in Strombolian eruptions; the main difference is the Strombolian sideromelane clasts may have been more viscous when ejected as reflected in the pyroclast shapes. Pyroclasts are smooth-skinned, light brown, and have vesicularities ranging from 20% to 70% (Heiken and Wohletz 1985 [DIRS 106122], pp. 6, and 34 to 41). Variations in pyroclast colors depend upon the absence or presence of phenocrysts and/or finely crystalline phases. There are gradations between sideromelane and tachylite (finely crystalline) pyroclasts and some grains can exhibit both textures.

- *Tachylite pyroclasts*–Finely crystalline, diktytaxitic textures are characteristic of most scoria bombs and ash from Strombolian eruptions. The "quench crystal" textures correlate with a slight increase in cooling times, perhaps caused by the clogging of the vent during slumping of talus into the crater or by decreased eruption rates (Heiken 1978 [DIRS 162817], Table 5).

  In hand specimens, tachylite bombs, scoria, and ash appear black (or red if oxidized). In transmitted light, a thin section of scoria also appears more or less opaque. In polished thin sections and when viewed with a scanning electron microscope at high enough magnification, tachylite pyroclasts have well-developed pyroxene and plagioclase laths on the order of a few micrometers to a few tens of micrometers wide, which are surrounded by dendritic growths of 0.2-μm- to 2-μm-wide pyroxene and Fe–Ti oxides. There are traces of glass between the dendritic phases.

- *"Glassy tachylite" pyroclasts*–Tephra from the Lathrop Wells volcano contains an unusual pyroclast type in which the vesicles are lined with glass, but the bulk of the grain has a diktytaxitic texture. These glass linings show deformation by growth of quench crystals beneath the linings.

- *Phenocrysts*–Most tephra from Strombolian eruptions contain phenocrysts, either whole or broken, that were separated during the fragmentation processes in the vent; some have thin glass coatings.

- *Lithic clasts*–Of special importance to interpreting subsurface processes during explosive eruptions are lithic clasts derived from magma flow in the dike or conduit formation due to the interaction between rising magma and wall rocks. Information can be derived concerning energies related to fragmentation and magma/groundwater interactions if the stratigraphy of the rock sequence underlying the volcano is known. Lithic clasts vary widely in size and shape, ranging from large angular blocks to individual sand grains.

6.1.3.5 Grain Size Limits and Terms for Pyroclastic Rocks

In addition to grain size of individual pyroclasts, grain size distribution for a pyroclastic deposit is commonly expressed in terms of the median clast diameter (Md) and the graphic standard deviation (or sorting) parameter, σ_ϕ, (see Heiken and Wohletz 1985 [DIRS 106122], pp. 5, 6, and 18).

Well sorted: $\sigma_\phi < 1\phi$

Moderately sorted: $\sigma_\phi = 1\phi$ to 2ϕ

Poorly sorted: $\sigma_\phi > 2\phi$

where: $\sigma_\phi=(\phi_{84} - \phi_{16})/2$. ϕ_{84} is the 84th percentile grain size and ϕ_{16} is the 16th percentile grain size expressed in ϕ units. Phi (ϕ) scale is a logarithmic transformation of the ratio of a grain diameter (in mm) to a standard grain diameter of 1 mm: $\phi = -\log_2 d$, where d is the particle diameter in mm.

6.2 FEATURES, EVENTS, AND PROCESSES

The development of a comprehensive list of features, events, or processes (FEPs) potentially relevant to postclosure performance of the Yucca Mountain repository is an ongoing, iterative process based on site-specific information, design, and regulations. Table 6-1 provides a list of igneous-related FEPs (DTN: MO0508SEPFEPLA.002 [DIRS 175064]) included in the TSPA-LA through the use of the results of the calculations described in this document. Details of the inclusion of igneous disruptive events FEPs are discussed in DTN: MO0508SEPFEPLA.002 [DIRS 175064], LA FEP List and Screening (Disruptive Events), Sections 6.2.1.7, 6.2.2.2, 6.2.2.3, 6.2.2.7, and 6.2.2.8). The rationale for exclusion of

igneous disruptive events FEPs are also discussed in DTN: MO0508SEPFEPLA.002 [DIRS 175064], LA FEP List and Screening (Disruptive Events).

For the igneous scenario, the TSPA-LA assumes that a hypothetical dike propagates upward, intersects the repository, provides a source for magma to enter the repository drifts, and magma and ash, potentially with entrained waste, are released to the surface via an eruptive conduit. The FEPs listed in Table 6-1 are part of the conceptual basis for such a scenario. This report does not provide a direct basis for the inclusion in TSPA-LA of the FEPs listed in Table 6-1, but this report provides supporting analyses to help constrain the potential consequences of the listed FEPs. As such, a partial treatment of the included FEPs is provided herein, and the results of this analysis report and listed FEPs are considered to be implicitly included in the TSPA-LA. It has been determined that the TWP (BSC 2006 [DIRS 178448], Table 2.2) does not reflect the current FEPs applicable to this analysis report, because FEP 1.2.04.07.0C (Ash Redistribution via Soil and Sediment Transport) is addressed in *Redistribution of Tephra and Waste by Geomorphic Processes Following a Potential Volcanic Eruption at Yucca Mountain, Nevada* (MDL-MGR-GS-000006, Rev 00) (SNL 2007 [DIRS 179347]). The current included FEPs that are applicable to this report are listed in Table 6-1.

Table 6-1. Disruptive Events FEPs Applicable to this Analysis Report

FEP Number	FEP Name	Relevant Section(s)
1.2.03.03.0A	Seismicity associated with igneous activity	6.3.3.2
1.2.04.03.0A	Igneous intrusion into repository	6.3.2.1, 6.3.2.2, 6.3.2.3, 6.3.2.4, 6.3.3.1, 6.3.3.2
1.2.04.04.0A	Igneous intrusion interacts with EBS components	6.3.2.1, 6.3.2.2, 6.3.2.3, 6.3.2.4; 6.3.3.1, 6.3.3.2, 6.3.3.3, 6.3.4.5
1.2.04.06.0A	Eruptive conduit to surface intersects repository	6.3.2.1, 6.3.2.2, 6.3.2.3, 6.3.2.4; 6.3.4.1, 6.3.4.2, 6.3.4.3, 6.3.4.4
1.2.04.07.0A	Ashfall	6.3.4.1, 6.3.4.2, 6.3.4.3, 6.3.4.4, 6.3.4.5

Source: DTN: MO0508SEPFEPLA.002 [DIRS 175064].
EBS = engineered barrier system.

6.3 ERUPTIVE PROCESSES ANALYSIS

There are several characteristics of igneous activity that need to be constrained in order to predict potential consequences of a volcanic event were one to occur at Yucca Mountain. These are:

- Geometry of shallow intrusive features such as dikes and conduits
- Properties (e.g., composition, density, viscosity, temperature) of magmas that might interact with repository structures and materials
- Dynamic processes associated with magma ascent at shallow depths and subsequent eruption
- Maximum magnitudes of dike-induced earthquakes

- Duration of igneous processes and volumes of igneous material involved in those processes

- Emplacement and characteristics of eruptive products.

This report provides information on these characteristics and processes based upon a combination of theory and data from several volcanic features in the Yucca Mountain region that are analogous to a potential volcanic event at Yucca Mountain. In some cases, information is used from volcanoes outside the Yucca Mountain region if they provide insight and are appropriately analogous to a potential Yucca Mountain event. Particular emphasis is given to the Lathrop Wells volcano, located about 18 km south of the proposed Yucca Mountain repository site. It is the youngest volcano in the region (~80,000 years; Heizler et al. 1999 [DIRS 107255], p. 803) and, therefore, its deposits have been least modified by surficial processes and preserve the best record of eruptive processes. In addition, quarry operations have produced excellent exposures of the main cone, allowing combined observations of both distant and proximal deposits. Specific aspects of the Lathrop Wells volcano are described in sections below, and detailed field descriptions of deposits and inferred eruptive processes at this volcano are provided in Appendix C. It is inferred that a volcano that might form at Yucca Mountain in the next few tens of thousands of years will exhibit similar eruptive processes to those recorded in the deposits at Lathrop Wells volcano.

6.3.1 Summary of Intrusive and Eruptive Phenomena Associated with Quaternary Volcanoes in the Yucca Mountain Region

There are eight Quaternary volcanoes in the Yucca Mountain region (Figure 6-1), which are hawaiitic in composition (Vaniman et al. 1982 [DIRS 101031], p. 343; Valentine and Perry 2006 [DIRS 177495], Table 1). Lathrop Wells volcano, with an age of ~80 thousand years (ka), is the youngest volcano in the region. Because if its young age and relatively better preservation, and therefore usefulness as an analogue for a potential future eruption at Yucca Mountain, the composition (Section 6.3.2) and physical volcanology (Appendix C) of this volcano are discussed in more detail than the other volcanoes. Two volcanoes with ages ~0.37 million years (Ma; Hidden Cone) and ~0.32 Ma (Little Black Peak) occur at Sleeping Butte and provide the next oldest volcanic analogue (Appendix D). The oldest of the Quaternary volcanoes are about 1 Ma in age and form an arcuate, ~11–km-long chain of five volcanoes in Crater Flat (Appendix E). These Quaternary volcanoes share many characteristics. All of the volcanoes have one or two lava flow fields that extend between 0.4 km to 1.8 km from the cone, and all but one of them have a single scoria cone (or cone remnant for the older, more eroded volcanoes) that represents the area from which all eruptive products emanated. Makani volcano has no scoria cone remnant, but lavas vented from its eastern side and flowed about 400 m to the west-southwest (Appendix E). The remnant volumes of each volcano are indicated in Table 6-2. Lathrop Wells volcano, with a total volume estimated at 0.12 km^3, is the largest (this partly reflects its better state of preservation). Red Cone and Black Cone volcanoes likely had original volumes that were similar to that of Lathrop Wells, but some of that volume has been removed by erosion. Makani is the smallest volcano.

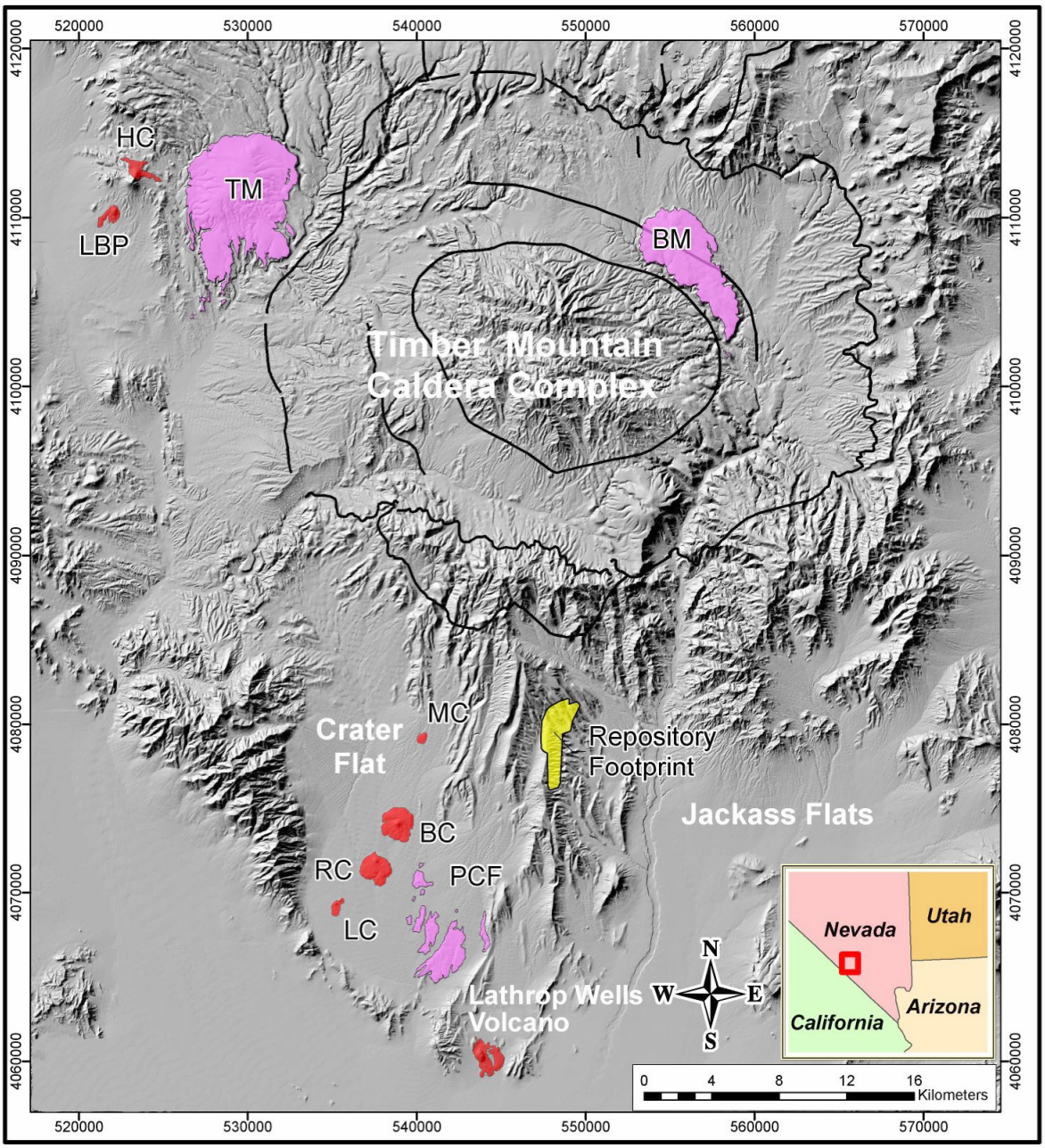

NOTES: Geology from Wahl et al. (1997 [DIRS 112289], plate 1). Pliocene volcanoes (pur ple) are Thirsty Mountain (TM), Buckboard Mesa (BM), and Pliocene Crater Flat (PCF). Pleistocene volcanoes (red) in Crater Flat (LC – Little Cones, RC – Red Cone, BC – Black Cone, MC – Makani Cone) are ~1 Ma (Fleck et al. 1996 [DIRS 105337], Table 2; Perry et al. 1998 [DIRS 144335], Table 2a; Appendix E). Little Black Peak (LBP) and Hidden Cone (HC) are ~0.32 and 0.37 Ma, respectively (Fleck et al. 1996 [DIRS 105337], Table 2). Lathrop Wells volcano is ~80 ka (Heizler et al. 1999 [DIRS 107255], p. 803). Figure modified from Valentine and Perry (2006 [DIRS 177495], Figure 1).

Figure 6-1. Digital Elevation Model of the Yucca Mountain Area Showing Distribution of Pliocene and Pleistocene Basaltic Volcanoes, and Caldera Outlines from Mid-Miocene Activity

The general phenomena associated with formation of small volume basaltic volcanoes in continental settings, including the Yucca Mountain region, are illustrated schematically in Figure 6-2. Magma propagates upward through the Earth's crust in fluid-driven cracks (dikes). The strike-length scale of a dike is apparently related to the length scale, or footprint, of the magma source zone in the mantle; Valentine and Perry (2006 [DIRS 177495], p. 4) show that these length scales have generally decreased from Pliocene to Quaternary times in the Yucca Mountain region, such that Quaternary dikes probably have lengths from several hundred meters to ~2 km. If Quaternary dikes ascend in swarms of two or more, one dike in a swarm will be the "master" dike that feeds an eruption, while others are subsidiary. Most observed dikes in the Yucca Mountain region occupy preexisting normal fault planes (Appendix F; Valentine and Krogh 2006 [DIRS 177282], p. 218) and it is likely that fault motion accompanies intrusion by magma, which reduces friction across the fault plane (Valentine and Krogh 2006 [DIRS 177282], p. 225). Contrasts in elastic properties of the surrounding rocks and bedding plane weaknesses can also result in localized lateral injection of magma (sills; Valentine and Krogh 2006 [DIRS 177282], p. 227). Where the master dike intersects the Earth's surface it might feed an early phase of fissure eruptions, but based upon the character of the Quaternary volcanoes in the Yucca Mountain region and upon observations at historical analogues, it is inferred that magma flow focuses relatively rapidly into a main conduit that supplies the bulk of eruptive products (Appendices C and E). The characteristics of these various subsurface features are discussed and quantified in Section 6.3.3.

Table 6-2. Estimated Volumes of Quaternary Volcanic Centers in the Yucca Mountain Region

Volcano Name	Volume (km^3)[†]	Brief Description
Black Cone	0.06[‡]	Single cone with two lava flow fields
Red Cone	0.06	Single cone with two lava flow fields
Little Cones	0.03[§]	Two small cones, each with a lava flow field (mostly buried by alluvium) extending southward
Makani	0.004[#]	Small lava field with minor pyroclastics
Little Black Peak	0.014	Single cone with lavas that extend from its base
Hidden Cone	0.03	Single cone on side of Sleeping Butte with two lava fields
Lathrop Wells	0.12	Single cone with two lava flow fields

NOTES: [†]Volumes calculated by reconstructing a sloping planar paleosurface beneath each volcano (determined by elevation of points around the edge of each volcano, assuming that this is close to the contact between volcanic products and the paleosurface unless noted otherwise), and integrating the digital elevation data above that surface. The volume estimates do not account for distal fallout deposits that may have existed but are now obscured or missing due to posteruptive surficial processes.

[‡]Bradshaw and Smith (1994 [DIRS 101996], p. 168) estimate the volume of Black Cone volcano to be 0.067 ± 0.015 km^3.

[§]Combined volume of SW and NE Little Cone volcanoes and their lava flow fields. Assumes each of the two lava fields is 10-m thick and buried by an average of 10 m of alluvium.

[#]Assumes 5 m partial burial of volcanic products, in addition to those exposed on the surface.

Once magma intersects the surface it will erupt by both explosive processes that produce pyroclastic deposits and by effusive processes that produce lavas. The types of pyroclastic deposits at Quaternary volcanoes in the Yucca Mountain region indicate that eruptions ranged from relatively weak bursts of volcanic gas and coarse fluidal fragments of magma (ejected along ballistic trajectories up to a few hundred meters in height) that are characteristic of Strombolian eruptions (Chouet et al. 1974 [DIRS 178064], p. 4,961; Valentine et al. 2005

[DIRS 177782], p. 629), to energetic, relatively continuous jets (eruption columns) of volcanic gas, lapilli, and ash-size magma fragments that rose up to several kilometers height and were dispersed both locally and downwind to be deposited by fallout mechanisms. The latter type of eruption, referred to as violent Strombolian, produced deposits of as much as 1-cm thickness up to 20 km from the Lathrop Wells volcano (Appendix C), while the relatively weaker Strombolian eruptions produced pyroclastic deposits only within a few hundred meters of the vent. The scoria cones at Lathrop Wells volcano and the ~1-Ma volcanoes of Crater Flat appear to have been built by combinations of Strombolian and violent Strombolian mechanisms (Appendices C and E). The Quaternary volcanoes all have lava flow fields that were produced by stacking and internal inflation of many individual lava flow units. Based upon historical analogues and upon field observations at Lathrop Wells volcano (Appendix C), lavas probably vented from the bases of the cones, partly simultaneously with explosive activity at the cone summits. Duration of eruptive activity at any one of the volcanoes likely ranged from several months to ~2 to 3 years, with pyroclastic cone-building activity during part of that time (~1 to 3 months). Specific parameters associated with eruptive activity are discussed and quantified in Section 6.3.4.

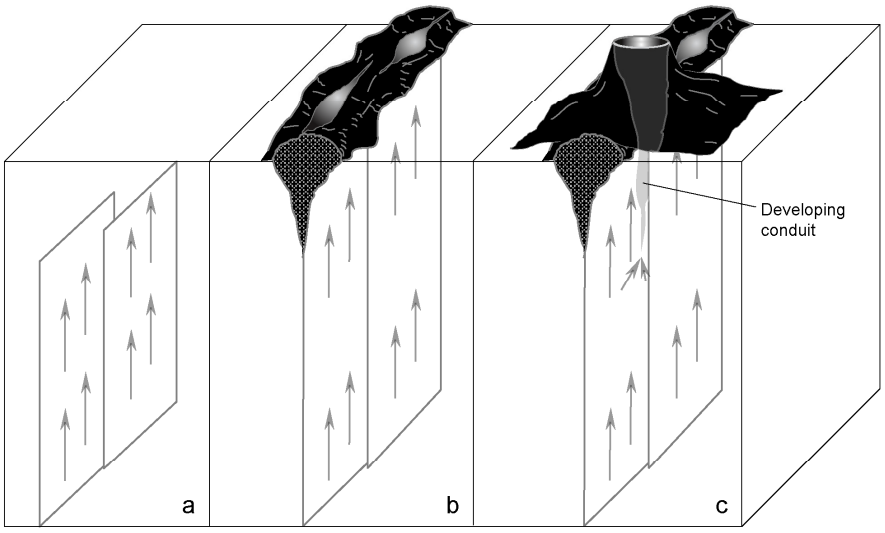

Figure 6-2. Sequence of Events in Formation of a Small Basaltic Volcano, Starting with Upward Dike Propagation (Left Side), to Initial Fissure Eruptions (Center), to Formation of a Conduit and Main Cone (Right)

6.3.2 Physical and Chemical Characteristics of Quaternary Basalt Magma in the Yucca Mountain Region

6.3.2.1 Magma Chemistry

Magma-chemistry data are used to determine parameters for important (physical or constitutive) variables such as magma viscosity, temperature, and density, that affect magma ascent (pressure, density, velocity of multiphase flow, etc.) and eruption on the Earth's surface (eruption velocity, particle size distribution, cloud height). Because of the extensive data available, and its compositional similarity to the other Quaternary volcanoes in the Yucca Mountain region, Lathrop Wells volcano is used here as a compositional proxy for a potential future volcano at Yucca Mountain. The major element variation for Lathrop Wells is based on 45 chemical analyses (DTN: LA000000000099.002 [DIRS 147725]) that adequately describe the basaltic magmas generated during the Quaternary period in Crater Flat and are typical of hawaiitic compositions. Table 6-3 lists the means and other statistical parameters associated with the 12 most abundant oxides from these analyses. The 45 analyses chosen represent the interiors of dense basalt flows suitable for accurate chemical analyses (i.e., other samples are screened due to effects of oxidation or other alteration). Appendix C (Table C-1) also provides chemical compositions of early- and late-erupted lavas from the monogenetic eruptive sequence.

Table 6-3. Mean Lathrop Wells Lava Chemistry with Associated Statistics

SiO_2		TiO_2		Al_2O_3	
Mean	48.50	Mean	1.93	Mean	16.74
Standard Error	0.09	Standard Error	0.01	Standard Error	0.03
Median	48.57	Median	1.93	Median	16.75
Mode	48.55	Mode	1.97	Mode	16.87
Standard Deviation	0.58	Standard Deviation	0.06	Standard Deviation	0.22
Sample Variance	0.34	Sample Variance	0.00	Sample Variance	0.05
Count	45	Count	45	Count	45
Fe_2O_3T[a]		Fe_2O_3[b]		FeO[b]	
Mean	11.63	Mean	1.74	Mean	8.90
Standard Error	0.03	Standard Error	0.00	Standard Error	0.02
Median	11.58	Median	1.74	Median	8.86
Mode	11.56	Mode	1.73	Mode	8.84
Standard Deviation	0.22	Standard Deviation	0.03	Standard Deviation	0.17
Sample Variance	0.05	Sample Variance	0.00	Sample Variance	0.03
Count	45	Count	45	Count	45
MnO		MgO		CaO	
Mean	0.17	Mean	5.83	Mean	8.60
Standard Error	0.00	Standard Error	0.02	Standard Error	0.03
Median	0.17	Median	5.83	Median	8.55
Mode	0.17	Mode	5.88	Mode	8.41
Standard Deviation	0.00	Standard Deviation	0.11	Standard Deviation	0.22
Sample Variance	0.00	Sample Variance	0.01	Sample Variance	0.05
Count	45	Count	45	Count	45

Table 6-3. Mean Lathrop Wells Lava Chemistry with Associated Statistics (Continued)

Na_2O		K_2O		P_2O_5	
Mean	3.53	Mean	1.84	Mean	1.22
Standard Error	0.01	Standard Error	0.01	Standard Error	0.00
Median	3.55	Median	1.84	Median	1.22
Mode	3.59	Mode	1.84	Mode	1.21
Standard Deviation	0.09	Standard Deviation	0.04	Standard Deviation	0.03
Sample Variance	0.01	Sample Variance	0.00	Sample Variance	0.00
Count	45	Count	45	Count	45

Source: DTN: LA000000000099.002 [DIRS 147725].

NOTE: All values except count are in wt %.

[a] Total iron is reported as Fe_2O_3T.

[b] Fe_2O_3 and FeO were recalculated assuming a 0.15 mole fraction of ferric iron (Fe_2O_3).

The following sample analyses are from Perry and Straub (1996 [DIRS 106490], Appendix A; DTN: LA000000000099.002 [DIRS 147725]) was used to develop the statistics in this table: LW11FVP, LW12FVP, LW74FVP, LW45FVP, LW72FVP, LW73FVP, LW100FVP, LW120FVP, LW121FVP, LW30FVP, LW31FVP, LW32FVP, LW63FVP, LW64FVP, LW65FVP, LW66FVP, LW67FVP, LW110FVP, LW115FVP, LW20FVP, LW21FVP, LW22FVP, LW23FVP, LW06FVP, LW07FVP, LW40FVP, LW41FVP, LW44FVP, LW55FVP, LW56FVP, LW19FVP, LW25FVP, LW26FVP, LW27FVP, LW28FVP, LW29FVP, LW04FVPA, LW54FVP, LW57FVP, LW58FVP, LW05FVPA, LW59FVP, LW60FVP, LW61FVP, LW62FVP.

6.3.2.2 Water Content of Primary Basaltic Magma

Eruptive styles in the Yucca Mountain region ranged from violent Strombolian on one end of the spectrum to quiescent a'a' lava on the other (Perry et al. 1998 [DIRS 144335], Chapter 2). Eruption style was primarily controlled by volatile content (which is dominated by water) and the rate at which volatiles were exsolved from the magma. The inferred eruptive styles indicate a large range in volatile contents and, hence, water content of Yucca Mountain region magmas. In addition, variations in energy are suggested at individual volcanic centers of the Quaternary Crater Flat field and Lathrop Wells volcanoes.

Amphibole, possibly of magmatic origin, is found as a rare and sparse phase in some Quaternary Crater Flat basalts. Knutson and Green (1975 [DIRS 106299], p. 126, Figure 1), performing experiments on material similar in composition to Yucca Mountain region basalts, observed that magmatic amphibole was stabilized at water contents of between 2 wt % and 5 wt %. Baker and Eggler (1983 [DIRS 122601], p. 387) showed that at 2 kbar pressure, water content in excess of 4.5 wt % is required to stabilize amphibole in high-alumina basalt similar to Yucca Mountain region basalts. Nicholis and Rutherford (2004 [DIRS 173945]) conducted analyses of water content in melt inclusions as well as phase equilibria experiments on samples from Lathrop Wells and northeast Little Cone volcanoes. Out of 21 melt inclusions analyzed, 19 had H_2O contents in the range of 1.2 wt % to 1.7 wt %, and the remaining two inclusions had 2.9 wt % and 3.5 wt % (Nicholis and Rutherford 2004 [DIRS 173945], p. 490). Nicholis and Rutherford (2004 [DIRS 173945], p. 490) refer to results by Luhr and Housh (2002 [DIRS 178118]) that reach as high as 4.6 wt % H_2O in melt inclusions as well as up to 930 ppm CO_2. Nicholis and Rutherford (2004 [DIRS 173945], p. 491) conclude that the Lathrop Wells magmas may have contained 1.9 wt % to 4.6 wt % H_2O. This range is consistent with the experimental data mentioned above by Knutson and Green (1975 [DIRS 106299]) and Baker and Eggler (1983

[DIRS 122601]). Even if a particular concentration of volatiles could be tied to a particular eruptive style, the Yucca Mountain region post-Miocene (i.e., 5 Ma) record is sparse; therefore, it is difficult to rigorously define a probability distribution function for primary magma water content for use in TSPA. Therefore, it is recommended that water content of magmas for a potential future eruption at Yucca Mountain be assumed to have a uniform probability of any value between 1.0 wt % and 5.0 wt %.

Direct measurements of water in mafic (low silica) magmas or magmatic products from a range of tectonic settings indirectly support the recommended parameter values and cover the range of values that can be reasonably expected for future basaltic igneous activity. Garcia et al. (1989 [DIRS 122542], Table 1, p. 10,527), Byers et al. (1985 [DIRS 122532], Figure 4, p. 1,891), and Muenow et al. (1979 [DIRS 125093], Table 1, p. 74) found total water contents in Hawaiian tholeiites and transitional alkalic basalts that range from near 0% to nearly 1%. These melts probably represent higher degrees of partial melting than Yucca Mountain region basalts, so their low water contents are expected. On the other hand, Gaetani et al. (1993 [DIRS 144274], pp. 332 to 334) and Sisson and Grove (1993 [DIRS 144351], p. 163) present experimental evidence that high-alumina basalt and basaltic andesite magmas commonly contain up to several wt % water. Sisson and Layne (1993 [DIRS 122549], Table 1, p. 622) measured water contents in glass inclusions from arc basalts and basaltic andesites that range from 1% to 6%. True magmatic values could be somewhat lower because of concentration of water in the inclusions, which is caused by partial crystallization of the melt after entrapment. Water contents of 0.2% to 2% have been reported for back arc basin lavas and 1.2% to 3% for island arc tholeiites and boninites (Danyushevsky et al. 1993 [DIRS 149303], Tables 1 and 4, pp. 349 and 358).

6.3.2.3 Mole Percent of Constituents in Volcanic Gas

A survey of data compilations from the literature, including volcanoes from convergent, divergent, and hot-spot tectonic settings, must suffice to constrain the relative proportions of major gas constituents in Yucca Mountain region basalts owing to the absence of current activity in the Yucca Mountain region from which gases could be directly sampled. Three types of data exist in the literature:

- Measurements of emitted volcanic gases
- Measurements of gases trapped in volcanic glass or melt inclusions
- Experiments on gas solubilities in silicate melts.

The first type of data is more directly relevant to eruptive scenarios at Yucca Mountain because the gases released from an igneous event will include corrosive species. Also, gases will fractionate between the magma and the gas phases during exsolution. Consequently, gas composition data for glasses may not directly represent their relative abundances in the gas phase after exsolution.

Measured concentrations of volcanic-gas constituents were taken from a compilation by Symonds et al. (1994 [DIRS 101029], Tables 3 to 5), and only the data for mafic centers were included in the present analysis. Data in Table 6-4 include hawaiite from Mount Etna; tholeiitic basalt from Momotombo, Poas, Kilauea, Ardoukoba, and Erta Ale; nephelenite from

Nyiragongo; and alkali basalt from Surtsey. Statistics listed in Table 6-4 were calculated by first computing the mean for each of the volcanic centers from the data reported by Symonds et al. (1994 [DIRS 101029], Tables 3 to 5) and then using these individual means to generate the overall statistics.

Table 6-4. Mole Percent Concentration of Volcanic Gases and Associated Uncertainty Estimates

	H_2O	H_2	CO_2	CO	SO_2
Mean	73.16	1.17	14.28	0.57	9.45
Square Root of the Sum of the Squares	17.97	0.89	16.03	0.59	8.90
Standard Deviation	19.81	0.67	15.32	0.75	8.95
	S_2	HCl	HF	H_2S	f_{O_2}*
Mean	0.41	0.87	0.17	0.74	–10.63
Square Root of the Sum of the Squares	0.63	0.21	0.04	1.04	1.92
Standard Deviation	0.40	1.12	0.08	0.69	1.80

Source: Symonds et al. (1994 [DIRS 101029], Tables 3-5, 88 analyses.

NOTE: * f_{O_2} is listed as log bars.

This is a closed data set, indicating that each parameter (other than f_{O_2}) must vary between 0% and 100%. A species such as H_2O will rarely be present at levels less than 50% and probably has some mean or median value of geologic significance. If data from a sufficient number of eruptions and individual volcanoes were gathered, a normal distribution of values seems likely. As for the minor species, which are also corrosive, the cited uncertainties are quite large relative to mean values. Thus, it seems likely that adequate conservatism will be accommodated by a normal, or even a uniform, distribution.

6.3.2.4 Magmatic Temperatures, Viscosities, and Densities

Many direct measurements of magmatic temperatures have been made for erupting lavas. However, this is only possible when water contents are low enough, or rates of magmatic outgassing are slow enough, to permit direct measurement. Thus, although direct measurements are available for the low end of the spectrum of water content, experiments must be relied upon to constrain magmatic temperatures for magmas with elevated water content.

Table 6-5 presents calculated saturation pressures, liquidus temperatures, viscosities, and densities for magma of Lathrop Wells composition for variable water contents ranging from 0 wt % to 4 wt %. The values are derived and interrelationships are discussed in the following paragraphs of this section.

Yucca Mountain region basaltic lavas are generally aphyric to sparsely porphyritic (Perry and Straub 1996 [DIRS 106490], p. 6), which indicates that they erupted at near-liquidus or super-liquidus temperatures. The liquidus temperature for dry basaltic magmas increases with increasing pressure. Wet liquidi, however, have negative slopes, so that water-bearing magmas may exist at a temperature less than that of the dry liquidus. Jaupart and Tait (1990 [DIRS 118292], p. 219) present a simple expression for the solubility of water in basaltic magma:

$$n = 6.8 \times 10^{-8} P^{0.7} \quad \text{(Eq. 6-1)}$$

where n is the mass fraction of water and P is the pressure in Pascals. As magmas decompress, not only will they tend to exsolve more fluid, they will also tend to crystallize. Magma is saturated with respect to water when the pressure is such that n equals the initial water content. Table 6-5 shows saturation pressures, calculated from Equation 6-1, for initial water contents of 0.5 wt %, 1.0 wt %, 2.0 wt %, 3.0 wt %, and 4.0 wt % (wt % = 100 times the mass fraction). At lower pressures, water vapor would begin to exsolve and form bubbles within the magma (see also Section 6.3.4.2).

Table 6-5. Calculated Saturation Pressures, Liquidus Temperatures, Viscosities, and Densities as a Function of Water Content for Lathrop Wells Magmas

Water Content (wt %)	Saturation Pressure (Pa)	Liquidus Temperature (°C)	Viscosity (log poise)	Density (kg/m^3)
0	1×10^5	1,169	2.678	2,663
0.5	9.0×10^6	1,153	2.572	2,633
1	2.4×10^7	1,137	2.472	2,605
2	6.5×10^7	1,106	2.284	2,556
3	1.2×10^8	1,076	2.112	2,512
4	1.7×10^8	1,046	1.957	2,474

NOTE: Derived using mean Lathrop Wells compositions from Table 6-3, Eqs. 6-1 and 6-2; Eq. 3 from Shaw (1972 [DIRS 126270]) Saturation pressures are calculated for each value of water content (n) using Equation 6-1. Liquidus temperatures are calculated for each value of saturation pressure using Equation 6-2 as described in the text. Viscosity (η, in poise) is calculated by $\log(\eta) = \ln(\eta)/2.303$, where $\ln(\eta)$ is defined in terms of composition and temperature (K) by Equation 3 of Shaw (1972 [DIRS 126270], p. 873), with $c_\eta = -6.40$ and $c_T = 1.50$, using the procedure defined by Shaw (1972 [DIRS 126270], p. 876 and example on p. 878). For conversion to SI units, 1 Pa-sec = 10 poise. Density of the melt for each water content, saturation pressure, and liquidus temperature is calculated using the equation and values (partial molar volume, thermal expansion, and compressibility) in Table 3 of Lange and Carmichael (1990 [DIRS 147767], p. 36) and as described in the text. Representative values of partial molar volume (26.7 cm^3/gram formula weight), thermal expansion (9.5×10^{-3} cm^3/mole·K), and compressibility (-3.2×10^{-4} cm^3/mole-bar) were selected for the H_2O component based on Ochs and Lange (1999 [DIRS 144330], p. 1,316, Table 2; and Abstract, p. 1,314).

Using saturation pressures derived from Table 6-5, the following expression of Sisson and Grove (1993 [DIRS 122564], p. 178) can be used to estimate multiple phase-saturation (liquidus) temperatures in the magmas:

$$T(°\text{C}) = 969 - (33.1 \times H_2O) + 0.0052\,(P_b - 1) + 742.7 \times Al^{\#} - 138 \times NaK^{\#} + 125.3 \times Mg^{\#} \quad \text{(Eq. 6-2)}$$

where

H_2O = wt % of water
P_b = pressure in bars (note that elsewhere in this document pressure is in Pascals)
$Al^{\#}$ = ratio of mass fractions of $Al_2O_3/(Al_2O_3 + SiO_2)$
$NaK^{\#}$ = ratio of mass fractions of $(Na_2O + K_2O)/(Na_2O + K_2O + CaO)$
$Mg^{\#}$ = molar $Mg/(Mg + 2Fe_2O_3T)$.

It should be noted that $Al^{\#}$, $NaK^{\#}$, and $Mg^{\#}$ do not vary as a function of water content in Lathrop Wells magmas as these parameters simply express relative proportions.

Liquidus temperatures for Lathrop Wells magmas with different hypothetical water contents were calculated as follows. First, the mean Lathrop Wells composition (from Table 6-3) was normalized to 100% (anhydrous). Then, major element oxides were renormalized to sum to 99.5 wt %, 99.0 wt %, 98.0 wt %, 97.0 wt %, and 96.0 wt %. To these values, 0.5 wt %, 1.0 wt %, 2.0 wt %, 3.0 wt %, and 4.0 wt % H_2O were added, respectively, so that the sum of the renormalized major element oxide content and water content sum to 100 wt % in each case. With these new hypothetical compositions, and the saturation pressure calculated as described above, Equation 6-2 was used to compute the liquidus temperatures shown in Table 6-5. The same hypothetical compositions and calculated temperatures were used to calculate bubble- and crystal-free viscosity using the method of Shaw (1972 [DIRS 126270], pp. 873 and 878).

Density can also be calculated as a function of composition (including water content), pressure, and temperature using the formulation and data of Lange and Carmichael (1990 [DIRS 147767], Table 3) with additional data for H_2O (Ochs and Lange 1999 [DIRS 144330], p. 1,315). Equation 2 from Ochs and Lange (1999 [DIRS 144330], p. 1,315) produces the molar volume of the silicate liquid, which only requires a simple conversion to density. The density conversion can be done as follows. Assume that 100 g of magma are present. In doing the calculation, one converts the weight of each oxide (equivalent to the wt %) to the number of moles of each constituent. These terms can be summed to give a total number of moles. The density is then equal to the inverse of the product of molar volume (cm^3/mole) and number of moles per 100 g of liquid. This result, in g/cm^3, can then be converted to kg/m^3 as shown in Table 6-5.

The liquidus temperature for a mildly alkalic basalt similar in composition to the mean Lathrop Wells lava composition at atmospheric pressure is between 1,174°C and 1,188°C (Mahood and Baker 1986 [DIRS 104663], Tables 1 and 2). Mahood and Baker (1986 [DIRS 104663]) temperature calculations are close to temperatures reported by Knutson and Green (1975 [DIRS 106299], Figure 1) for a hawaiite that is also similar in composition to Lathrop Wells basalt. Yoder and Tilley (1962 [DIRS 122589], Figure 28) published experimental results on the water-saturated liquidus for a high-alumina basalt, which indicated that at 1.75×10^8 Pa water pressure, the liquidus was more than 100°C cooler than the 10^5 Pa liquidus temperature, similar to Table 6-5. The calculated liquidus temperatures are higher than those obtained by phase equilibria experiments using samples from Lathrop Wells volcano, as reported by Nicholis and Rutherford (2004 [DIRS 173945], p. 490, Figure 2). For example, under water-saturated conditions, the experimental liquidus temperature at a pressure of 120 MPa is ~1,035°C, compared to the theoretical value of 1,076°C (Table 6-5), and the liquidus temperature at a pressure of 170 MPa is ~1,015°C, compared to the calculated value of 1,046°C. For the

purposes of modeling magma-repository interactions, a range of liquidus temperatures for a given pressure could be used to account for the differences between the theoretical and experimental results.

The presence of bubbles and crystals complicates the calculation of viscosity beyond the pure liquid values show in Table 6-5. As mentioned above, phenocrysts are only present in volume fractions of a few percent in Quaternary eruptive products in the Yucca Mountain region, so it is reasonable to ignore their effects on viscosity. Groundmass crystals, which grow during final ascent, emplacement, and cooling of eruptive products may act to increase the effective viscosity of the magma during these final processes. The effects of gas bubbles are more important for the magmas of interest. *Final Report of the Igneous Consequences Peer Review Panel, with Appendices* (Detournay et al. 2003 [DIRS 169660], Appendix 2, Section A2.6.1) provides a detailed discussion of the effects of bubbles including a plot (Detournay et al. 2003 [DIRS 169660], Figure 2B, Appendix 2) of relative viscosity (i.e., relative to the viscosity of pure liquid) that incorporates the effects of surface tension, shear strain rate, and bubble volume fraction. This plot can be used to estimate the effects of bubbles on flow of magma into drifts and conduit (below the fragmentation level; see Section 6.3.4.2) and lava flow processes, which are explored in detail in *Magma Dynamics at Yucca Mountain, Nevada* (BSC 2005 [DIRS 174070]).

6.3.3 Characteristics of Shallow Intrusive Features

The geometrics of several subvolcanic features in the Yucca Mountain region are discussed before considering the eruptive processes at the Earth's surface. They are considered in order of decreasing age.

6.3.3.1 Dikes and Dike Swarms

Direct observations of subsurface dikes and conduits, which conducted magma and volatiles toward a volcanic vent, are uncommon. Access to subsurface levels is hindered either by the young age of a volcano, wherein subsurface exposures are absent or limited, or by older age where feeder dikes may be exposed by erosion but the eruptive products—clues to eruption phenomena—have been removed by erosion. In the Yucca Mountain region, however, three preserved eruptive centers of late Miocene age provide direct access to shallow subsurface dikes and their eruptive products (Basalt Ridge, 9.1 ± 0.7 Ma; east Basalt Ridge, 8.8 ± 0.1 Ma (Perry et al. 1998 [DIRS 144335], p. 2-18); Paiute Ridge, 8.58 ± 0.07 Ma (Ratcliff et al. 1994 [DIRS 106634], p. 416)). These features yield analogue information on dike characteristics beneath eruptive centers that can be generalized to describe subsurface processes active during intrusion and eruption of small-volume volcanoes. The intruded host rocks are welded and non-welded ignimbrite sheets and fallout, similar to the setting at the Yucca Mountain site. In addition, the 3.7-Ma basalts of southeastern Crater Flat provide a younger (Pliocene) analogue for Yucca Mountain region volcanism. Although these Pliocene eruptive products have not been sufficiently eroded to expose plumbing below the paleosurface, dikes are exposed where they intrude into the lower parts of their own pyroclastic deposits. These, along with Quaternary volcanoes where no intrusions are yet exposed, provide indirect evidence on the nature of feeder dikes and are also discussed in this section. Appendix F provides location (Figure F-2) and detailed discussion of the analogue volcanic sites, which is summarized below.

Exposures to subvolcanic depths of up to 270 m are accessible in steep canyons that define Basalt Ridge and east Basalt Ridge, Nevada (BSC 2005 [DIRS 174070], Figure 6-6). The canyon walls expose the subsurface approach of planar dike sets of alkali basalt upward toward their eruptive vents, and the overlying ridges preserve many of the eruptive products of linear fissure eruptions and up to three focused eruptive vents per center (Figure F-11). The orientation of the subsurface feeder dikes parallels most normal faults in the area, and the dike at east Basalt Ridge clearly occupies a normal fault from its deepest exposures upward to the surface; this dike is almost continuously exposed for 4.3-km length. The near-vertical dike and fault orientation at the deepest exposure is N28°E and curves to a north-south strike, as do other faults in the area (Orkild et al. 1969 [DIRS 106460], plate 1). At depths of 250 m to 150 m below the paleosurface, feeder dikes from these examples are single tabular masses 10-m to 12-m wide with occasional swelling to 15 m. They often follow preexisting, vertical cooling joints where developed in the host ignimbrites. At shallower levels, the feeder dikes can bifurcate into closely spaced, multiple (5 to 6) dikes with overall widening of the intruded zone to ~25 m. Basalt Ridge includes exposure of a ~3-m-thick sill extending ~30 m into a nonwelded pumiceous tuff about 35 m below the paleosurface. Within the vertical dike, incorporation of pebble-size pieces of host rock xenoliths along the margins is common, while boulder-size pieces are far less common. Rotation and fusing of blocks of the silicic tuff is common. At east Basalt Ridge, further widening of the dike zone (up to 40-m thick at 35-m depth) occurred toward the paleosurface as overburden stresses became reduced during ascent, and flaring into an 80-m- to 100-m-wide, funnel-shaped vent within 25 m of the surface marks the eruptive source vent. In summary, the two small-volume eruptive centers at Basalt Ridge expose single-feeder dikes at depths slightly shallower than the proposed Yucca Mountain repository, which bifurcate into multiple closely spaced, small dikes with up to 100% widening of the intruded zone as they approach the surface, and which flare into a wide vent only at very shallow depths (Figure F-9).

At Paiute Ridge, Nevada, exposures of five or more alkali-basalt dikes, small sills, and at least one conduit, extend downward from shallow levels to >250 m below the paleosurface (Appendix F). Similar to the Basalt Ridge area, the host rocks include ignimbrite sheets and fallout deposits, as well as older carbonates and shales. Numerous preexisting high-angle faults provided pathways for several of the dikes, and there is evidence for fault-widening accompanying dike intrusion (Valentine and Krogh 2006 [DIRS 177282] pp. 225 and 228, pp. 217 and 229). The major dike orientations follow the faulted structural grain of the area and range between N20°W and N25°W, with shorter variations to between due North and N5°W. Smaller, discontinuous dike segments range between N10°E and N45°E. Dikes occur as single dikes or in swarms of up to four and are up to 5-km long in outcrop. Dike width varies from 1 m to 9 m, with most in the 2-m to 6-m range (CRWMS M&O 1998 [DIRS 123201], pp. 5-31 and 5-33); at one locality, one dike swells to 20-m width over ~30 m of strike length near an overlying sill. Some single dikes are composed of multiple overlapping, en echelon segments. Lateral intrusions of magma into sill bodies occurred by local rotation of principal stresses near contacts of strong Paleozoic carbonate rocks and weaker overlying tuffs within hanging walls of faults; sills appear to have been emplaced as shallow as ~30 m and as deep as 200 m (Byers and Barnes 1967 [DIRS 101859]; Valentine and Krogh 2006 [DIRS 177282]. Dike spacing ranges from 250 m to 1,440 m for dikes greater than 1,000-m long, and from 12 m to 135 m where they form a dike set radial to a preserved conduit. Absolute depth of these intrusive features is estimated to range from 100 m to 250 m. The reconstruction used to estimate depth is complicated by relief on the preeruptive surface and by faulting into a graben structure; however,

the difference in elevation between the 20-m-wide dike exposure and the base of an effusive lava flow 1,100 m to the east suggests <100-m depth in this area of the intrusion. In summary, Paiute Ridge is an intrusive dike and sill complex whose emplacement and final configuration were greatly influenced by preexisting normal faults and the contrasting lithologies of the host rocks.

Pliocene (3.7 Ma, Fleck et al. 1996 [DIRS 105337], Table 2) alkali basalt flows fed by linear eruptive vents and several focused vents are exposed within Crater Flat basin, about 10 km southwest of Yucca Mountain crest. The flows and vent-facies rocks are exposed along northeast-trending, southeast-dipping normal faults, which parallel the edges of the basin. However, the feeder dikes and eruptive vents are oriented between N10°W and N5°E and predate the northeast-trending faults (Appendix F; Potter et al. 2003 [DIRS 160060], plate 1). Therefore, fault alignment controlled both the ascent of basaltic magma feeding the eruptions and the (younger) orientation of the erosional remnants of the fissure system (Carr 1982 [DIRS 101519], p. 7; Brocher et al. 1998 [DIRS 100022] p. 967). The rocks comprise near-vent pyroclastic deposits, scattered scoria clasts, and lava flows, whose features are diagnostic of eruptions from fissures, which extend approximately 3.5 km (Appendix F). Nearly all loose pyroclastic materials, such as would form scoria cones or cone aprons, are removed by erosion, exposing the cores of vents including welded spatter, bombs, clastogenic and effusive lava flows, and the linear outcrops of narrow, en echelon feeder dikes. The dikes are typically about 1-m to 3-m wide, and occur singly and in swarms in zones up to 75-m wide. The position and orientation of the dikes within the fissure deposits indicate that they are remnants of feeder dikes that intruded into their overlying pyroclastic products as the eruptions proceeded; no intrusions into underlying country rock are exposed. Therefore, these basalts preserve the eroded surface remnants of a small-volume volcanic event which was confined to a narrow axis of linear dikes intruded parallel to or along normal faults as they approached the near surface.

Field analogue studies of Quaternary (< 1.8 Ma) small-volume volcanoes in Crater Flat offer insight and inferences into subvolcanic environments. Recent interpretations of the ~1-Ma-old Red Cone, Black Cone, and Makani volcanoes (Appendix D) support the conclusion that each of these small-volume eruptions represent a monogenetic event from a single vent fed by single structurally controlled feeder dikes, and not expressions of polycyclic eruptions from numerous vents scattered throughout their lava fields (Vaniman and Crowe 1981 [DIRS 101620], pp. 15 and 18; Smith et al. 1994 [DIRS 101996], p. 168). In particular, numerous isolated mounds of proximal pyroclastic material within the lava fields at Red Cone and Black Cone are cannibalized pieces of early cone-building material that were dislodged and rafted away by lavas flowing from flank eruptions, rather than individual source vents (Appendix D). Observations of anomalies in high-resolution aeromagnetic data collected from the Crater Flat area show that there is close association between locations of these volcanoes and underlying faults (Perry et al. 2005 [DIRS 177379], p. 485, Figure 1). In the case of Black Cone and Makani volcano, inferred structural control by separate north–south trending faults implies that individual feeder dikes fed these separate volcanic events; Makani volcano also exhibits a ~north-south-trending dike within its pyroclast deposit (Appendix D). In spite of the apparent northeast alignment of Quaternary cones in Crater Flat, suggesting control by a single dike or dike set with length of 10 km to 12 km, these events are likely controlled by individual dikes occupying north-south faults formed during east-west extension of Crater Flat basin. The actual number of dikes beneath the eruptive centers cannot be resolved from the aeromagnetic data.

The Lathrop Wells volcano (77.3±6 ka; Heizler et al. 1999 [DIRS 107255], Table 8a) is the youngest and best-preserved volcano in the Yucca Mountain region and an appropriate analogue for potential eruptive activity in the area (Detournay et al. 2003 [DIRS 169660], pp. 12 to 13). Appendix C details interpretation of recent field work and concludes that the Lathrop Wells volcano originated with fissure eruptions along a probable single northwest-trending dike, then focused into a single vent marked by the current cone. Early Strombolian bursts of molten pyroclasts from the vent were succeeded by a more energetic violent Strombolian phase, which built the majority of the cone with loose scoria lapilli, bombs, and subordinate ash. Similar to the Crater Flat cones and flows discussed above, flank eruptions of lava at Lathrop Wells dragged pyroclastic material from the growing cone and rafted it into positions away from the vent, giving the appearance of numerous scattered vents surrounded by lavas. Alignment of some of the rafted pyroclast mounds (plus other data from geochemical analyses, geomorphological studies, and partial excavation of several mounds) led earlier workers to infer up to three or more dikes fed the cone and lava field (Perry et al. 1998 [DIRS 144335], pp. 2-43 to 2-45). The Lathrop Wells dike is considered to underlie the northwest elongation of the cone and be reflected in the northwest-trending oxidation zone that discolors that cone. Recent quarry excavation on the southern midflank of the cone has exposed spatter and agglutinate from the early cone-building phase; a N7°W direction between the exposed agglutinate and the center of the cone's summit crater provides a reasonable estimate for orientation of the fissure that initiated eruption at Lathrop Wells volcano.

In summary, field measurements along with aeromagnetic data at analogue basaltic volcanoes have removed some of the speculation that has characterized the discussion of Yucca Mountain region dike orientation and width and number of dikes per swarm, both at the Earth's surface and at depths near the proposed repository level of ~300 m. The latter depth is most relevant to analyses of potential intersection of dikes with repository drifts, including the intrusive case; the surface or near-surface data partially address consequences for the eruptive case. The data set is nonetheless small for deep dike exposures, and the recommended distributions for dike widths, number of dikes, dike spacing and orientation are developed from field analogue data.

Because the dike widths in the regional analogues range over only one order of magnitude, a normal distribution for dike widths is appropriate for description. The normal distribution of dike widths can be described as having a mean of 8 m, a minimum of 1 m and 95th percentile of 12 m.

From the preceding discussion, it is clear that the term "dike swarm" used here refers to a limited number of narrow, closely spaced dikes in the shallow subsurface and not to the many dike intrusions typical of volcanic rift zones or shield volcanoes as summarized by Walker (1999 [DIRS 178457], p. 22, Figure 1). Table 6-6 shows the estimated probability distribution for the number of dikes in a "swarm" at repository depth that is recommended for TSPA.

Table 6-6. Probability Distribution for the Number of Dikes in a Swarm at Repository Depth

Number of Dikes	Probability Distribution
1	0.40
2	0.25
3	0.15
4	0.10
5	0.10

In addition to the number of possible dikes, the spacing between dikes is another important variable. For the Paiute Ridge intrusion, mean dike spacing for dikes greater than 1-km long is ~995 m (maximum 1,440 m; minimum 250 m) (Byers and Barnes 1967 [DIRS 101859]). For the 3.7-Ma-old Crater Flat basalts, dike spacing is ~385 m (Perry et al. 1998 [DIRS 144335], Appendix 2-M1). In each example, some dike splitting or en echelon geometry may occur that provides less than one meter spacing. In order to capture the variability observed in the field, the recommended dike spacing (measured edge-to-edge) for the Yucca Mountain region can be judged as a random uniform distribution ranging from 0.5 m to 1,500 m.

The orientation of potential dike intrusions at repository level affects the number of drifts intersected by a dike (because of repository layout) and requires a distribution to estimate the number of affected waste packages for igneous consequences modeling. Field observations of dike intrusions in the region, regardless of age, show that most dikes in these small magmatic systems occupy steeply dipping faults from depths of >250 m to their eruptive paleosurfaces. Dikes that cannot be shown to occupy preexisting planes of weakness often parallel the faulted or fractured structural grain (e.g., Paiute Ridge). The observations suggest that dike orientation at repository depths at Yucca Mountain would also be controlled primarily by preexisting extensional faults by capture of the ascending magma. Crustal-stress arguments reason that dike orientations from depth would align along directions roughly perpendicular to the least principal stress in the absence of preexisting weaknesses (faults or fractures); field observations show that at shallow depths orientations of dikes are largely controlled by preexisting structures and thus can deviate from orientations controlled solely by crustal stress orientation. The orientation of mapped faults within the Yucca Mountain block near the repository footprint (Day et al. 1998 [DIRS 100027], plate 1) is bimodal (~N10°E and N20°W) and overlapping. A distribution of potential dike orientations at repository level (~300 m beneath the surface) should reflect those orientations plus or minus some angle of variability. Therefore, preferred directions for dike orientations are projected in the ~N10°E ± 15° and N20°W ± 15° ranges, which generally describe the bimodal fault-distribution. In azimuths measured clockwise from north, these directions are 010° ± 15° and 160° ± 15°. The probability is considered higher for the 010° ± 15° range because those directions are roughly perpendicular to the WNW-direction of least principal stress (Zoback and Zoback 1980 [DIRS 108658], Table 2). Table 6-7 and Figure 6-3 show a distribution for dike azimuth that captures the structural influence at repository-level on dike ascent and the deeper crustal (regional) control. In brief, the northern swath of 145° to 030° azimuths reflects the dominance of shallow structural control recognized in the regional volcanic analogues (Appendices C, D, E, and F); the azimuths centered on 030° reflect the influence that the regional stress field might have in influencing orientations of dikes near the surface, as well as the "tail" (~ 050° to 100°); the 100° to 140° azimuths describe the low probability that

ascending dikes will obtain orientations that are parallel (120° ± 20°) to the least horizontal principle stress.

The distribution differs from the probability distribution for dike azimuth from the 1996 probabilistic volcanic hazard analysis (PVHA; BSC 2004 [DIRS 169989], Figure 6-20, Table 6-10). The PVHA elicitation process produced an aggregated expert assessment of the distribution whose mode reflects a dominant influence by least principle stress arguments (i.e., a mode centered on ~ N30°E or 030°), although many experts also acknowledge control of magma ascent by shallow structures (CRWMS 1996 [DIRS 100116], e.g., pp. MD-2, WD-7). The secondary mode in the PVHA distribution centered on ~170° azimuth (BSC 2004 [DIRS 169989], Figure 6-20, Table 6-10) accounts for the influence of the NNW-trending existing faults and fractures at the Yucca Mountain site.

Table 6-7. Probability Distribution Function for Potential Dike Orientations at Repository Depth

Azimuth (degrees from North)	Probability
0 to 009	0.130
010 to 019	0.120
020 to 029	0.100
030 to 039	0.090
040 to 049	0.070
050 to 059	0.050
060 to 069	0.030
070 to 079	0.020
080 to 089	0.020
090 to 099	0.010
100 to 109	0.005
110 to 119	0.005
120 to 129	0.005
130 to 139	0.005
140 to 149	0.030
150 to 159	0.070
160 to 169	0.110
170 to 179	0.130

NOTE: Probabilities may not sum to one due to rounding.

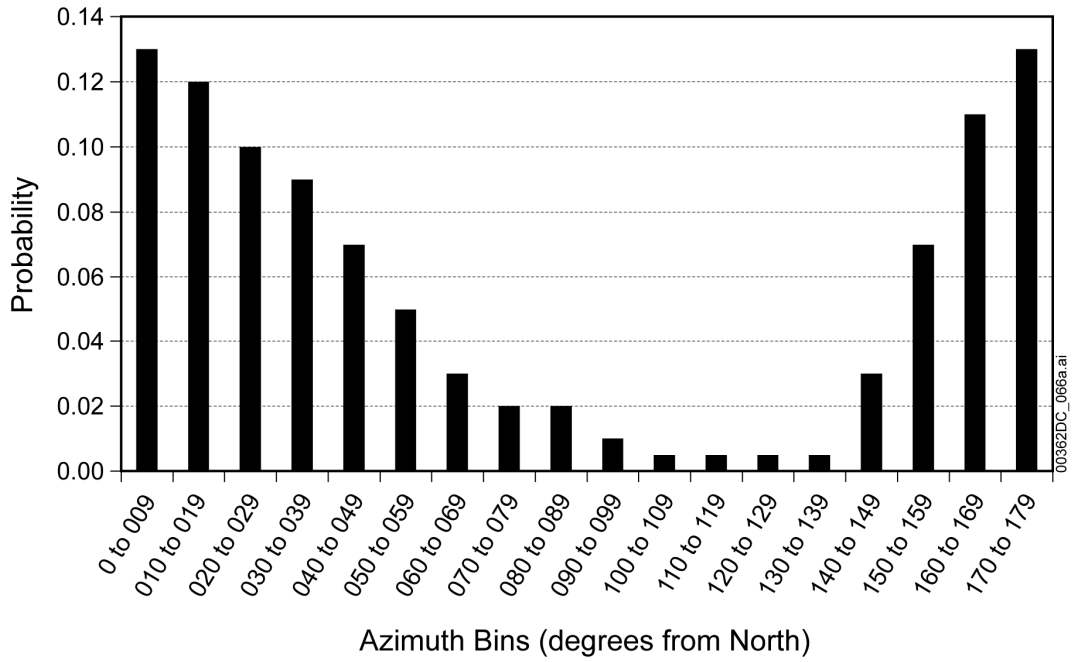

Figure 6-3. A Probability Distribution Function for Potential Dike Orientations at Repository Depth

Dike-length measurements from analogue studies in the Yucca Mountain region obtain data from various elevations, but do not yield much continuous information from repository depths. Exposures from the surface to depths of ~250 m show minor dike bifurcation at depths less than about 100 m (except near the vent) and continuity of tabular dikes below 100 m (in terms of a singular dike and its orientation). Lengths measured in the field (Appendix F, Table F-1) range from a minimum of ~0.5 km at Paiute Ridge to ~4.3 km or more at east Basalt Ridge; inferred dike lengths at the near-surface for Pliocene-Pleistocene volcanoes in the Yucca Mountain region range from 0.4 km for Makani volcano up to 5 km for Thirsty Mountain (Figure D-1); the eight youngest (≤1 my) volcanoes have inferred dike lengths of <1.8 km (Valentine and Perry 2006 [DIRS 177495], Table 1). Therefore, the dike-length distribution for intrusion at repository depth should be normal, with minimum of 0.4 km, a mean of 2 km, a 95th percentile of 6 km, and truncated at 8 km. The distribution reflects those data that represent the youngest intrusive activities within the waning basaltic field in the Yucca Mountain region.

6.3.3.2 Dike-Induced Earthquakes

Worldwide, geodetic measurements, cointrusive seismicity, and field observations indicate a propagating dike incrementally forms small normal faults, fissures, tensile cracks, and grabens at the surface above the dike. The magma-induced surface faults with cointrusive displacements of up to several meters can form aseismically or be accompanied by shallow depth, low-magnitude earthquake swarms (Hackett et al. 1996 [DIRS 169781], pp. 147 and 158). The volcanic earthquake swarms can include high frequency earthquakes that can generate ground motions similar to those generated by tectonic induced earthquakes. The volcanic earthquake swarms typically occur ahead of the propagating dike tip and are thought to result from slip along suitably oriented existing fractures that lie within an ambient differential stress region. If the ambient state of stress is such that existing faults are near failure, then the stress perturbation due

to dike intrusion can induce failure along these faults (Rubin 1995 [DIRS 164118], p. 321; Rubin and Gillard 1998 [DIRS 169786], p. 10,017 and 10,026; Rubin et al. 1998 [DIRS 169787], p. 10,011). Dike-induced rupturing of fractures and faults near the dike tip, the subject of this discussion, form in the shallow crust at depths less than 4 km to 5 km, where differential stress and rigidity are lower than at depth (Smith et al. 1996 [DIRS 101020], p. 6,284). Hence, rupture areas and the maximum magnitudes of strain release associated with dike intrusion are small, in comparison with regional faults that extend to the brittle-ductile transition.

Numerical and scaled empirical experiments on dike intrusion provide information on the relationships between dike geometry, stress and strain distribution, and surface deformation (Mastin and Pollard 1988 [DIRS 169783], p. 13,228 and Figure 12; Rubin 1992 [DIRS 169784], Figure 6). Dike intrusion produces a broad zone of uplift that results from magma-induced compressional stress alongside the dike, with a narrow zone of subsidence that forms above the dike and results from tensile stress near the dike tip. Normal faults and fissures form where the tensile zone interacts with the earth surface. Fissures form in two symmetrical zones above the dike, and form progressively inward with dilation of the dike. Most fissures are oriented parallel to the dike plane. As dilation continues, dip-slip movement occurs on the fissures, producing normal faults and a central graben. The down-dip extent of faults is small, and they extend only slightly deeper than the dike top. Depth to the dike top can be estimated from the graben widths (Mastin and Pollard 1988 [DIRS 169783], p. 13,228).

Maximum magnitudes of dike-induced earthquakes can be estimated for the Yucca Mountain region using an approach following Smith et al. (1996 [DIRS 101020], p. 6,284). In the absence of observed volcanic seismicity (as in the Yucca Mountain region), the geometry of surface deformation features such as surface lengths of normal faults and fissures and graben widths can be used to estimate fault dimensions. Empirical relationships between fault dimensions and magnitude can then be used to estimate maximum magnitudes of potential dike-induced earthquakes. To estimate the maximum magnitudes of dike-induced earthquakes for the Yucca Mountain region, surface-fault length is equated to the dike-length distribution at repository depth, which has a minimum of 0.4 km, a mean of 2.0 km, a 95th percentile of 6.0 km, and a cutoff at 8.0 km (Section 6.3.3.1). The dike lengths can be equated to potential surface-rupture lengths (SRL) and, for SRLs of 0.4 km, 2.0 km, 6.0 km, and 8.0 km, yield maximum moment magnitudes of 4.6, 5.4, 6.0, and 6.1, respectively, for the Yucca Mountain region using $M = 5.08 + 1.16 \log_{10}$ (SRL); where M is moment magnitude (Wells and Coppersmith 1994 [DIRS 107201], Figure 9).

The estimated maximum magnitudes of dike-induced earthquakes for the Yucca Mountain region are compared to maximum magnitude ranges:

- Estimated for normal faults, fissures, and graben widths in volcanic rift zones worldwide and in the eastern Snake River Plain (Smith et al. 1996 [DIRS 101020], Tables 1 and 2)
- Estimated for fault width using a volcanic crust 4-km thick (referred to as depth to the level of neutral buoyancy shown by Smith et al. (1996 [DIRS 101020], Table 2)
- Calculated for instrumentally observed earthquakes at active volcanic rift zones (Smith et al. 1996 [DIRS 101020], Figure 5).

The maximum magnitudes estimated for the Yucca Mountain region overlap maximum-magnitude estimates derived from surface lengths in volcanic rift zones worldwide and the eastern Snake River Plain. They exceed estimates based on observed seismicity at active volcanic rift zones and fault widths in volcanic rift zones worldwide, the eastern Snake River Plain, and a 4-km-thick volcanic crust (Figure 6-4). Magnitudes of dike-induced earthquakes that are calculated using tectonic-fault dimensions will be maximum magnitudes, for the following reasons (Smith et al. (1996 [DIRS 101020], pp. 6,284 and 6,285):

- The crustal rigidity of the shallow, fractured crust in active volcanic areas is probably lower than the rigidity of typical midcrustal regions where most tectonic fault ruptures nucleate

- Commonly high b values (> 1.0) are associated with volcanic seismicity, indicating the effective differential stress in the shallow crust of active volcanic regions is lower than for typical midcrustal regions (b is the slope of the Gutenberg-Richter magnitude-frequency relationship log N = a – bM; where M is magnitude; N is the number of earthquakes with magnitudes greater than M occurring in a given time period; “a” and “b” are constants that describe the linear relationship, “a” is the intercept)

- Rupture along dike-induced normal faults and fissures occurs incrementally rather than as a sudden catastrophic release of strain, where only the latter gives rise to energy release that is proportional to the dimensions of the entire fault rupture.

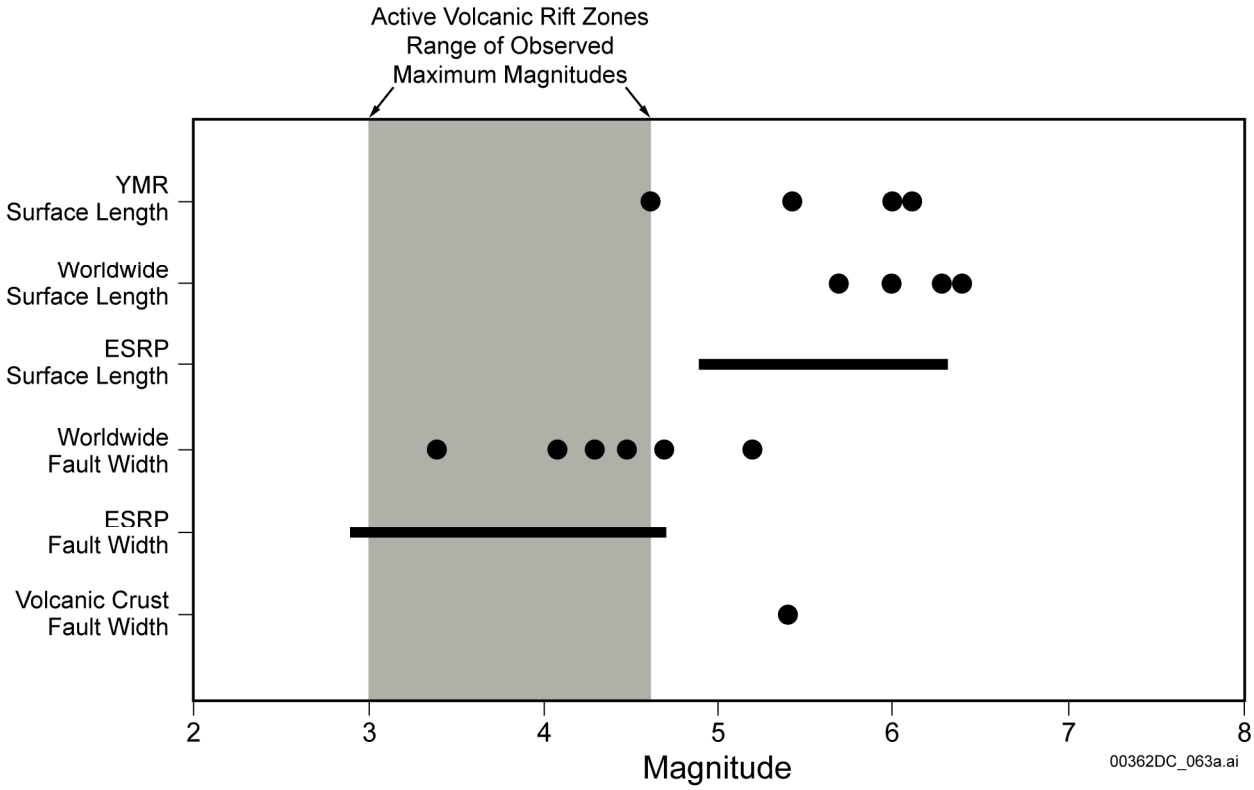

Source: Yucca Mountain region dike surface length (this report); other data (Smith et al. 1996 [DIRS 101020], Tables 1 and 2, Figure 5).

ESRP = Eastern Snake River Plain.

NOTE: Bars indicate upper and lower values of the mean plus and minus the standard deviation, respectively, and solid circles indicate single calculated values. Yucca Mountain region values are discussed in text. Other maximum magnitude (M) values shown are: M 5.7, 6.0, 6.3, and 6.4 for surface lengths of faults and fissures in volcanic rift zones worldwide; M 5.6 ± 0.7 for surface lengths of faults and fissures in eastern Snake River Plain volcanic rift zones; M 3.4, 4.1, 4.3, 4.5, 4.7, and 5.2 for fault widths derived from graben widths in volcanic rift zones worldwide; M 3.8 ± 0.9 for fault widths derived from graben widths in eastern Snake River Plain volcanic rift zones; M 5.4 for a fault width equivalent to a volcanic crust 4-km thick; and M 3.8 ± 0.8 for the range of instrumentally observed seismicity at active volcanic rift zones (shaded).

Figure 6-4. Plot of Calculated and Observed Maximum Magnitudes for Dike-Induced Earthquakes

For example, surface faulting with well over 1-m displacement was observed to accompany a fissure eruption near Krafla caldera in Iceland, but the associated earthquakes did not exceed magnitude 2.5 (Brandsdottir and Einarsson 1979 [DIRS 155852], p. 209).

In addition to earthquakes associated with dike formation itself, it is also possible that dike intrusion could trigger slip on a preexisting tectonic fault. In the Yucca Mountain region, the state of stress is close to failure (Stock et al. 1985 [DIRS 101027], pp. 8701 and 8702). Stress perturbations associated with dike intrusion could alter the state of stress in the vicinity of a preexisting fault sufficiently to cause the fault to slip in an earthquake. By triggering slip on a preexisting tectonic fault, dike intrusion could generate an earthquake with a magnitude that is larger than that caused directly by dike formation (i.e., larger than earthquakes observed within active volcanic rift zones; Figure 6-4). Such a process could affect the timing of a specific earthquake on a pre-existing fault, but should not affect the long-term average rate of movement, which would be driven by the larger-scale tectonic state of stress.

Smith et al. (1996 [DIRS 101020], pp. 6,287 and 6,288) selected a maximum magnitude for dike-induced earthquakes in the eastern Snake River Plain to be consistent with the maximum magnitudes derived from fault width and rupture area. They reasoned that the maximum magnitude estimates derived from fault width and rupture area measured in the eastern Snake River Plain were internally consistent, and they were consistent with observed magnitudes during dike injection in worldwide volcanic rift zones. Following this approach, magnitudes ranging from 4.6 to 6.1 are reasonable estimates for potential dike-induced earthquakes in the Yucca Mountain region.

6.3.3.3 Conduits

An important issue in defining the consequences of a potential volcanic event that intersects the repository is the size, shape, and number of conduits that transport magma and, potentially, radioactive waste, to the surface during eruption. This section summarizes the information from analogue sites that is related to conduits. The best data for describing conduits come from field studies of basaltic volcanic vents or necks exposed by erosion where direct measurements can be made of conduit diameter and variation with depth. Several sites of Yucca Mountain region Miocene and younger basaltic volcanoes provide data that constrains, to some degree, conduit size and depth for a small-volume basaltic eruption. Another source of information for conduit depth is abundance of wall-rock xenoliths incorporated into eruptive products. Both sources are summarized below and are detailed in Appendices C through F.

East Basalt Ridge–East Basalt Ridge, Nevada, provides the most direct evidence of dike/conduit transition for the area. A radiometric age of 8.8 ± 0.1 Ma for east Basalt Ridge is provided by Perry et al. (1998 [DIRS 144335], p. 2-18). As discussed in Section 6.3.3.1, the 10-m- to 12-m-wide dike at 250 m below the paleosurface gradually widens toward the surface; at 90-m depth, the dike is 15-m wide with evidence of increasing interaction with the wall rocks (Figure F-9). At ~25-m depth, the now 40-m-wide dike zone abruptly flares upward to ~100 m width and merges into its eruptive products. There is a large boulder of host rock incorporated into the lower flared interval, but it is equivocal whether it was dragged upward from near its current position or foundered from the overlying flared interval. The transition depth from dike to conduit is arbitrary in this case and can be conservatively argued to occur between 90 m and 25 m below the paleosurface. The surface geology indicates that the eruption was initially dominated by fissure eruption along the dike, culminating in about three focused vents distributed along strike, rather than feeding a single volcanic cone.

Paiute Ridge–Paiute Ridge, Nevada, is another analogue where erosion has exposed a subsurface remnant of a probable conduit at a depth of 50 m to 100 m beneath its paleosurface (Appendix F; Figure F-9). The Paiute Ridge intrusive complex is dated 8.58 ± 0.07 Ma (Ratcliff et al. 1994 [DIRS 106634], p. 416). The conduit shape is complex, roughly elliptical, and reflects intersection of four prominent dikes and several short (radial?) dikes. The core of the edifice is dense, vertically jointed basalt and measures ~100 m by 70 m and represents a focused-flow pathway toward the overlying vent (now eroded). The dense core is surrounded by an irregular zone of intense mixing of basalt magma with brecciated, rhyolitic wall rock. The overall size, inclusive of the mixed zone, is ~220 m by 110 m. Ledges of basalt dipping in toward the conduit resemble cone sheets and some may have been vents (boccas) for effusive flows near the flanks of a now-eroded cone. The cone-sheet geometry and close network of

dikes and breccias at the conduit, plus evidence of nearby eruptive products, imply interaction with host rock at a range of shallow depths with decreasing overburden stresses (Valentine and Krogh 2006 [DIRS 177282], p. 229). The conduit likely represents very shallow, subvolcanic plumbing of focused magma flow directly beneath the eruptive vent.

Pliocene Crater Flat– The Crater Flat site is described in detail in Appendix F. Alkali basaltic rocks of Pliocene age (~3.7 Ma; Fleck et al. 1996 [DIRS 105337], Table 2) are preserved in southeastern Crater Flat, 10 km southwest of the repository site at Yucca Mountain, and comprise ~0.6 km^3 in volume. Erosion and tilting along normal faults have exposed the shallow interiors of three to five vent areas for this volcanic event, which was dominated by emplacement of lavas except for locations very close to the vents. Vents are aligned along three en echelon, north–south trending segments that are characterized by dikes and local patches of pyroclastic material over a total length of ~3.5 km. The vent areas have accumulations of variably welded scoria, spatter, and breccia that are partly intruded by dikes. The distribution of pyroclastic deposits around vents suggests that they may have originally formed pyroclastic cones, one on the order of at least 200 m in diameter (Perry et al. 1998 [DIRS 144335], Appendix 2-M1). It is likely that minor eruptive activity occurred along the entire fissure at various stages, but that most volume flux was focused at the vents. The exposures of Crater Flat volcanic rocks do not extend below the preeruptive surface. This volcanic activity occurred during a phase when the overall volume flux of the entire volcanic field was significantly larger than is recorded in Quaternary events, and this is reflected by the fissure-fed, lava-dominant nature of this site and other Pliocene volcanoes in the region (Valentine and Perry 2006 [DIRS 177495], p. 4).

Quaternary Crater Flat volcanoes–Five small volcanoes erupted in Crater Flat at approximately 1 Ma (Little Cones, Red Cone, Black Cone, and Makani volcano); their radiometric ages are indistinguishable. The characteristics of the volcanoes and interpretations of eruption processes and durations for each are described in detail in Appendix E. Erosion has not yet exposed the magma feeder systems for these volcanoes, but some inferences can be made based upon surface exposures. Four of the five volcanoes probably began with eruptions along short fissures (Valentine and Perry 2006 [DIRS 177495], p. 2) that rapidly focused into a single main conduit for each volcano, from which most of the pyroclastic products and lavas emanated. Lavas probably erupted largely from the bases of the cones, while pyroclastic material erupted from the crater at the summit of each cone. The breakout vents, or boccas, for the lavas are small (few square meters) and likely are connected to the main conduits at very shallow levels, at or just above the contact between volcanic products and the preeruptive ground surface, and therefore do not have a primary effect on geometry at depths of 200 m to 400 m. One of the Quaternary volcanoes, Makani, apparently did not erupt long enough to focus completely into a distinct central vent around which a scoria cone could be formed; most of its products, which comprise a very small volume, are short lava flows that emanated from a fissure about 400-m long.

Lathrop Wells volcano–The youngest basaltic volcano in the Yucca Mountain region is Lathrop Wells volcano (~80 ka; Heizler et al. 1999 [DIRS 107255], p. 799) and it is the best preserved. Appendix C details the geology and evolution of the Lathrop Wells volcanic event. The scoria cone shows minimal erosion and there are no exposures of plumbing within or beneath the cone. Quarried exposures of interior agglutinate in the southern part, however, imply that the elongated axis of the cone reflects the orientation of the initial fissure eruption, which preceded focusing

into a single conduit and vent. Studies of xenolith host rock incorporated into the Lathrop Wells eruptive products show that the volume of xenolithic material in cone and tephra (excluding lava) can be represented by a single, cylindrically shaped conduit with diameter of ~18 m extending the depth of the underlying silicic tuff section, or ~335 m (Appendix C). Additional studies (Appendix F) imply that the representative volume is distributed over a conduit that narrows with depth and that has significant flaring within 50 m to 100 m directly beneath the cone.

Summary–The analogue sites support a model wherein conduits flare rapidly in the uppermost 50 m of host rock beneath small-volume basaltic volcanoes that were formed by eruptions driven by magmatic volatiles (i.e., not by explosive interaction between magma and groundwater or surface waters). This magmatic-volatile driving mechanism is most consistent with interpretations of eruption mechanisms at all of the analogue sites studied, in particular the Quaternary volcanoes of the Yucca Mountain region. Appendix F describes in detail the data supporting the inference of shallow conduit flaring and corroborates this with published theoretical models of conduit flow in basaltic eruptions. Based upon the eroded analogues, roughly circular conduits do not reach down to repository depths of 300 m, implying that the effective "conduit diameter" at that depth would be the dike width; therefore, it is recommended that the dike width (chosen from a distribution, Section 6.3.3.1) be used as a minimum conduit diameter for TSPA. The east Basalt Ridge dike locally swells to ~15 m at the deepest (~250 m) level exposed. Xenolith data from eruptive deposits at the Lathrop Wells volcano suggest that the maximum diameter of its conduit in the ~300 m depth range would be ~21 m (see detailed discussion in Appendix C). This is an upper bound for two reasons: (1) it assumes that all of the eruptive products (cone, tephra sheet, and lavas) have the same (mean) lithic content as deposits in the Lathrop Wells cone, and (2) it assumes that the conduit has a constant diameter from the surface to the base of the Miocene tuffs (~335 m beneath the volcano). It is likely that, as with the eroded analogues, the conduit at Lathrop Wells volcano flares rapidly within the uppermost 50 m beneath the volcano. Nevertheless, because it is impossible to constrain the Lathrop Wells conduit geometry it is recommended that 21 m be used as the 95th percentile value for conduit width in TSPA. Therefore, the range of conduit diameters sampled for eruptive modeling in TSPA should be a normal distribution with a minimum value that is determined by the dike width of a given realization, a 95th percentile value of 21 m, and a mean of 15 m.

Each of the Quaternary volcanoes in the Yucca Mountain region appear to have formed one conduit. Given that a volcano forming in the Yucca Mountain region during the next 10,000 yrs to 1,000,000 yrs is likely to be similar to those that have formed during the Quaternary, it is most likely that a future volcano will also form only one conduit. Table 6-8 presents the probability distribution function for number of conduits associated with a future volcano recommended for TSPA. The distribution is based on the Quaternary record of volcanism in the Yucca Mountain region.

Table 6-8. Probability Distribution Function for Number of Conduits Associated with a Future Volcano

Number of Conduits	Probability
1	0.85
2	0.10
3	0.05

The probability distribution shown in Table 6-8 reflects the Quaternary record of one conduit per event, but allows that a future volcano might have more than one conduit (as many as three, which is observed in the larger-volume, fissure dominated, Pliocene Crater Flat volcanic rocks).

A final point regarding conduits is the observation that spacing between surface vents (equated to conduit spacing at depth) does not appear to have a characteristic length (Appendix F). Analogue data discussed in Appendix F (Table F-1) suggests a minimum spacing of about 500 m and a maximum spacing of about 2 km. This is not well constrained by abundant field data or by known processes and should be described as a random uniform probability.

6.3.4 Eruptive Processes and Resulting Pyroclastic Deposits

Section 6.3.1 through 6.3.3 and Appendices C through E describe the variety of intrusive and effusive features that accompanied formation of the Quaternary volcanoes of the Yucca Mountain region. Much of the dynamics of volcanic eruptions is determined by the interplay of volatiles with silicate melt and with surrounding country rocks. Strombolian eruptions are indicative, for example, of the growth and coalescence of large bubbles or gas pockets in a slowly rising magma column beneath a vent. As these bubbles grow in size their rise velocity relative to the surrounding basaltic melt increases, so that they ascend through the magma column and burst as they reach the vent, throwing out large fluid chunks of magma as lapilli and bombs. McGetchin et al. (1974 [DIRS 115469], Figure 14) described the process of cone growth associated with Strombolian eruptions. Violent Strombolian eruptions, on the other hand, may represent situations where gas bubbles remain small and, when the ascending bubbly magma fragments (see below), it forms small clasts in the ash and lapilli size range. Lavas represent relatively bubble-poor magmas, but can erupt simultaneously with violent Strombolian activity from the same conduit (Luhr and Simkin 1993 [DIRS 144310], Figures 33 And 94; Appendix C). The solubilities of volatiles such as H_2O and CO_2 in basaltic magmas are proportional to pressure (Jaupart and Tait 1990 [DIRS 118292], p. 219). At depth (for example, in a magma chamber), magmas will have relatively high volatile contents. As they ascend through progressively lower lithostatic pressure, they will become oversaturated and bubbles will nucleate. Continued rise results in increasing numbers and sizes of bubbles (caused by combined exsolution of volatiles and decompression and coalescence growth of the bubbles). These two processes increase the specific volume of the magma, and as a consequence, its velocity also increases gradually (according to conservation of mass). Explosive eruption occurs when, at shallow depths, the magma reaches a foamy state, and with further decompression, it fragments, switching from being a melt with dispersed bubbles to a gas with dispersed fragments or clots of melt. At and above this fragmentation depth, the gas-melt mixture accelerates rapidly until it leaves the volcanic vent at speeds of tens to a few hundreds of meters per second. A further complication in this sequence of events is the possibility of loss of volatiles through the walls of the conduit or dike as magma ascends. This action can reduce the effective volatile content for the eruption.

The dynamics of magma ascent, and particularly fragmentation processes, are currently a topic of intense research in the volcanological community. Most recent advances in this area focus on silicic rather than basaltic magmas. The reasons for this are twofold. First, silicic magmas are responsible for the most explosive eruptions and present the most severe hazard to populations; understanding their dynamics is key in mitigating these hazards. Second, silicic magmas have viscosities several orders of magnitude higher than basaltic magmas. This condition greatly

reduces the effects of bubbles rising more rapidly than their host melts and coalescing with each other. Thus, theoretical modeling is made more tractable by having to consider only nucleation, decompression growth, and growth by diffusion of exsolving volatiles into bubbles. In other words, the dynamics are closely approximated by a "homogeneous flow" approach, in which the gas and melt move at about the same velocity everywhere and are in thermal equilibrium. However, the rise of basaltic magmas with their lower viscosities is complicated by the potential for rapid rise and coalescence of bubbles (Vergniolle and Jaupart 1986 [DIRS 115585], pp. 12,842 through 12,846). Extreme results of this process are represented by classic Strombolian bursts, which are basically large bubbles rising through and bursting at the top of a magma column, producing eruptions of mostly gas with small amounts of melt (fragments of bubble walls) thrown out ballistically. Another example is the Hawaiian fire fountain eruptions, which have been observed to erupt molten pyroclasts with H_2O vapor content much higher than the H_2O solubility at depth. A general theory for the rise of basaltic magmas, accounting fully for the important two-phase flow effects, does not exist. Instead, the treatment below simplifies the problem by assuming homogeneous flow.

6.3.4.1 Magma Ascent Rate below Volatile Exsolution Depth

Wilson and Head (1981 [DIRS 101034]) developed a theory for the ascent of basaltic magmas along dikes and cylindrical conduits using the homogeneous flow simplification (Section 5, Assumption 4). Ascent can be driven by a high-pressure source or by a net buoyancy of the magma (including melt, bubbles, and crytstals) with respect to the surrounding rocks. At depth, where magma is under sufficient pressure that all volatiles are dissolved, the ascent velocity for bouyancy-driven flow, u_f, is (Wilson and Head 1981 [DIRS 101034], p. 2,974):

$$u_f = \frac{A\eta}{4K\rho_m r}\left[\left(1+\frac{64 g_c r^3 (\rho_c-\rho_m)K\rho_m}{A^2\eta^2}\right)^{1/2}-1\right] \quad \text{(Eq. 6-3)}$$

where

A = 64 (circular conduit) or 24 (dike)
η is magma viscosity
K = 0.01
ρ_m is the melt density (no bubbles)
ρ_c is the wall rock density
r is the conduit radius or dike half width
g_c is gravitational acceleration

The flow described in Equation 6-3 can occur only when $\rho_c > \rho_m$, and only applies if there are no bubbles in the magma.

6.3.4.2 Volatile Exsolution and Fragmentation

As magmas rise, volatiles may begin to exsolve. The solubility of water (n), the major volatile species in basalt, is approximated by Equation 6-1 (Jaupart and Tait 1990 [DIRS 118292], p. 219). The depth at which exsolution of water vapor begins to occur is the depth at which the magma becomes saturated with respect to its original water content, which, assuming lithostatic pressure ($P = \rho_c g_c d$, where d is depth; see Section 5, Assumption 3), can be derived as:

$$d_{exs} = \frac{\left(n_i / 6.8\times10^{-8}\right)^{10/7}}{\rho_c g_c} \qquad \text{(Eq. 6-4)}$$

where,

d_{exs} is exsolution depth in meters (m)
n_i is the initial dissolved mass fraction of water at the magma's depth of origin,
ρ_c is the average density of the crust above d_{exs} in kg/m^3
g_c is gravitational acceleration (m/s^2).

This relation is plotted in Figure 6-5. The mass fraction of water exsolved from a basaltic magma, n_{exs}, at a given depth is:

$$n_{exs} = n_i - n \qquad \text{when } d < d_{exs} \qquad \text{(Eq. 6-5a)}$$

$$n_{exs} = 0 \qquad \text{when } d > d_{exs} \qquad \text{(Eq. 6-5b)}$$

The density of the mixture of silicate melt and water vapor bubbles (ρ_{mix}) can be calculated from (Wilson and Head 1981 [DIRS 101034], p. 2,983):

$$\frac{1}{\rho_{mix}} = \frac{n_{exs}}{\rho_g} + \frac{(1-n_{exs})}{\rho_m} \qquad \text{(Eq. 6-6)}$$

The density of the gas phase (ρ_g) can be calculated using the ideal gas law:

$$\rho_g = \frac{P}{RT} \qquad \text{(Eq. 6-7)}$$

where R is the gas constant for water (in this report, a value of 461 J/kg-K is used) and T is temperature. If it is assumed that the pressure in a conduit or dike is determined by the lithostatic pressure, ρ_g can be computed as a function of depth d:

$$\rho_g = \frac{\rho_c g_c d}{RT} \qquad \text{(Eq. 6-8)}$$

Equations 6-1 and 6-4 to 6-8 can be used to calculate the mixture density for any initial volatile content at any depth, which may be useful for estimating the interactions between the mixture and the repository. The mixture density can also be expressed in terms of gas volume fraction, ϕ, as:

$$\rho_{mix} = \phi\rho_g + (1-\phi)\rho_m \quad \text{(Eq. 6-9)}$$

Rearranging, the gas volume fraction is here derived as:

$$\phi = \frac{\rho_{mix} - \rho_m}{\rho_g - \rho_m} \quad \text{(Eq. 6-10)}$$

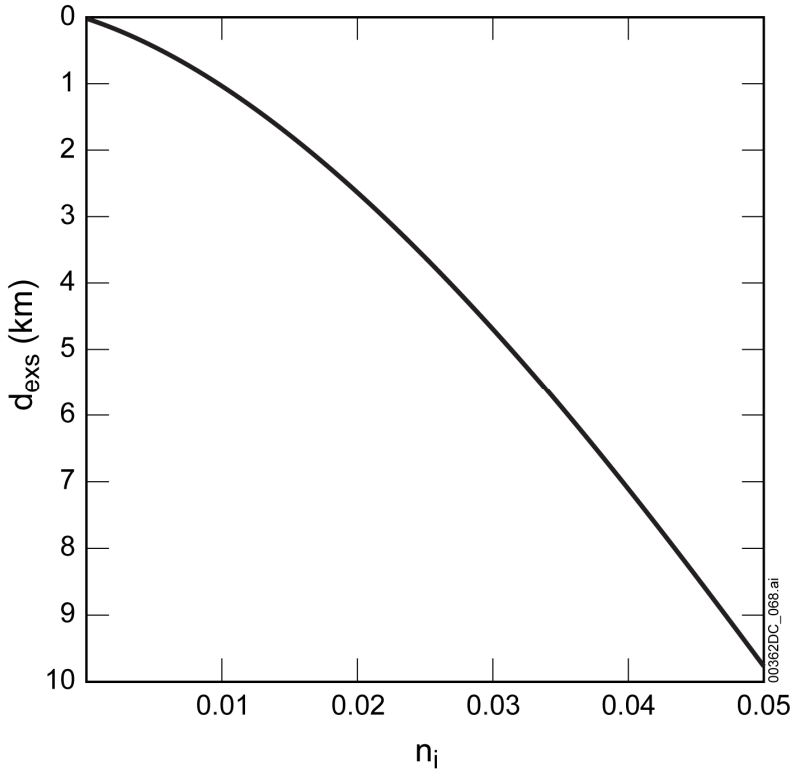

Source: Plot of Equation 6-4.

NOTE: For illustration purposes only. The calculations assume that pressure in the magma column is lithostatic and that bubble nucleation kinetics can be ignored. The average (shallow) crustal density (ρ_c) is taken to be 2,500 kg/m^3, as an example. d_{exs} is depth at which exsolution begins; n_i is dissolved water (H_20) content up to 0.05.

Figure 6-5. Plot of the Depth at which Volatile Exsolution Begins in a Basalt as a Function of Initial Dissolved Water Content

Figure 6-6 shows the depth at which fragmentation occurs in rising basaltic magma, assuming that:

- Flow is steady and homogeneous, the system is closed (no gas loss into country rock), and bubble nucleation and growth kinetics can be ignored (Section 5, Assumption 4)

- Vertical pressure profile in the dike/conduit below the fragmentation depth is very close to the lithostatic pressure profile (Section 5, Assumption 3)

- Gas volume fraction at which fragmentation commences can be established.

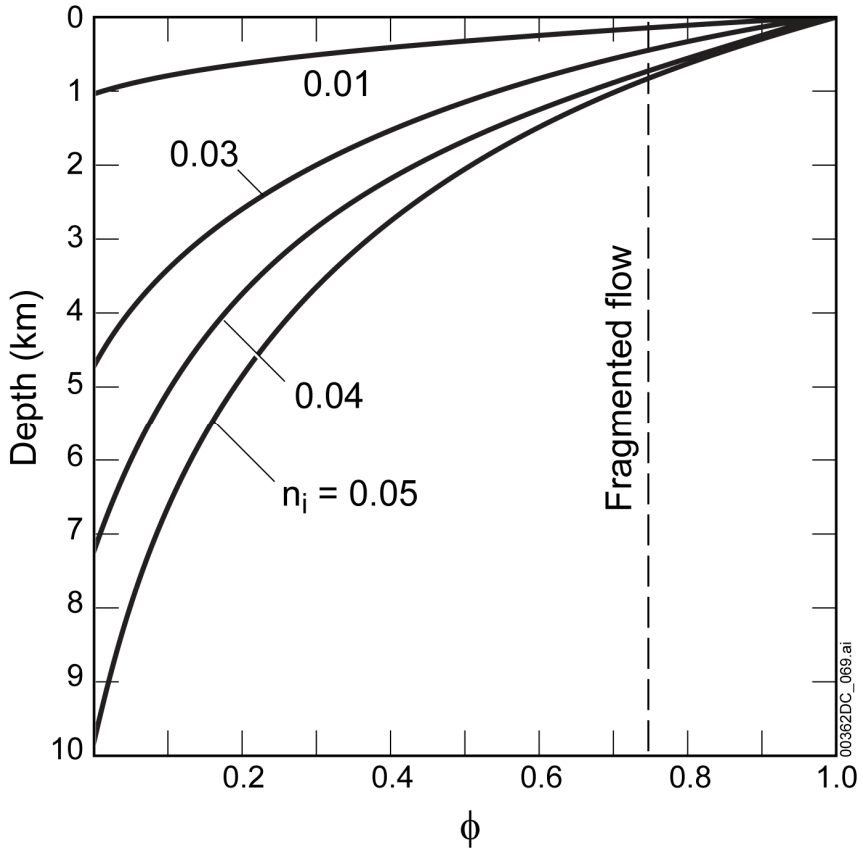

Source: Plot of Equation 6-10.

NOTE: For illustration purposes only. Calculations assume ρ_c = 2,500 kg/m^3, ρ_m = 2,500 kg/m^3, T = 1,300 K, and R = 461 J kg/K. The dashed line defines a critical gas volume fraction (ϕ) of 0.75, which, in this report, is assumed to be the threshold for fragmentation of the magma. Plot is derived by solving Equations 6-1 and 6-5 as functions of depth (d) for a given value of n_i, Equations 6-8 and 6-6, and finally Equation 6-10 for each value of n_i = 0.01, 0.03, 0.04, and 0.05 (curve for n_i = 0.02 curve, which plots symmetrically between n_i = 0.01 and n_i = 0.03 curves, is omitted for clarity).

Figure 6-6. Example Plot of the Variation of Gas Volume Fraction with Depth for a Basalt, Assuming Pressure in the Magma is Lithostatic and for Four Values of Initial Dissolved Water Content

The limitations of the first assumption have already been discussed. The second assumption is very good at depths where ϕ is small, but it becomes less accurate toward the fragmentation depth, and it is probably very inaccurate above the fragmentation depth. The uncertainty has no impact on the analysis because at these shallow depths, fragmented flow has almost certainly been obtained. Hence, the second assumption is a good estimate of the "average" fragmentation depth for a variety of different scenarios. The third assumption is currently a subject of intense research. The commonly assumed critical fragmentation value of $\phi = 0.75$ (Mader 1998 [DIRS 144419], p. 55) is adopted as a reasonable estimate in Figure 6-6, given how little is

understood about this process with regard to basaltic magmas. Recent studies have demonstrated, however, that fragmentation can take place in a range of $0.60 < \phi < 0.95$ (Mader 1998 [DIRS 144419], p. 56). With all these assumptions, Figure 6-6 illustrates that estimated fragmentation depths for initial volatile contents between 0 wt % and 5 wt % range from about 0 m to 1,200 m.

6.3.4.3 Velocity as a Function of Depth above Exsolution Depth

Descriptions of the magma velocity, conduit/dike dimensions, and magma pressure as functions of depth (d) require, even with the homogeneous-flow approximation and a steady-state assumption, solution of three coupled equations (Wilson and Head 1981 [DIRS 101034], p. 2,974, Eqs. 16 to 18). Two of these equations are ordinary differential equations. The detailed solution of these equations for a range of parameters appropriate to volcanism in the Yucca Mountain region is beyond the scope of this report. However, Wilson and Head (1981 [DIRS 101034], p. 2,983) provide some plots that relate eruption velocity, u_{erupt}, (where the magma–gas mixture exits the vent) to initial dissolved water content (n_i) of the magma, assuming that the pressure in the conduit/dike is equal to lithostatic pressure. Their solutions, shown with the curves in Figures 6-7 and 6-8, are for values of n_i up to approximately 0.02 for dike (fissure) and circular conduit geometries.

The velocity of magma ascending from some depth to the vent probably can be estimated with sufficient accuracy for modeling by simplifying such that velocity increases linearly from $0.01u_{erupt}$ at d_{exs} to $0.1u_{erupt}$ at the fragmentation depth, thence increasing linearly to u_{erupt} at the vent (u_{erupt} obtained from Figures 6-7 and 6-8). Using such an approach will account for the greater accelerations that are thought to occur above the fragmentation depth and the more gradual acceleration below it. In addition, this approach guarantees consistency in the calculations of velocity at various depths (as opposed to random sampling from distributions at different depths).

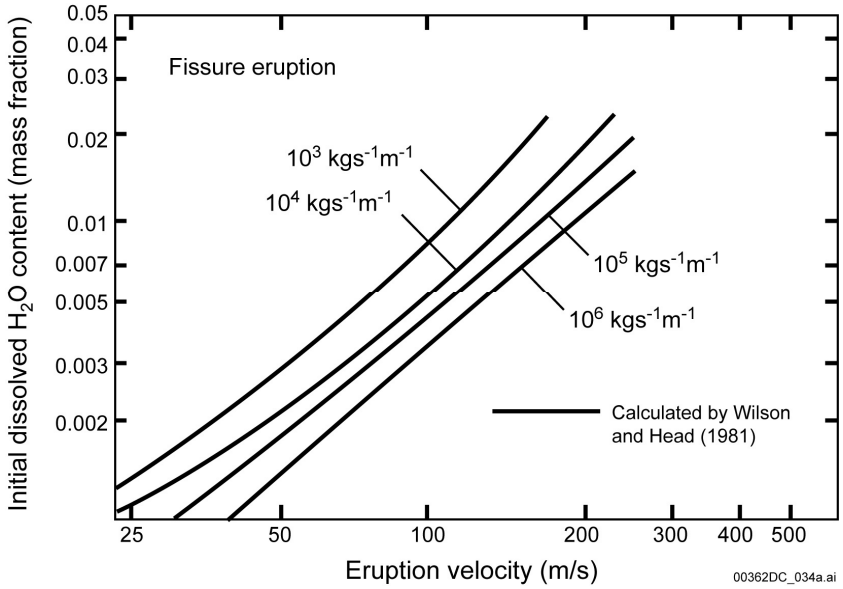

Source: Wilson and Head 1981 [DIRS 101034]; plot of equations 16 to 18 from reference.

NOTE: Solid curves show values for the variation of eruption velocity (u_{erupt}) with initial dissolved water content (n_i) calculated by Wilson and Head (1981 [DIRS 101034], p. 2,983), which assume homogeneous flow and lithostatic pressure in the rising magma column.

Figure 6-7. Plot of the Variation of Eruption Velocity with Initial Dissolved Water Content for Various Mass Discharge Rates Along a Fissure

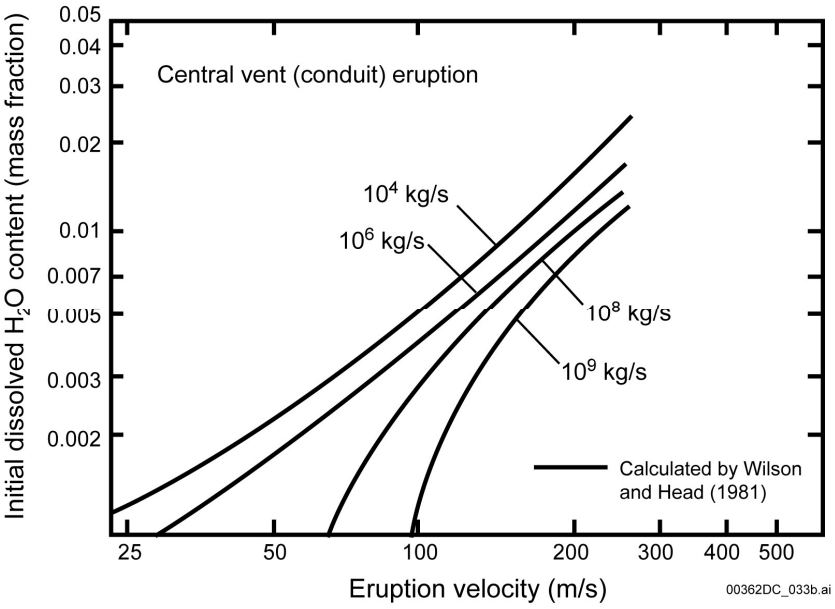

Source: Wilson and Head 1981 [DIRS 101034]; plot of equations 16 to 18 from reference.

NOTE: Solid curves show values for the variation of eruption velocity (u_{erupt}) with initial dissolved water content (n_i) calculated by Wilson and Head (1981 [DIRS 101034], p. 2,983), based on the assumption of homogeneous flow and lithostatic pressure in the rising magma column.

Figure 6-8. Plot of the Variation of Eruption Velocity with Initial Dissolved Water Content for Various Mass Discharge Rates from a Circular Conduit

6.3.4.4 Eruption Volume and Duration

For the purposes of predicting how much radioactive waste might be erupted and subsequently dispersed over significant distances, were a volcano to form at Yucca Mountain, it is important to provide constraints on volumes of fallout tephra. Tephra that is energetically ejected from the volcanic vent through violent Strombolian mechanisms would account for the furthest dispersed product of any expected eruption in the Yucca Mountain region. The literature on analogue cones and their tephra volumes is limited, but fallout tephra volumes are generally about two times their cone volumes, based upon data that includes Tolbachik 1 (ratio 1.3), Tolbachik 2 (ratio 1.0), Sunset Crater (ratio 1.6), Heimaey (ratio 0.8), Serra Gorda (ratio 1.4), Cerro Negro (ratio 1.7, based upon eruptions from 1850 through 1995), and Parícutin (ratio 5.9, which is by far the greatest) (NRC 1999 [DIRS 151592], Table 3). The average of these ratios is 1.9. At Lathrop Wells volcano, estimated tephra fall volume is about 0.07 km^3 and the cone volume is 0.02 km^3 (Appendix C), for a ratio of 3.5. The volume of lavas at Lathrop Wells is 0.03 km^3, indicating that the total volume of eruptive products from that volcano (not corrected for porosity or vesicularity) is about 0.12 km^3 (Appendix C). Volumes of all Quaternary volcanoes in the Yucca Mountain region are provided in Table 6-2. The population of Quaternary scoria cones (8) in the Yucca Mountain region is small and does little to constrain the probability of one particular volume relative to another, which suggests that a uniform probability distribution of eruptive volumes is appropriate for predicting future potential volcanic events at Yucca Mountain.

The minimum potential volume can be accounted for using a similar tephra/cone ratio for NE Little Cone (the smallest volcanic cone in the Yucca Mountain region), whose dimensions are provided by Stamatakos et al. (1997 [DIRS 138819], pp. 322 and 328). The cone diameter is 230 m and the height is 40 m, which accounts for 15 m of the exposed cone material and 25 m that is buried (by 10 m of lava and 15 m of younger alluvium, as interpreted from ground magnetic survey data). Assuming a 50% erosion of the cone height similar to that used by *Issue Resolution Status Report Key Technical Issue: Igneous Activity* (NRC 1999 [DIRS 151592], Section 4.2.5.3.1, Table 3) for SW Little Cone, the total height of NE Little Cone would have been 80 m (2 × 40 m). Using the equation for a cone ($V=1/3\pi r^2 h$; where r is the radius of 115 m and h is the cone height of 80 m), the resulting volume for NE Little Cone is approximately 0.001 km^3 (or about 1.1×10^6 m^3). Using a tephra/cone ratio of 4 (similar to Lathrop Wells volcano) yields a tephra volume of 0.004 km^3, which is chosen as a minimum volume of fallout tephra for a potential future eruption. The potential maximum volume can be estimated from the Lathrop Wells data by doubling the volume of tephra from that volcano. This volume, 0.14 km^3, represents a tephra/cone ratio of 7 compared with the Lathrop Wells cone volume. This is intended to capture the potential maximum tephra in the waning volcanic field.

In addition to constraining volumes of volcanic eruptions for the purposes of predicting the effects of an igneous event on the repository, it is important to constrain the duration of various processes. Wood (1980 [DIRS 116536], p. 402) states that over 90% of historical basaltic eruptions last less than 12 months, although notable exceptions exist. Appendices C and E discuss potential time scales for the entire eruptive duration for some of the Quaternary volcanoes in the Yucca Mountain region based upon lava flow lengths and cone dimensions and comparison with historical analogues. For example, the Lathrop Wells volcano is inferred to have erupted for at least seven months, with cone building and several episodes of violent

Strombolian eruption columns during part of that time (~1 day to 100 days, likely a few weeks; Appendix C.9). Emplacement of individual lava fields at Red Cone and Black Cone volcanoes would have required at least 9 to 12 months, and the presence of two lava fields at each volcano therefore implies eruptive activity lasting on the order of two years, based on their length (Appendix D). Unfortunately, erosion of the cones and fallout deposits (if they existed originally) from the older volcanoes precludes any estimates of duration of pyroclastic activity there. Assuming that the estimated volume of tephra originally associated with NE Little Cone, which is about 5% that of Lathrop Wells, represents the smallest potential pyroclastic event in the Yucca Mountain region, it is reasonable to assume that the total duration of NE Little Cone explosive activity would be about 5% of the duration of the pyroclastic activity at Lathrop Wells, or between about one hour and five days. Note that for all of these volcanoes it is likely that violent Strombolian eruption columns occurred in several episodes, each producing a layer of fallout as at Lathrop Wells volcano (Appendix C). The suggested duration of an entire igneous event (including emplacement of lavas and pyroclastic deposits) can be described as a lognormal probability distribution with a mode of seven months (reflecting the Lathrop Wells estimate), a minimum of 1 month, and a 90th percentile of 3 years. This distribution captures the historical data as applied to the lengths and volumes of basaltic eruptive products in the Yucca Mountain region.

Table 6-9 lists several historical eruptive events and duration, power, and estimated mass discharge rates for their respective violent Strombolian episodes. The mass discharge rates can be used to define realizations of a potential eruptive event in the Yucca Mountain region. To illustrate how the parameters in Table 6-9 are interrelated, one approach for creating a realization for duration, power, and volume of a violent Strombolian eruptive phase would follow the steps below:

- Determine a total volcano volume by sampling from a distribution of volumes that captures the volumes of Quaternary Crater Flat volcanoes. An alternative would be to use the volume of the Lathrop Wells volcano since it is the best-characterized analogue to a potential future Yucca Mountain volcano.

- Determine the entire volcanic event duration by sampling the recommended distribution.

- Determine a mass discharge rate (or eruptive power) for an individual violent Strombolian phase by sampling from a probability distribution based upon data from historical analogue eruptions (Table 6-9). The mass discharge rate distribution can encompass the range of values in Table 6-9 as log uniform with minimum of 7.4×10^2 kg/s and maximum of 7.4×10^5 kg/s.

- Determine the duration for violent Strombolian phase by sampling the log-uniform distribution (18 hours to 75 days, as shown in Table 6-9 in log-seconds). Ensure that this duration does not exceed the duration of the entire volcanic event (second bullet).

- Calculate the total violent Strombolian volume erupted by multiplying mass discharge rate (derived from power) by duration. Ensure that this volume is within the range of 0.004 km^3 to 0.14 km^3 that encompasses potential tephra fall deposits in the Yucca Mountain region, and that this volume does not exceed the total volume of the volcano (first bullet).

These steps maintain consistency in durations and volumes of different phases of a volcanic event, and allow for the possibility of a violent Strombolian phase lasting the full duration of the event, as well as producing the full volume of the event. Other approaches may be equally valid.

Table 6-9. Explosive Eruptive Events, Duration, Power, and Estimated Mass Discharge Rates Used to Develop Probability Distributions for Eruptive Plume Dispersal Calculations

Event	Log (*t*) (*t* in s) [a]	Log (*Po*) (*Po* in W) [a]	Mass Discharge Rate (kg/s) [b]
Cerro Negro, 1992	4.8	12.0	7.4×10^5
Tolbachik, 1975	6.1	11.7	3.7×10^5
Parícutin, 1944 I	5.6	11.1	9.3×10^4
Parícutin, 1944 II	6.8	11.5	2.3×10^5
Parícutin, 1946	6.8	9.0	7.4×10^2
Heimaey, 1973	6.4	9.9	5.9×10^3

[a] Jarzemba (1997 [DIRS 100460], p. 136).
[b] Mass discharge rates based on T = 1,350 K and magma heat capacity c_p = 1,000 J K^{-1} kg^{-1} (Best 1982 [DIRS 147740], p. 301). Mass discharge rate = $Po(c_pT)^{-1}$.

6.3.4.5 Entrainment of Wall Rock and Repository Materials in Ascending Magma

There are no natural analogues or appropriate experimental data representing the interception of engineered systems, with or without the equivalent of waste fuel, by extrusive magma. A variety of processes would affect the entrainment of waste by rising magma and its subsequent dispersal. Some of these processes are volcanological in nature, and some are related to the nature of the engineered system. Each process is associated with its own uncertainties.

Engineered barrier system–Engineered barrier system processes that may influence the amount of waste entrained involve those that govern the fraction of waste that escapes from packages, and those governing the final grain-size distribution of that waste. Regarding waste escape, the integrity of waste canisters within an erupting mixture is largely unknown. DOE performance assessments have assumed the waste package fails upon contact with basaltic magma (Reamer 1999 [DIRS 119693], p. 82). In current analyses (e.g., *Number of Waste Packages Hit by Igneous Intrusion* (BSC 2005 [DIRS 174066], Section 5.1)), the assumption is that waste packages in drifts intersected by magma provide no protection for the waste.

Waste Form–Pressurized-water reactor fuels are composed of uranium oxide, processed by superheated steam into a fine powder whose crystallites are ~0.2 μm in size, with a specific surface area of about 2 m^2 g^{-1} (Dehaudt 2001 [DIRS 164019], p. 61). The powder is shaped in a uniaxial press, densified by sintering, and ground along its perimeter to ~6 mm diameter. Following sintering, the UO_2 grain size averages 9 μm (Dehaudt 2001 [DIRS 164019], p. 63). The fuel pellets are inserted into rods of zirconium alloy clad, about 1 cm in outside diameter

(Dehaudt 2001 [DIRS 164019], p. 60), with a small gap between the pellets and the clad to accommodate the escape of fission gases and slight volume change of the pellets. During power production, thermal fractures break the pellet up into several pieces and the clad becomes more brittle (Dehaudt 2001 [DIRS 164019], Section 5.2.5). At high burnup (>30 GWd/tM), the fuel and clad fuse together (Piron 2001 [DIRS 162396], p. 41).

During volcanic disruption, the fuel pellets could be disaggregated by both physical and chemical processes, including:

- Volatilization and recondensation of volatile radionuclides
- Dissolution of spent-fuel oxides into magmatic melt
- Mechanical disaggregation by impact, abrasion, or shock waves
- Oxidation of the clad and UO_2 waste-form pellets, causing disintegration of both.

Some waste may enter the biosphere by volatilization of fission products containing chlorine, iodine, or cesium. *Radionuclide Screening* (BSC 2004 [DIRS 160059], p. 39), shows that ^{137}Cs is the only volatile radioisotope to have any significant dosage effect in the eruptive igneous scenario. Due to its short half-life (30 years), its effect is minimal in the postclosure stage of the repository. These volatile radionuclides are, therefore, neglected. Dissolution of spent-fuel oxides into magmatic melt has apparently not been studied and insufficient data are available for quantifying the outcome. Since this process could reduce the quantity of waste available for atmospheric dispersion, for modeling the waste is considered as particulate and available for atmospheric dispersal with tephra (BSC 2005 [DIRS 174067], Section 5.2.4).

Mechanical disaggregation of waste pellets could occur by abrasion, impact, or shock waves. The final grain size of the waste resulting from these processes would vary depending on the energy and duration of those processes, the number of times waste pellets are subjected to them, and the strength of the waste (which depends on alteration). No known work examines the size reduction that could result from conditions related to volcanic extrusion. Fragmentation of waste-form pellets by crushing and grinding (BSC 2005 [DIRS 174067], Appendix H), and by penetration of high-energy devices into shipping casks (Sandoval et al. 1983 [DIRS 156313], Table 4.3.2), suggest possible fragment-size distributions, though the fragmentation mechanisms in these tests may bear little resemblance to those in natural eruptions. Studies of xenolith size in eruptive deposits and their relation to host-rock size distributions may also provide useful constraints, but have yet to be undertaken.

Oxidation of waste pellets is common and well-studied, though most such studies have been conducted at temperatures well below magmatic (BSC 2004 [DIRS 169987], Section 6.2.2.2). In warm (~100°C to 400°C), humid environments, oxidation of spent fuel in the presence of air occurs rapidly; in dry air it takes place more slowly, and in humid environments without air very slowly or not at all (BSC 2004 [DIRS 169987], Section 6.2.2.2). At temperatures greater than 500°C, however, waste can be oxidized by pure steam (BSC 2004 [DIRS 169987], Section 6.2.2.2) to form thin coatings on preexisting UO_2 grains or, under moisture-saturated conditions, dehydrated schoepite crystals tens to hundreds of microns in length (BSC 2004 [DIRS 169987], Section 6.2.2.2). Oxidation of grain surfaces partially disaggregates the waste and increases specific surface area, making it more easily soluble in water (BSC 2004 [DIRS 169987], Section 6.2.2.2). During a volcanic eruption, oxidation of waste pellets could

occur below the ground surface in the presence of magmatic gas, or above the ground surface following ejection, though, in the latter case, oxidation would slow dramatically as the ambient gas cools and dries out. Codell (2003 [DIRS 165503], Section IIB and IIE) indicates that time scales for magma/waste and atmospheric transport are too short to support significant oxidation of waste. The rate of oxidation at magmatic temperature and the effect of oxidation on disaggregation and final grain size are not known in any quantitative way.

Volcanic Processes–Uncertainties are inherent in the following volcanic processes:

- Interaction between a rising dike and the perturbed stress field around repository drifts
- Interaction between rising, vesiculating magma and partially open drifts (e.g., would magma flow like lava for long distances down the drifts, would it pile up quickly to block the drift and, therefore, allow magma in the dike to continue rising, or would it explode down the drift as a pyroclastic mixture?)
- Depth to which conduits might extend (i.e., if a wide conduit is formed but extends only 200 m below the surface, then it will not have as large a disruptive effect on the repository).

Wall-rock xenoliths are incorporated into rising magma by mechanical disruption of dike walls and during conduit growth, but they do not provide a perfect analogue for engineered materials that could be disrupted by magma flooding a repository drift. There are a few data available on the interaction of magma with undisturbed country rock and subsequent eruption of the lithic debris for the range of eruptive styles that can be reasonably expected at Yucca Mountain. For example, Valentine and Groves (1996 [DIRS 107052], pp. 79 to 84) report data on the quantity of wall rock debris erupted from various depths during Strombolian, Hawaiian, effusive, and hydrovolcanic activity at two volcanoes. The hydrovolcanic eruptions reported by Valentine and Groves contained between 0.32 and 0.91 volume fraction of wall rock debris, with most of that originating in the uppermost ~510 m of the dike/conduit feeder systems. Strombolian, Hawaiian, and effusive eruptions ejected much lower volumes of wall rock debris, commonly resulting in total volume fractions of 10^{-3} to 10^{-5}. Doubik and Hill (1999 [DIRS 115338], p. 60) state that the Lathrop Wells volcano has a relatively high average lithic volume fraction of 9×10^{-3} for xenoliths greater than 1 mm, based on image analysis of unspecified locations at the cone. It is possible that all the locations studied by Doubik and Hill were located in a quarry that exposes proximal cone deposits. Clarification of this issue has required analysis of more exposures at Lathrop Wells and is discussed in Appendix C2.7, where it is shown that Doubik and Hill (1999 [DIRS 115338]) may have overestimated the lithic content for Lathrop Wells. Addressing this issue is important because Doubik and Hill (1999 [DIRS 115338], p. 61) cite similarity of lithic content as a justification for using the relatively large and violent Tolbachik eruptions as analogues for the Lathrop Wells volcano (and, hence, potential eruptions at Yucca Mountain).

6.3.5 Characteristics of Strombolian and Violent Strombolian Deposits

6.3.5.1 Bulk Grain Size

As described in Section 6.3.3, explosive eruptive styles of Quaternary volcanoes in the Yucca Mountain region include both Strombolian and violent Strombolian. Strombolian eruptions are characterized by short-duration bursts that throw relatively coarse fragments of melt out of the vent on ballistic trajectories. Most of the fragments (clasts) are deposited immediately around the vent, with only a very small fraction of finer particles rising higher and being dispersed by wind to form minor fallout sheets. Violent Strombolian eruptions, on the other hand, are characterized by vertical eruption of a high-speed jet of a gas-clast mixture, and fragments or clasts tend to be finer grained; it is this type of eruptive phase that poses a greater hazard due to its ability to disperse more, potentially contaminated volcanic ash higher (several kilometers) into the atmosphere and to deposit ash further downwind. The Lathrop Wells cone and tephra have characteristics that indicate much of the eruptive style was violent Strombolian (Appendix C) and, therefore, the Lathrop Wells grain sizes are relevant to selecting a distribution to describe a potential Yucca Mountain region eruption.

Particle-size distributions have been measured at individual stratigraphic sections in the tephra-fall deposits from Lathrop Wells volcano (DTN: LA0302GH831811.002 [DIRS 162864]). The particles span a range of sizes dependent largely on the settling velocities of particles of different mass and distance from the vent (Figure C-2 and C-9). Table 6-10 and Figure 6-9 show data from one such tephra section located 2.5 km NNW of the Lathrop Wells cone summit, likely along the main depositional axis of the ash cloud during the majority of the eruption (Appendix C). The median grain sizes measured in four samples from this section are relatively small, ranging from 0.65 mm to 1.30 mm; the means range from 0.71 mm to 1.76 mm, but the majority of the deposit consists of grains with mean size around 1 mm. The deposit can be described as representative of the violent Strombolian phase of the eruption that resulted in increased fragmentation, higher loft of the ash, and further downwind displacement. A size distribution for TSPA that reflects these small grain sizes is appropriate for forecasting grain sizes of a potential violent Strombolian basaltic eruption at the proposed Yucca Mountain repository.

Table 6-10. Grain Size Variations in Tephra Fall for Section B (see Figure C-8)

Sample Number	Md_ϕ (median)	Md (mm)	Graphic Mean (mm)
DK-LW-007	0.15	0.90	1.09
DK-LW-006	0.32	0.80	1.00
DK-LW-005	0.62	0.65	0.71
DK-LW-004	-0.38	1.30	1.76

Source: Values calculated from data in DTN: LA0302GH831811.002 [DIRS 162864] or from Figure 6-9.

NOTES: Md_ϕ (median) = median grain size in ϕ units (defined in Section 6.1.3.5).
Md (mm) = median grain size in mm.
Graphic Mean (mm) = $(\phi_{16} + \phi_{50} + \phi_{84})/3$.

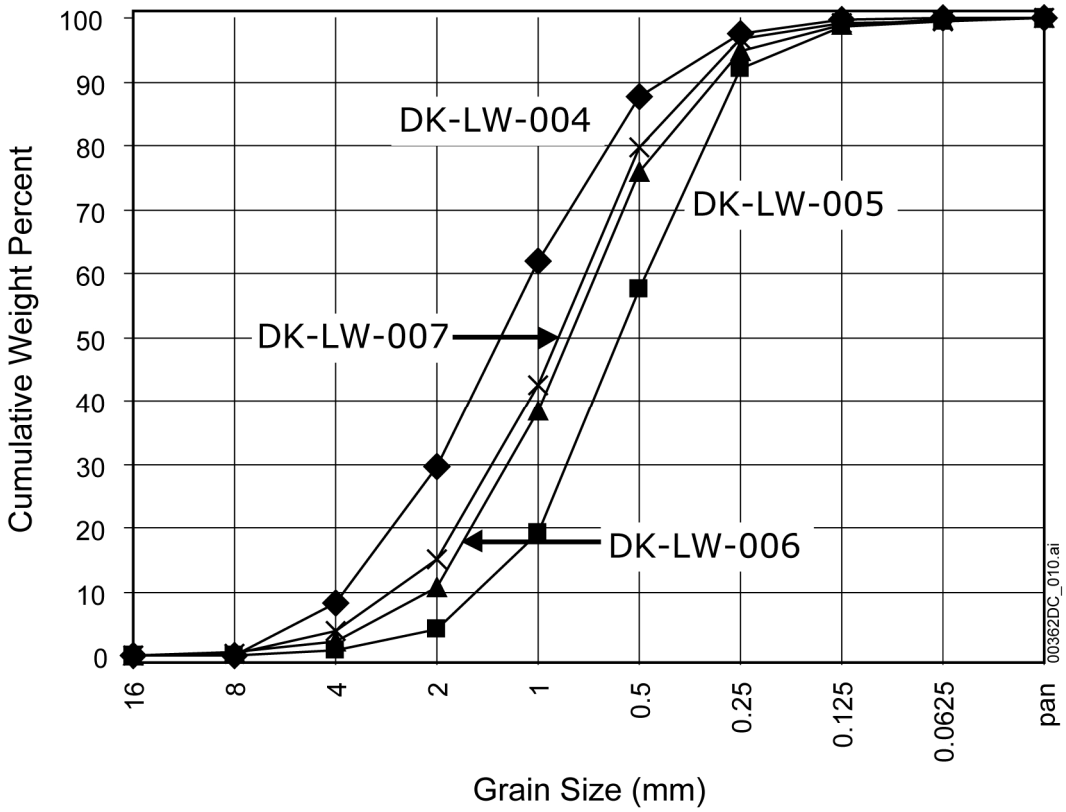

Source: DTN: LA0302GH831811.002 [DIRS 162864].

Figure 6-9. Grain Size Variations in a Lathrop Wells Volcano Tephra Fall Located 2.5 km NNW from the Vent

Therefore, the mean bulk particle size for describing an energetic violent Strombolian eruption for the Yucca Mountain area can be sampled from a log-triangular distribution with a minimum of 0.01 mm, mode of 0.1 mm, and maximum of 1.0 mm, to cover 2 orders of magnitude. The size range accounts for the smaller bulk particle sizes for violent Strombolian eruptions integrated over the entire deposit. For a given mean-particle diameter, the standard deviation, $\sigma_{\phi,}$ can be sampled from a uniform distribution between $\sigma_{\phi} = 1$ and $\sigma_{\phi} = 3$ (described below).

Table 6-11 lists corroborative examples of bulk eruptive clast-size distributions for three historic violent Strombolian eruptions (Tolbachik and Cerro Negro 1971 and 1968; Maleyev and Vande-Kirkov 1983 [DIRS 144325], pp. 61 and 62; Rose et al. 1973 [DIRS 116087], p. 342) and for one typical Strombolian eruption (Etna Northeast crater; McGetchin et al. 1974 [DIRS 115469], p. 3,264, Figure 8). Mean clast diameters for the violent Strombolian phases range from 0.19 mm to 0.37 mm, with standard deviations from 1.5 σ_{ϕ} to 2.5 σ_{ϕ} units (defined in Section 6.1.3.5). Furthermore, Jarzemba (1997 [DIRS 100460], p. 137) used a log-triangular distribution with a minimum of 0.1 mm, median of 1 mm, and maximum of 100 mm. The upper range accounts for larger lapilli sizes and small blocks and bombs, but these clasts would fall ballistically on or near the cone and would not contribute much or any mass to a downwind tephra deposit. Therefore, the recommended upper limit of 1.0 mm for the TSPA distribution gives some additional conservatism to calculations in *Atmospheric Dispersal and Deposition of*

Tephra from Potential Volcanic Eruption at Yucca Mountain, Nevada (BSC 2005 [DIRS 174067]) and TSPA.

Given a mean clast size, the standard deviation of the particle size is needed to supply sufficient information on the particle size distribution. Table 6-11 provides information on the graphic standard deviation, σ_ϕ (defined in Section 6.1.3.5), for the violent Strombolian eruptions at Tolbachik and Cerro Negro. It is recommended that, for a given mean-particle diameter, σ_ϕ be sampled from a uniform distribution between $\sigma_\phi = 1$ and $\sigma_\phi = 3$, which is chosen simply to bracket the values in Table 6-11.

Table 6-11. Estimated Bulk Clast Size Distribution Parameters for Three Violent Strombolian Eruptions (Tolbachik and Cerro Negro 1971 and 1968) and One Strombolian Eruption (Etna 1971)

	Violent Strombolian Eruptions			Strombolian Eruption
	Combined Great Tolbachik N. Breakthrough[a]	Cerro Negro 1971 (Overall)[b]	Cerro Negro 1968 (Overall)[b]	Bulk Etna Northeast Crater[c]
Median (mm)	0.3	0.24	0.15	95
Graphic Mean (mm)	0.37	0.23	0.19	110
Graphic Standard Deviation (σ_ϕ)	2.5	1.5	1.83	3.48

Sources: [a]Derived from data presented in Maleyev and Vande-Kirkov 1983 [DIRS 144325], pp. 61 to 62.
[b]Rose et al. 1973 [DIRS 116087], p. 342.
[c]Estimated from McGetchin et al. 1974 [DIRS 115469], p. 3,264, Figure 8.

6.3.5.2 Clast Characteristics

The clasts produced by Strombolian and violent Strombolian eruptions can be quite different in character. Strombolian eruptions produce a much higher proportion of coarse clasts, with the mean diameter commonly being greater than 10 cm (Table 6-11). Common Strombolian clast types include ribbon, spindle, and cowpie bombs. Ribbon and spindle bombs take their shape as they are stretched and torn or as they spin through the air on their dominantly ballistic paths; these shapes indicate the hot, fluid state of the clasts during flight. Cowpie bombs are very hot and fluid when they hit the ground. All these clasts are hot during flight and deposition because of their large size (low surface-area-to-volume ratio minimizes heat loss) and low eruption height (they have less time to cool before hitting the ground). These large clasts may have vesicle (bubble) volume fractions up to about 70%. Smaller clasts, in the millimeter to centimeter range, tend to be subequant vesicular scoria clasts, and they can have a range of vesicularities (for example, the Cinder Cone eruption at Lassen Volcanic National Park, California, produced scoria with vesicularities of 20% to 70%; Heiken and Wohletz 1985 [DIRS 106122], p. 34). Finer ash-sized clasts tend to be less vesicular, and can range from irregular to fluidal to blocky in shape.

Violent Strombolian eruptions carry clasts much higher in the air, providing more cooling time; the clasts also cool more quickly because they have a much higher degree of fragmentation. A much larger proportion of the clasts is in the millimeter to centimeter size range compared to Strombolian eruptions, and most of these clasts have irregular shapes and relatively high vesicularities.

In violent Strombolian eruptions, the long-range, downwind transport and fallout of clasts becomes an important issue for YMP TSPA calculations. Transport and deposition of clasts depend on their settling velocity in air, which in turn depends on their bulk density (the melt density corrected for the porosity, or vesicularity, of the clasts) and shape. Calculations of clast dispersal commonly use a shape factor, $F = (b + c)/2a$, where a, b, and c are the lengths of the longest, medium, and shortest axes of the clasts. Clasts produced by these types of eruptions can have a range of shapes. Jarzemba (1997 [DIRS 100460], p. 139) used a value of $F = 0.5$ as a shape factor likely to be representative of common clast shapes, which in the absence of further data, is recommended for TSPA calculations for the YMP.

Density of erupted particles varies with particle size because larger particles tend to have a higher fraction of vesicles (bubble voids) than small particles. Detailed data are lacking, but it is recommended that the particle density be varied as follows:

- For particle diameters less than or equal to 0.01 mm, the particle density is 0.8 of the magma density (which is taken to have an average density value of 2,600 kg/m^3 for a Lathrop Wells-type magma). This value is based on a fine-particles void fraction of 0.2 due to vesicles.

- For particle diameters greater than or equal to 10 mm, the particle density is 0.4 of the magma density. This value is based on a void fraction of 0.6 due to vesicles.

- Between 0.01 mm and 10 mm, the density should decrease linearly with the logarithm of the diameter. This accounts for increasing vesicularity with increasing clast size.

6.3.5.3 Density of Fallout Deposits

Bulk in situ density of fallout deposits typically ranges from 300 kg/m^3 to 1,500 kg/m^3 (Sparks et al. 1997 [DIRS 144352], p. 366), but is rarely directly measured, particularly for basaltic deposits such as are most likely in the Yucca Mountain region. Blong (1984 [DIRS 144263], p. 208) has measured a range of fallout deposits that have a density of approximately 1,000 kg/m^3. There are two reasonable ways of treating deposit density in TSPA calculations: 1) simply use 1,000 kg/m^3, or 2) use a sample from a normal distribution of deposit densities ranging from 300 kg/m^3 to 1,500 kg/m^3 with a mean of 1,000 kg/m^3.

6.4 POTENTIAL ERUPTION SCENARIO AT THE YUCCA MOUNTAIN REPOSITORY

A future basaltic magma intrusion into the subsurface of Yucca Mountain followed by a surface eruption of scoria, lava, and ash would have relatively predictable physical volcanological consequences. Based on the properties of basaltic magma and the eruption processes discussed in Sections 6.1 through 6.3, one scenario of a surface eruption is compiled below. This scenario is proposed as a guide to a likely sequence of eruption phenomena at the surface and is not proposed as a conservative event sequence; it is based upon investigations of Yucca Mountain region volcanoes with emphasis on recent (≤1 my) geological history. *Magma Dynamics at Yucca Mountain, Nevada* (BSC 2005 [DIRS 174070] details effects of a multiphase mixture of magma and gases intersecting a repository drift, as well as aspects of physical blockage of the

surface vent. Further effects of a magmatic dike intruding the drifts are discussed in *Dike/Drift Interactions* (BSC 2004 [DIRS 170028]). The calculation of the number of waste packages impacted by the magma intruding a repository is presented in *Number of Waste Packages Hit by Igneous Intrusion* (BSC 2005 [DIRS 174066]). Finally, models for eruption, ash-fall distribution, and redistribution of ash by surface processes are included in *Atmospheric Dispersal and Deposition of Tephra from a Potential Volcanic Eruption at Yucca Mountain, Nevada* (BSC 2005 [DIRS 174067]).

A. At approximately 300-m depth, a single vertical crack filled with vesiculating basaltic magma accelerates toward the ground surface. The dike at this depth is about 2 km in map view, and from 8 m to 10 m wide. Although ascent through the upper crust may be influenced by regional crustal stresses resulting in an approximately N30°E-S30°W orientation, the dike tip and magma front become captured by a steeply dipping fault plane, which at Yucca Mountain are oriented largely north-south. At the ground surface, a single fissure, trending ~north-south and several hundred meters long, opens up as the dike tip intersects the ground surface. Initially the fissure releases mainly magmatic gases and some rock fragments, but over a period of minutes to hours lapilli- to bomb-sized clots of magma begin to be ejected. The magma is 1,000°C to 1,100°C, of hawaiitic composition, and will have a volatile content dominated by H_2O that is 2% to 4% by mass. A fissure eruption proceeds to release a curtain of molten material to heights of a few hundred meters.

B. As eruption proceeds, lapilli and bombs accumulate along the fissure and eruption becomes increasingly focused toward one or a few closely spaced vents. Eventually one vent becomes the dominant point of eruption, and accumulation of material around that vent begins to form a main cone. As the cone grows it buries more and more of the original fissure system, but may retain some manifestation of the fissure either by having an elongated shape or by having satellite vents that continue to erupt at a slower rate at other points along the fissure. During initial cone growth, eruptions are dominated by Strombolian mechanisms that produce mainly coarse lapilli- and bomb-sized material that is ejected a few tens of meters to a few hundreds of meters into the air and is distributed around the vent according to ballistic paths. Much of the material is still very hot when it lands on the cone slopes, resulting in various degrees of welding or agglutination of clasts. Partly because of the welding, cone slopes might be steeper than angle of repose as they accumulate, resulting in periodic collapses or avalanches of material into the vent. This material may then be reerupted during subsequent explosions. Only brief periods of higher eruption columns might occur during this phase.

C. As the eruption continues, a more violent eruptive phase builds. During this phase the main vent produces sustained jets of relatively finely fragmented (ash to small bomb sizes) material, ejected from the vent at velocities of several tens of meters per second to perhaps as high as about 300 m/s. The eruptive jet mixes with atmospheric air, heats it, and the resulting mixture become buoyant with respect to the atmosphere and rises many hundreds of meters to several kilometers into the air. Atmospheric winds push the plume and its outward-spreading top in a

downwind direction. Clasts fall out of this plume after having a long enough residence time in the air to cool, and they accumulate as loose, nonwelded fallout deposits that are well sorted and that blanket the surrounding terrain. Cone growth continues as coarser clasts accumulate close to the vent after falling directly from the margins of the rising jet (but not following simple ballistic paths). Because the new cone-building deposits have no welding-induced cohesion, avalanching back into the vent and down the outer cone slopes is almost continuous. Variations in gas content, magma supply rate, and vent-choking due to avalanches result in pulsing of the eruptive jet or plume. Individual pulses (or violent Strombolian eruptive phases) may last between about half an hour to many days. Each of these eruptive phases produces a distinct layer of tephra on the cone slopes (where it might later be eradicated by avalanching) and in the surrounding tephra sheet, which might extend for tens of kilometers.

D. At any time during the above processes, there might be brief periods of explosive magma-groundwater interaction (as indicated by a small fraction of deposits at Lathrop Wells volcano; Appendix C). These events might eject up to several 100,000s of cubic meters of material that is relatively lithic-enriched compared to other eruption products. The events could produce thin fallout units or localized pyroclastic surge deposits. Accompanying explosions might destroy part of the growing cone, but this is rapidly "healed" by subsequent Strombolian or violent Strombolian events. Although hydrovolcanism is included as part of this scenario, it was discounted as a significant phenomenon by the PVHA since the depth to the saturated zone is ~600 m and there is negligible perched water present within the unsaturated zone at Yucca Mountain.

E. Lava flows may issue at any time (concurrently with explosive eruptions or separately) from the base of the main cone. Some of these flows might dislodge and raft pieces of the cone along the flow tops. If these rafted pieces contain welded/agglutinated beds that were produced during Strombolian eruptive phases, they might retain their original bedding structure as they are carried along the top of a flow and may be partially rotated. Other nonwelded masses may be partially disaggregated during transport.

F. Cone growth might occur only during a portion (~2 days to 21 days, subtracting out pauses in explosive activity) of the eruptive history of the volcano, which will likely be on the order of one month for this small-volume event but could be as long as about 15 years. During this time, an irregularly shaped conduit of average 15-m diameter has grown downward to 100 m to 200 m below the surface, formed by a combination of mechanical erosion and melting of host tuff. Though somewhat confined at depth, the conduit dimensions flare (widen) to increasing cross-sectional area above 100-m depth; directly beneath the pyroclastic deposits, the vent may be many times the conduit diameter at depth. At some point below the flare bottom, the feeder conduit merges with the underlying planar parent dike; the data suggest that this transition occurs above the planned repository level (~300 m). Away from the conduit, the dike magma cools slowly, its viscosity increases

due to crystal growth in the matrix, and magma transport is mostly vertical up the conduit with some lateral contribution to the magma flux.

G. The total erupted volume of the hypothetical new volcano will have been about 0.1 km^3. The volume will be dominated by the fallout tephra (from violent Strombolian phases), followed by lavas and finally by the main cone in a volume ratio of about 7:3:2, respectively. The new volcano would form a cone between 150-m to 200-m high, a lava field between 5 km^2 to 10 km^2 in area and ~20-m thick, and a tephra blanket that extends many kilometers, mainly in the direction of the prevailing wind. After eruption of magma ceases, volcanic gases will continue to leak from vents for many years as the subsurface magmas continue to cool and degas. Cooling of the surface lavas and cone may continue for many decades even after the degassing ends.

6.5 UNCERTAINTIES (INPUT)

6.5.1 Input Data and Uncertainty

Table 6-12 and the following sections summarize input data from Table 4.1 and their uncertainties for the analyses detailed in Section 6 this report. Column 5 in Table 6-12 lists "epistemic" uncertainty, which refers to the uncertainty that could be reduced by further knowledge, for example, by further sampling and analysis. The uncertainties associated with these inputs are discussed in the following sections.

Table 6-12. List of Input Data and Uncertainty Type

Input Name	Input Description	Input Source	Value or Distribution	Uncertainty Type
45 chemical analyses of products from Lathrop Wells volcano	Mean major-element chemical composition (and related statistics) of Lathrop Wells lava	DTN: LA000000000099.002 [DIRS 147725]	Means (see Table 6-3 for complete statistics) SiO_2-48.50% TiO_2-1.93% Al_2O_3-16.74% Fe_2O_3T-11.63% [Fe_2O_3 1.74%] [FeO 8.90%] MnO-0.17% MgO-5.83% CaO-8.60% Na_2O-3.53% K_2O-1.84% P_2O_3-1.22%	Epistemic
Tephra thicknesses, Lathrop Wells volcano	Thicknesses of tephra-fall deposits in vicinity of Lathrop Wells volcano	DTN: LA0305DK831811.001 [DIRS 164026]	Tephra thicknesses at various map points range from 1 cm to 304 cm	Epistemic
Particle-size data for tephra sheet from Lathrop Wells volcano	Sieve fractions of tephra samples, weight percentages of sieve fractions, and cumulative weight percentages of sieve fraction.	LA0302GH831811.002 [DIRS 162864]	See DTN: LA0302GH831811 .002 [DIRS 162864]	Epistemic

Table 6-12. List of Input Data and Uncertainty Type (Continued)

Input Name	Input Description	Input Source	Value or Distribution	Uncertainty Type
Lithic clasts measured at Lathrop Wells cone, Nevada	Manual counts of xenolith clasts in Lathrop Wells scoria cone exposed within the quarry	LA0302GH831811.003 [DIRS 162865]	Xenolith volume fraction is 0.0091 at the lowest elevation (2,886 ft) and 0.00014 at the highest elevation measured (3,146 ft).	Epistemic

6.5.1.1 Chemical Analyses of Products from the Lathrop Wells Volcano

There is a low degree of uncertainty associated with the mean chemical composition of Lathrop Wells volcano lava; the uncertainty is quantitatively provided in the statistical information in Table 6-3. These data are used to estimate physical properties of a future magma (of similar composition) as it ascends through the crust, intercepts and interacts with the repository, and erupts onto the surface. The statistics provided in Table 6-3 for the major element chemical composition data reflect the natural variations expected among multiple samples of the same lava flow, as well as the variations expected for multiple samples from different lava flows from the same monogenetic volcanic event. There is a very low degree of uncertainty associated with any one major oxide determination because of the tight clustering of values (reflected in their standard error and standard deviation) among 45 rock samples and the use of modern analytical methods of chemical analysis. Additional analyses would only serve to decrease the standard deviations of any one mean.

6.5.1.2 Tephra Thicknesses for the Lathrop Wells Volcano

There is a moderate degree of uncertainty associated with the determinations of tephra section thicknesses presented in Appendix C. These data are used to estimate the volume of ash and lapilli ejected during the more violent phases of the eruption—and the evolution of eruption type—for development of the volcanic history. Most recent excavations of tephra sections were limited to using a shovel, whereas excavations during several past field seasons were often done using a motorized backhoe. Most of the latter excavations were localized around the base of the cone and, therefore, provide constraints on the thicker accumulations of ash. The most recent excavations could not always expose the base of the tephra when the thickness of tephra was greater than about 1 m, due to its unconsolidated nature. Geologic evidence suggests that the tephra was covered and preserved by eolian sands and silts soon after deposition, but erosional stripping of some depositional sites has occurred. Therefore, the tephra thicknesses represent minimum values in nearly all cases.

6.5.1.3 Particle-Size Data for Tephra Sheet from Lathrop Wells Volcano

Uncertainty related to particle sizes measured for the tephra sheet from Lathrop Wells volcano is moderate due to the partial preservation of the deposit and the limited number of stratigraphic sections from which samples were acquired. Furthermore, the data used in Section 6.3.5.1 is a subset of the entire data set and represents one stratigraphic section located ~2.5 km from the source at cone summit. Justification for selection of these data is given in Section 6.3.5.1. The selected grain size data, however, are corroborated by data from well-studied historical

eruptions. The standard deviations provided along with the particle sizes capture a range that describes the finer grain sizes of violent Strombolian eruptive products, which is the most energetic eruption phenomena expected in the eruptive scenario. The impact of including larger sizes than those described would be to deposit a larger proportion of bigger clasts close to the vent (hence, not included in an eruption cloud that is subject to wind dispersal); the impact of smaller sizes would be to inject proportionally more very fine particles into the eruption cloud and disperse potentially contaminated ash over farther distances. The particle-size data provided adequately describes the bulk sizes of the violent Strombolian phase of an eruptive process within the Yucca Mountain region.

6.5.1.4 Lithic Clasts Measured at Lathrop Wells Cone, Nevada

Xenolith (or lithic) clast size volume fraction distribution as measured at Lathrop Wells volcano has a low to moderate degree of uncertainty. The xenoliths are Miocene age and incorporated into Quaternary basaltic magma ascending toward eruption at the surface. Uncertainty derives from the evolving and limited exposures within the quarry that give access to measurable sections. Clearly epistemic in nature, the data provide an estimate of the magma conduit diameter based on the thickness of Miocene tuffs beneath the vent. Conduit diameter is calculated using the mean of 18 measurements, which show a decrease in xenolith production with time. The impact of a larger mean volume fraction of xenoliths is a larger conduit diameter estimate at repository depth, but it is doubtful that significantly larger volume fractions of lithics will be uncovered in the growing quarry exposures because of the sector of the cone already provided in the quarry.

INTENTIONALLY LEFT BLANK

7. CONCLUSIONS

This report provides technical bases for parameter values that will be used for the TSPA-LA related to the effects of a volcanic eruption through the Yucca Mountain repository. Uncertainties in the output parameters are described in the text as appropriate and summarized in Table 7-1. The information and data in this report are based largely on literature values and simple calculations as described in Section 6 and discussed in *Data Qualification Report: Data Related to Characterization of Eruptive Processes for Use on the Yucca Mountain Project* (CRWMS M&O 2000 [DIRS 156980], p. 17). Other information that indirectly relates to assessment of a potential igneous disruption of the repository and posteruption processes, such as descriptions of the Lathrop Wells volcano, is based on field studies and supporting laboratory analyses.

7.1 SUMMARY OF SCIENTIFIC ANALYSIS

The technical product output (Table 7-1) of this scientific analysis report provides distributions for parameters for use in the YMP license application to describe the physical properties of basaltic magmas, volcanoes, eruptive processes, and volcanic products related to a volcanic eruption through the Yucca Mountain repository. The parameters and development of their distributions are detailed in Section 6 and compiled in Table 7-1. Other phenomena that relate to the progression of eruptive processes are qualitatively described, based on literature-derived data from observations of relevant volcanic eruptions worldwide and on data from Lathrop Wells volcano, Nevada (Appendix C). Lathrop Wells volcano is a particularly relevant source of information because it is the youngest volcanic event (~80,000 years) near Yucca Mountain and, along with other young basaltic cinder cones and flows in the area, forms the basis for the potential disruptive volcanic event for the repository. Therefore, processes that encompass volcanic eruption, cone construction, and ash-plume dispersal and deposition are depicted in this report. Other related reports cover topics that precede or follow in time the potential eruption scenario. Model development and results for dike propagation in the shallow crust and the effects of a magmatic dike intercepting a repository drift at atmospheric pressure are discussed in *Dike/Drift Interactions* (BSC 2004 [DIRS 170028]). The number of waste packages involved in a magmatic intrusion into a repository drift filled with waste packages is discussed in *Number of Waste Packages Hit by Igneous Intrusions* (BSC 2005 [DIRS 174066). Specific results from modeling and analysis of potential ash-plume eruption, dispersal, and deposition from violent Strombolian eruption of basaltic magma are described in *Atmospheric Dispersal and Deposition of Tephra from a Potential Volcanic Eruption at Yucca Mountain, Nevada* (BSC 2005 [DIRS 174067]). A conceptual and mathematical model for ash redistribution is also developed in *Atmospheric Dispersal and Deposition of Tephra from a Potential Volcanic Eruption at Yucca Mountain, Nevada* (BSC 2005 [DIRS 174067], Section 6.6, Appendix I).

Table 7-1. Technical Product Output

Parameter (number refers to Technical Data Parameter Dictionary number in the TDMS)	Recommended Values	Uncertainties	Restrictions on Subsequent Use
Number of volcanic conduits at repository depth (~300 m) (6469)	The probability of one conduit is 0.85; of two conduits is 0.10; and of three conduits is 0.05 (Table 6-8)	The distribution captures the uncertainty in the analogue volcanoes in the Yucca Mountain region.	None
Volcanic conduit diameter at repository depth (~300 m) (6838)	Normal distribution with mean of 15 m, minimum of 1 m, and a 95th percentile of 21 m. In addition, the conduit diameter cannot be smaller than the dike width chosen for the realization (Section 6.3.3.3).	The distribution captures the uncertainty from analogue volcanic centers in the Yucca Mountain region, including the possibility of conduit diameters greater than 21 m.	None
Volcanic dike width at repository depth (~300 m) (6472)	Normal distribution with mean of 8 m, a minimum of 1 m, and a 95th percentile of 12 m (Section 6.3.3.1)	The distribution captures the uncertainty from dikes feeding analogue eruptive centers in the Yucca Mountain region, including the possibility of dikes greater than 12 m at repository depth.	None
Number of volcanic dikes at repository depth (~300 m) associated with formation of a new volcano (8028)	The probability of one dike is 0.40; of two dikes is 0.25; of three dikes is 0.15; of four dikes is 0.10, and of five dikes is 0.10 (Table 6-6)	The distribution captures the uncertainty from analogue eruptive centers and their feeder dikes in the Yucca Mountain region.	None
Volcanic dike spacing at repository depth (~300 m) (8051)	Random uniform distribution with minimum of 0.5 m and maximum of 1,500 m (Section 6.3.3.1)	The distribution captures the uncertainty from analogue volcanic centers in the Yucca Mountain region.	None
Volcanic eruptive center spacing along a single dike (7069)	Random uniform distribution with minimum of 0.5 km, and maximum of 2 km (Table F-1)	The distribution captures most of the uncertainty from the analogue volcanoes in the Yucca Mountain region.	None
Volcanic dike length at repository depth (~300 m) (6834)	Normal distribution with minimum of 0.4 km, mean of 2 km, 95th percentile of 6 km; truncated at 8 km (Section 6.3.3.1)	The distribution captures the uncertainty from analogue volcanic eruptive centers in the Yucca Mountain region.	None
Volcanic dike azimuths at repository depth (~300 m) and above; also called dike orientation (6833)	Expected azimuths are 010° ± 15° and 160° ± 15°. Probability is higher for 010° ± 15° range because (1) the range is roughly perpendicular to the WNW-direction of least principal stress, and (2) there are existing faults with similar azimuths (see Section 6.3.3.1, Table 6-7, and Figure 6-3 for detailed distribution).	The distribution captures most of the uncertainty in mapped fault azimuths within the surface footprint of the Yucca Mountain repository.	None

Table 7-1. Technical Product Output (Continued)

Parameter (number refers to Technical Data Parameter Dictionary number in the TDMS)	Recommended Values	Uncertainties	Restrictions on Subsequent Use
Maximum magnitude of dike-induced earthquakes (8029)	Maximum moment magnitude is 6.1 (Section 6.3.3.2). Magnitudes were calculated from the recommended distribution of dike lengths.	The maximum magnitude provided for dike-induced earthquakes includes the uncertainty given for volcanic dike length observed in the Yucca Mountain region (see 6834).	None
Magma chemistry (6847)	Mean Lathrop Wells volcano basalt composition (Table 6-3)	Uncertainty (as standard deviation and sample variance) is given directly in Table 6-3 and is related simply to the variation in compositions measured directly on Lathrop Wells volcanic products.	None
Water content of magmas (8030)	Uniform distribution between 1 and 5 wt% (Section 6.3.2.2)	This distribution captures the range of values reported by Nicholis and Rutherford (2004 [DIRS 173945]) for Quaternary magmas in the Yucca Mountain region.	None
Gas composition of magma (8031)	Table 6-4	A measure of the uncertainty is provided in Table 6-4 of this report as the standard deviation; the uncertainty reflects the range of volcanic data from which the values are derived.	None
Magmatic temperatures (6849), viscosities (6848), and densities (8032)	Table 6-5. Calculated from theoretical relations or based upon experimental data described in Section 6.3.2.4. As an example, for water contents ranging from 4 to 0%, liquidus temperature ranges from 1,046°C to 1,169°C, liquidus viscosity ranges from 1.957 to 2.678 (log poise units), and liquidus density ranges from 2,474 kg/m^3 to 2,663 kg/m^3, based upon theoretical relations.	Uncertainties associated with theoretical values are expected to be less than about 5% because the mathematical relationships used to calculate the values are closely tied to experimental data. However, other uncertainties are introduced because magmas at shallow depth and during eruption typically are below liquidus temperature and contain variable quantities of crystals and bubbles, which affect the bulk material properties.	There are no restrictions on the subsequent use of these values, but values should be considered estimates rather than precise values.

Table 7-1. Technical Product Output (Continued)

Parameter (number refers to Technical Data Parameter Dictionary number in the TDMS)	Recommended Values	Uncertainties	Restrictions on Subsequent Use
Magma ascent rate below vesiculation depth (6474)	Equation 6-3	Uncertainties are related to processes and material properties not accounted for in Equation 6-3, for example, if there is a pressure-driving force in addition to buoyancy between the magma and surrounding rocks or if the rheology of the magma is non-Newtonian.	Subsequent use of Equation 6-3 should explicitly state the sources of uncertainty and the assumptions made in the theory.
Volatile exsolution depths in magma (8033)	Range from about 1 km to 10 km depth for water contents between 0.01 and 0.05 weight fraction (1 and 5 wt%) (Figure 6-5).	Uncertainties are related to the assumptions made in the theoretical approach: steady and homogeneous flow, and lithostatic pressure within the dike or conduit. The uncertainties could be large.	Subsequent use of Figure 6-5 should explicitly state the assumptions made in the theory and should not violate the theory.
Fragmentation depths of magma (6842)	Range from 100 to 850 m (approximately) for water contents between 1 and 5 wt% (Figure 6-6).	Uncertainties are related to incomplete understanding of the mechanisms of magma fragmentation, which has been observed to occur at gas volume fractions ranging from 0.60 to 0.95.	Subsequent use of these fragmentation depths should state explicitly that they assume fragmentation at a gas volume fraction of 0.75.
Volcanic eruption velocity as a function of depth (8034)	Eruption velocity u_{erupt} is estimated from Figures 6-7 and 6-8. Velocity then decreases linearly downward to $0.1u_{erupt}$ at the fragmentation depth. Below fragmentation depth, the velocity continues to decrease linearly to $0.01u_{erupt}$ at the depth where water exsolution begins.	Uncertainties are related to the validity of assumptions made in developing the theory that produces the curves in Figures 6-7 and 6-8 (steady, homogeneous flow, with lithostatic pressure in the rising magma column). Uncertainty in the velocity versus depth functions is associated with the simple linear nature of the recommended functions, whereas, in nature, the functions would probably be nonlinear.	Subsequent use of these velocity profiles should explicitly state the simplifications that are made to derive them.
Volcanic eruption duration for formation of an entire volcano (6839)	A lognormal probability distribution with mode of seven months, a minimum of 1 month, and 90th percentile of 3 years (Section 6.3.4.4).	The distribution includes the uncertainties associated with observations of historical, relevant scoria cone eruptions worldwide, including the possibility of a long duration eruption.	None
Duration of a single explosive phase constituting a violent Strombolian eruptive phase (8035)	A log-uniform probability ranging from 18 hours to 75 days (Section 6.3.4.4).	The distribution captures most of the uncertainty from the limited number of observed, relevant explosive phases during a volcanic eruption.	Duration cannot exceed the duration of the entire volcanic event.

Table 7-1. Technical Product Output (Continued)

Parameter (number refers to Technical Data Parameter Dictionary number in the TDMS)	Recommended Values	Uncertainties	Restrictions on Subsequent Use
Volcanic tephra fall or ash volume (7303)	Log-uniform distribution between 0.004 km^3 and 0.14 km^3 (Section 6.3.4.4).	This distribution, based on the Lathrop Wells volcano, captures the uncertainty associated with potential ash volume, based on the estimated volumes of Quaternary volcanoes in the YMR.	None
Mean particle size erupted during violent Strombolian eruption phases (6479)	Log-triangular distribution with a minimum of 0.01 mm, a mode of 0.1 mm, and a maximum of 1.0 mm (Section 6.3.5.1).	Uncertainties are due mainly to the rarity of relevant data in the published literature that pertain to the bulk erupted particle size from violent Strombolian eruptions. The distribution incorporates the range of values that have been estimated.	None
Standard deviation of volcanic particle size distribution for a given mean (8036)	Uniform distribution between σ_ϕ = 1 and σ_ϕ = 3 (Section 6.3.5.1).	Uncertainties are due mainly to the rarity of data in the published literature that pertain to the bulk erupted particle size from violent Strombolian eruptions. The distribution incorporates the range of values that have been estimated.	None
Clast characteristics of volcanic erupted particle (1107)	Shape factor of 0.5 (shape factor (F) = (b + c)/2a, where a, b, and c are the length of the longest, middle, and shortest axes of the particles) (Section 6.3.5.2).	Uncertainty is related to an absence of data in the published literature.	None
Density of volcanic erupted particles (61)	For particle diameters less than or equal to 0.01 mm, density is 0.8 of the magma density. For particles greater than 10 mm, density is 0.4 of the magma density. For particles between 0.01 mm and 10 mm, density should decrease linearly with increasing log diameter (Section 6.3.5.2).	Uncertainty is related to the wide range of vesicularities of clasts that can be erupted during a single volcanic event.	None
Volcanic tephra deposit density or ash settled density (7375)	Two approaches to treating deposit density in calculations: (1) use 1,000 kg/m^3, or (2) sample from a normal distribution of deposit densities ranging from 300 to 1,500 kg/m^3, with a mean of 1,000 kg/m^3(Section 6.3.5.3).	Uncertainties are due to a lack of published data.	None

7.2 OUTPUT PARAMETERS AND UNCERTAINTY

The output parameter distributions and their uncertainties, as summarized in Table 7-1 form the technical product output for this report (Output DTN: LA0612DK831811.001).

The qualitative descriptions of uncertainties in Table 7-1 are due to limited relevant published data on many parameters and to the small number of analogue volcanoes where relevant data were obtained. The recommended distributions indeed capture most of the spread of data provided in Section 6 and the appendices. Reasoned arguments, especially those that rely on the expected future eruptive event, support the basis that the phenomena inferred from old eruptive centers in the Yucca Mountain region adequately sample future eruptive processes. Confidence in the distributions is supported by the established trend of decreasing volcanic activity in the Yucca Mountain region (leading to "simpler" geometries of individual events), and the consistency of parameters that accompany that volcanism (e.g., the number of dikes associated with the Quaternary events). It is clear that the recommended distributions are representative of the past eruptive phenomena measured or inferred, while it is reasoned, rather than computed, from the data that the distributions are appropriate for future eruptions, while being consistent with Assumption 2 of Section 5.

8. INPUTS AND REFERENCES

8.1 DOCUMENTS CITED

103750 Altman, W.D.; Donnelly, J.P.; and Kennedy, J.E. 1988. *Qualification of Existing Data for High-Level Nuclear Waste Repositories: Generic Technical Position*. NUREG-1298. Washington, D.C.: U.S. Nuclear Regulatory Commission. TIC: 200652.

103597 Altman, W.D.; Donnelly, J.P.; and Kennedy, J.E. 1988. *Peer Review for High-Level Nuclear Waste Repositories: Generic Technical Position*. NUREG-1297. Washington, D.C.: U.S. Nuclear Regulatory Commission. TIC: 200651.

162795 Arrighi, S.; Principe, C.; and Rosi, M. 2001. "Violent Strombolian and Subplinian Eruptions at Vesuvius During Post-1631 Activity." *Bulletin of Volcanology, 63*, 126-150. New York, New York: Springer-Verlag. TIC: 253920.

122601 Baker, D.R. and Eggler, D.H. 1983. "Fractionation Paths of Atka (Aleutians) High-Alumina Basalts: Constraints from Phase Relations." *Journal of Volcanology and Geothermal Research, 18*, 387-404. Amsterdam, The Netherlands: Elsevier. TIC: 246252.

147740 Best, M.G. 1982. *Igneous and Metamorphic Petrology*. New York, New York: W.H. Freeman and Company. TIC: 247662.

144263 Blong, R.J. 1984. *Volcanic Hazards, A Sourcebook on the Effects of Eruptions*. Sydney, Australia: Academic Press. TIC: 247016.

101996 Bradshaw, T.K. and Smith, E.I. 1994. "Polygenetic Quaternary Volcanism at Crater Flat, Nevada." *Journal of Volcanology and Geothermal Research, 63*, 165-182. Amsterdam, The Netherlands: Elsevier. TIC: 224980.

155852 Brandsdottir, B. and Einarsson, P. 1979. "Seismic Activity Associated with the September 1977 Deflation of the Krafla Central Volcano in North-Eastern Iceland." *Journal of Volcanology and Geothermal Research, 6*, 197-212. Amsterdam, The Netherlands: Elsevier. TIC: 250651.

100022 Brocher, T.M.; Hunter, W.C.; and Langenheim, V.E. 1998. "Implications of Seismic Reflection and Potential Field Geophysical Data on the Structural Framework of the Yucca Mountain-Crater Flat Region, Nevada." *Geological Society of America Bulletin, 110*, (8), 947-971. Boulder, Colorado: Geological Society of America. TIC: 238643.

178156 Bruce, P. M. and Huppert, H. E. 1989. "Thermal Control of Basaltic Fissure Eruptions." *Nature, 342*, pp. 665-667. xxx, xx: xxx. TIC: TBD.

160059 BSC 2002. (Bechtel SAIC Company) *Radionuclide Screening*. ANL-WIS-MD-000006 REV 01. Las Vegas, Nevada: Bechtel SAIC Company. ACC: MOL.20020923.0177.

169989 BSC 2004. *Characterize Framework for Igneous Activity at Yucca Mountain, Nevada*. ANL-MGR-GS-000001 REV 02. Las Vegas, Nevada: Bechtel SAIC Company. ACC: DOC.20041015.0002; DOC.20050718.0007.

169987 BSC 2004. *CSNF Waste Form Degradation: Summary Abstraction*. ANL-EBS-MD-000015 REV 02. Las Vegas, Nevada: Bechtel SAIC Company. ACC: DOC.20040908.0001; DOC.20050620.0004.

170027 BSC 2004. *Development of Earthquake Ground Motion Input for Preclosure Seismic Design and Postclosure Performance Assessment of a Geologic Repository at Yucca Mountain, NV*. MDL-MGR-GS-000003 REV 01. Las Vegas, Nevada: Bechtel SAIC Company. ACC: DOC.20041111.0006; DOC.20051130.0003.

170028 BSC 2004. *Dike/Drift Interactions*. MDL-MGR-GS-000005 REV 01. Las Vegas, Nevada: Bechtel SAIC Company. ACC: DOC.20041124.0002; DOC.20050622.0002.

174067 BSC 2005. *Atmospheric Dispersal and Deposition of Tephra from a Potential Volcanic Eruption at Yucca Mountain, Nevada*. MDL-MGR-GS-000002 REV 02. Las Vegas, Nevada: Bechtel SAIC Company. ACC: DOC.20050825.0001; DOC.20050908.0001; DOC.20060306.0008.

173981 BSC 2005. *Features, Events, and Processes: Disruptive Events*. ANL-WIS-MD-000005 REV 03. Las Vegas, Nevada: Bechtel SAIC Company. ACC: DOC.20050830.0008.

174070 BSC 2005. *Magma Dynamics at Yucca Mountain, Nevada*. ANL-MGR-GS-000005 REV 00. Las Vegas, Nevada: Bechtel SAIC Company. ACC: DOC.20050829.0006.

174066 BSC 2005. *Number of Waste Packages Hit by Igneous Intrusion*. ANL-MGR-GS-000003 REV 02. Las Vegas, Nevada: Bechtel SAIC Company. ACC: DOC.20050829.0001.

175539 BSC 2005. *Q-List*. 000-30R-MGR0-00500-000-003. Las Vegas, Nevada: Bechtel SAIC Company. ACC: ENG.20050929.0008.

178448 BSC 2006. *Technical Work Plan for: Igneous Activity Assessment for Disruptive Events*. TWP-WIS-MD-000007 REV 09 ICN 01. Las Vegas, Nevada: Bechtel SAIC Company. ACC: DOC.20060814.0018.

122532 Byers, C.D.; Garcia, M.O.; and Muenow, D.W. 1985. "Volatiles in Pillow Rim Glasses from Loihi and Kilauea Volcanoes, Hawaii." *Geochimica et Cosmochimica Acta, 49*, 1887-1896. New York, New York: Pergamon Press. TIC: 246241.

101859 Byers, F.M., Jr. and Barnes, H. 1967. *Geologic Map of the Paiute Ridge Quadrangle, Nye and Lincoln Counties, Nevada*. Map GQ-577. Washington, D.C.: U.S. Geological Survey. ACC: HQS.19880517.1104.

104639 Byers, F.M., Jr.; Carr, W.J.; Orkild, P.P.; Quinlivan, W.D.; and Sargent, K.A. 1976. *Volcanic Suites and Related Cauldrons of Timber Mountain-Oasis Valley Caldera Complex, Southern Nevada*. Professional Paper 919. Washington, D.C.: U.S. Geological Survey. TIC: 201146.

101519 Carr, W.J. 1982. *Volcano-Tectonic History of Crater Flat, Southwestern Nevada, as Suggested by New Evidence from Drill Hole USW-VH-1 and Vicinity*. Open-File Report 82-457. Denver, Colorado: U.S. Geological Survey. ACC: NNA.19870518.0057.

100969 Champion, D.E. 1991. "Volcanic Episodes Near Yucca Mountain as Determined by Paleomagnetic Studies at Lathrop Wells, Crater Flat, and Sleeping Butte, Nevada." *High Level Radioactive Waste Management, Proceedings of the Second Annual International Conference, Las Vegas, Nevada, April 28-May 3, 1991. 1*, 61-67. La Grange Park, Illinois: American Nuclear Society. TIC: 204272.

178064 Chouet, B.; Hamisevicz, N.; and McGetchin, T.R. 1974. "Photoballistics of Volcanic Jet Activity at Stromboli, Italy." *Journal of Geophysical Research, 79*, (32), 4961-4976. Washington, D.C.: American Geophysical Union. TIC: 258645.

157236 Christiansen, R.L.; Lipman, P.W.; Carr, W.J.; Byers, F.M., Jr.; Orkild, P.P.; and Sargent, K.A. 1977. "The Timber Mountain-Oasis Valley Caldera Complex of Southern Nevada." *Geological Society of America Bulletin, 88*, (7), 943-959. Boulder, Colorado: Geological Society of America. TIC: 201802.

165503 Codell, R. 2003. "Alternative Igneous Source Term Model for the Yucca Mountain Repository." *Proceedings of the 10th International High-Level Radioactive Waste Management Conference (IHLRWM), March 30-April 2, 2003, Las Vegas, Nevada.* Pages 405-412. La Grange Park, Illinois: American Nuclear Society. TIC: 254559.

102647 Connor, C.B.; Lane-Magsino, S.; Stamatakos, J.A.; Martin, R.H.; LaFemina, P.C.; Hill, B.E.; and Lieber, S. 1997. "Magnetic Surveys Help Reassess Volcanic Hazards at Yucca Mountain, Nevada." *Eos, Transactions, 78*, (7), 73, 77, 78. Washington, D.C.: American Geophysical Union. TIC: 234580.

102740 Crowe B.M. 1986. "Volcanic Hazard Assessment for Disposal of High-Level Radioactive Waste." Chapter 16 of *Active Tectonics: Impact on Society*. Washington, D.C.: National Academy Press. TIC: 216663.

100110 Crowe, B.; Perry, F.; Geissman, J.; McFadden, L.; Wells, S.; Murrell, M.; Poths, J.; Valentine, G.A.; Bowker, L.; and Finnegan, K. 1995. *Status of Volcanism Studies for the Yucca Mountain Site Characterization Project*. LA-12908-MS. Los Alamos, New Mexico: Los Alamos National Laboratory. ACC: HQO.19951115.0017.

100972 Crowe, B.; Self, S.; Vaniman, D.; Amos, R.; and Perry, F. 1983. "Aspects of Potential Magmatic Disruption of a High-Level Radioactive Waste Repository in Southern Nevada." *Journal of Geology, 91*, (3), 259-276. Chicago, Illinois: University of Chicago Press. TIC: 216959.

101839 Crowe, B.M. and Carr, W.J. 1980. *Preliminary Assessment of the Risk of Volcanism at a Proposed Nuclear Waste Repository in the Southern Great Basin*. Open-File Report 80-357. Denver, Colorado: U.S. Geological Survey. ACC: HQS.19880517.1140.

100973 Crowe, B.M. and Perry, F.V. 1990. "Volcanic Probability Calculations for the Yucca Mountain Site: Estimation of Volcanic Rates." *Proceedings of the Topical Meeting on Nuclear Waste Isolation in the Unsaturated Zone, FOCUS '89, September 17-21, 1989, Las Vegas, Nevada*. Pages 326-334. La Grange Park, Illinois: American Nuclear Society. TIC: 212738.

101532 Crowe, B.M.; Wohletz, K.H.; Vaniman, D.T.; Gladney, E.; and Bower, N. 1986. *Status of Volcanic Hazard Studies for the Nevada Nuclear Waste Storage Investigations. LA-9325-MS. Volume II*. Los Alamos, New Mexico: Los Alamos National Laboratory. ACC: NNA.19890501.0157.

178143 Crowe, Bruce M.; Perry, Frank V. 1991. *Preliminary geologic map of the Sleeping Butte volcanic centers*. LA-12101-MS. 1. Los Alamos, NM: Los Alamos National Laboratory. ACC: MOL.19980409.0362. TIC: 201913.

174074 Crumpler, L.S. 2003. "Natural Scoria Cone Half-Section, East Grants Ridge: A Test of Basalt Pyroclastic Eruption Models." *Geology of the Zuni Plateau, New Mexico Geological Society Fifty-Fourth Annual Field Conference, September 24-27, 2003*. Lucas, S.G., Semken, S.C., Berglof, W.R., and Ulmer-Scholle, D.S., eds. Pages 155-164. Socorro, New Mexico: New Mexico Geological Society. TIC: 257282.

173900 Crumpler, L.S. 1980. "An Alkali-Basalt through Trachyte Suite, Mesa Chivato Mount Taylor Volcanic Field, New Mexico: Summary." *Geological Society of America Bulletin, Part I, 91*, (1), 253-255. Boulder, Colorado: Geological Society of America. TIC: 257320.

100116 CRWMS M&O 1996. *Probabilistic Volcanic Hazard Analysis for Yucca Mountain, Nevada*. BA0000000-01717-2200-00082 REV 0. Las Vegas, Nevada: CRWMS M&O. ACC: MOL.19971201.0221.

123201 CRWMS M&O 1998. "Physical Processes of Magmatism and Effects on the Potential Repository: Synthesis of Technical Work through Fiscal Year 1995." Chapter 5 of *Synthesis of Volcanism Studies for the Yucca Mountain Site Characterization Project*. Deliverable 3781MR1. Las Vegas, Nevada: CRWMS M&O. ACC: MOL.19990511.0400.

170965 CRWMS M&O 1999. *Final Report on Qualification of Volcanism Isotope, Trace-Element, and Halogen Data Using Procedure YAP-SIII.1Q/Rev. 3/ICN 0*. Las Vegas, Nevada: CRWMS M&O. ACC: MOL.19990406.0471.

156980 CRWMS M&O 2000. *Data Qualification Report: Data Related to Characterization of Eruptive Processes for Use on the Yucca Mountain Project*. TDR-NBS-GS-000016 REV 00. Las Vegas, Nevada: CRWMS M&O. ACC: MOL.20000810.0002.

149303 Danyushevsky, L.V.; Falloon, T.J.; Sobolev, A.V.; Crawford, A.J.; Carroll, M.; and Price, R.C. 1993. "The H_2O Content of Basalt Glasses from Southwest Pacific Back-Arc Basins." *Earth and Planetary Science Letters, 117*, 347-362. Amsterdam, The Netherlands: Elsevier. TIC: 246102.

178142 Dartevelle, S., and G. A. Valentine 2005. "Early-time multiphase interactions between basaltic magma and underground openings at the proposed Yucca Mountain radioactive waste repository." *Geophysical Research Letters, 32*, 1-5. Washington, DC: American Geophysical Union. Submit to RPC

100027 Day, W.C.; Dickerson, R.P.; Potter, C.J.; Sweetkind, D.S.; San Juan, C.A.; Drake, R.M., II; and Fridrich, C.J. 1998. *Bedrock Geologic Map of the Yucca Mountain Area, Nye County, Nevada*. Geologic Investigations Series I-2627. Denver, Colorado: U.S. Geological Survey. ACC: MOL.19981014.0301.

164019 Dehaudt, P. 2001. "Physical and Chemical State of the Nuclear Spent Fuel After Irradiation." Section 5.2 of *Synthesis on the Long Term Behavior of the Spent Nuclear Fuel*. Poinssot, C., ed. CEA-R-5958(E). Volume I. Paris, France: Commissariat à l'Énergie Atomique. TIC: 253976.

162799 Delaney, P.T. 1982. "Rapid Intrusion of Magma into Wet Rock: Groundwater Flow due to Pore Pressure Increases." *Journal of Geophysical Research, 87*, (B9), 7739–7756. Washington, D.C.: American Geophysical Union. TIC: 254049.

145370 Delaney, P.T. and Gartner, A.E. 1997. "Physical Processes of Shallow Mafic Dike Emplacement Near the San Rafael Swell, Utah." *Geological Society of America Bulletin, 109*, (9), 1177-1192. Boulder, Colorado: Geological Society of America. TIC: 247421.

162800 Delaney, P.T. and Pollard, D. 1978. "Basaltic Subvolcanic Conduits Near Shiprock, New Mexico: Magma Flow, Heat Transport, and Brecciation of Host Rocks." *Eos Transactions, 59*, (12), 1212. Washington, D.C.: American Geophysical Union. TIC: 254390.

162801 Delaney, P.T. and Pollard, D.D. 1981. *Deformation of Host Rocks and Flow of Magma During Growth of Minette Dikes and Breccia-Bearing Intrusions Near Ship Rock, New Mexico*. Geological Survey Professional Paper 1202. Washington, D.C.: U.S. Geological Survey. TIC: 254050.

169660 Detournay, E.; Mastin, L.G.; Pearson, J.R.A.; Rubin, A.M.; and Spera, F.J. 2003. *Final Report of the Igneous Consequences Peer Review Panel, with Appendices*. Las Vegas, Nevada: Bechtel SAIC Company. ACC: MOL.20031014.0097; MOL.20030730.0163.

178158 Diez, M.; Connor, C. B.; Connor, L.; and Savov, I. P. 2005. "Magma Dynamics and Conduit Growth Mechanisms Inferred from Exposed Volcano Conduits at the San Rafael Subvolcanic Field, Utah." *Eos, Transactions (Supplement)*, *86*, (52), V33A-0662. Washington, D.C.: American Geophysical Union. TIC: 258374.

162802 Dobran, F. 2001. "Conduit Erosion." Volcanic *Processes, Mechanisms in Material Transport*. Pages 480-484. New York, New York: Kluwer Academic/Plenum Publishers. TIC: 254051.

115338 Doubik, P. and Hill, B.E. 1999. "Magmatic and Hydromagmatic Conduit Development During the 1975 Tolbachik Eruption, Kamchatka, with Implications for Hazards Assessment at Yucca Mountain, NV." *Journal of Volcanology and Geothermal Research, 91*, 43-64. Amsterdam, The Netherlands: Elsevier. TIC: 246029.

178114 Duncan, A.M.; Guest, J.E.; Stofan, E.R.; Anderson, S.W.; Pinkerton, H.; and Calvari, S. 2004. "Development of Tumuli in the Medial Portion of the 1983 Aa Flow-Field, Mount Etna, Sicily." *Journal of Volcanology and Geothermal Research, 132*, 173-187. New York, New York: Elsevier. TIC: 258348.

105284 Farmer, G.L.; Perry, F.V.; Semken, S.; Crowe, B.; Curtis, D.; and DePaolo, D.J. 1989. "Isotopic Evidence on the Structure and Origin of Subcontinental Lithospheric Mantle in Southern Nevada." *Journal of Geophysical Research, 94*, (B6), 7885-7898. Washington, D.C.: American Geophysical Union. TIC: 201800.

178115 Ferrucci, M.; Pertusati, S.; Sulpizio, R.; Zanchetta, G.; Pareschi, M.T.; and Santacroce, R. 2005. "Volcaniclastic Debris Flows at La Fossa Volcano (Vulcano Island, Southern Italy): Insights for Erosion Behaviour of Loose Pyroclastic Material on Steep Slopes." *Journal of Volcanology and Geothermal Research, 145*, 173-191. New York, New York: Elsevier. TIC: 258479.

105337 Fleck, R.J.; Turrin, B.D.; Sawyer, D.A.; Warren, R.G.; Champion, D.E.; Hudson, M.R.; and Minor, S.A. 1996. "Age and Character of Basaltic Rocks of the Yucca Mountain Region, Southern Nevada." *Journal of Geophysical Research, 101*, (B4), 8205-8227. Washington, D.C.: American Geophysical Union. TIC: 234626.

144274 Gaetani, G.A.; Grove, T.L.; and Bryan, W.B. 1993. "The Influence of Water on the Petrogenesis of Subduction-Related Igneous Rocks." *Nature, 365*, 332-335. London, England: Macmillan Journals. TIC: 246792.

178144 Gaffney, E.S. and Damjanac, B. 2006. "Localization of Volcanic Activity: Topographic Effects on Dike Propagation, Eruption and Conduit Formation." *Geophysical Research Letters, 33*, 1-4. Washington, D.C.: American Geophysical Union. TIC: 258505.

122542 Garcia, M.O.; Muenow, D.W.; Aggrey, K.E.; and O'Neil, J.R. 1989. "Major Element, Volatile, and Stable Isotope Geochemistry of Hawaiian Submarine Tholeiitic Glasses." *Journal of Geophysical Research, 94*, (B8), 10525-10538. Washington, D.C.: American Geophysical Union. TIC: 246240.

178116 Gutmann, J.T. 1979. "Structure and Eruptive Cycle of Cinder Cones in the Pinacate Volcanic Field and the Controls of Strombolian Activity." *Journal of Geology, 87*, 448-454. Chicago, Illinois: University of Chicago Press. TIC: 258343.

178149 Gutmann, J.T. 2002. "Strombolian and Effusive Activity as Precursors to Phreatomagmatism : Eruptive Sequence at Maars of the Pinacate Volcanic Field, Sonora, Mexico." *Journal of Volcanology and Geothermal Research, 113*, 345-356. Amsterdam, Netherlands: Elsevier Science BV. TIC: 258349.

169781 Hackett, W.R.; Jackson, S.M.; and Smith, R.P. 1996. "Paleoseismology of Volcanic Environments." Chapter 4 of *Paleoseismology*. McCalpin, J.P., ed. San Diego, California: Academic Press. TIC: 256139.

124671 Hallett, R.B. 1992. "Volcanic Geology of the Rio Puerco Necks." *San Juan Basin IV: New Mexico Geological Society, 43rd Annual Field Conference, September 30-October 3, 1992*. Lucas, S.G.; Kues, B.S.; Williamson, T.E.; and Hunt, A.P.; eds. 135-144. Socorro, New Mexico: New Mexico Geological Society. TIC: 239345.

124674 Head, J.W., III and Wilson, L. 1989. "Basaltic Pyroclastic Eruptions: Influence of Gas-Release Patterns and Volume Fluxes on Fountain Structure, and the Formation of Cinder Cones, Spatter Cones, Rootless Flows, Lava Ponds and Lava Flows." *Journal of Volcanology and Geothermal Research, 37*, 261-271. Amsterdam, The Netherlands: Elsevier. TIC: 235982.

162817 Heiken, G. 1978. "Characteristics of Tephra from Cinder Cone, Lassen Volcanic National Park, California." *Bulletin of Volcanology, 41-2*, 119–130. New York, New York: Springer-Verlag. TIC: 235508.

106122 Heiken, G.H. and Wohletz, K. 1985. *Volcanic Ash*. Berkeley, California: University of California Press. TIC: 242991.

107255 Heizler, M.T.; Perry, F.V.; Crowe, B.M.; Peters, L.; and Appelt, R. 1999. "The Age of Lathrop Wells Volcanic Center: An $^{40}Ar/^{39}Ar$ Dating Investigation." *Journal of Geophysical Research, 104*, (B1), 767-804. Washington, D.C.: American Geophysical Union. TIC: 243399.

151040 Hill, B.E.; Connor, C.B.; Jarzemba, M.S.; La Femina, P.C.; Navarro, M.; and Strauch, W. 1998. "1995 Eruptions of Cerro Negro Volcano, Nicaragua, and Risk Assessment for Future Eruptions." *Geological Society of America Bulletin, 110*, (10), 1231-1241. Boulder, Colorado: Geological Society of America. TIC: 245102.

178117 Holm, R.F. 1987. "Significance of Agglutinate Mounds on Lava Flows Associated with Monogenetic Cones: An Example at Sunset Crater, Northern Arizona." *Geological Society of America Bulletin, 99*, 319-324. Boulder, Colorado: Geolgical Society of America. TIC: 258344.

178066 Hooper, D.M. and Sheridan, M.F. 1998. "Computer-Simulation Models of Scoria Cone Degradation." *Journal of Volcanology and Geothermal Research, 83*, 241-267. New York, New York: Elsevier. TIC: 258353.

178161 Houghton, B. F.; Wilson, C. J. N.; and Smith, I. E. M. 1999. "Shallow-seated Controls on Styles of Explosive Basaltic Volcanism: A Case Study from New Zealand." *Journal of Volcanology and Geothermal Research, 91*, pp. 97-120. TIC: TBD.

109119 Jackson, J.A., ed. 1997. *Glossary of Geology*. 4th Edition. Alexandria, Virginia: American Geological Institute. TIC: 236393.

100460 Jarzemba, M.S. 1997. "Stochastic Radionuclide Distributions After a Basaltic Eruption for Performance Assessments of Yucca Mountain." *Nuclear Technology, 118*, 132-141. Hinsdale, Illinois: American Nuclear Society. TIC: 237944.

118292 Jaupart, C. and Tait, S. 1990. "Dynamics of Eruptive Phenomena." Chapter 8 of *Modern Methods of Igneous Petrology: Understanding Magmatic Processes*. Nicholls, J. and Russell, J.K., eds. Reviews in Mineralogy Volume 24. 213-238. Washington, D.C.: Mineralogical Society of America. TIC: 246394.

111236 Keating, G.N. and Valentine, G.A. 1998. "Proximal Stratigraphy and Syn-Eruptive Faulting in Rhyolitic Grants Ridge Tuff, New Mexico, USA." *Journal of Volcanology and Geothermal Research, 81*, 37-49. Amsterdam, The Netherlands: Elsevier. TIC: 246096.

174077 Keating, G.N.; Geissman, J.W.; and Zyvoloski, G.A. 2002. "Multiphase Modeling of Contact Metamorphic Systems and Application to Transitional Geomagnetic Fields." *Earth and Planetary Science Letters, 198*, 429-448. New York, New York: Elsevier. TIC: 257642.

178148 Kilburn, C.R.J., and Lopes, R.M.C. 1991. "General Patterns of Flow Field Growth: Aa and Blocky Lavas." *Journal of Geophysical Research, 96*, (B12), 19,721-19,732. Washington, DC: American Geophysical Union (AGU). TIC: 258363.

106299 Knutson, J. and Green, T.H. 1975. "Experimental Duplication of a High-Pressure Megacryst/Cumulate Assemblage in a Near-Saturated Hawaiite." *Contributions to Mineralogy and Petrology, 52*, 121-132. Berlin, Germany: Springer-Verlag. TIC: 225057.

100909 Kotra, J.P.; Lee, M.P.; Eisenberg, N.A.; and DeWispelare, A.R. 1996. *Branch Technical Position on the Use of Expert Elicitation in the High-Level Radioactive Waste Program*. NUREG-1563. Washington, D.C.: U.S. Nuclear Regulatory Commission. TIC: 226832.

147767 Lange, R.L. and Carmichael, I.S.E. 1990. "Thermodynamic Properties of Silicate Liquids with Emphasis on Density, Thermal Expansion and Compressibility." Chapter 2 of *Modern Methods of Igneous Petrology: Understanding Magmatic Processes*. Nicholls, J. and Russell, J.K., eds. Reviews in Mineralogy Volume 24. 25-64. Washington, D.C.: Mineralogical Society of America. TIC: 246394.

174240 Laughlin, A.W.; Perry, F.V.; Damon, P.E.; Shafiqullah, M.; WoldeGabriel, G.; McIntosh, W.; Harrington, C.D.; Wells, S.G.; and Drake, P.G. 1993. "Geochronology of Mount Taylor, Cebollita Mesa, and Zuni-Bandera Volcanic Fields, Cibola County, New Mexico." *New Mexico Geology, 15*, (4), 81-92. Socorro, New Mexico: New Mexico Bureau of Mines and Mineral Resources. TIC: 225061.

178152 Lorenz, V. 1986. "On the Growth of Maars and Diatremes and Its Relevance to the Formation of Tuff Rings." *Bulletin of Volcanology, 48*, pp. 265-274. TIC: 259009.

178118 Luhr, J.F. and Housh, T.B. 2002. "Melt Volatile Contents in Basalts from Lathrop Wells and Red Cone, Yucca Mountain Region (SW Nevada): Insights from Glass Inclusions." *Eos (Transactions), American Geophysical Union, 83*, (47), F1496. Washington, D.C.: American Geophysical Union. TIC: 258364.

144310 Luhr, J.F. and Simkin, T., eds. 1993. *Paricutin, The Volcano Born in a Mexican Cornfield*. Phoenix, Arizona: Geoscience Press. TIC: 247017.

178155 Macedonio, G.; Dobran, F.; and Neri, A. 1994. "Erosion Processes in Volcanic Conduits and Application to the AD 79 Eruption of Vesuvius." *Earth and Planetary Science Letters, 121*, 137-152. New York, New York: Elsevier. TIC: 258775.

144419 Mader, H.M. 1998. "Conduit Flow and Fragmentation." *The Physics of Explosive Volcanic Eruptions*. Gilbert, J.S. and Sparks, R.S.J., eds. Geological Society Special Publication No. 145. Pages 51-71. London, United Kingdom: Blackwell Scientific Publications. TIC: 247115.

104663 Mahood, G.A. and Baker, D.R. 1986. "Experimental Constraints on Depths of Fractionation of Mildly Alkalic Basalts and Associated Felsic Rocks: Pantelleria, Strait of Sicily." *Contributions to Mineralogy and Petrology, 93*, 251-264. New York, New York: Springer-Verlag. TIC: 225072.

144325 Maleyev, Ye.F. and Vande-Kirkov, Yu.V. 1983. "Features of Pyroclastics of the Northern Breakthrough of the Great Tolbachik Fissure Eruption and the Origin of Its Pale-Grey Ash." *The Great Tolbachik Fissure Eruption, Geological and Geophysical Data 1975-1976*. Fedotov, S.A. and Markhinin, Ye.K., eds. Pages 57–71. New York, New York: Cambridge University Press. TIC: 247236.

178119 Martin, U. and Németh, K. 2006. "How Strombolian is a "Strombolian" Scoria Cone? Some Irregularities in Scoria Cone Architecture from the Transmexican Volcanic Belt, near Volcán Ceboruco, (Mexico) and Al Haruj (Libya)." *Journal of Volcanology and Geothermal Research, 155*, 104-118. New York, New York: Elsevier. TIC: 258481.

178163 Mastin, L. G. 2002. "Insights into Volcanic Conduit Flow from an Open-Source Numerical Model." *Geoch. Geophys. Geosyst., 3*, (7), pp. 1-18. TIC: 256346.

124749 Mastin, L.G. 1991. "The Roles of Magma and Groundwater in the Phreatic Eruptions at Inyo Craters, Long Valley Caldera, California." *Bulletin of Volcanology, 53*, 579-596. Heidelberg, Germany: Springer-Verlag. TIC: 239071.

170144 Mastin, L.G. and Ghiorso, M.S. 2000. *A Numerical Program for Steady-State Flow of Magma-Gas Mixtures Through Vertical Eruptive Conduits*. Open-File Report 00-209. Vancouver, Washington: U.S. Geological Survey. ACC: MOL.20040629.0228.

169783 Mastin, L.G. and Pollard, D.D. 1988. "Surface Deformation and Shallow Dike Intrusion Processes at Inyo Craters, Long Valley, California." *Journal of Geophysical Research, 93*, (B11), 13,221-13,235. Washington, D.C.: American Geophysical Union. TIC: 256132.

162826 McBirney, A.R. 1959. "Factors Governing Emplacement of Volcanic Necks." *American Journal of Science, 257*, (1), 431–448. New Haven, Connecticut: Yale University, Sterling Tower. TIC: 254240.

176089 McFadden, L.D.; McDonald, E.V.; Wells, S.G.; Anderson, K.; Quade, J.; and Forman, S.L. 1998. "The Vesicular Layer and Carbonate Collars of Desert Soils and Pavements: Formation, Age and Relation to Climate Change." *Geomorphology, 24*, 101-145. New York, New York: Elsevier. TIC: 257875.

105023 McFadden, L.D.; Wells, S.G.; and Jercinovich, M.J. 1987. "Influences of Eolian and Pedogenic Processes on the Origin and Evolution of Desert Pavements." *Geology, 15*, (6), 504-508. Boulder, Colorado: Geological Society of America. TIC: 241037.

115469 McGetchin, T.R.; Settle, M.; and Chouet, B.A. 1974. "Cinder Cone Growth Modeled after Northeast Crater, Mount Etna, Sicily." *Journal of Geophysical Research, 79*, (23), 3257-3272. Washington, D.C.: American Geophysical Union. TIC: 246027.

178169 Minor, S. A.; Orkild, P. P.; Sargent, K. A.; Warren, R. G.; Sawyer, D. A.; and Workman, J. B. 1998. *Digital Geologic Map of the Thirsty Canyon NW Quadrangle, Nye County, Nevada*. U.S. Geological Survey Open File Report 98-623. Denver, Colorado: U.S. Geological Survey. ACC: TBD.

178154 Mitchell, K.L. 2005. "Coupled Conduit Flow and Shape in Explosive Volcanic Eruptions." *Journal of Volcanic and Geothermal Research, 143*, 187-203. New York, New York: Elsevier. TIC: 258779.

178166 Morrissey, M. M. and Chouet, B. A. 1997. "A Numerical Investigation of Choked Flow Dynamics and Its Application to the Triggering Mechanism of Long-Period Events at Redoubt Volcano, Alaska." *Journal of Geophysical Research, 102*, pp. 7965-7983. ACC: MOL.20070215.0153.

125093 Muenow, D.W.; Graham, D.G.; Liu, N.W.K.; and Delaney, J.R. 1979. "The Abundance of Volatiles in Hawaiian Tholeiitic Submarine Basalts." *Earth and Planetary Science Letters, 42*, 71-76. Amsterdam, The Netherlands: Elsevier. TIC: 246833.

178160 Németh, K. and White, J.D.L. 2003. "Reconstructing Eruption Processes of a Miocene Monogenetic Volcanic Field from Vent Remnants: Waipiata Volcanic Field, South Island, New Zealand." *Journal of Volcanology and Geothermal Research, 124*, 1-21. New York, New York: Elsevier. TIC: 258910.

173945 Nicholis, M.G. and Rutherford, M.J. 2004. "Experimental Constraints on Magma Ascent Rate for the Crater Flat Volcanic Zone Hawaiite." *Geology, 32*, (6), 489-492. Boulder, Colorado: Geological Society of America. TIC: 256878.

151592 NRC (U.S. Nuclear Regulatory Commission) 1999. "Issue Resolution Status Report Key Technical Issue: Igneous Activity." Rev. 2. Washington, D.C.: U.S. Nuclear Regulatory Commission. Accessed September 18, 2000. TIC: 247987. http://www.nrc.gov/NMSS/DWM/ia-rev2.htm

163274 NRC 2003. *Yucca Mountain Review Plan, Final Report*. NUREG-1804, Rev. 2. Washington, D.C.: U.S. Nuclear Regulatory Commission, Office of Nuclear Material Safety and Safeguards. TIC: 254568.

144330 Ochs, F.A., III and Lange, R.A. 1999. "The Density of Hydrous Magmatic Liquids." *Science, 283*, 1314-1317. Washington, D.C.: American Association for the Advancement of Science. TIC: 246839.

106460 Orkild, P.P.; Sargent, K.A.; and Snyder, R.P. 1969. *Geologic Map of Pahute Mesa, Nevada Test Site and Vicinity, Nye County, Nevada*. Miscellaneous Geologic Investigations Map I-567. Washington, D.C.: U.S. Geological Survey. TIC: 217639.

178157 Papale, P.; Neri, A.; and Macedonio, G. 1998. "The Role of Magma Composition and Water Content in Explosive Eruptions 1. Conduit Ascent Dynamics." *Journal of Volcanology and Geothermal Research, 87*, 75-93. New York, New York: Elsevier. TIC: 258778.

170145 Parfitt, E.A. 2004. "A Discussion of the Mechanisms of Explosive Basaltic Eruptions." *Journal of Volcanology and Geothermal Research, 134*, 77-107. New York, New York: Elsevier. TIC: 256202.

106490 Perry, F.V. and Straub. K.T. 1996. *Geochemistry of the Lathrop Wells Volcanic Center*. LA-13113-MS. Los Alamos, New Mexico: Los Alamos National Laboratory. ACC: MOL.19961015.0079.

173994 Perry, F.V.; Baldridge, W.S.; DePaolo, D.J.; and Shafiqullah, M. 1990. "Evolution of a Magmatic System During Continental Extension: The Mount Taylor Volcanic Field, New Mexico." *Journal of Geophysical Research, 95*, (B12), 19,327-19,348. Washington, D.C.: American Geophysical Union. TIC: 257257.

177379 Perry, F.V.; Cogbill, A.H.; and Kelley, R. E. 2005. "Uncovering Buried Volcanoes at Yucca Mountain." *Eos, Transactions, 86*, (47), 485, 488. Washington, D.C.: American Geophysical Union. TIC: 258001.

144335 Perry, F.V.; Crowe, B.M.; Valentine, G.A.; and Bowker, L.M., eds. 1998. *Volcanism Studies: Final Report for the Yucca Mountain Project*. LA-13478. Los Alamos, New Mexico: Los Alamos National Laboratory. TIC: 247225.

106499 Peterman, Z.E.; Spengler, R.W.; Singer, F.R.; and Dickerson, R.P. 1996. *Geochemistry of Outcrop Samples from the Raven Canyon and Paintbrush Canyon Reference Sections, Yucca Mountain, Nevada*. Open-File Report 94-550. Denver, Colorado: U.S. Geological Survey. ACC: MOL.19970204.0213.

178120 Pinkerton, H. and Sparks, R.S.J. 1976. "The 1975 Sub-Terminal Lavas, Mount Etna: Case History of the Formation of a Compound Lava Field." *Journal of Volcanology and Geothermal Research, 1*, 167-182. Amsterdam, The Netherlands: Elsevier. TIC: 258354.

162396 Piron, J.P. 2001. "Presentation of the Key Scientific Issues for the Spent Nuclear Fuel Evolution in a Closed System." Section 5.1 of *Synthesis on the Long Term Behavior of the Spent Nuclear Fuel*. Poinssot, C., ed. CEA-R-5958(E). Volume I. Paris, France: Commissariat à l'Énergie Atomique. TIC: 253976.

160060 Potter, C.J.; Dickerson, R.P.; Sweetkind, D.S.; Drake, R.M., II; Taylor, E.M.; Fridrich, C.J.; San Juan, C.A.; and Day, W.C. 2002. *Geologic Map of the Yucca Mountain Region, Nye County, Nevada*. Geologic Investigations Series I-2755. Denver, Colorado: U.S. Geological Survey. TIC: 253945.

178165 Pyle, D. M. 2000. "Sizes of Volcanic Eruptions." *Encyclopedia of Volcanoes,* San Diego, California: Academic Press. TIC: TBD.

162829 Pyle, D.M. 1995. "Assessment of the Minimum Volume of Tephra Fall Deposits." *Journal of Volcanology and Geothermal Research, 69*, (3-4), 379-382. New York, New York: Elsevier. TIC: 254749.

162830 Quareni, F.; Ventura, G.; and Mulargia, F. 2001. "Numerical Modelling of the Transition from Fissure- to Central-Type Activity on Volcanoes: A Case Study from Salina Island, Italy." *Physics of the Earth and Planetary Interiors, 124*, (3-4), 213–221. New York, New York: Elsevier. TIC: 254053.

106634 Ratcliff, C.D.; Geissman, J.W.; Perry, F.V.; Crowe, B.M.; and Zeitler, P.K. 1994. "Paleomagnetic Record of a Geomagnetic Field Reversal from Late Miocene Mafic Intrusions, Southern Nevada." *Science, 266*, 412-416. Washington, D.C.: American Association for the Advancement of Science. TIC: 234818.

178162 Rout, D.J.; Cassidy, J.; Locke, C.A.; and Smith, I.E.M. 1993. "Geophysical Evidence for Temporal and Structural Relationships within the Monogenetic Basalt Volcanoes of the Auckland Volcanic Field, Northern New Zealand." *Journal of Volcanology and Geothermal Research, 57*, 71-83. Amsterdam, The Netherlands: Elsevier. TIC: 258777.

119693 Reamer, C.W. 1999. "Issue Resolution Status Report (Key Technical Issue: Igneous Activity, Revision 2)." Letter from C.W. Reamer (NRC) to Dr. S. Brocoum (DOE/YMSCO), July 16, 1999, with enclosure. ACC: MOL.19990810.0639.

178153 Richter, D. H.; Eaton, J. P.; Murata, K. J.; Ault, W. U.; and Krivoy, H. L. 1970. *Chronological Narrative of the 1959-60 Eruption of Kilauea Volcano, Hawaii*. Geological Survey Professional Paper 537-E. Denver, Colorado: U.S. Geological Survey. ACC: TBD.

178121 Riedel, C.; Ernst, G.G.J.; and Riley, M. 2003. "Controls on the Growth and Geometry of Pyroclastic Constructs." *Journal of Volcanology and Geothermal Research, 127*, 121-152. New York, New York: Elsevier. TIC: 258482.

116087 Rose, W.I., Jr.; Bonis, S.; Stoiber, R.E.; Keller, M.; and Bickford, T. 1973. "Studies of Volcanic Ash from Two Recent Central American Eruptions." *Bulletin Volcanologique, XXXVII-3*, 338-364. New York, New York: Springer-Verlag. TIC: 246073.

178141 Rossi, M.J. 1997. "Morphology of the 1984 Open-Channel Lava Flow at Krafla Volcano, Northern Iceland." *Geomorphology, 20*, 95-112. New York, New York: Elsevier. TIC: 258350.

178122 Rowland, S.K. and Walker, G.P.L. 1987. "Toothpaste Lava: Characteristics and Origin of a Lava Structural Type Transitional Between Pahoehoe and Aa." *Bulletin of Volcanology, 49*, 631-641. New York, New York: Springer-Verlag. TIC: 258478.

169784 Rubin, A.M. 1992. "Dike-Induced Faulting and Graben Subsidence in Volcanic Rift Zones." *Journal of Geophysical Research, 97*, (B2), 1839-1858. Washington, D.C.: American Geophysical Union. TIC: 256133.

164118 Rubin, A.M. 1995. "Propagation of Magma-Filled Cracks." *Annual Review of Earth and Planetary Sciences, 23*, 287-336. Palo Alto, California: Annual Reviews. TIC: 254554.

169786 Rubin, A.M. and Gillard, D. 1998. "Dike-Induced Earthquakes: Theoretical Considerations." *Journal of Geophysical Research, 103*, (B5), 10,017-10,030. Washington, D.C.: American Geophysical Union. TIC: 256130.

169787 Rubin, A.M.; Gillard, D.; and Got, J-L. 1998. "A Reinterpretation of Seismicity Associated with the January 1983 Dike Intrusion at Kilauea Volcano, Hawaii." *Journal of Geophysical Research, 103*, (B5), 10,003-10,015. Washington, D.C.: American Geophysical Union. TIC: 256131.

156313 Sandoval, R.P.; Weber, J.P.; Levine, H.S.; Romig, A.D.; Johnson, J.D.; Luna, R.E.; Newton, G.J.; Wong, B.A.; Marshall, R.W., Jr.; Alvarez, J.L.; and Gelbard, F. 1983. *An Assessment of the Safety of Spent Fuel Transportation in Urban Environs*. SAND82-2365. Albuquerque, New Mexico: Sandia National Laboratories. ACC: NNA.19870406.0489.

100075 Sawyer, D.A.; Fleck, R.J.; Lanphere, M.A.; Warren, R.G.; Broxton, D.E.; and Hudson, M.R. 1994. "Episodic Caldera Volcanism in the Miocene Southwestern Nevada Volcanic Field: Revised Stratigraphic Framework, $^{40}Ar/^{39}Ar$ Geochronology, and Implications for Magmatism and Extension." *Geological Society of America Bulletin, 106*, (10), 1304-1318. Boulder, Colorado: Geological Society of America. TIC: 222523.

178164 Scandone, R. 1979. "Effusion Rate and Energy Balance of Paricutin Eruption (1943-1952), Michoacan, Mexico." *Journal of Volcanic and Geothermal Research, 6*, 49-59. Amsterdam, The Netherlands: Elsevier. TIC: 258776.

178123 Self, S.; Kienle, J.; and Huot, J-P. 1980. "Ukinrek Maars, Alaska, II. Deposits and Formation of the 1977 Craters." *Journal of Volcanology and Geothermal Research, 7*, 39-65. Amsterdam, The Netherlands: Elsevier. TIC: 258483.

126270 Shaw, H.R. 1972. "Viscosities of Magmatic Silicate Liquids: An Empirical Method of Prediction." *American Journal of Science, 272*, 870-889. New Haven, Connecticut: Yale University, Kline Geology Laboratory. TIC: 246470.

144351 Sisson, T.W. and Grove, T.L. 1993. "Experimental Investigations of the Role of H2O in Calc-Alkaline Differentiation and Subduction Zone Magmatism." *Contributions to Mineralogy and Petrology, 113*, 143-166. New York, New York: Springer-Verlag. TIC: 246909.

122564 Sisson, T.W. and Grove, T.L. 1993. "Temperatures and H_2O Contents of Low-MgO High-Alumina Basalts." *Contributions to Mineralogy and Petrology, 113*, 167-184. New York, New York: Springer-Verlag. TIC: 246251.

122549 Sisson, T.W. and Layne, G.D. 1993. "H_2O in Basalt and Basaltic Andesite Glass Inclusions from Four Subduction-Related Volcanoes." *Earth and Planetary Science Letters, 117*, 619-635. Amsterdam, The Netherlands: Elsevier. TIC: 246239.

150228 Slate, J.L.; Berry, M.E.; Rowley, P.D.; Fridrich, C.J.; Morgan, K.S.; Workman, J.B.; Young, O.D.; Dixon, G.L.; Williams, V.S.; McKee, E.H.; Ponce, D.A.; Hildenbrand, T.G.; Swadley, W C; Lundstrom, S.C.; Ekren, E.B.; Warren, R.G.; Cole, J.C.; Fleck, R.J.; Lanphere, M.A.; Sawyer, D.A.; Minor, S.A.; Grunwald, D.J.; Laczniak, R.J.; Menges, C.M.; Yount, J.C.; Jayko, A.S.; Mankinen, E.A.; Davidson, J.G.; Morin, R.L.; and Blakely, R.J. 2000. *Digital Geologic Map of the Nevada Test Site and Vicinity, Nye, Lincoln and Clark Counties, Nevada, and Inyo County, California, Revision 4; Digital Aeromagnetic Map of the Nevada Test Site and Vicinity, Nye, Lincoln, and Clark Counties, Nevada, and Inyo County, California; and Digital Isostatic Gravity Map of the Nevada Test Site and Vicinity, Nye, Lincoln, and Clark Counties, Nevada, and Inyo County, California*. Open-File Report 99-554—A, —B, and —C. Denver, Colorado: U.S. Geological Survey. TIC: 248049; 251985; 251981.

101020 Smith, R.P.; Jackson, S.M.; and Hackett, W.R. 1996. "Paleoseismology and Seismic Hazards Evaluations in Extensional Volcanic Terrains." *Journal of Geophysical Research, 101*, (B3), 6277-6292. Washington, D.C.: American Geophysical Union. TIC: 238265.

179347 SNL 2007. *Redistribution of Tephra and Waste by Geomorphic Processes Following a Potential Volcanic Eruption at Yucca Mountain, Nevada*. MDL-MGR-GS-000006 REV 00. Las Vegas, Nevada: Sandia National Laboratories.

144352 Sparks, R.S.J.; Bursik, M.I.; Carey, S.N.; Gilbert, J.S.; Glaze, L.S.; Sigurdsson, H.; and Woods, A.W. 1997. *Volcanic Plumes*. 574. New York, New York: John Wiley & Sons. TIC: 247134.

138819 Stamatakos, J.A.; Connor, C.B.; and Martin, R.H. 1997. "Quaternary Basin Evolution and Basaltic Volcanism of Crater Flat, Nevada, from Detailed Ground Magnetic Surveys of the Little Cones." *Journal of Geology, 105*, 319-330. Chicago, Illinois: University of Chicago. TIC: 245108.

101027 Stock, J.M.; Healy, J.H.; Hickman, S.H.; and Zoback, M.D. 1985. "Hydraulic Fracturing Stress Measurements at Yucca Mountain, Nevada, and Relationship to the Regional Stress Field." *Journal of Geophysical Research, 90*, (B10), 8691-8706. Washington, D.C.: American Geophysical Union. TIC: 219009.

178150 Strong, M., and Wolff, J. 2003. "Compositional Variations within Scoria Cones." *Geology, 31*, (2), 143-146. Boulder, CO: Geological Society of America (GSA). TIC: 258339.

178124 Sumner, J.M. 1998. "Formation of Clastogenic Lava Flows During Fissure Eruption and Scoria Cone Collapse: The 1986 Eruption of Izu-Oshima Volcano, Eastern Japan." *Bulletin of Volcanology, 60*, 195-212. New York, New York: Springer-Verlag. TIC: 258365.

178125 Sumner, J.M.; Blake, S.; Matela, R.J.; and Wolff, J.A. 2005. "Splatter." *Journal of Volcanology and Geothermal Research, 142*, 49-65. New York, New York: Elsevier. TIC: 258351.

101029 Symonds, R.B.; Rose, W.I.; Bluth, G.J.S.; and Gerlach, T.M. 1994. "Volcanic-Gas Studies: Methods, Results, and Applications." Chapter 1 of *Volatiles in Magmas*. Carroll, M.J. and Holloway, J.R., eds. Reviews in Mineralogy Volume 30. Washington, D.C.: Mineralogical Society of America. TIC: 238061.

178126 Taddeucci, J.; Pompilio, M.; and Scarlato, P. 2004. "Conduit Processes During the July-August 2001 Explosive Activity of Mt. Etna (Italy): Inferences from Glass Chemistry and Crystal Size Distribution of Ash Particles." *Journal of Volcanology and Geothermal Research, 137*, 33-54. New York, New York: Elsevier. TIC: 258480.

175382 Taddeucci, J.; Spieler, O.; Kennedy, B.; Pompilio, M.; Dingwell, D.B.; and Scarlato, P. 2004. "Experimental and Analytical Modeling of Basaltic Ash Explosions at Mount Etna, Italy, 2001." *Journal of Geophysical Research, 109*, (B08203), 1-9. Washington, D.C.: American Geophysical Union. TIC: 257706.

174076 Thaden, R.E.; Santos, E.S.; and Raup, O.B. 1967. *Geologic Map of the Grants Quadrangle, Valencia County, New Mexico*. Map GQ-681. Washington, D.C.: U.S. Geological Survey. ACC: MOL.20050912.0101.

178151 Thorarinsson, S., Steinthorsson S., Einarsson Th., Kristmannsdottir, H., and Osk 1973. "The eruption on Heimaey, Iceland." *Nature, 241*, 372-375. London, England: Nature Publishing Group.

101030 Turrin, B.D.; Champion, D.; and Fleck, R.J. 1991. " $^{40}Ar/^{39}Ar$ Age of the Lathrop Wells Volcanic Center, Yucca Mountain, Nevada." *Science, 253*, (5020), 654-657. Washington, D.C.: American Association for the Advancement of Science. TIC: 225167.

177295 Valentine, G.A. 1987. "Stratified Flow in Pyroclastic Surges." *Bulletin of Volcanology, 49*, (4), 616-630. Berlin, Germany: Springer-Verlag. TIC: 258477.

107052 Valentine, G.A. and Groves, K.R. 1996. "Entrainment of Country Rock During Basaltic Eruptions of the Lucero Volcanic Field, New Mexico." *Journal of Geology, 104*, 71-90. Chicago, Illinois: University of Chicago Press. TIC: 246146.

177271 Valentine, G.A. and Harrington, C.D. 2006. "Clast Size Controls and Longevity of Pleistocene Desert Pavements at Lathrop Wells and Red Cone Volcanoes, Southern Nevada." *Geology, 34*, (7), 533-536. Boulder, Colorado: Geological Society of America. TIC: 258393.

177282 Valentine, G.A. and Krogh, K.E.C. 2006. "Emplacement of Shallow Dikes and Sills Beneath a Small Basaltic Volcanic Center - The Role of Pre-Existing Structure (Paiute Ridge, Southern Nevada, USA)." *Earth and Planetary Science Letters, 246*, 217-230. New York, New York: Elsevier. TIC: 258400.

177495 Valentine, G.A. and Perry, F.V. 2006. "Decreasing Magmatic Footprints on Individual Volcanoes in a Waning Basaltic Field." *Geophysical Research Letters, 33*, 1-5. Washington, D.C.: American Geophysical Union. TIC: 258439.

177782 Valentine, G.A.; Krier, D.; Perry, F.V.; and Heiken, G. 2005. "Scoria Cone Construction Mechanisms, Lathrop Wells Volcano, Southern Nevada, USA." *Geology, 33*, (8), 629-632. Boulder, Colorado: Geological Society of America. TIC: 258340.

177296 Valentine, G.A.; Palladino, D.M.; Agosta, E.; Taddeucci, J.; and Trigila, R. 1998. "Volcaniclastic Aggradation in a Semiarid Environment, Northwestern Vulcano Island, Italy." *Geological Society of America Bulletin, 110*, (5), 630-643. Boulder, Colorado: Geological Society of America. TIC: 258484.

101620 Vaniman, D. and Crowe, B. 1981. *Geology and Petrology of the Basalts of Crater Flat: Applications to Volcanic Risk Assessment for the Nevada Nuclear Waste Storage Investigations*. LA-8845-MS. Los Alamos, New Mexico: Los Alamos Scientific Laboratory. ACC: HQS.19880517.1541.

101031 Vaniman, D.T.; Crowe, B.M.; and Gladney, E.S. 1982. "Petrology and Geochemistry of Hawaiite Lavas from Crater Flat, Nevada." *Contributions to Mineralogy and Petrology, 80*, 341-357. Berlin, Germany: Springer-Verlag. TIC: 201799.

115585 Vergniolle, S. and Jaupart, C. 1986. "Separated Two-Phase Flow and Basaltic Eruptions." *Journal of Geophysical Research, 91*, (B12), 12,842-12,860. Washington, D.C.: American Geophysical Union. TIC: 239308.

112289 Wahl, R.R.; Sawyer, D.A.; Minor, S.A.; Carr, M.D.; Cole, J.C.; Swadley, W C; Laczniak, R.J.; Warren, R.G.; Green, K.S.; and Engle, C.M. 1997. *Digital Geologic Map Database of the Nevada Test Site Area, Nevada.* Open-File Report 97-140. Denver, Colorado: U.S. Geological Survey. TIC: 245880.

178061 Walker, G.P.L. 1973. "Lengths of Lava Flows." *Philosophical Transactions of the Royal Society of London. Series A, Mathematical and Physical Sciences, 274*, 107-118. London, England: Royal Society of London. TIC: 225821.

178457 Walker, G.P.L. 1999. "Volcanic Rift Zones and Their Intrusion Swarms." *Journal of Volcanology and Geothermal Research, 94,* 21-34. [New York, New York]: Elsevier. TIC: 258644.

107201 Wells, D.L. and Coppersmith, K.J. 1994. "New Empirical Relationships Among Magnitude, Rupture Length, Rupture Width, Rupture Area, and Surface Displacement." *Bulletin of the Seismological Society of America, 84*, (4), 974-1002. El Cerrito, California: Seismological Society of America. TIC: 226273.

107015 Wells, S.G.; Crowe, B.M.; McFadden, L.D.; Turrin, B.D.; Champion, D.E.; and Fleck, R.J. 1992. "Measuring the Age of the Lathrop Wells Volcanic Center at Yucca Mountain." *Science, 257*, 555-558. Washington, D.C.: American Association for the Advancement of Science. TIC: 225168.

178074 Wells, S.G.; Dohrenwend, J.C.; McFadden, L.D.; Turrin, B.D.; and Mahrer, K.D. 1985. "Late Cenozoic Landscape Evolution on Lava Flow Surfaces of the Cima Volcanic Field, Mojave Desert, California." *Geological Society of America Bulletin, 96*, (12), 1518-1529. Boulder, Colorado: Geological Society of America. TIC: 217544.

107208 Wells, S.G.; McFadden, L.D.; Renault, C.E.; and Crowe, B.M. 1990. "Geomorphic Assessment of Late Quaternary Volcanism in the Yucca Mountain Area, Southern Nevada: Implications for the Proposed High-Level Radioactive Waste Repository." *Geology, 18*, 549-553. Boulder, Colorado: Geological Society of America. TIC: 218564.

144406 Wells, S.G.; McFadden, L.D.; Renault, C.E.; and Crowe, B.M. 1991. "Reply on Geomorphic Assessment of Late Quaternary Volcanism in the Yucca Mountain Area, Southern Nevada: Implications for the Proposed High-Level Radioactive Waste Repository." *Geology, 19*, 661-662. Boulder, Colorado: Geological Society of America. TIC: 225179.

124930 White, J.D.L. 1991. "Maar-Diatreme Phreatomagmatism at Hopi Buttes, Navajo Nation (Arizona), USA." *Bulletin of Volcanology, 53*, (4), 239-258. Berlin, Germany: Springer-Verlag. TIC: 239072.

178127 Williams, R.S., Jr. and Moore, J.G. n.d. *Man Against Volcano: The Eruption on Heimaey, Vestmannaeyjar, Iceland.* Denver, Colorado: U.S. Geological Survey. ACC: MOL.20060905.0198.

101034 Wilson, L. and Head, J.W., III 1981. "Ascent and Eruption of Basaltic Magma on the Earth and Moon." *Journal of Geophysical Research, 86*, (B4), 2971-3001. Washington, D.C.: American Geophysical Union. TIC: 225185.

140956 Wohletz, K.H. 1986. "Explosive Magma-Water Interactions: Thermodynamics, Explosion Mechanisms, and Field Studies." *Bulletin of Volcanology, 48*, 245-264. Berlin, Germany: Springer-Verlag. TIC: 225183.

110071 WoldeGabriel, G.; Keating, G.N.; and Valentine, G.A. 1999. "Effects of Shallow Basaltic Intrusion into Pyroclastic Deposits, Grants Ridge, New Mexico, USA." *Journal of Volcanology and Geothermal Research, 92*, (3), 389-411. New York, New York: Elsevier. TIC: 246037.

162860 Wood, C.A. 1980. "Morphometric Analysis of Cinder Cone Degradation." *Journal of Volcanology and Geothermal Research, 8*, 137–160. Amsterdam, The Netherlands: Elsevier. TIC: 225186.

116536 Wood, C.A. 1980. "Morphometric Evolution of Cinder Cones." *Journal of Volcanology and Geothermal Research, 7*, 387-413. Amsterdam, The Netherlands: Elsevier. TIC: 225565.

178146 Wood, Y.A.; Graham, R.C.; Wells, S.G. 2002. "Surface Mosaic Map Unit Development for a Desert Pavement Surface." *Journal of Arid Environments, 52*, 305-317. Oxford, Great Britain: Elsevier Science Ltd. TIC: 258356.

178147 Wood, Y.A.; Graham, R.C.; Wells, S.G. 2005. "Surface Control of Desert Pavement Pedologic Process and Landscape Function, Cima Volcanic Field, Mojave Desert, California." *Catena, 59*, 205-230. Amsterdam, Netherlands: Elsevier BV. TIC: 258346.

163662 Woods, A.W.; Sparks, S.; Bokhove, O.; LeJeune, A-M.; Conner, C.B.; and Hill, B.E. 2002. "Modeling Magma-Drift Interaction at the Proposed High-Level Radioactive Waste Repository at Yucca Mountain, Nevada, USA." *Geophysical Research Letters, 29*, (13), 19-1 through 19-4. Washington, D.C.: American Geophysical Union. TIC: 254467.

162861 Wylie, J.J.; Helfrich, K.R.; Dade, B.; Lister, J.R.; and Salzig, J.F. 1999. "Flow Localization in Fissure Eruptions." *Bulletin of Volcanology, 60*, (8), 432–440. New York, New York: Springer-Verlag. TIC: 254054.

122589 Yoder, H.S., Jr. and Tilley, C.E. 1962. "Origin of Basalt Magmas: An Experimental Study of Natural and Synthetic Rock Systems." *Journal of Petrology, 3*, (3), 342-532. London, England: Oxford University Press. TIC: 247024.

108658 Zoback, M.L. and Zoback, M. 1980. "State of Stress in the Conterminous United States." *Journal of Geophysical Research, 85*, (B11), 6113-6156. Washington, D.C.: American Geophysical Union. TIC: 218504.

108617 Zreda, M.G.; Phillips, F.M.; Kubik, P.W.; Sharma, P.; and Elmore, D. 1993. "Cosmogenic ^{36}Cl Dating of a Young Basaltic Eruption Complex, Lathrop Wells, Nevada." *Geology, 21*, (1), 57-60. Boulder, Colorado: Geological Society of America. TIC: 225192.

8.2 CODES, STANDARDS, REGULATIONS, AND PROCEDURES

176544 10 CFR 63. Energy: Disposal of High-Level Radioactive Wastes in a Geologic Repository at Yucca Mountain, Nevada. Internet Accessible.

LS-PRO-0203, *Q-List and Classification of Structures, Systems, and Components.*

SCI-PRO-001, *Qualification of Unqualified Data.*

SCI-PRO-005, *Scientific Analyses and Calculations.*

IM-PRO-003, *Software Management.*

8.3 SOURCE DATA, LISTED BY DATA TRACKING NUMBER

147725 LA000000000099.002. Major Element, Trace Element, Isotopic, and Mineral Chemistry Data from Lathrop Wells. Submittal date: 08/02/1995.

162864 LA0302GH831811.002. Grain Size of Tephra from Tephra Deposits Around the Lathrop Wells Volcano, Nevada. Submittal date: 02/19/2003.

162865 LA0302GH831811.003. Lithic Clasts Measured at Lathrop Wells Cone, Nevada. Submittal date: 02/25/2003.

164026 LA0305DK831811.001. Locations and Thicknesses of Tephra (Ashfall) from Lathrop Wells Cone, Nevada. Submittal date: 05/09/2003.

171286 LA0306GH831811.001. SEM Photos-Types of Pyroclasts from Tephra Deposits Around the Lathrop Wells Volcano, Nevada. Submittal date: 06/16/2003.

178757 LA0609DK831811.001. Volumes of Lathrop Wells Volcano (Nevada) Cone, Lava Flows, and Tephra Sheet.

175064 MO0508SEPFEPLA.002. LA FEP List and Screening. Submittal date: 08/22/2005.

8.4 OUTPUT DATA, LISTED BY DATA TRACKING NUMBER

LA0612DK831811.001. Technical Product Output for ANL-MGR-GS-000002, Rev. 03.

8.5 SOFTWARE

Mastin, L.G. and Ghiorso, M.S. 2000. Conflow: A numerical model for conduit flow and thermodynamic open source code. U.S. Geologic Survey. Vancouver, WA. BSC SCM 611575.

INTENTIONALLY LEFT BLANK

APPENDIX A

QUALIFICATION OF INPUT DATA

APPENDIX A – QUALIFICATION OF INPUT DATA

External sources have provided unqualified data that have been used as direct input to this document. The inputs from these sources are qualified for intended use within the document using the criteria found in SCI-PRO-005, *Scientific Analyses and Calculations*. These criteria represent a subset of the methods and attributes required for qualification of data per SCI-PRO-001, *Qualification of Unqualified Data.* The following information is provided for each source: The full reference citation, a description of the data that were used from the source, and the extent to which the data demonstrate the properties of interest. In addition, one or more of the following criteria is also addressed:

- Reliability of data source
- Qualifications of personnel or organizations generating the data
- Prior uses of the data
- Availability of corroborating data.

The criteria described above meet the requirements of SCI-PRO-005, and are provided as justification that the data that have been used from these sources are considered qualified for intended use.

A.1 BLONG 1984

Reference–Blong, R.J. 1984 [DIRS 144263]. *Volcanic Hazards, A Sourcebook on the Effects of Eruptions.* Sydney, Australia: Academic Press. TIC: 247016.

Description of Use–Quaternary basalts of the Yucca Mountain region display textural and depositional facies that indicate a range of eruptive processes. Explosive processes, in which fragments, or clots, of melt were erupted in a stream of gas, are evidenced by the presence of scoria cones and remnants of ash fallout blankets. This reference is used as one of the sources of input for bulk in situ density of fallout deposits, setting a typical value of 1,000 kg/m^3.

Extent to which the Data Demonstrate the Properties of Interest–The calculations that are run to provide a feed to the TSPA require input values for the density of tephra deposits or settled ash. The values that are used from the Blong reference are recommended as one of two reasonable ways of treating these deposit densities, in that they are representative of a range of values. The range of values is compared with data from Sparks et al. (1997 [DIRS 144352]), which sets typical ranges from 300 kg/m^3 to 1,500 kg/m^3.

Qualifications of Personnel and Organizations Generating the Data–Emeritus Professor Russell Blong retired as Director of Risk Frontiers[1] in July 2003 after more than 30 years on the staff at Macquarie University.

[1] Risk Frontiers (formerly the Natural Hazards Research Centre) is regarded as a world leader in quantitative natural hazards risk assessment and risk management. Risk Frontiers, based at Sydney's Macquarie University, is a not-for-profit research organization sponsored by the Australian insurance community. For ten years, it has provided insurers with sophisticated research-based solutions. Other applications include emergency management, land use

Dr. Blong holds Masters degrees in Geography (Auckland) and Engineering Science and a Ph.D. in Geomorphology (Sydney). He has researched a wide range of natural hazards and their consequences including volcanic, earthquake, flood, and landslide hazards and their consequences in Australia, the South Pacific, and Asia. His other interests include building damage assessments, loss modeling, and integrated risk rating. He has published ten books and more than 200 research papers. He is a former president of the International Society for the Prevention and Mitigation of Natural Hazards (the Natural Hazards Society). One of his books on volcanic hazards is considered a sourcebook on volcanic risk. It is probably the most complete reference on volcanic hazards, including their effects on people, infrastructure, and economic activity.

A.2 JARZEMBA 1997

Reference–Jarzemba, M.S. 1997. "Stochastic Radionuclide Distributions After a Basaltic Eruption for Performance Assessments of Yucca Mountain." *Nuclear Technology, 118,* 132-141. [Hinsdale, Illinois]: American Nuclear Society. TIC: 237944. [DIRS 100460]

Description of Use–Section 6.3.4.4 discusses the potential eruption volume and duration. Jarzemba (1997 [DIRS 100460], p. 136) is the source for the log time values from eight different analogue volcanic eruptions from around the world. These values are presented in Table 6-9. Section 6.3.5.2 discusses potential pyroclast shape factors (F) used in clast dispersal calculations. Jarzemba (1997 [DIRS 100460], p. 139) used a value of F = 0.5 and that value is recommended here for TSPA calculations.

Extent to which the Data Demonstrate the Properties of Interest–Section 6.3.4.4 develops parameters that will be used to develop probability distributions for Eruptive Plume Dispersal calculations. The necessary inputs include the duration and power of explosive, eruptive events, as well as the mass discharge rates. Jarzemba (1997 [DIRS 100460]) provides values for duration and power from various volcanic eruptions around the world and is consistent with similar calculations being run for the NRC. Section 6.3.5.2 develops a clast shape factor for use in TSPA calculations of clast dispersal in the atmosphere. Jarzemba (1997 [DIRS 100460], p. 139) used a value of F=0.5, which is considered to be representative of the range of common clast shapes.

Qualifications of Personnel or Organizations Generating the Data and Prior Use of the Data–Southwest Research Institute provides technical support for NRC Yucca Mountain programs, thus the Institute can be considered to have the necessary credentials to provide qualified data. Studies have been underway by the DOE Yucca Mountain Project, as well as by the Center for Nuclear Waste Regulatory Analysis at the Southwest Research Institute, which provides technical support for NRC Yucca Mountain programs. This reference publishes some of the work that was conducted by Southwest Research Institute for the NRC. The referenced data have been acquired by Southwest Research Institute under contract to NRC. While the specific data (log time of the eruption duration) has not been specifically quoted by the NRC, this specific reference (Jarzemba 1997 [DIRS 100460]) is referred to by the NRC in "Issue

planning and floodplain management. As well as Australia, these tools are currently being used in Europe, North America, and Asia.

Resolution Status Report (Key Technical Issue: Igneous Activity, Revision 2)" (Reamer 1999 [DIRS 119693]).

Dr. Jarzemba earned his Ph.D. in 1993 in Nuclear Engineering and an undergraduate degree in Engineering Physics from Ohio State University. Dr. Jarzemba has over 15 years of research and professional experience. At the time of publication, Dr. Jarzemba was a research scientist with Southwest Research Institute. Dr. Jarzemba is the author and coauthor of numerous books and publications.

A.3 SISSON AND GROVE 1993

Reference–Sisson, T.W. and Grove, T.L. 1993. "Experimental Investigations of the Role of H_2O in Calc-Alkaline Differentiation and Subduction Zone Magmatism." *Contributions to Mineralogy and Petrology, 113,* 143-166. New York, New York: Springer-Verlag. TIC: 246909.

Description of Use–Section 6.3.2.4 presents an approach to determining the temperatures of magmas with elevated water content. Sisson and Grove (1993 [DIRS 122564]) is a source of an equation that represents their experimental work, which expresses the relationship between temperature and the weight percentage of water, pressure, and composition of magmas. This analysis uses this expression to determine the liquidus temperatures for Lathrop Wells magmas with different hypothetical water contents.

Extent to which the Data Demonstrate the Properties of Interest–Direct measurements of physical properties of erupting magma are difficult to obtain, especially in those magmas with elevated water content. Thus, although direct measurements are available for the low end of the spectrum of water content, experiments must be relied upon to constrain magmatic temperatures for magmas with water contents equivalent to the higher end of the potential range being evaluated in the Yucca Mountain region. The experimental results presented by Sisson and Grove (1993 [DIRS 144351]) provide a mathematical representation of temperature, and water content in magmas that are similar in composition to those seen at Lathrop Well volcano and other volcanism in the Yucca Mountain region.

Qualifications of Personnel and Organizations Generating the Data–Dr. Sisson earned his Ph.D. in Geology from the Massachusetts Institute of Technology and has over 25 years of professional and research experience. His current research includes the use of a high-temperature, high-pressure experimental laboratory to determine:

- The depths at which magmas are stored before eruptions
- How volatile concentrations influence eruption styles
- How magma ascent rates control the growth of gas bubbles that power explosive eruptions
- How magmas form by melting of diverse source-rocks.

Experimental and petrologic research led to his election in 2000 as a Fellow of the Mineralogical Society of America. In addition, he leads the Undersea Hazards of Hawaiian Volcanoes task, a collaborative effort between the U.S. Geological Survey and the Japan Marine Science and Technology Center to use deep-diving submersibles and remotely operated vehicles to understand the growth, deformation, and collapse of Earth's largest ocean island volcanoes. As task leader, he coordinates research efforts between United States and Japanese participants and guides research activities. Other research has been to study deep marine volcanic rocks that erupted early in the growth of Kilauea Volcano. Results bear on the melting processes that initiated growth of Kilauea, Earth's most active volcano, and on the stability of volcano flanks.

Dr. Grove holds a Ph.D in Geology from Harvard University. He has over thirty years of professional and research experience. Dr. Grove's research focus is on the processes that have led to the chemical differentiation of the crust and mantle of the Earth and on the processes of formation and evolution of the interiors of other planets, including the moon, Mars, and meteorite parent bodies. The development of new experimental techniques has allowed examination of the role of H_2O in magmatic processes. The results of the experiments are used with thermodynamic and kinetic theory to develop models of physical conditions and chemical exchange processes.

A.4 SPARKS, BURSIK, CAREY, GILBERT, GLAZE, SIGURDSSON, AND WOODS 1997

Reference–Sparks, R.S.J.; Bursik, M.I.; Carey, S.N.; Gilbert, J.S.; Glaze, L.S.; Sigurdsson, H.; and Woods, A.W. 1997. *Volcanic Plumes.* 574. New York, New York: John Wiley & Sons. TIC: 247134. [DIRS 144352]

Description of Use–Quaternary basalts of the Yucca Mountain region display textural and depositional facies that indicate a range of eruptive processes. Explosive processes, in which fragments, or clots, of melt were erupted in a stream of gas, are evidenced by the presence of scoria cones and remnants of ash fallout blankets. The Sparks et al. (1997 [DIRS 144352]) reference is used as one of the sources of input for bulk in situ density of fallout deposits, setting typical ranges from 300 kg/m^3 to 1,500 kg/m^3.

Extent to which the Data Demonstrate the Properties of Interest–The calculations that are run to provide a feed to the TSPA require input values for the density of tephra deposits or settled ash. The values that are used from Sparks et al. (1997, are recommended as one of two reasonable ways of treating these deposit densities, by providing a range of values. The range of values is compared with data from Blong (1984 [DIRS 144263]) that provide an approximation of 1,000 kg/m^3.

Qualifications of Personnel or Organizations Generating the Data and Prior Use of the Data–While the data (bulk in situ density of fallout deposits) has not been specifically quoted by the NRC, this specific reference (Sparks et al. 1997 [DIRS 144352]) is referred to by the NRC in "Issue Resolution Status Report (Key Technical Issue: Igneous Activity, Revision 2)" (Reamer 1999 [DIRS 119693]).

Dr. Sparks is currently Research Professor and Director of the Centre for Environmental and Geophysical Flows at the University of Bristol, U.K. His research interests are in volcano dynamics, igneous petrology, and application of fluid mechanics to understanding flow processes in the earth and the environment. Dr. Sparks authored and coauthored numerous books and articles on volcanology.

Dr. Bursik holds a Ph.D. in Geology, from the California Institute of Technology (1989). The title of his dissertation was *Volcanotectonic Evolution of the Mono Basin, Eastern California.* Dr. Bursik's currently serves as Professor, Department of Geology, State University of New York at Buffalo. His research is mostly in the area of geological fluid mechanics and surface processes. He is also interested in erosion in semiarid regions, landform change related to wildfires, growth of deltas, the hydraulics of the Niagara River, and the coupling between faulting and volcanism. His field areas include San Francisco Volcanic Field, Arizona; Mammoth Mountain-Mono Craters, California; Kamchatka, Russia, and Colima and Popocatepetl volcanoes, Mexico.

Dr. Carey holds a Ph.D in Geological Oceanography from University of Rhode Island (1983). He has over 29 years of research and professional experience. His current position is Professor of Oceanography at the Graduate School of Oceanography, University of Rhode Island. Dr. Carey's current research interests can be subdivided into three main areas, all of which are related to the study of explosive volcanism at convergent plate boundaries. The three areas include computer simulation of explosive eruption processes (tephra fallout and eruption column dynamics); the petrology and physical properties of magmas involved in explosive volcanism, and; the origin and characteristics of marine volcaniclastic sediments adjacent to island arcs and continental margins. Dr. Carey is also currently working on research projects in Indonesia (Krakatau volcano), Iceland, and the West Indies (Kick'em Jenny) volcano) where he uses subbottom geophysical surveys with CHIRP and bubble pulser systems together with gravity and SCUBA coring and ROVs to investigate the nature of volcaniclastic deposits on the seafloor.

Dr. Gilbert is a Senior Lecturer at the University of Lancaster, United Kingdom. Her main research interests include physical and chemical effects of volcanic ash on vegetation and soil; subglacial volcanism processes, products, and hazards; volcanic facies as indicators of climate change; and volcanic pollutant dispersal in the atmosphere. Dr. Gilbert has extensive fieldwork skills, as well as expertise in laboratory based volcanology experiments and analytical geochemistry and has authored and coauthored numerous peer-reviewed journal articles.

The other authors of this volume, Drs. L.S. Glaze, H. Sigurdsson, and A.W. Woods, each represent many years of experience in geoscience academics and research, including specific expertise in geophysics, geochemistry, and oceanography.

A.5 SYMONDS, ROSE, BLUTH, AND GERLACH 1994

Symonds, R.B.; Rose, W.I.; Bluth, G.J.S.; and Gerlach, T.M. 1994. "Volcanic-Gas Studies: Methods, Results, and Applications." Chapter 1 of *Volatiles in Magmas.* Carroll, M.J. and Holloway, J.R., eds. Reviews in Mineralogy Volume 30. Washington, D.C.: Mineralogical Society of America. TIC: 238061. [DIRS 101029]

Description of Use–This reference provides data tables containing gas concentrations from various convergent-plate (Table 3), divergent-plate (Table 4), and hot-spot (Table 5) volcanoes. The tables are a compilation of the study results performed by the authors and other volcanologists. The values of the gas concentrations (total of 88 sample analyses) listed in the tables have been used in the analysis report to arrive at the mean value, square root of the sum of the squares and the standard deviation of the tabulated concentrations (Table 6-4). As such, the gas analyses results listed in the reference are a direct input to the statistical measurements obtained in Section 6.3.2.3.

Extent to which the Data Demonstrate the Properties of Interest–The referenced gas concentrations from Symonds et al. 1994 [DIRS 101029], provide a range of gas compositions from a variety of volcanic centers from around the world. For the purpose of including hawaiite from Mount Etna; tholeiitic basalt from Momotombo, Poas, Kilauea, Ardoukoba, and Erta Ale; nephelenite from Nyiragongo; and alkali basalt from Surtsey. The data from these mafic centers are considered to be representative of a range of volcanism that may be analogous to potential volcanic activity in the Yucca Mountain region. The use of these data must suffice to constrain the relative proportions of major gas constituents in Yucca Mountain region basalts owing to the absence of current volcanic activity in the Yucca Mountain region from which gases could be directly sampled.

Qualifications of Personnel and Organizations Generating the Data–Dr. Symonds earned his Ph.D. and M.S. degrees in Geology from Michigan Technological University. He has over 20 years of research and professional experience in volcanology, including over 10 years experience as a research geologist with the United States Geological Survey, Cascade Volcano Observatory, Vancouver, Washington. At the time of publication, Dr. Symonds was a research scientist with the United States Geological Survey, Cascade Volcano Observatory. Dr. Symonds has authored and coauthored numerous peer reviewed professional articles on volcanology.

Dr. Rose has earned a B.A. and a Ph.D from Dartmouth College, in the field of Earth Sciences. With more than 30 years of professional experience and over 150 published papers on volcanic studies, Dr. Rose has investigated multispecies and regional gas measurements of volcanic emissions, ash/aerosol interactions, aircraft hazards, distal ash fallout patterns, quantitative retrievals of ash particles, and detection of ice in volcanic clouds. He developed the first methodology to use infrared satellite data for quantitative retrievals of ash particles, size, and cloud mass. Dr. Rose received the Bowen Award, presented by the Volcanology, Geochemistry, and Petrology Section of the American Geophysical Union in 2002.

Dr. Bluth holds a Ph.D in Geochemistry from Pennsylvania State University in addition to a B.A. in Geology and an M.S. in Geochemistry. Dr. Bluth has more than 15 years of professional experience, including the study of high-temporal resolution links between degassing and subsurface dynamics by merging of volcanic seismic and gas emission data for Montserrat Volcano, sponsored by the National Science Foundation (2003 to present), volcanic hazard studies in Guatemala (2001 to present). These studies focused on remote sensing evaluation of volcanic activity, ground-based gas and thermal measurements and the development algorithms and software interface to study volcanic hazards for the Pacific Disaster Center, in Maui, Hawaii. Dr. Bluth authored and coauthored numerous professional publications on volcanology and geologic sciences.

Dr. Gerlach earned his B.S. and M.S. in Geology from the University of Wisconsin, with emphasis on physics and geophysics. In 1974, he graduated from the University of Arizona with a Ph.D. in Geology. Dr. Gerlach has more than 30 years of professional experience, including 14 years as a member of the Volcano Emissions Project, which is headquartered at the Cascades Volcano Observatory. The position requires international leadership through scientific contributions on the geochemistry of volcanic gas emissions, their application in assessing volcano hazards, their relationship to magmatic and hydrothermal processes, and their impact on the atmosphere, climate change, ecosystems, and human health. Dr. Gerlach authored and coauthored numerous professional publications on volcanology and geologic sciences.

A.6 WILSON AND HEAD 1981

Wilson, L. and Head, J.W., III. 1981. "Ascent and Eruption of Basaltic Magma on the Earth and Moon." *Journal of Geophysical Research, 86,* (B4), 2971-3001. Washington, D.C.: American Geophysical Union. TIC: 225185. [DIRS 101034]

Description of Use–This reference provides equations and resulting plots used to estimate the:

- Ascent velocity of magma at depth were magma is under sufficient pressure where all volatiles are dissolved (Section 6.3.4.1)
- Density of the mixture of silicate melt and water vapor bubbles (Section 6.3.4.2)
- Velocity of the magma and magma pressure as a function of depth (Section 6.3.4.3).

The report contains a discussion of the development of the equations, as well as associated limitations and assumptions. The report was coauthored by Dr. Lionel Wilson, Lunar and Planetary Unit, Department of Environmental Sciences, University of Lancaster, Lancaster, LA1 4YQ, United Kingdom; and Dr. James W. Head III, Department of Geological Sciences, Brown University, Providence, Rhode Island.

Extent to which the Data Demonstrate the Properties of Interest–As discussed in Assumption 4, rising magma, composed of melt liquid and volatile gases, can be considered homogeneous and characterized by equilibrium between melt and exsolved volatiles, even though actual ascent velocities of melt and bubbles (exsolved volatiles) are different. Since a general theory for multiphase ascent of basaltic magmas that encompasses the potential range of magmas in the Yucca Mountain region is not yet available, Wilson and Head (1981 [DIRS 101034]) provide a mathematical approach to estimating ascent velocity for magma with varying range of initial water content (0% to 2+%). Utilizing this approach, this analysis extends those curves to include potential magmas containing up to 5% initial dissolved water content.

Qualifications of Personnel or Organizations Generating the Data–Dr. Lionel Wilson and Dr. James William Head, III, are internationally recognized scientists in the fields of volcanology and earth and planetary science. Both have authored and coauthored numerous books and professional papers related to their fields of expertise.

Dr. Wilson is Professor Emeritus of Earth and Planetary Sciences, Department of Environmental Science, Lancaster University, U.K. Dr. Wilson worked at Lancaster University from 1970

through 1997, and continues to occupy a one-quarter position, his main responsibility being to lead the Planetary Science Research Group. He also coedits *Journal of Volcanology and Geothermal Research.* In addition to his position at Lancaster University, Dr. Wilson holds positions at Brown University (Planetary Geosciences Group) and the Hawaii Institute of Geophysics and Planetology. He is on the Science Advisory Board for the Geophysics Department of the University of Alaska. He was elected (2004) as one of 41 distinguished scientists as a Fellow of the American Geophysical Union, the largest professional body for Geophysicists and earth-scientists in the world.

Dr. Head is a Louis and Elizabeth Scherck Distinguished Professor, Department of Geological Sciences, at Brown University, Providence, Rhode Island. He received his B.S. from Washington and Lee University (1964) and his Ph.D from Brown University (1969). From 1968 to 1972, Dr. Head worked for NASA and participated in the Apollo Lunar Exploration Program activities of landing site selection, astronaut field and science training, surface geologic traverse planning, mission operations, and data analysis. Over the past 25 years, he has served on numerous national and international committees concerned with the various aspects of earth and planetary science and space research.

A.7 STAMATAKOS, CONNOR, AND MARTIN

Reference–Stamatakos, J.A.; Connor, C.B.; and Martin, R.H. 1997. "Quaternary Basin Evolution and Basaltic Volcanism of Crater Flat, Nevada, from Detailed Ground Magnetic Surveys of the Little Cones." *Journal of Geology, 105,* 319-330. Chicago, Illinois: University of Chicago. TIC: 245108. [DIRS 138819]

Description of Use–Stamatakos et al. (1997 [DIRS 138819], pp. 322 and 328) estimate the dimensions and the amount of alluvium accumulation for the Little Cones. This estimate is used to determine the amount of the eruptive volume of the NE Little Cone, which is used to estimate the potential minimum eruption volume in the Yucca Mountain region.

Extent to which the Data Demonstrate the Properties of Interest–Section 6.3.4.4 discusses the potential distribution of the volume of material from eruptive volcanic cones in the Yucca Mountain region. The Little Cones at Crater Flats represent some of the most recent volcanism, and, because of their size, are used as an analogue for eruptive volume at the minimum end of the distribution. Studies of this volcanic complex have been underway by the DOE's Yucca Mountain Project, as well as by the Center for Nuclear Waste Regulatory Analysis at the Southwest Research Institute. The Center provides technical support for NRC Yucca Mountain programs and this reference publishes some of the work that was conducted under that program. The paper provides an estimate of the original dimensions and the amount of alluvium accumulation (25 m) of Little Cones that is combined with other data and observations to determine the distribution of this parameter that is used in other analyses of eruptive events.

Qualifications of Organizations Generating the Data and Prior Use of the Reference–Southwest Research Institute provides technical support for NRC Yucca Mountain programs, thus the Institute can be considered to have the necessary credentials to provide qualified data. Studies have been underway by the DOE Yucca Mountain Project, as well as by the Center for Nuclear Waste Regulatory Analysis at the Southwest Research Institute, which provides

technical support for NRC Yucca Mountain programs. This reference publishes some of the work that was conducted by Southwest Research Institute for the NRC. The referenced data have been acquired by Southwest Research Institute under an NRC contract. While the specific data (25 m of alluvium accumulation, 230-m diameter and 15-m height of Little Cone) has not been specifically quoted by the NRC, this specific reference (Stamatakos et al. 1997 [DIRS 138819]) is referred to by the NRC in "Issue Resolution Status Report (Key Technical Issue: Igneous Activity, Revision 2)" (Reamer 1999 [DIRS 119693]).

A.8 LANGE AND CARMICHAEL 1990; OCHS AND LANGE 1999

References–Lange, R.L. and Carmichael, I.S.E. 1990. "Thermodynamic Properties of Silicate Liquids with Emphasis on Density, Thermal Expansion and Compressibility." Chapter 2 of *Modern Methods of Igneous Petrology: Understanding Magmatic Processes.* Nicholls, J. and Russell, J.K., eds. Reviews in Mineralogy Volume 24. 25-64. Washington, D.C.: Mineralogical Society of America. TIC: 246394. [DIRS 147767]

Ochs, F.A., III and Lange, R.A. 1999. "The Density of Hydrous Magmatic Liquids." *Science, 283,* 1314-1317. Washington, D.C.: American Association for the Advancement of Science. TIC: 246639. [DIRS 144330]

Description of Use–Section 6.3.2.4 discusses the methods used to calculate estimated temperatures, viscosities, and densities of magmas with varying water contents. The two references listed above provided a method for calculation of magma density as a function of composition (including water content), pressure, and temperature. The approach used the formulation and data from Lange and Carmichael (1990 [DIRS 147767], Table 3) with additional data for H_2O (Ochs and Lange 1999 [DIRS 144330], p. 1,315). Equation 2 from Ochs and Lange (1999 [DIRS 144330], p. 1,315) produces the molar volume of the silicate liquid, which then requires a simple conversion to density.

Extent to which the Data Demonstrate the Properties of Interest–The two references discussed above provide a theoretical and mathematical approach to calculating densities of magmas. This analytical method represents the state of the art in understanding the relationship of chemical composition and other physical properties of basaltic magmas. The density calculations were based on the mean chemical composition of extruded materials from the Lathrop Wills cone, utilizing calculated temperatures and pressures that were also derived and discussed in Section 6.3.2.4. The calculations were run for a range of water contents from 0 wt% to 4 wt%.

Qualifications of Personnel and Organizations Generating the Data–Dr. Lange holds a Ph.D. in Geology from the University of California, Berkeley, and has over 15 years of professional and research experience. She currently holds the position of Associate Professor at the Department of Geological Sciences at the University of Michigan-Ann Arbor. Professor Lange's research involves field studies of volcanic rocks in Mexico, Wyoming, and California, as well as experimental studies on magmatic liquids at high temperatures and pressures. Current topics of study by Professor Lange and her research group include the:

- Origin of continental crust and its internal stratification; measurements of thermodynamic properties of magmatic liquids
- Entropy and volume of solution of H_2O in silicate melts
- Phase equilibria of hydrous basalts in the lower crust
- Argon age-dating chronology
- Geographic Information Systems methods applied to quantifying eruption rates at continental arcs
- Acoustic interferometry applied to silicate melts at high temperatures and pressures.

Dr. Ian Carmichael earned his Ph.D. in Geology at Imperial College of Science, University of London, and has over 50 years of professional and research experience in the field of igneous petrology. He is currently Professor at the Department of Earth and Planetary Science, University of California, Berkeley, where he has been associated since 1964. He is internationally recognized as one of the leading experts in the field of igneous petrology and his textbooks are used widely within the field. Dr. Carmichael has authored and coauthored over 150 peer-reviewed journal articles and books.

Mr. Ochs completed his M.A. in Geology in 1996 at the University of Michigan-Ann Arbor, where he was a graduate student studying with Dr. Lange.

Reliability of Data Source–Lange and Carmichael (1990 [DIRS 147767]) appear as Chapter 2 of *Modern Methods of Igneous Petrology: Understanding Magmatic Processes*, which is the 24th volume of a collection of journal articles and monographs published in conjunction with a series of short courses sponsored by the Mineralogical Society of America. Referred to as the Reviews in Mineralogy Series, Volume 24 represents the seventeenth year of published material accompanying courses in the subjects of mineralogy, petrology, crystallography, and geochemistry. The courses are conducted in conjunction with annual meetings of professional organizations such as the Geological Society of America and the American Geophysical Union. The editors of the volume, in addition to their own reviews and feedback to authors, also manage the peer review process.

The findings of the Ochs and Lange (1999 [DIRS 144330]) research, undertaken at University of Michigan-Ann Arbor, were reported in *Science,* which is published by the American Association for the Advancement of Science. Science is a weekly journal that publishes significant original scientific research, plus reviews and analyses of current research and science policy. All articles published in *Science* are peer reviewed and are expected to present important new research results of broad significance and must meet stringent guidelines published by the editors. The American Association for the Advancement of Science is an international non-profit organization dedicated to advancing science around the world by serving as an educator, leader, spokesperson and professional association. In addition to organizing membership activities, AAAS publishes the journal *Science*, as well as many scientific newsletters, books, and reports, and spearheads programs that raise the bar of understanding for science worldwide. Founded in

1848, American Association for the Advancement of Science serves some 262 affiliated societies and academies of science, serving 10 million individuals. *Science* has the largest paid circulation of any peer-reviewed general science journal in the world.

A.9 SHAW 1972

Reference–Shaw, H.R. 1972. "Viscosities of Magmatic Silicate Liquids: An Empirical Method of Prediction." *American Journal of Science, 272,* 870-889. New Haven, Connecticut: Yale University, Kline Geology Laboratory. TIC: 246470. [DIRS 126270]

Description of Use–Section 6.3.2.4 discusses the methods used to calculate estimated temperatures, viscosities, and densities of magmas of similar chemical compositions, with varying water contents. In addition to the other physical properties, the hypothetical compositions and calculated temperatures were used to calculate bubble- and crystal-free viscosity using an approach described in the Shaw reference.

Extent to which the Data Demonstrate the Properties of Interest–Direct measurements of physical properties of erupting magma are difficult to obtain, especially in those magmas with water content at the higher end of the range projected for magmas in the Yucca Mountain region. Thus, experiments and calculated values must be relied upon to constrain the physical properties for magmas being evaluated in this analysis report. The method outlined by Shaw provides an approach for calculating viscosity of multi-component anhydrous silicate liquids using four partial molar coefficients of silica.

Reliability of Data Source– Shaw, a staff member of the U.S. Geological Survey at the time of this 1972 publication, presented his method for calculating viscosity of silicate magmas in the American Journal of Science. Founded in 1818, the American Journal of Science is the oldest scientific journal in the United States that has been published continuously. The Journal is devoted to geology and related sciences and publishes articles from around the world presenting results of major research from all earth sciences. All articles are subject to peer review prior to publication. Readers are primarily earth scientists in academia and government institutions from around the world.

A.10 JAUPART AND TAIT 1990

Reference–Jaupart, C. and Tait, S. 1990. "Dynamics of Eruptive Phenomena." Chapter 8 of *Modern Methods of Igneous Petrology: Understanding Magmatic Processes.* Nicholls, J. and Russell, J.K., eds. Reviews in Mineralogy Volume 24. 213-238. Washington, D.C.: Mineralogical Society of America. TIC: 246394. [DIRS 118292]

Description of Use–This analysis report uses Jaupart and Tait (1990 [DIRS 118292]) as a source for an equation that represents the solubility of water in basaltic magmas, as related to pressure. The saturation pressures that are derived from this equation are then used as part of the analysis that provides an estimate of multi-phase saturation.

Extent to which the Data Demonstrate the Properties of Interest–Section 6.3.2.4 discusses the methods used to calculate estimated temperatures, viscosities, and densities of magmas with varying water contents. To complete the calculations of these physical properties, values for

saturation pressure were required for varying weight percent of water. The Jaupart and Tait (1990 [DIRS 118292]) reference provides simplified expressions of the solubility of gases in silicate melts, including water in basalt. They state that the simplified equations relating water solubility to pressure only are sufficient for use in systems of low concentrations of water. The expression is judged sufficient for the use in this report, which is calculating saturated pressures for water contents from 1 wt% to 4 wt%.

Reliability of Data Source–The Jaupart and Tait (1990 [DIRS 118292]) reference appears as Chapter 8 of *Modern Methods of Igneous* Petrology*: Understanding Magmatic Processes*, which is the 24th volume of a collection of journal articles and monographs published in conjunction with a series of short courses sponsored by the Mineralogical Society of America. Referred to as the Reviews in Mineralogy Series, Volume 24 represents the seventeenth year of published material accompanying courses in the subjects of mineralogy, petrology, crystallography, and geochemistry. The courses are conducted in conjunction with annual meetings of professional organizations such as the Geological Society of America and the American Geophysical Union. The editors of the volume, in addition to their own reviews and feedback to authors, also manage the peer review process of all materials that are published in these volumes. These volumes are considered by the scientific community to represent the current state of knowledge in the various disciplines.

A.11 WOOD 1980

Reference–Wood, C.A. 1980. "Morphometric Evolution of Cinder Cones." *Journal of Volcanology and Geothermal Research, 7,* 387-413. Amsterdam, The Netherlands: Elsevier. TIC: 225565. [DIRS 116536]

Description of Use–The data compiled and published by Wood (1980 [DIRS 116536]) were used in formulating the values used for eruption duration for explosive eruptions that form scoria cones. The range reported by Wood gives a duration of 1 day to 15 years, with a median value of 50 days. The data presented in the Wood article are also used to estimate the duration of the cone-forming eruption at Lathrop Wells, which has volcanological characteristics consistent with other Quaternary volcanoes of the Yucca Mountain region.

Extent to which the Data Demonstrate the Properties of Interest–This reference provides data on the duration of eruption as related to volcanic cone height and estimated cone volume for twelve cones from around the world that have formed through explosive eruption. Based on these observations of rates of cone growth as a function of time, a cone the size as that at the Lathrop Wells volcano (140-m high, 0.018-km^3 volume) might have formed over a period between about 2 days and 21 days.

Qualifications of Personnel and Organizations Generating the Data–Dr. Wood (University of North Dakota.) is a volcanologist with 25 years of experience using remote sensing and other techniques to study volcanoes. His Ph.D is in Planetary Science (Brown University, 1979). In addition to having published 180 professional papers and abstracts on volcanoes and other geologic topics he is a member of the NASA EOS Interdisciplinary Team on Volcanology and a volcano Principle Investigator on the SIR-C Shuttle radar mission. His current position is Professor and Chair at Department of Space Studies, University of North Dakota, Grand Forks.

APPENDIX B

ADDRESSING YMRP ACCEPTANCE CRITERIA

APPENDIX B – ADDRESSING YMRP ACCEPTANCE CRITERIA

The following information describes how this analysis addresses *Yucca Mountain Review Plan, Final Report* (YMRP) (NRC 2003 [DIRS 163274], Sections 1.5.3, 2.2.1.3.2.3, 2.2.1.3.10.3, and 2.2.1.3.11.3) acceptance criteria. Only those acceptance criteria that are applicable to this report (see Section 4.2) are discussed. In most cases, the applicable acceptance criteria are not addressed solely by this report; rather, the acceptance criteria are fully addressed when this report is considered in conjunction with other analysis and model reports that describe igneous FEPs. Where a sub-criterion includes several components, only some of those components may be addressed, and are included here.

B.1 DESCRIPTION OF SITE CHARACTERIZATION WORK CRITERIA

YMRP (NRC 2003 [DIRS 163274], Section 1.5.3), Acceptance Criteria:

Acceptance Criterion 1: **The "General Information" section of the License Application contains an adequate description of Site Characterization activities.**

1. An adequate overview is provided of the site characterization activities related to geology; hydrology; geochemistry; geotechnical properties and conditions of the host rock; climatology, meteorology, and other environmental sciences; and the reference biosphere.

   Field studies and analyses were conducted in the Yucca Mountain region to characterize the geology and volcanic activity. Results of field studies, available data in literature sources, external reviews, and expert elicitation were used to develop parameter values and distributions that can be used to model processes of the shallow subsurface and surface volcanic activity relevant to a repository at Yucca Mountain. Characteristics of eruptive conduits, dike widths, dike swarms, and dike-induced earthquakes are described in Sections 6.3.3.1 and 6.3.3.2. Characteristics of igneous material (magma chemistry and magma physical properties) are described in Section 6.3.2. Eruptive processes, including magma ascent rate, volatile exsolution and fragmentation, velocity as a function of depth above exsolution depth, eruption volume and duration, entrainment of wall rock and repository materials in ascending magma, and characteristics of Strombolian and violent Strombolian eruption deposits, are described in Section 6.3.4. Uncertainties are described in Sections 6.5, and 7.

Acceptance Criterion 2: The "General Information" section of the license application contains an adequate description of site characterization results.

1. A sufficient understanding is provided of current features and processes present in the Yucca Mountain region.

   This report provides basic descriptive information about the volcanic eruptive products and processes that resulted in the surface deposition of the scoria cone, lava flows, and tephra fall associated with the Lathrop Wells volcano (Section 6.3; Appendix C). The Lathrop Wells volcano is the youngest volcanic expression known in the Yucca Mountain region and is considered to exemplify the type of eruptive phenomena that

would occur during a future eruption of basaltic magma in the region. The Lathrop Wells volcano is the southernmost surface expression of the Crater Flat Volcanic Zone, which, in large part, defines the probabilistic volcanic hazard for the repository (*Characterize Framework for Igneous Activity at Yucca Mountain, Nevada,* BSC 2003 [DIRS 169989], Section 6.4.1.5). The eruptive volumes of scoria (cone), lava, and tephra are used to develop parameter values and distributions for use in the model report *Atmospheric Dispersal and Deposition of Tephra from a Potential Volcanic Eruption at Yucca Mountain, Nevada* (BSC 2005 [DIRS 174067]). The eruptive processes at Lathrop Wells volcano, as inferred from analysis of lithologies preserved in the cone and tephra sheet, help define the processes of mass ejection from the volcanic vent for both proximal (ballistic) and distal (ash cloud) distances. Further, this report defines properties of magma that directly influence the interaction of a magma-filled dike(s) with a subsurface repository that are direct inputs to TSPA.

2. Adequate information is provided for evolution of future events and processes likely to be present in the Yucca Mountain region that could affect repository safety.

   This report provides basic descriptive information about the volcanic eruptive processes that are characteristic of the Yucca Mountain region, as exemplified by features observed at Lathrop Wells volcano (Section 6; Appendix C). Parameter values are developed for use in models of igneous processes or as inputs to TSPA-LA models that support the analysis of the direct-release and indirect-release volcanic scenarios. The report identifies information that has been collected from the Yucca Mountain region, as well as information developed from studies at analog sites or developed from the review of published literature. The report also provides the technical basis for the use of the Lathrop Wells volcanic center as the most appropriate analog for a future volcanic eruption through the repository at Yucca Mountain.

B.2 MECHANICAL DISRUPTION OF ENGINEERED BARRIERS

YMRP (NRC 2003 [DIRS 163274], Section 2.2.1.3.2.3) Acceptance Criteria

Acceptance Criterion 1: System Description and Model Integration Are Adequate.

1. Total system performance assessment adequately incorporates important design features, physical phenomena, and couplings, and uses consistent and appropriate assumptions throughout the mechanical disruption of engineered barrier abstraction process.

   This analysis report describes physical phenomena associated with magmatic intrusion into and volcanic eruption through a repository. It lists appropriate assumptions, parameter values, and distributions that directly or indirectly influence that type of disruption. The values provided are to be used appropriately and consistently throughout analyses of the mechanical disruption of engineered barriers, although no specific analyses of potential disruptions are given in this report. This report provides the technical basis for the parameters, assumptions, and conceptual models used in modeling magmatic intrusion and volcanic eruption at the proposed repository given in *Dike/Drift Interactions* (BSC 2004 [DIRS 170028]) and *Atmospheric Dispersal and Deposition of*

Tephra from a Potential Volcanic Eruption at Yucca Mountain, Nevada (BSC 2005 [DIRS 174067]).

2. The description of geological and engineering aspects of design features, physical phenomena, and couplings, that may affect mechanical disruption of engineered barriers, is adequate. For example, the description may include materials used in the construction of engineered barrier components, environmental effects (e.g., temperature, water chemistry, humidity, radiation, etc.) on these materials, and mechanical-failure processes and concomitant failure criteria used to assess the performance capabilities of these materials. Conditions and assumptions in the abstraction of mechanical disruption of engineered barriers are readily identified and consistent with the body of data presented in the description.

   Descriptions of geologic aspects of igneous and volcanic phenomena are provided in this report, including basic physical descriptions of magmatic transport in subsurface and surface environments. The physical and chemical characteristics of Quaternary basalt magma are discussed in Section 6.3. Characteristics of shallow intrusive features are provided in Section 6.3.3. Magmatic pressures, volatile content and exsolution, temperatures, and densities are discussed in Section 6.3.4. Descriptions of analogue volcanoes, including aspects of their subsurface plumbing (dikes and conduits) are in Sections 6.3.3.1 and 6.3.3.3 and in Appendices C, D, E, and F). Surface and near-surface phenomena associated with eruption are given in Section 6.3.4. Finally, Section 6.3.5 discusses the characteristics of Strombolian and violent Strombolian eruptions.

Acceptance Criterion 2: Data Are Sufficient for Model Justification.

1. Not applicable to this report. Geological and engineering values, used in the license application to evaluate mechanical disruption of engineered barriers, are adequately justified. Adequate descriptions of how the data were used, interpreted, and appropriately synthesized into the parameters are provided.

2. Sufficient data have been collected on the geology of the natural system, engineering materials, and initial manufacturing defects, to establish initial and boundary conditions for the total system performance assessment abstraction of mechanical disruption of engineered barriers.

   Geological and physical volcanological descriptions of analogue volcanoes (natural systems) in the Yucca Mountain region are given in this analysis report. The analogue descriptions (Appendices C, D, E, and F), the physical and mathematical descriptions of magmas and magmatic processes (Sections 6.3.3 and 6.3.4), and the parameter values and distributions of volcanic phenomena (Section 7.1, developed in Section 6) provide information to help establish initial and boundary conditions to the total system performance assessment abstraction of the mechanical disruption of engineered barriers.

3. Data on geology of the natural system, engineering materials, and initial manufacturing defects, used in the total system performance assessment abstraction, are based on appropriate techniques. These techniques may include laboratory experiments, site-

specific field measurements, natural analog research, and process-level modeling studies. As appropriate, sensitivity or uncertainty analyses used to support the DOE total system performance assessment abstraction are adequate to determine the possible need for additional data.

The data presented in this report include descriptions, and parameter values and distributions for volcanic phenomena in Section 6 and Appendices C, D, E, and F. The data were developed from relevant scientific literature and from past and recent field studies of natural analogue volcanoes that form the basis of the volcanological hazard for the Yucca Mountain repository. Field studies have been documented in scientific notebooks under approved quality assurance procedures and are summarized in Appendices C, D, E, and F. The physical and chemical characteristics of Quaternary basalt magma are discussed in Section 6.3.2. Characteristics of shallow intrusive features and provided in Section 6.3.3, as well as in Appendix F. Magmatic pressures, volatile content and exsolution, temperatures, and densities are discussed in Section 6.3.4.

B.3 DESCRIPTION OF VOLCANIC DISRUPTION OF WASTE PACKAGES CRITERIA

YMRP (NRC 2003 [DIRS 163274, Section 2.2.1.3.10.3), Acceptance Criteria:

Acceptance Criterion 1: System description and model integration are adequate.

1. Total system performance assessment adequately incorporates important design features, physical phenomena, and couplings, and uses consistent and appropriate assumptions throughout the volcanic disruption of the waste package abstraction process.

   This report provides basic descriptive information about the volcanic eruptive processes that are characteristic of the Yucca Mountain region, as exemplified by features observed at Lathrop Wells volcano (Section 6.3; Appendix C). Parameter values are developed for use in models of igneous processes or as inputs to TSPA-LA models that support the analysis of the direct-release and indirect-release volcanic scenarios. This report describes the basis for the parameters used in such models (e.g., *Dike/Drift Interactions* (BSC 2004 [DIRS 170028]), but does not perform the waste package abstraction process.

2. Models used to assess volcanic disruption of waste packages are consistent with physical processes generally interpreted from igneous features in the Yucca Mountain region and/or observed at active igneous systems.

   This report provides basic descriptive information about the volcanic eruptive processes that are characteristic of the Yucca Mountain region, as exemplified by features observed at Lathrop Wells volcano (Section 6.3; Appendix C). Parameter values are developed for use in models of igneous processes or as inputs to TSPA-LA models that support the analysis of the direct-release and indirect-release volcanic scenarios. Chemical characteristics of igneous material are described in Section 6.3.2. Characteristics of eruptive conduits, dike widths, dike swarms, and dike-induced

earthquakes are described in Section 6.3.3. The processes associated with volcanic eruptions are described in Section 6.3.4, and processes that might entrain radioactive waste in eruption products are described in Section 6.3.4.5. Finally, ash plumes and associated deposits are described in Section 6.3.5. The report describes the basis for the parameters used in the volcanic scenarios and traces the outputs forward into analyses that use these parameters. The report identifies information that has been collected from the Yucca Mountain region, as well as information developed from studies at analog sites or developed from the review of published literature. The report also provides the technical basis for the use of the Lathrop Wells volcanic center as the most appropriate analog for a future volcanic eruption through the repository at Yucca Mountain. A potential eruption scenario at the Yucca Mountain repository is described in Section 6.4.

3. Models account for changes in igneous processes that may occur from interactions with engineered repository systems.

   Not applicable. This report does not address changes in igneous processes that might occur as a result of interactions with engineered repository systems. Possible changes have been analyzed and documented in *Dike/Drift Interactions* (BSC 2004 [DIRS 170028]).

4. Guidance in NUREG-1297 and NUREG-1298 (Altman et al. 1988 [DIRS 103597]; 1988 [DIRS 103750]) or other acceptable approaches is followed.

   External sources have been used as direct input to this document. The inputs from these sources are qualified for intended use within the document using the criteria found in SCI-PRO-005. These criteria represent a subset of the methods and attributes required for qualification of data per SCI-PRO-001. These methods and attributes are based on those that are presented in NUREG-1298 (Altman et al. 1988 [DIRS 103750]), which are meant to provide "the level of confidence in the data … commensurate with their intended use."

   The data contained in DTN: LA000000000099.002 [DIRS 147725], Major Element, Trace Element, Isotopic, and Mineral Chemistry Data from Lathrop Wells, were qualified in *Final Report on Qualification of Volcanism Isotope, Trace-element, and Halogen Data Using Procedure YAP-SIII.1Q/REV 3/ICN 0 {Qualification of Unqualified Data}* (CRWMS M&O 1999 [DIRS 170965]).

   The requirements, methods and, attributes for qualification of unqualified data, as outlined in the two procedures discussed above, are based on the guidance that is presented in NUREG 1298.

Acceptance Criterion 2: Data are sufficient for model justification.

1. Parameter values used in the license application to evaluate volcanic disruption of waste packages are sufficient and adequately justified. Adequate description of how the data were used, interpreted, and appropriately synthesized into the parameters is provided.

Section 6.3 provides basic descriptive information about the volcanic eruptive processes that are characteristic of the Yucca Mountain region. The report describes the synthesis of the information and basis for parameter values that are used to model igneous processes and inputs to TSPA-LA models that support the analysis of the direct-release and indirect-release volcanic scenarios. The report also traces the parameter outputs forward into analyses and models that use these parameters. A potential eruption scenario at the Yucca Mountain repository is described in Section 6.4.

2. Data used to model processes affecting volcanic disruption of waste packages are derived from appropriate techniques. These techniques may include site-specific field measurements, natural analog investigations, and laboratory experiments.

   The report identifies information that has been collected from site-specific field measurements in the Yucca Mountain region as well as information that has been developed from studies at analog sites or developed from the review of published literature. Data have also been obtained from samples collected and analyzed by procedures governed by a strict quality assurance program. Data, parameters, and other inputs are described in Section 4.1. A potential eruption scenario at the Yucca Mountain repository is described in Section 6.4. Data uncertainties for inputs to, and outputs from, this analysis and limitations on use of outputs are described in detail in Sections 6.5, 7.1, and 7.2. The report also provides the technical basis for the Lathrop Wells volcanic center being the most appropriate analog for a future volcanic eruption through the repository at Yucca Mountain.

3. Sufficient data are available to integrate features, events, and processes relevant to the volcanic disruption of waste packages into process-level models, including determination of appropriate interrelationships and parameter correlations.

   The report identifies information that has been collected from the Yucca Mountain region as well as information that has been developed from studies at analog sites or developed from the review of published literature. FEPs relevant to this analysis are discussed in Section 6.2. These FEPs have guided the approach to field observation and collection/analysis of appropriate samples and sample parameters. Sufficient data are collected to help integrate the relevant FEPs into process-level models (Section 4.1). The report describes the relevant eruptive processes and describes the development of parameters based on the integration of those FEPs. Characteristics of igneous material are described in Section 6.3.2. Relationships between various magma characteristics and their effects on an eruption are described in Section 6.3.4. Processes related to entrainment of waste in an ascending magma are described in Section 6.3.4.5, and ash plumes and their deposits are discussed in Section 6.3.5. The physical volcanology of the Lathrop Wells volcano and its suitability as an analog for a future eruption through the repository are discussed in Appendix C. A potential eruption scenario at the Yucca Mountain repository is described in Section 6.4. Process-level models that use the parameters developed from these processes are described in other reports (e.g., *Dike/Drift Interactions* (BSC 2004 [DIRS 170028]). Output parameters from this analysis and associated uncertainties are described in

Sections 7.1 and 7.2. Interrelationships and correlations between parameters are described in Section 6.

4. Where sufficient data do not exist, the definition of parameter values and associated uncertainty is based on appropriate use of expert elicitation, conducted in accordance with NUREG-1563 (Kotra et al. 1996 [DIRS 100909]). If other approaches are used, the U.S. Department of Energy adequately justifies their use.

   The dike length distribution developed from analogue volcanoes in the Yucca Mountain region was used as input to the calculation in Section 6.3.3.2.

B.4 DESCRIPTION OF AIRBORNE TRANSPORT OF RADIONUCLIDES CRITERIA

YMRP (NRC 2003 [DIRS 163274], Section 2.2.1.3.11.3), Acceptance Criteria

Acceptance Criterion 1: System description and model integration are adequate.

1. Total system performance assessment adequately incorporates important design features, physical phenomena, and couplings and uses consistent and appropriate assumptions throughout the airborne transport of radionuclides abstraction process.

   This analysis report develops parameter values and distributions that directly or indirectly influence the airborne transport of radionuclide particles via surface volcanic eruption of basaltic magma after intersection with the waste-packages-filled drifts. This report provides the technical basis for the parameters, assumptions, and conceptual models used in modeling the airborne transport of radionuclides in *Atmospheric Dispersal and Deposition of Tephra from a Potential Volcanic Eruption at Yucca Mountain, Nevada* (BSC 2005 [DIRS 174067]).

2. Models used to assess airborne transport of radionuclides are consistent with physical processes generally interpreted from igneous features in the Yucca Mountain region and/or observed at active igneous systems.

   Physical processes of eruption and emplacement of basaltic particulate matter are described in this report. Parameters that define many aspects of the processes and resulting deposits are developed for use in downstream models used to assess the airborne transport of radionuclides. The report provides basic descriptive information about the volcanic eruptive processes that are characteristic of the Yucca Mountain region, as exemplified by features observed at Lathrop Wells volcano. Characteristics of eruptive conduits, dike widths, and dike swarms are described in Sections 6.3.3.1 and 6.3.3.3. Chemical characteristics of igneous material are described in Section 6.3.2. The processes associated with volcanic eruptions are described in Section 6.3.4, and processes that could entrain radioactive waste in eruption products are described in Section 6.3.4.5. Finally, ash plumes and associated deposits are described in Section 6.3.5. The report carefully identifies information that has been collected from the Yucca Mountain region as well as information developed from studies at analog sites or developed from the review of published literature. A

potential eruption scenario at the Yucca Mountain repository is described in Section 6.4. The report also provides the technical basis for the use of the Lathrop Wells volcanic center as the most appropriate analog for a future volcanic eruption through the repository at Yucca Mountain (Appendix C).

3. Models account for changes in igneous processes that may occur from interactions with engineered repository systems.

   This report discusses ash particle sizes as measured from the tephra deposit from the Lathrop Wells volcano (Appendix C) and from several historical eruptions (Section 6.3.5.1). Section 6.3.4.5 describes processes that could entrain radioactive waste in eruption products after interaction with the engineered repository. The range in ash particle sizes provides the input for incorporating waste particles within the eruption column that is described and modeled in *Atmospheric Dispersal and Deposition of Tephra from a Potential Volcanic Eruption at Yucca Mountain, Nevada* (BSC 2005 [DIRS 174067]). Physical properties of eruptions that may lead to variations in the eruptive dispersal and deposition of ash and waste particles are addressed in this report, including magma velocity above the vesiculation depth, variable volatile content of magma and its effects on velocity of magma ascent, conduit diameter, and a range of possible mass discharge rates that affect ash column characteristics. Interactions of a dike of ascending magma with engineered repository design features, including drifts, waste packages, and waste form are discussed in *Dike/Drift Interaction* (BSC 2004 [DIRS 170028]).

4. Guidance in NUREG-1297 and NUREG-1298 (Altman et al. 1988 [DIRS 103597]; 1988 [DIRS 103750]) or in other acceptable approaches for peer review and data qualifications is followed.

   Data used to develop parameter values and distributions for output from this report were qualified for intended use (Section 4 and Appendix A).

Acceptance Criterion 2: Data are sufficient for model justification.

1. Parameter values used in the license application to evaluate airborne transport of radionuclides are sufficient and adequately justified. Adequate description of how the data were used, interpreted, and appropriately synthesized into the parameters is provided.

   This report provides basic descriptive information about the volcanic eruptive processes that are characteristic of the Yucca Mountain region. This report provides the technical basis for the parameters used in modeling the airborne transport of radionuclides in *Atmospheric Dispersal and Deposition of Tephra from a Potential Volcanic Eruption at Yucca Mountain* (BSC 2005 [DIRS 174067]). A potential eruption scenario at the Yucca Mountain repository that might result in airborne transport of radionuclides is described in Section 6.4. The report also traces the parameter outputs forward into analyses that use these parameters.

2. Data used to model processes affecting airborne transport of radionuclides are derived from appropriate techniques. These techniques may include site-specific field measurements, natural analog investigations, and laboratory experiments.

   The report identifies information that has been collected from site-specific field measurements in the Yucca Mountain region as well as information that has been developed from the studies at analog sites or developed from the review of published literature (Section 6.3). A potential eruption scenario at the Yucca Mountain repository is described in Section 6.4. Data uncertainties for inputs to, and outputs from, this analysis and limitations on use of outputs are described in detail in Sections 6.5, 7.1 and 7.2. The report also provides the technical basis for the Lathrop Wells volcanic center being the most appropriate analog for a future volcanic eruption through the repository at Yucca Mountain.

3. Sufficient data are available to integrate features, events, and processes relevant to the airborne transport of radionuclides into process-level models, including determination of appropriate interrelationships and parameter correlations.

   The report identifies information that has been collected from site-specific field measurements in the Yucca Mountain region as well as information that has been developed from studies at analog sites or developed from the review of published literature (Sections 4 and 6). FEPs relevant to this analysis are discussed in Section 6.2. The report describes the relevant eruptive processes and describes the development of parameters based on the integration of those processes. Characteristics of igneous material are described in Section 6.3.2. Relationships between various magma characteristics and their effects on an eruption are described in Section 6.3.4. Processes related to entrainment of waste in an ascending magma are described in Section 6.3.4.5, and ash plumes and their deposits are discussed in Section 6.3.5. The physical volcanology of the Lathrop Wells volcano and its suitability as an analog for a future eruption through the repository are discussed in Appendix C. A potential eruption scenario at the Yucca Mountain repository is described in Section 6.4. Process-level models that use the parameters developed from these processes are described in other reports (e.g., *Dike/Drift Interactions* (BSC 2004 [DIRS 170028]). Interrelationships and correlations between parameters are described in Section 6.

Acceptance Criterion 3: Data uncertainty is characterized and propagated through the model abstraction.

1. Models use parameter values, assumed ranges, probability distributions, and bounding assumptions that are technically defensible, and reasonably account for uncertainties and variabilities, and do not result in an under-representation of the risk estimate.

   The report identifies information that has been collected from the Yucca Mountain region as well as information that has been developed from studies at analog sites or developed from the review of published literature. Data uncertainties for inputs to, and outputs from, this analysis and limitations on use of outputs are described in detail

in Sections 6.5, 7.1 and 7.2. The report also traces the parameter outputs forward into analyses that use these parameters. However, the report does not discuss the specific uses of the parameters in the downstream models, nor does the report discuss potential effects of parameter variations on the representation of risk.

2. Parameter uncertainty accounts quantitatively for the uncertainty in parameter values derived from site data and the available literature (i.e., data precision) and the uncertainty introduced by model abstraction (i.e., data accuracy).

   Data uncertainties for inputs to, and outputs from, this analysis and limitations on use of outputs are described in detail in Sections 6.5, 7.1 and 7.2. The report also traces the parameter outputs forward into analyses that use these parameters. However, the report does not discuss how the parameters are used in the downstream models, nor does this report discuss methods used to abstract parameter values into the downstream, process-level models.

3. Where sufficient data do not exist, the definition of parameter values and associated uncertainty is based on the appropriate use of expert elicitation, conducted in accordance with NUREG-1563 (Kotra et al. 1996 [DIRS 100909]). If other approaches are used, the U.S. Department of Energy adequately justifies their use.

   Expert elicitation was not used to develop parameter values pertinent to airborne transport of radionuclides described in this report.

APPENDIX C

ERUPTIVE AND GEOMORPHIC PROCESSES AT THE LATHROP WELLS SCORIA CONE VOLCANO

APPENDIX C – ERUPTIVE AND GEOMORPHIC PROCESSES AT THE LATHROP WELLS SCORIA CONE VOLCANO

C.1 INTRODUCTION

Lathrop Wells volcano is the youngest of eight small-volume, alkali basalt Quaternary volcanoes in the Southwestern Nevada Volcanic Field (Fleck et al. 1996 [DIRS 105337]; Perry et al. 1998 [DIRS 144335]). It is located 18 km south of the U.S. Department of Energy proposed repository for high-level nuclear waste and spent nuclear fuel at Yucca Mountain (Figure C-1). Because of its relatively young age (~80 ka; Heizler et al. 1999 [DIRS 107255], p. 799) and good state of preservation, the volcano provides key information on the nature of a potential future volcanic event at Yucca Mountain (over periods of 10^4 to 10^6 years) that is used for repository risk assessments (Crowe 1986 [DIRS 102740], pp. 253 and 257). In addition, Lathrop Wells volcano preserves much evidence for the complex and often overlooked range of processes that accompany formation and geomorphic evolution of small scoria-cone volcanoes that are the most abundant type of continental volcanic landform (Wood 1980 [DIRS 116536], p. 388).

In addition to outcrops and excavated pits for tephra fallout characterization, commercial quarrying of the Lathrop Wells cone over the last 15 years has exposed sequential views of the internal structure that provide clues to the sequence of eruptive processes. Volcanic activity began with initial Strombolian eruptions accompanied by lava effusion onto a gently sloping alluvial plain. Pyroclastic activity evolved towards increasingly energetic violent Strombolian eruptions as time progressed, while lavas continued to effuse from the base of the growing cone (Figure C-2a, b). Two main types of volcanic surfaces were generated by the eruptive activity: (1) scoria cone, and (2) surfaces with abundant pyroclastic material (either fallout or rafted cone material). After eruptions ceased, these surface types evolved differently, while eolian and colluvial processes buried and preserved parts of the fallout deposit. With respect to geomorphic interpretations of different volcanic surfaces, the degree of cone or lava surface degradation is often used as an indicator of relative age (e.g., Wood 1980 [DIRS 162860], p. 149; Hooper and Sheridan 1998 [DIRS 178066], p. 242; Wells et al. 1985 [DIRS 178074], p. 1,518; Wells et al. 1990 [DIRS 107208], Figure 2; Bradshaw and Smith 1994 [DIRS 101996], p. 168). Appendix E discusses the importance of accounting for different initial characteristics of the volcanic surfaces in order to avoid erroneous interpretations of relative ages of lava fields associated with the ~1-Ma volcanoes in Crater Flat. Previous geomorphic interpretations of Lathrop Wells as a polycyclic volcano (Wells et al. 1990 [DIRS 107208], p. 551) also failed to account for the different initial surface characteristics.

The conclusions about Lathrop Wells volcano, along with other basaltic centers in the southern Nevada region, provide analogue information for three main issues that are important in risk assessment for the proposed Yucca Mountain repository: (1) the nature of subsurface plumbing of a volcanic event were one to intersect the 250-m- to 350-m-deep repository, namely the number and size of dikes and conduits that might transport radioactive waste to the surface (e.g., Crowe et al. 1983 [DIRS 100972], p. 264; Doubik and Hill 1999 [DIRS 115338], p. 60; Woods et al. 2002 [DIRS 163662], pp. 19-1 and 19.3; Dartevelle and Valentine 2005 [DIRS 178142], p. 1); (2) the volumes of erupted materials associated with the waning basaltic volcanism in the Yucca Mountain region; and (3) types of explosive activity that might disperse

contaminants over distances of ~20 km or greater (e.g., Jarzemba 1997 [DIRS 100460], p. 138; Appendix F) .

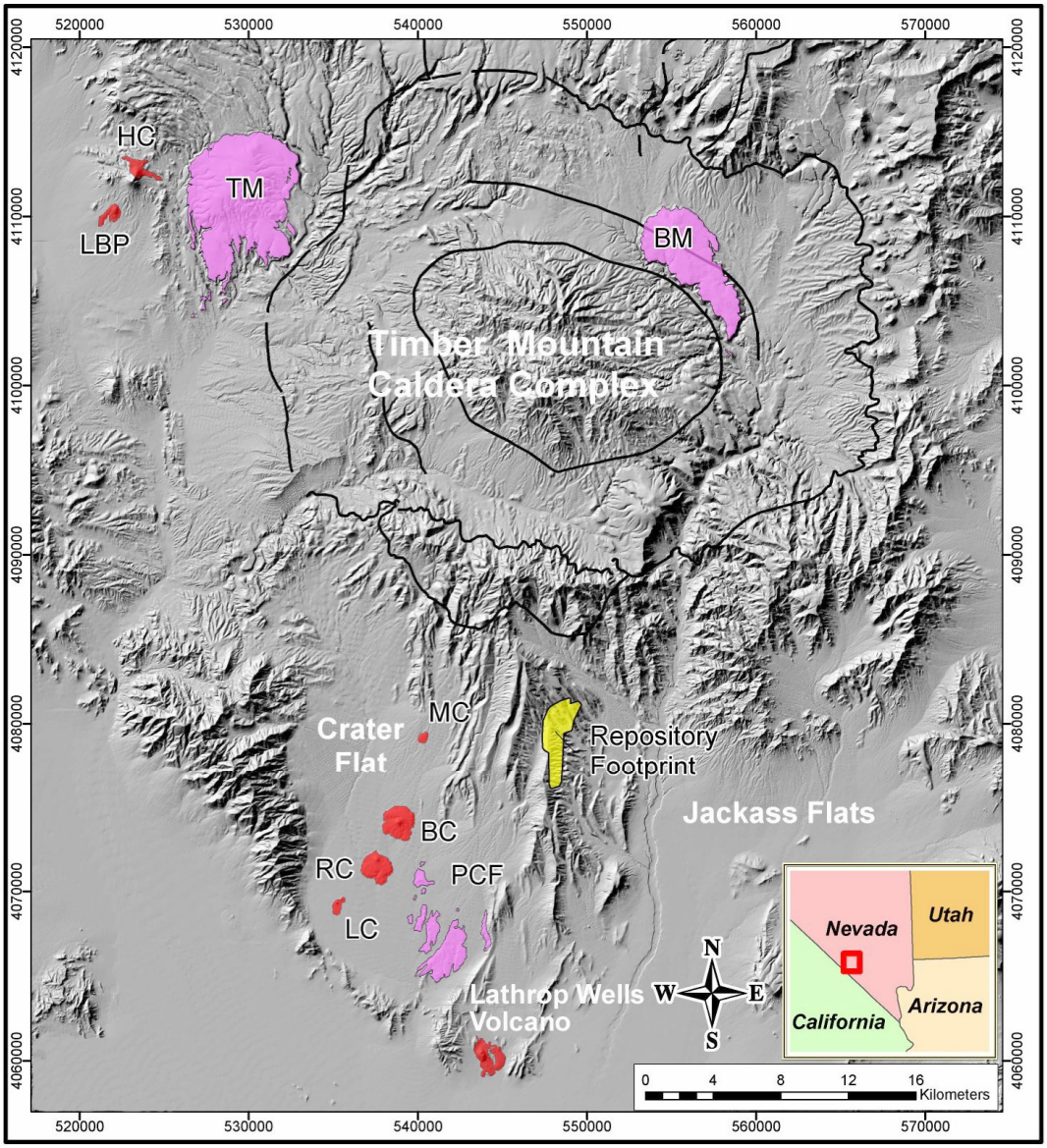

NOTES: Geology from Wahl et al. (1997 [DIRS 112289], plate 1). Pliocene volcanoes (pur ple) are Thirsty Mountain (TM), Buckboard Mesa (BM), and Pliocene Crater Flat (PCF). Pleistocene (red) volcanoes in Crater Flat (LC – Little Cones, RC – Red Cone, BC – Black Cone, MC – Makani Cone) are ~1 Ma (Fleck et al. 1996 [DIRS 105337], Table 2; Perry et al. 1998 [DIRS 144335], Table 2a; Appendix E). Little Black Peak (LBP) and Hidden Cone (HC) are ~0.32 and 0.37 Ma, respectively (Fleck et al. 1996 [DIRS 105337], Table 2). Lathrop Wells volcano (LW) is ~80 ka (Heizler et al. 1999 [DIRS 107255], p. 803). Figure modified from Valentine and Perry (2006 [DIRS 177495], Figure 1).

Figure C-1. Digital Elevation Model of the Yucca Mountain Area Showing Distribution of Plio-Pleistocene Basaltic Volcanoes, and Caldera Outlines from Mid-Miocene Activity

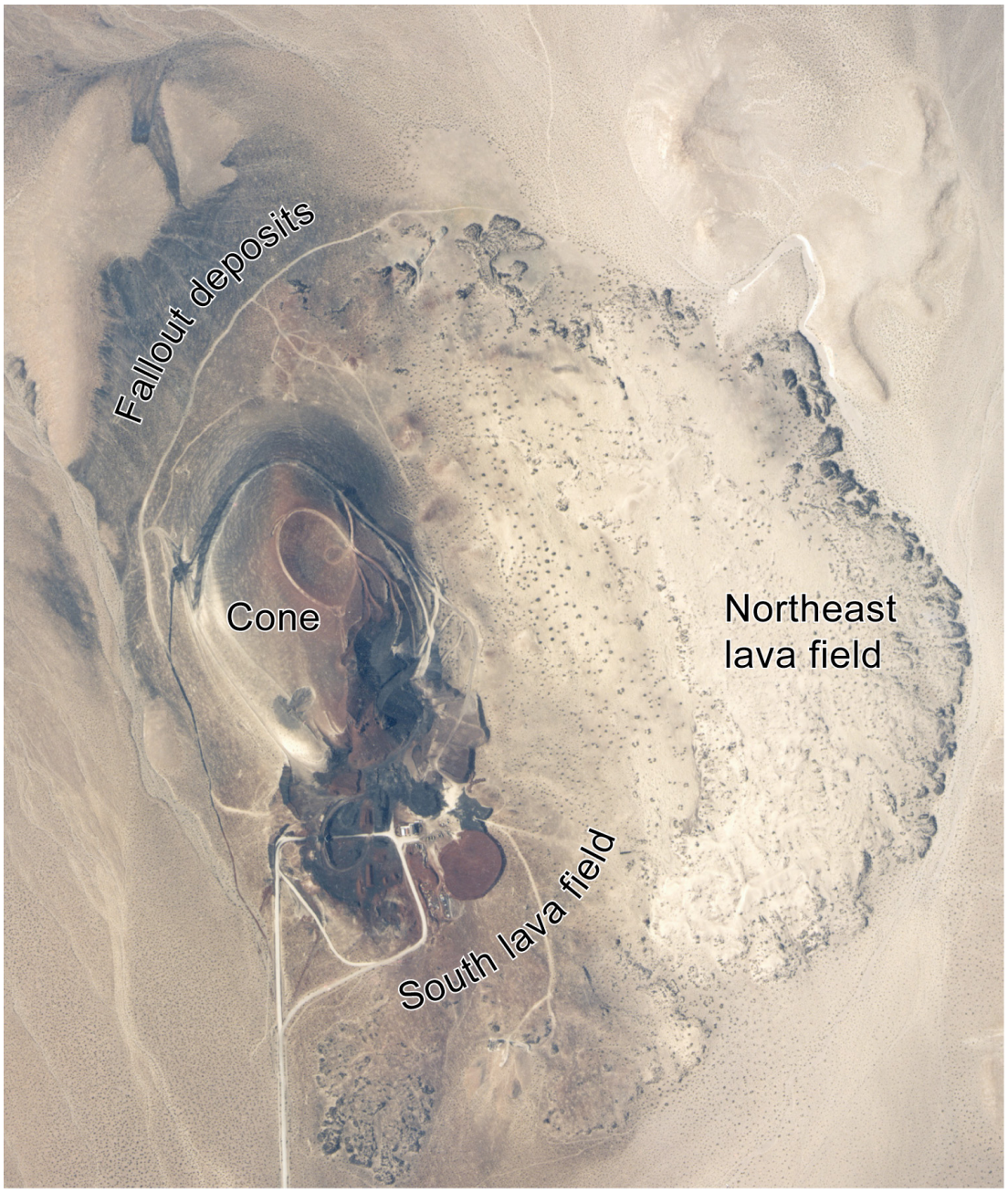

Figure C-2a. Aerial View of Lathrop Wells Volcano

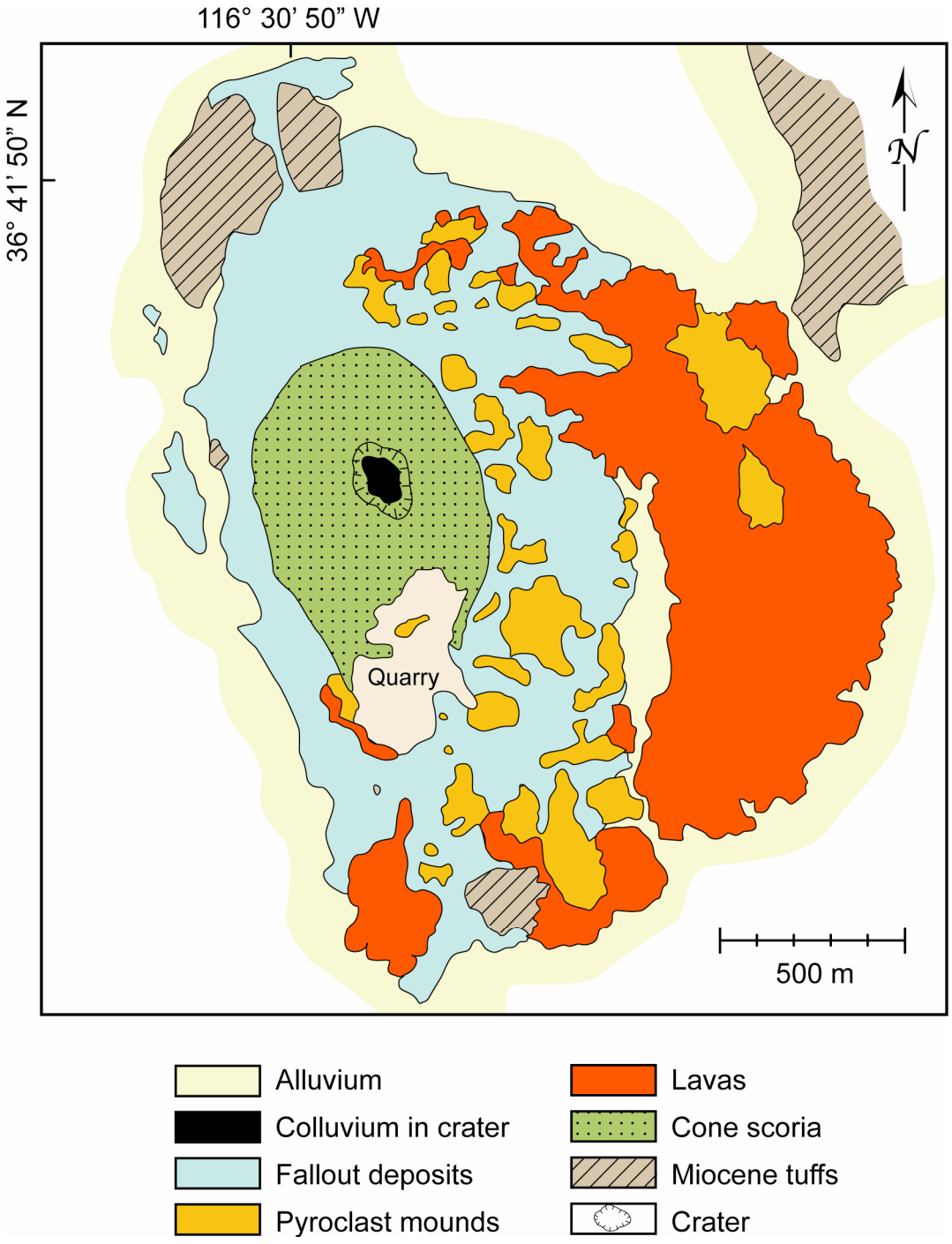

Source: Modified from Perry et al. 1998 [DIRS 144335].

Figure C-2b. Geologic Map of Lathrop Wells Volcano

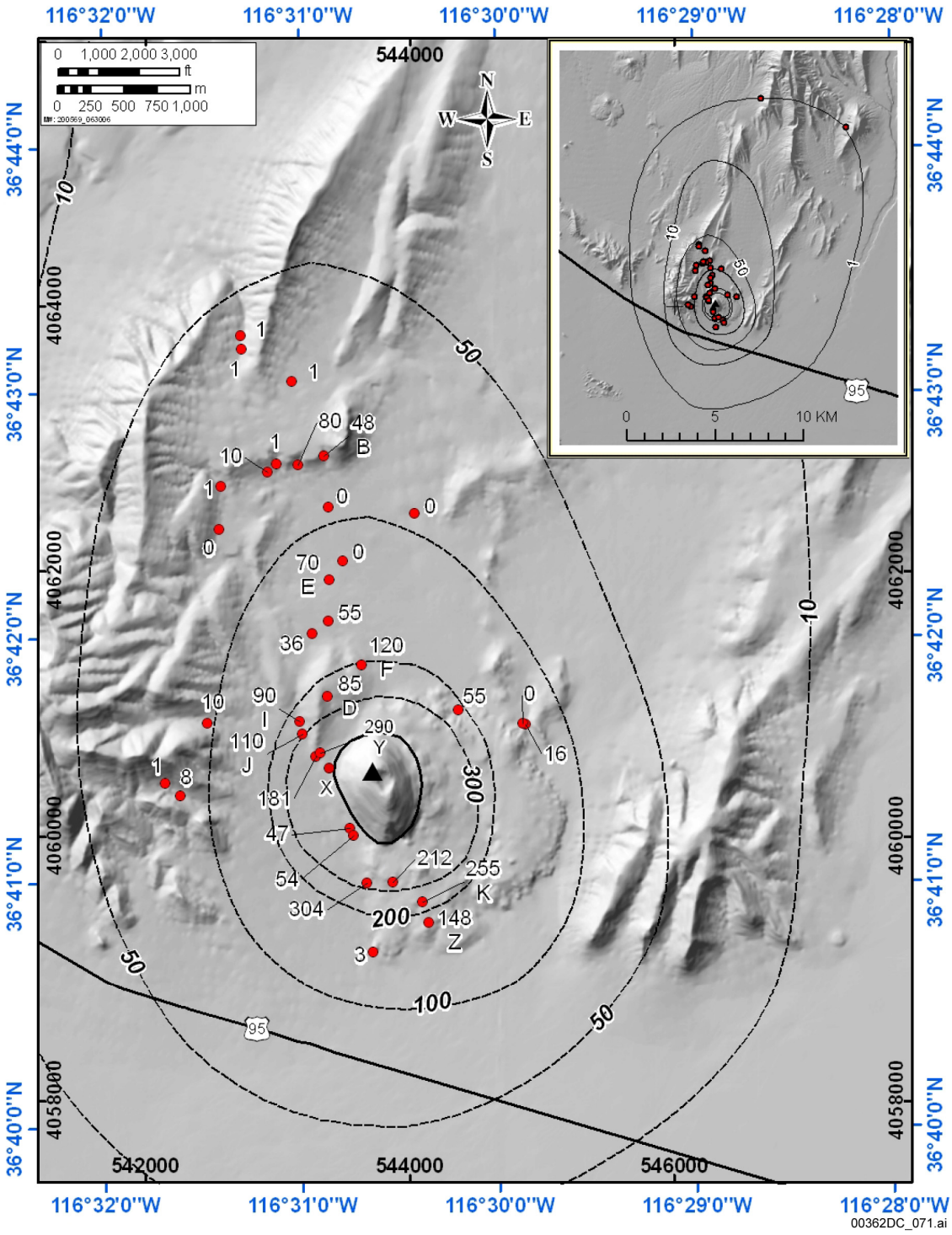

NOTES: Contours (units in cm) represent fallout isopachs (approximate, due to incomplete preservation and exposure of the deposits). Inset shows possible regional extent based upon thin (~1 cm) remnants of ash in distal locations. Tephra thickness data are from DTN: LA0305DK831811.001 [DIRS 164026]. Lettered stations refer to stratigraphic columns in Figure C-8. Red circles are measurement points with thicknesses in cm. Triangle marks summit of Lathrop Wells cone. Solid oval outlines base of Lathrop Wells cone.

Figure C-2c. Distribution of Volcanic Products at Lathrop Wells

C.2 GEOLOGIC SETTING

Volcanism in the Southwestern Nevada Volcanic Field began in the mid-Miocene with eruptions at several large calderas and silicic volcanic centers (Figure C-1; Sawyer et al. 1994 [DIRS 100075], p. 1,305). Silicic volcanism in the area around Yucca Mountain began to wane after ~11.45 Ma with the eruption of the Ammonia Tanks Tuff, finally ending with eruptions that formed the Black Mountain caldera ~9.4 Ma (Sawyer et al. 1994 [DIRS 100075], Table 1). Waning silicic activity gave way to large basaltic centers, with volumes up to ~10 km^3, during late Miocene. Basaltic volcanism continued sporadically in the region, with a general decrease in volume per volcano, including the most recent eruption that produced the Lathrop Wells volcano at ~80 ka (Crowe 1986 [DIRS 102740], p. 253; Fleck et al. 1996 [DIRS 105337], Table 2; Perry et al. 1998 [DIRS 144335], p. 2-40; Heizler et al. 1999 [DIRS 107255], p. 767; Valentine and Perry 2006 [DIRS 177495], Figure 2).

Basin-and-Range faulting has produced a dominant north-south grain of normal faults that intersects the northwest-southeast trending Walker Lane shear zone along the southwestern margin of the volcanic field. Lathrop Wells volcano is located in the transition between dominantly north-south trending normal faults to the right-lateral shear of the Walker Lane. In detail, the volcano resides at the intersection of closely spaced splays of the northwest-trending Windy Wash and the northeast-trending Stagecoach Road normal fault systems that define the southern extent of narrow, linear ridges of Miocene-age ignimbrites of Yucca Mountain. Within these fault systems, the volcano is located on an eastward tilted fault block, between major west-dipping normal faults, that is partly covered by a thin veneer of alluvial fan deposits (Potter et al. 2002 [DIRS 160060], plate 1). Based upon these observations and those at other basaltic volcanoes in the region back to the Miocene (e.g., Valentine and Krogh 2006 [DIRS 177282], Figure 2, p. 221), it is likely that the dike system that fed Lathrop Wells eruptions occupied a normal fault at shallow depths.

C.3 PREVIOUS WORK

Lathrop Wells volcano was first evaluated from a nuclear waste disposal and risk-assessment perspective by Crowe and Carr (1980 [DIRS 101839], p. 1). Numerous other investigations (Vaniman and Crowe 1981 [DIRS 101620], p. 1; Crowe et al. 1983 [DIRS 100972], p. 259, Crowe et al. 1986 [DIRS 101532], p. 1; Crowe 1986 [DIRS 102740], p. 247; Champion 1991 [DIRS 100969], p. 61; Wells et al. 1990 [DIRS 107208]; Wells et al. 1991 [DIRS 144406], p. 661; Wells et al. 1992 [DIRS 107015] p. 555; Turrin et al. 1991 [DIRS 101030, p. 654; Zreda et al. 1993 [DIR 108617], p. 57; Perry et al. 1998 [DIRS 144335], p. 2-105; Valentine et al. 2005 [DIRS 177782], p. 629; Valentine and Harrington 2006 [DIRS 177271] , pp. 533 to 535; Appendix E, this report) added geochronologic, petrologic, geomorphic, paleomagnetic, and volcanological data and interpretations for Lathrop Wells volcano and the several nearby scoria cones that together compose the Crater Flat volcanic zone. Despite the numerous papers that touch upon the Lathrop Wells volcano, the literature remains confused on several aspects of its eruption sequence and a clear understanding of that sequence has not emerged previously. For example, some workers refer to the entire sequence as “Strombolian” and infer the presence of multiple vents scattered throughout the lava fields (e.g., Perry et al. 1998 [DIRS 144335], p. 2-46) with eruptions potentially separated by substantial periods of time (although not explicitly stated, the time intervals implied by Wells et al. (1990 [DIRS 107208]) must be on the

order of 10^3 to 10^4 years or more), while Wohletz (1986 [DIRS 140956], p. 262) infers the occurrence of a major hydrovolcanic explosion phase accompanied by formation of a tuff ring early in the eruptive sequence. After more than a decade of debate on the age of the Lathrop Wells event, including evidence from K–Ar dating, cosmogenic ^{3}He and ^{36}Cl exposure ages (Zreda et al. 1993 [DIRS 108617], Table 1), and paleomagnetic and geomorphic studies, Heizler et al. (1999 [DIRS 107255], p. 257) concluded that reproducible ^{40}Ar/^{39}Ar ages of 77.3 ± 6.0 ka and 76.6 ± 4.9 ka (2σ) for the early and late erupted lavas, respectively, represent the most probable age (for simplicity, ~80 ka) for the volcano.

C.4 OVERVIEW OF COMPOSITION AND ERUPTIVE SEQUENCE

Compositionally, Lathrop Wells is an alkali basalt (Table C-1) with an Mg value of ~54 that reflects substantial fractionation of the parent magma (Vaniman and Crowe 1981 [DIRS 101620], p. 36; Crowe et al. 1995 [DIRS 100110], p. 4 to 9; Perry and Straub, 1996 [DIRS 106490], p. 5). Most of the volcanic products are sparsely porphyritic, with 1 vol % to 4 vol % olivine phenocrysts and a groundmass dominated by plagioclase; however, two lobes of the early lava field and the lower cone deposits also contain 1 vol % to 4 vol % plagioclase phenocrysts up to 1-mm long (Perry and Straub 1996 [DIRS 106490], p. 6, Figure 8). Based on strontium and neodymium isotopic compositions, elevated concentrations of rare earth elements, strontium, barium, and thorium, and lower rubidium relative to typical alkali basalts, previous workers have concluded that Lathrop Wells magma was derived from an enriched lithospheric mantle source (Vaniman et al. 1982 [DIRS 101031], p. 353; Farmer et al. 1989 [DIRS 105284], p. 7,885; Perry et al. 1998 [DIRS 144335], p. 4-24). Small but systematic geochemical differences occur between early and late-erupted magmas as reflected in the two flow fields (Table C-1; Perry and Straub 1996 [DIRS 106490], p. 7; Perry et al. 1998 [DIRS 144335], p. 4-14). Early lavas are generally 0% to 2% nepheline normative, while late lavas are generally 0% to 2% hypersthene normative, primarily because of slightly lower Na_2O content at the same SiO_2 content in the late lavas. Incompatible trace element differences between early and late flows show both relative depletion and enrichment in the later flows. Thorium and rubidium values are 15% to 20% higher in the late flows, while strontium, neodymium, and samarium values are 5% to 10% lower. Perry et al. (1998 [DIRS 144335], p. 4-19) tested several mechanisms to account for these differences including fractional crystallization, crustal contamination, and magma mixing. They concluded that none of these mechanisms can account for the observed geochemical trends and hypothesized the differences are due to processes that occurred in the mantle source during melting and melt withdrawal. Nicholis and Rutherford (2004 [DIRS 173945], p. 492) studied phenocryst-melt equilibria of Lathrop Wells lava and nearby Crater Flat volcanic products, and concluded that magma-ascent rates exceeded 0.04 m/s to account for formation of microlitic plagioclase textures found in the lavas. Nicholis and Rutherford (2004 [DIRS 173945]) calculate that the ascending magma was near-water-saturated with temperature of ~975°C to 1,000°C and with ~1.2 wt % to 4.6 wt % H_2O based upon their own analyses of melt inclusions and those of Luhr and Housh (2002 [DIRS 178118], p. 1,221).

Table C-1. Representative Compositions of Early and Late Stage Lavas from Lathrop Wells Volcano

Sample	LW22FVP	LW61FVP
	Western Lobe of South Lava Field	Late Breakout from Northeast Lava Field
Major Elements	**wt %**	**wt %**
SiO_2	47.43	48.65
TiO_2	2.06	1.83
Al_2O_3	16.60	16.87
Fe_2O_3	12.15	11.45
MnO	0.18	0.18
MgO	6.13	5.70
CaO	8.40	8.79
Na_2O	3.55	3.39
K_2O	1.80	1.80
P_2O_5	1.31	1.17
Total	99.60	99.82
Trace Elements	**ppm**	**ppm**
V	184.6	187.6
Cr	106.2	110.3
Co	31.5	29.8
Ni	61.7	46.9
Rb	14.0	19.8
Sr	1,555.9	1,450.2
Y	23.5	22.6
Zr	381.8	370.5
Ba	1,314.8	1,375.7
Sc	18.7	19.7
La	92.6	94.1
Ce	184	179
Sm	12.7	12.0
Eu	3.28	3.06
Tb	1.17	1.10
Yb	2.42	2.34
Lu	0.356	0.338
Hf	7.17	7.12
Ta	1.39	1.37
Th	6.05	7.29

Source: DTN: LA000000000099.002 [DIRS 147725].

The volcano consists of a scoria cone and two lava fields (Figure C-2; Valentine et al. 2005 [DIRS 177782], p. 628 to 629), and remnants of a scoria fallout deposit that extends up to ~20 km from the vent. The cone was 140-m high (before summit quarrying) with an elongate base and its summit encloses a crater that is partially filled by colluvium and eolian sediments. The outer cone slopes consist entirely of loose scoria lapilli, sparse blocks and bombs, and of

eolian sediments that are mixed in the upper few decimeters. Several meters of scoria have been erosionally removed from the cone rim and moved down the cone slopes by creep and fluvial processes (Perry et al. 1998 [DIRS 144335], p. 2-67). Lava flow fields extend from the base of the cone on its northeast, east, and south sides, covering an area of 1.95 km^2 with average flow thickness of ~15 m and steep flow fronts. The lavas were emplaced on the low-angle (1° to 2°), south-sloping surface of the basin similar to lavas produced by the ~1-Ma volcanoes in nearby Crater Flat (Appendix E), although at Lathrop Wells the lavas locally flowed around a low ridge of Miocene tuff that is partly straddled by the volcano.

The relative timing of emplacement of the cone, fallout deposits, and lava fields is shown schematically in Figure C-3. Early cone building was accomplished by Strombolian explosions from eruption along a short fissure that is now buried by the cone (Valentine and Perry 2006 [DIRS 177495], p. 2). This early explosive activity resulted in little, if any, fallout deposition beyond the cone itself, and was accompanied by effusion of lavas that formed the south lava field. Activity was soon confined to a single eruptive vent and became increasingly energetic, producing sustained eruption columns of well-fragmented, highly vesicular basalt lapilli and ash characteristic of violent Strombolian mechanisms. The bulk of the cone was built by this violent Strombolian activity (Valentine et al. 2005 [DIRS 177782], pp. 631 to 632), along with emplacement of fallout deposits that buried most of the early, south lava field. The northeast lava field was emplaced late with respect to pyroclastic activity; these lavas overlie fallout deposits but also are locally (north of the cone) covered with a veneer of fallout. One of the last eruptive events recorded at the cone was a summit explosion, which deposited fist-size and smaller pieces of distinctive basalt-xenolith breccia around the cone base (Doubik and Hill 1999 [DIRS 115338], p.60).

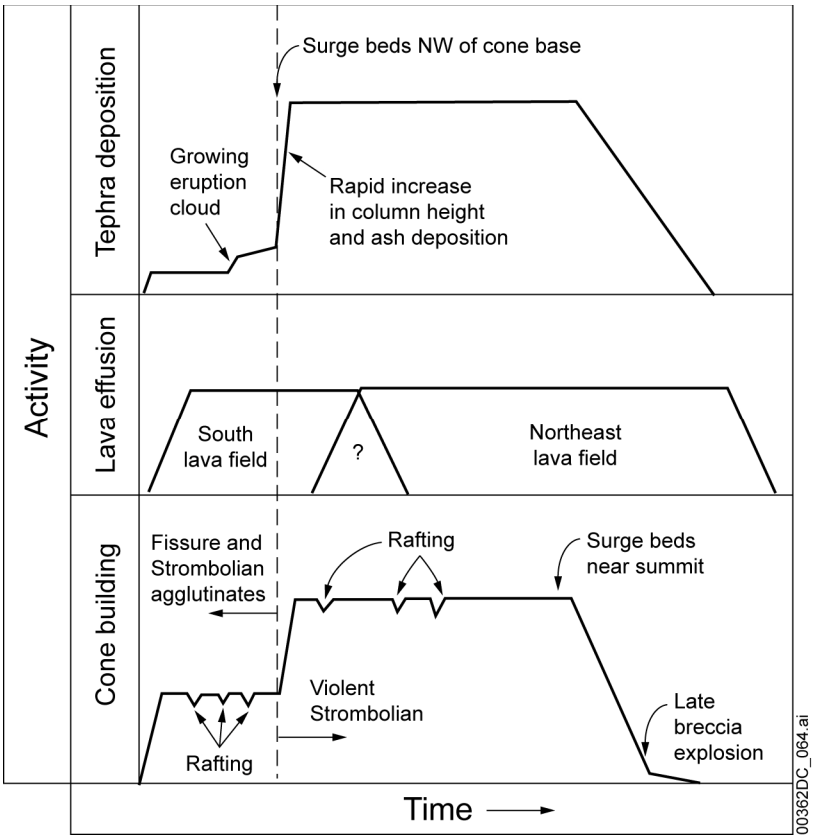

Figure C-3. Schematic Diagram Showing the Relative Timing of Emplacement of Scoria Cone, Fallout, and Lava Fields at the Lathrop Wells Volcano

C.5 PRODUCTS OF THE STROMBOLIAN ERUPTIVE PHASE

C.5.1 Early (lower) Cone

Quarrying of the southern cone slope has exposed an early phase of the cone composed of welded spatter and agglutinate (~40 m above the base level of the cone; Figure C-4). These deposits are dull red, massive to crudely bedded, partly welded bomb-and-coarse-lapilli agglutinate, and are the only deposits observed in the cone that have plagioclase phenocrysts. Clasts range from roughly equant, angular to subrounded lapilli and blocks (probably representing variably recycled fragments of broken bombs) to large (~1 m) fluidal spindle and ribbon bombs. Some small bombs have irregular, ragged shapes that fold around underlying clasts, indicating that the bombs were molten upon impact. Sparse bombs have cauliflower surface textures that indicate some quenching by wet steam or liquid water. In the quarry, deposits are partly welded but there is little compaction deformation of clasts. This facies is consistent with deposition of coarse bombs that traveled on relatively low ballistic paths with limited in-flight cooling, as well as ejecting recycled bombs and bomb fragments that avalanched into the vent, indicative of Strombolian eruptions (see McGetchin et al. 1974 [DIRS 115469], p. 3,267; Valentine et al. 2005 [DIRS 177782], p. 630). In quarry exposures this early cone-building facies is in sharp contact with, and mantled by, overlying beds of well-sorted scoria lapilli of the later violent Strombolian eruptions.

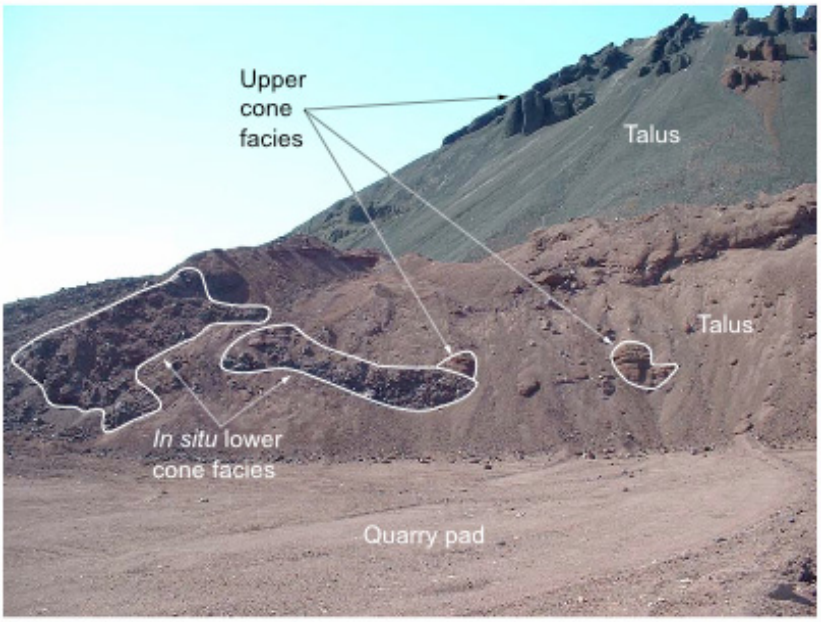

Figure C-4. Cone-Building Deposits Associated with the Early, Strombolian Phase of Activity, Overlain by Cone Deposits from the Later Violent Strombolian Phase (as Exposed by Quarry Operations in Late 2001)

Although in situ exposures of the early cone-building facies are limited and transient because of quarry activities, features of the contemporaneous south lava field provide additional clues about the nature of the early cone. As described in Section 6.3.3.1, the many mounds of pyroclastic material dispersed across the lava field are the result of rafting of cone material atop lava flows. Most of the rafted mounds preserve facies (either intact or partly disintegrated during transport on the lavas) that are identical to the in situ facies described above. One large raft is an intact sequence of densely welded spatter grading upward over ~2 m into moderately welded bombs and lapilli. The densely welded spatter indicates that the early cone building included periods of sustained, relatively rapid accumulation of hot, fluid clasts (Head and Wilson 1989 [DIRS 124674], p. 267; Sumner et al. 2005 [DIRS 178125], p. 54). Some of the lavas produced during early cone building may have originated as clastogenic flows. These observations suggest that at cones with unexposed internal stratigraphy, rafted mounds on top of associated lava flows provide an indirect way to determine styles of pyroclastic activity within the cones (see also Holm 1987 [DIRS 178117], p. 319). Additionally, the relative abundance of rafted mounds on the south lava field at Lathrop Wells indicates that slumping and cone "deconstruction" by rafting was a major part of the early cone-building phase (see also Appendix E).

C.5.2 South Lava Field

The south lava field extends ~800 m from the southern base of the cone (prior to quarry operations), implying an average effusion rate on the order of 1 m^3/s (Walker 1973 [DIRS 178061], Figure 4). The surface of the lava field is buried by fallout over much of proximal and medial portions. The lavas initially flowed directly southward around the west side of a small hill of Miocene ignimbrite, and then south-southeastward around the east side of the hill, to form a western and an eastern part of the lava field. The western part has margins

characterized by lobes that are commonly 20-m to 80-m wide and extend a few tens of meters to nearly 200 m from the main part of the lava field. Surface textures such as linear or arcuate squeeze-up ridges, lava tumuli, and ripply surface ridges (formed on the top of lava channels on the axes of long lobes) are more abundant toward the distal edges of the lava field where they are less obscured by the southward-thinning fallout deposits (Figure C-5). Flow fronts are clearly preserved and are characterized by steep margins, typically 2-m to 4-m high, of blocky lava. Down stepping of marginal flow lobes as they extend outward onto the desert floor represents breakouts from the lobes. This indicates the presence of a tube network that fed lava toward distal margins and provided material for lateral growth of the lava field (see also, for example, Pinkerton and Sparks 1976 [DIRS 178120], p. 181; Appendix E, this report). One small lobe of lava (now buried by quarry tailings) extends ~100 m southwest of the cone base. This lobe and the western part of the south lava field are the only lavas that contain plagioclase phenocrysts and on this basis are inferred to be a very early lava of the same type that was erupted by Strombolian activity during early cone building.

An additional characteristic of the south lava field is the presence of many mounds, typically 20 m to 40 m in diameter and up to ~2-m high, of coarse pyroclastic material. There are four main types of mounds. One type is composed, on the crest of the mound, of partly welded, angular fragments with variable vesicularity. This mound type ranges from linear (~10-m long by 1-m to 2-m wide) to circular in map view, and may represent lava-flow-top breccia that was uplifted as tumuli, although the detailed structure is indeterminate due to partial burial by the fallout scoria. The coarse breccia may have been pushed upward (driven by internal inflation of the underlying lava) so that it partly protrudes above the fallout deposits, or it may have been blanketed with fallout that has since been stripped off the steepest surfaces by erosion (e.g., Appendix E). A second type of mound consists of loose, scattered accumulations of decimeter-sized ribbon and spindle bombs, and may also contain rotated slabs of agglutinate.

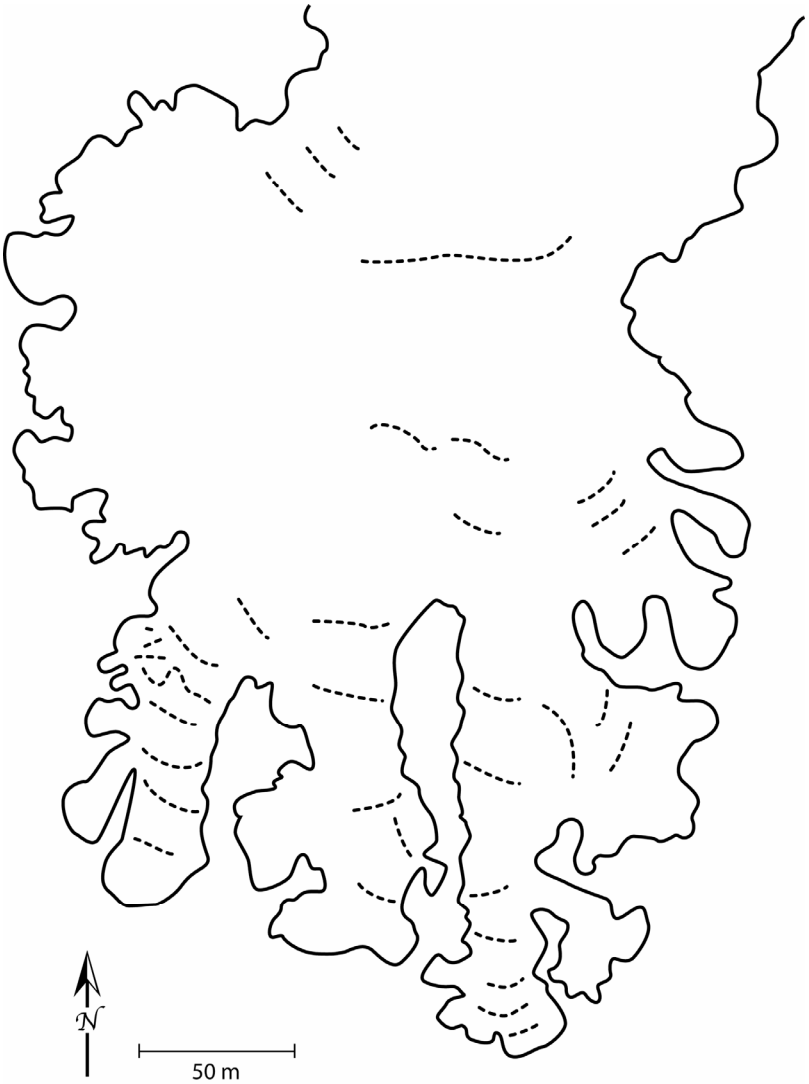

Figure C-5. Map of Western Part of the South Lava Field, Showing Lobate Flow Margins (Solid Lines) and Pressure Ridge and Squeeze-Up Features (Dashed Lines)

A narrow dike-like lava squeeze-up, 20-cm to 30-cm thick and about 20-m long with an arcuate shape, occurs at the southern foot of one such mound (Figure C-6a). A third type of mound consists of a coherent mass of variably welded spatter and agglutinate that preserves original bedding (Figure C-6b and c). The latter two mound types represent pyroclasts deposited in the main cone, during early Strombolian eruptions, that were subsequently dislodged by flowing lava and rafted to their final locations (see also Gutmann 1979 [DIRS 178116], p. 450; Holm 1987 [DIRS 178117], p. 324; Luhr and Simkin 1993 [DIRS 144310], pp. 89 and 95; Appendix E, this report). This is supported by the presence of plagioclase phenocrysts similar to those found in the early cone deposits. The preservation and orientation of bedding in the final rafted mass depend upon the degree of welding of the original beds where they formed on the cone. Partial break-up of non- to partly welded masses during rafting could be expected. A final type of pyroclast mound is composed of jumbled blocks of very coarse spatter distributed in a circular pattern ~10 m to 15 m in diameter, interpreted to be the collapsed remnants of a hornito (rootless spatter vent). The pyroclastic debris from each of these mounds, together with the fallout

deposits that blanket most of the south lava field, combine to obscure the flow surfaces. The interpretations of these different types of pyroclast mounds are consistent with observations of historical eruptions (e.g., Williams and Moore 1976 [DIRS 178127], p. 8; Luhr and Simkin 1993 [DIRS 144310], pp. 89 and 95; Sumner 1998 [DIRS 178124], Figure 9) and interpretations of similar features at other small basaltic volcanoes (e.g., Gutmann 1979 [DIRS 178116], p. 450; Holm 1987 [DIRS 178117], p. 324; Appendix E, this report), but differ from previous workers at Lathrop Wells who inferred that the mounds were separate eruptive vents. Perry et al. 1998 ([DIRS 144335], p. 2-56), argued that the fact that some mounds have internally coherent magnetization is most consistent with an interpretation that they are vents, but many of the mounds obtained their magnetic signal when they cooled within the cone and retained this as they were carried intact atop the lavas.

C.6 PRODUCTS OF THE VIOLENT STROMBOLIAN PHASE

C.6.1 Cone Deposits

The upper approximately two-thirds of the cone (Figure C-4) is composed of beds typically ~10-cm to greater than 1-m thick that slope outward near the angle of repose (~30°) in lower exposures and shallow slightly with elevation. The beds range from planar over lateral distances of tens of meters, to lenticular. They are composed of relatively well-sorted, loose, vesicular scoria lapilli. Internal structure within many planar beds, such as slight variation in grain sizes, can in many cases be traced continuously over tens of meters laterally and up slope, indicating deposition by fallout. Other planar beds have internal structure indicative of a component of grain avalanching, such as horizons rich in inversely graded, clast-supported coarse lapilli that are lenticular over a few meters distance. Near the top of the quarry, some planar beds "roll over" to dip inward toward the crater center, while maintaining relatively constant thickness; others are truncated by ventward-dipping beds. The rollover geometry is indicative of deposition by fallout mantling the cone. No welding is observed in this facies, including very proximal crater wall deposits exposed by quarrying, and fluidal bombs comprise a minor component of the deposits. Riedel et al. (2003 [DIRS 178121], p. 126) and Martin and Nemeth (2006 [DIRS 178119], p. 105) discussed the role of fallout from sustained violent Strombolian eruption columns in this phase of cone building, as opposed to ballistic emplacement of coarse bombs during the earlier Strombolian phase that is consistent with the classical model presented by McGetchin et al. (1974 [DIRS 115469], Figure 14). Six meters below the south rim of the crater, quarrying temporarily exposed a 40-cm-thick, well-sorted, laminated-to-thinly bedded, planar- and cross-stratified ash (median clast diameter $Md \approx 0.1$ mm to 0.2 mm; Figure C-7a and b), sandwiched between massive beds of poorly sorted, nonwelded, clast-supported, angular scoria lapilli ($Md \approx 8$ mm; Figure C-7b).

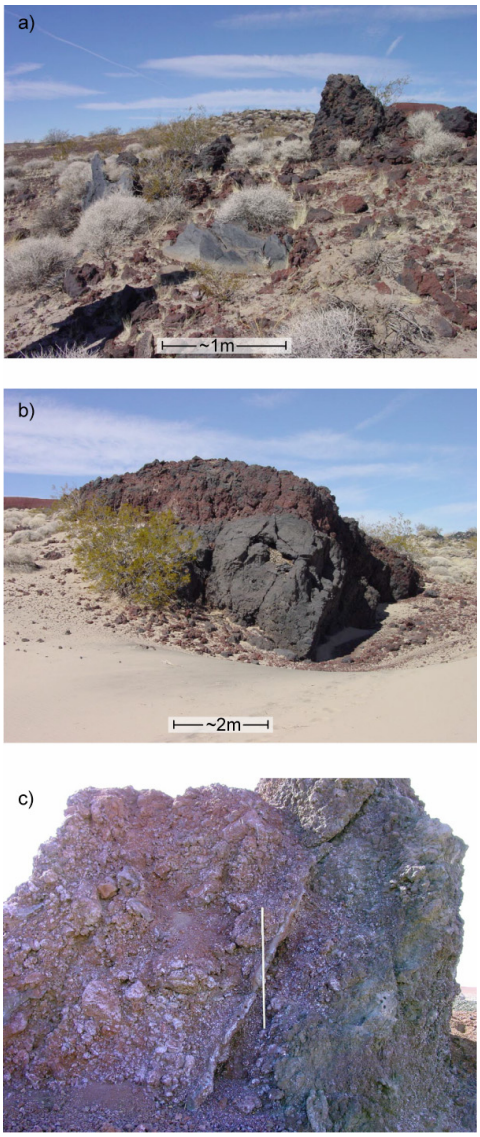

NOTES: (a) Mound consisting of broken slabs or masses of partly welded agglutinate. This example has a narrow, arcuate squeeze-up (rootless dike) along its leading edge (emplacement direction was toward the photographer).

(b) Pyroclast mound composed of an intact, tilted block of bedded spatter and agglutinate, near eastern margin of south lava field. Black lower portion is densely welded spatter. Red upper part is moderately welded agglutinate. The block tilts downward away from the photographer.

(c) Internal structure of an intact pyroclast mound, showing steeply tilted bedding of partly welded agglutinate. A thin layer of spatter crosses the middle of the meter stick. A thick mantle of fallout lapilli beds (from violent Strombolian eruptions at the cone) covered this rafted block prior to quarrying activities, such that it had a subdued, rounded morphology.

Figure C-6. Examples of Two Types of Pyroclast Mounds on the South Lava Field

The lamellae, consisting of alternating coarse and fine ash, range from 3-mm to 15-mm thick and dip conformably 30° to 35° toward the crater. The unit pinches out within ~50 m to the west, and the eastern extent was covered. Upper and lower contacts are parallel to the internal bedding and no scouring is evident, although cross stratification indicates a component of lateral transport. Plastically deformed bedding that surrounds a 4-cm-diameter clast suggests the beds

were moist during deposition. Scanning electron microscopic analysis reveals equant, rounded grains of tachylite with smooth, glassy vesicle wall remnants and less abundant sideromelane. This ash was deposited by a localized density current mechanism, possibly partial collapse or heavy fallout from an ash-rich eruption column. For example, Taddeucci et al. (2004 [DIRS 178126], p. 35) and Taddeucci et al. (2004 [DIRS 175382], Figure 1), mention observations of such processes during eruptions of Mt. Etna, Italy in 2001.

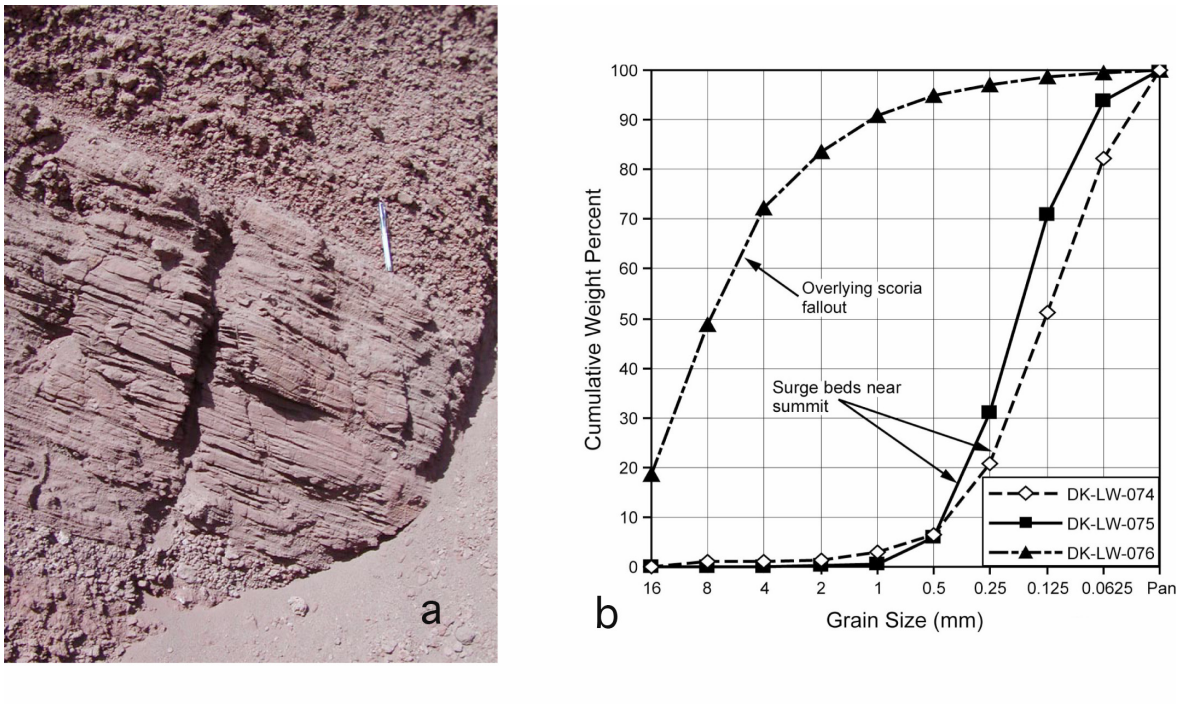

NOTES: (a) Cross-stratified ash deposit interbedded with scori a lapilli deposits in upper cone. Bedding dips in toward the center.
(b) Cumulative grain-size distribution for cross-stratified ash deposit (samples DK-LW-74,76) and overlying scoria lapilli bed (sample DK-LW-76) that is typical of the upper cone-forming deposits.

Figure C-7. Cross-stratified Ash Deposit

The cone and crater are elongate with an axis oriented N12°W. Before quarrying, the rim had two peaks on its opposing north and south sides, both higher than the west and east sides of the rim. Many cones around the world are asymmetric because of strong winds or directed fountaining during eruptions. In such cases, one quadrant of the rim will be elevated. The two-peaked nature of the Lathrop Wells rim is difficult to explain by these mechanisms. Instead, it can be argued that the cone shape reflects the fact that rafting of cone material atop lava flows mainly occurred from the eastern base of the cone. The higher base level of the cone on its eastern side (Section C.8.3) reflects accumulation of lavas around one or more lateral breakouts (boccas, now buried by scoria) that were the source for the flows. Slumping of cone material onto departing lava flows removed material from the side of the cone, resulting in its elongate shape and reducing the height of the eastern rim. Accumulation of proximal fallout scoria during violent Strombolian eruptions healed or buried any scarps that may have been produced by slumping (see also Holm 1987 [DIRS 178117], p. 321; Luhr and Simkin 1993 [DIRS 144310], p. 89). If rafting had not occurred, the cone may have had a more circular base and rim, and the

southern and northern parts of the rim would have been connected along the eastern quadrant by a rim that maintained a constant, or gently northward-rising, elevation; the eastern flank would also have had a slope closer to the angle of repose instead of the 24° slope that it exhibits now. This interpretation builds upon earlier work (summarized by Perry et al. 1998 [DIRS 144335], p. 2-41) that inferred the elongate shape might partly reflect the orientation of a feeder dike/fissure (inherited from early cone building eruptions). An additional process that might have contributed to the two-peaked characteristic of the rim is a change in wind direction during violent Strombolian eruptions (Section C.6.2).

C.6.2 Fallout Deposits beyond the Cone

Ten stratigraphic columns of fallout deposits beyond the cone were measured in pits (Figure C-8, Table C-2). Erosion of the deposits in most areas, and burial beneath alluvial sediments in others, greatly limit detailed reconstruction of their distribution. Maximum measured fallout thickness is 304 cm in a section measured 700 m south of the vent, although deposits clearly thicken closer to the cone. Grain size data for the deposits (Figure C-9), along with characteristic planar-parallel bedding that mantles preexisting topography (except for very steep lava surface features), are consistent with the interpretation that most of these deposits originated by fallout from sustained buoyant eruption columns. Individual beds range from centimeters to decimeters in thickness. Some are massive while others show reverse-to-normal grading indicative of waxing and waning eruption column events; indeed, each bed probably represents a pulse in explosive activity. Most beds have clast-supported textures. Some beds consist of angular or slightly ragged, glassy and highly vesicular clasts, many of which appear to be fragments of small ribbons; these beds consist of juvenile clasts that might have been shredded from an annulus of magma in the conduit by the eruptive jet. Other beds are dominated by variably rounded and abraded scoria clasts that appear to have been recycled by avalanching and churning in the vent. The fallout deposits are nearly xenolith free, with the exception of a layer referred to as “salt and pepper” (Columns F, E, and B; Figure C-8) that occurs near the base the sequence in the northern and northwestern quadrants of the fallout distribution and one instance south of the cone (see isopachs on Figure C-2c). This distinctive layer contains a few percent of coarse, ash-sized, Miocene tuff xenoliths.

Table C-2. Coordinates of Measured Stratigraphic Sections of Fallout Deposits

Column	Latitude	Longitude
Z	N36° 40’ 49.4”	W116° 30’ 22.9”
K	N36° 40’ 54.8”	W116° 30’ 26.0”
X	N36° 41’ 28.6”	W116° 30’ 49.5”
Y	N36° 41’ 31.8”	W116° 30’ 54.1”
J	N36° 41’ 36.1”	W116° 31’ 02.4”
I	N36° 41’ 39.2”	W116° 31’ 03.1”
D	N36° 41’ 42.7”	W116° 30’ 53.5”
F	N36° 41’ 53.0”	W116° 30’ 44.2”
E	N36° 42’ 14.0”	W116° 30’ 53.9”
B	N36° 42’ 44.3”	W116° 30’ 55.3”

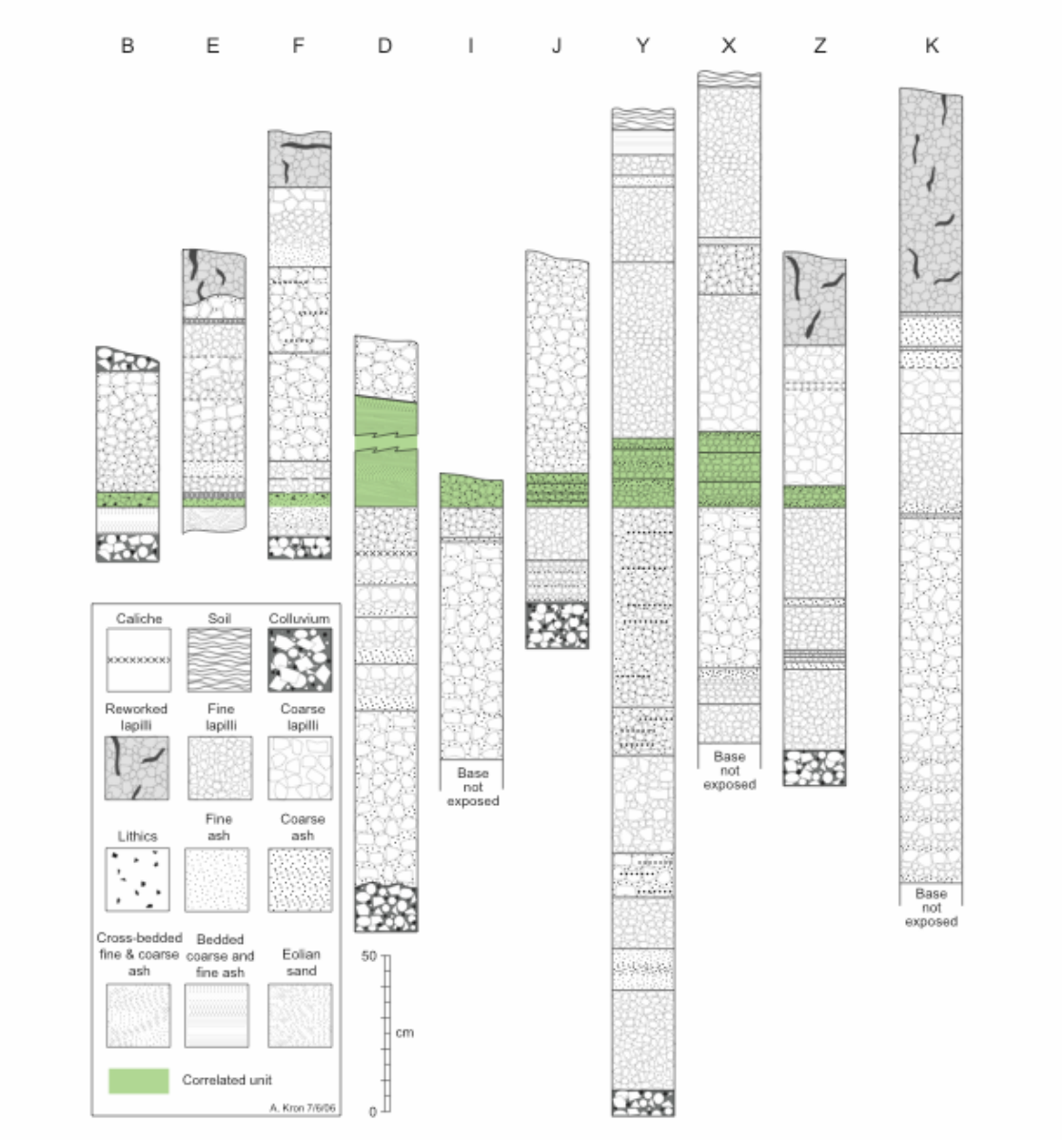

NOTES: Columns are drawn with respect to an inferred common datum (stratigraphic level) that corresponds to the emplacement of the localized cross-laminated ash unit described in Section C.6.2, inferring that similar thin, planar ash layers observed elsewhere correlate with that unit. This interpretation is not considered unique.

Section D is a composite section of two neighboring sequences: one is 85-cm thick, the other is ~140-cm thick and is complicated by the laminated ash unit that is correlated. On Figure C-2, the 85-cm-thick sequence is chosen to represent a thickness for the purpose of contouring isopachs.

Figure C-8. Stratigraphic Columns (Locations Shown in Figures C-2 and Table C-2) of Fallout Deposits at Ten Sites Ranging up to 2.5 Km from the Vent

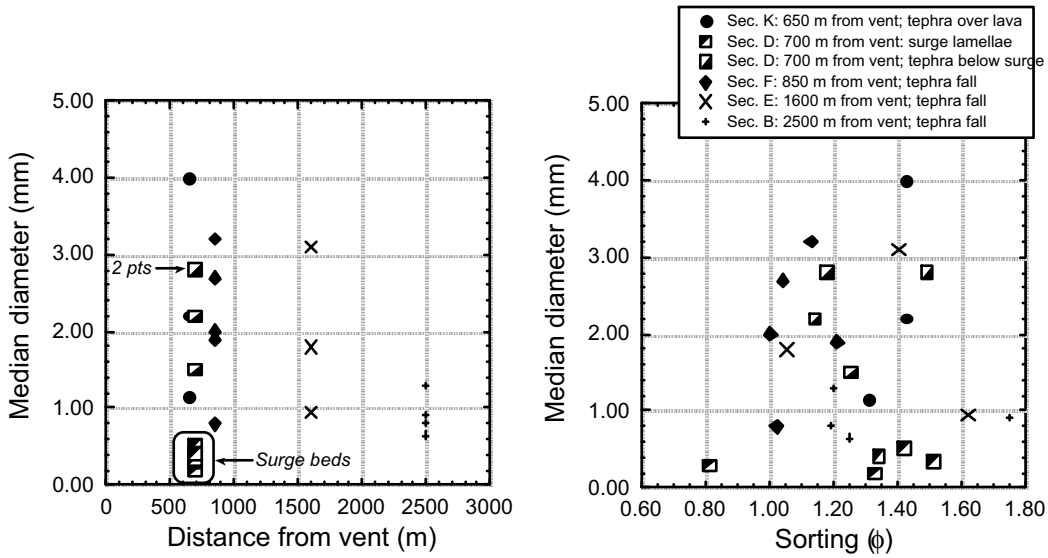

NOTES: (a) Plot of median diameter (Md_ϕ) against distance from vent and against sorting parameter.
(b) For deposits associated with fallout beyond the cone."Surge" samples refer to the package of laminated and cross-laminated beds northwest of the cone.

Figure C-9. Plot of Median Diameter (Md_ϕ) Against Distance from Vent and Sorting

Northwest of the cone, the fallout deposits blanketed an arcuate hill of Miocene ignimbrite (see Figure C-2a). Near the middle of the fallout sequence along the cone-facing flank of this hill (within 200 m to 300 m from the cone base) there is a deposit of finely laminated and cross-laminated ash (grain size parameters are plotted on Figure C-9 for comparison with other units in the fallout sequence) that reaches 120 cm in thickness. The deposit thins to the northeast and southwest and is only found in this limited area; its total volume amounts to less than 0.03% of the volume of eruptive products from the volcano. Cross laminations within the deposit indicate that its emplacement involved lateral transport with an active bed load. There are three possible origins for this deposit that is interbedded with otherwise normal fallout facies:

(1) Short-lived hydrovolcanic activity that produced a pyroclastic surge (base surge) event during the violent Strombolian activity (Vaniman and Crowe 1981 [DIRS 101620], p. 21). Wind may have pushed the surge in the downwind direction (e.g., Self et al. 1980 [DIRS 178123], p. 51) and blocking of the density stratified current by the tuff hill may have focused deposition in that area (Valentine 1987 [DIRS 177295], p. 625). Rounded quartz grains (comprising up to 5 vol % of the clasts) in the deposit might have been ejected by such eruptions from eolian deposits on the paleosurface beneath the volcano. However, the lack of any clear, correlative hydrovolcanic blast record in the well-exposed cone sequence and the lack of strong palagonitization of the deposits do not strongly support the hydrovolcanic mechanism. Correlation of this unit with the cross laminated deposit near the cone rim (Section C.6.1) cannot be ruled out, although it is unlikely that the two are related given their highly localized distribution in different directions from the crater.

(2) Heavy fallout from an ash-rich eruption column (referred to as "local collapse" by Taddeucci et al. 2004b [DIRS 175382], Figure 1, in their observations of analogous processes at Mt. Etna) that was bent toward the north-northwest by wind, may have produced a weak density current. As in the above mechanism this current may have been blocked by topography and thus preferentially deposited on the volcano-facing side of the hill. The presence of abraded ash particles (Figure C-10) and rounded quartz grains is consistent with a strong wind that could have bent the eruption column, added to the lateral component of flow in the weak density current, and also mixed in some eolian grains.

(3) Strong wind blowing to the north-northwest across recently deposited fallout might have remobilized ash-sized particles, mixed the ash with eolian particles, and deposited them on the windward side of the hill much like the mechanism that has produced sand ramps around the bases of many hills and ridges in the area. This mechanism involves no eruptive mechanism at all (actually, it calls for a lull in pyroclastic activity which is consistent with different dispersal directions for individual fallout beds as discussed below) and provides a mechanism for both mixing eolian sand with basalt grains and substantially abrading the basalt grains. Given the limited preservation of the deposits it is difficult to distinguish between these mechanisms. The evidence does not support the inference by Wohletz (1986 [DIRS 140956], p. 262) that these laminated and cross-laminated deposits record a major, initial hydrovolcanic phase of eruptions that produced a tuff ring.

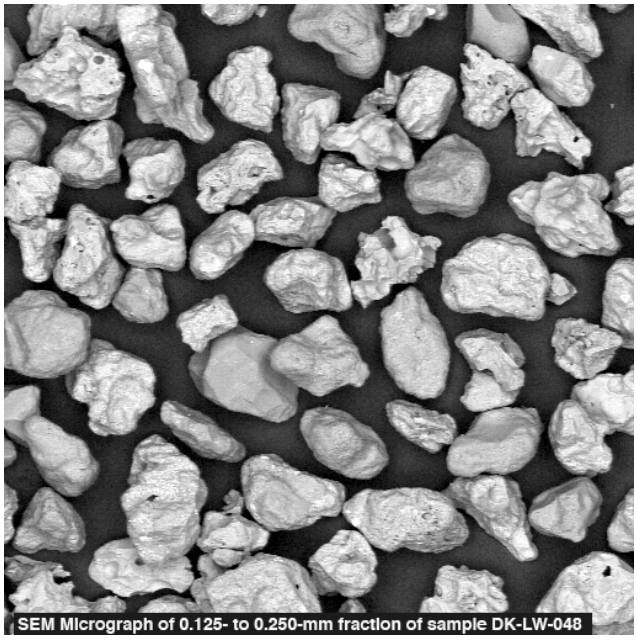

Source: LA0306GH831811.001 [DIRS 171286].

NOTE: For illustration purposes only. Abrasion and rounding by transport are visible in some grains.

Figure C-10. Scanning Electron Photomicrograph of Ash from the Laminated and Cross-Laminated Sequence within the Fallout Deposits ~200 m to 300 m Northwest of the Cone (Column D; Table C-2)

Lateral correlation of individual layers is ambiguous for most of the fallout sequence at Lathrop Wells, but some variations and local correlations do provide clues about the dispersal of different parts of the sequence. For example, there is a thin distinctive doublet of ash layers near the base of the sequence that probably correlates the lower beds of section Y (too narrow to show on Figure C-8) and sections Z and K to the south of the vent. This doublet is absent to the north and is replaced in sections F and E by the above-mentioned salt-and-pepper layer. This indicates that separate fallout units were dispersed in different directions, some to the south and some (most?) to the north. The isopach map (Figure C-2c) must be viewed as a composite result, and cannot be simply related to column height and wind directions. Based upon analogy with historical eruptions that produced similarly dispersed fallout beds (e.g., Hill et al. 1998 [DIRS 151040], p. 1,236, Figure 5; Arrighi et al. 2001 [DIRS 162795], pp. 145 and 146), it can be inferred that individual eruption column events might have reached sustained heights up to a few kilometers. Many stratigraphic columns have distinct zones in their midsections that are characterized by ash layers. Although in most places these are planar bedded and do not show any clear evidence of lateral transport (i.e., they were likely deposited by simple fallout), it is possible that they are lateral equivalents of the laminated and cross-laminated ash unit described in the previous paragraph. Figure C-8 presents the stratigraphic columns in a manner that "normalizes" them to a common datum that assumes this correlation of ash layers is true. However, as there are other potential interpretations, it would be difficult to prove such correlations.

C.6.3 Northeast lava field

The northeast lava flow field extends from the northeast base of the cone, reaching up to 400 m northward. This proximal portion of the lava field is mantled by fallout scoria from the violent Strombolian eruptive phase and has several pyroclast mounds on it, while the main eastern portion of the field has little scoria on its top but does overlie fallout deposits and has sparse pyroclast mounds. These relationships indicate that the lava field formed late relative to pyroclastic eruptions and might have continued growing after they had ceased. The pyroclast mounds rise 5 m to 15 m above the surrounding lava surface and have rounded tops, and are characterized by loose scoria clasts in the large lapilli to small block size range and are blocky in shape. Only one mound was observed containing larger clasts that are fragments of broken fluidal bombs, as well as large blocks of dense, poorly vesicular basalt up to 1 m in size. One mound in the proximal area has a lava squeeze-up on one of its margins.

Mounds of pyroclasts within the northeast lava field are apparently more aligned along flow direction of associated lava than those on the south lava field. Perry et al. (1998 [DIRS 144335], p. 2-41) considered the alignment of mounds, along with observations from trenching their margins, to indicate the trend of fissures and vents for surrounding lava flows. In contrast, the mounds are interpreted here to be material that was rafted from the cone by lava effusion during the violent Strombolian cone-building phase. This is consistent with the grain size and lack of agglutination in the mounds of the northeast lava field (compare with mounds on the south lava field that commonly are agglutinated or welded and retain some original bedding, having been scavenged from the early, Strombolian cone). The alignment of mounds simply reflects flow direction of proximal lavas that carried the rafts.

Northeast of the cone the medial to distal parts of the northeast lava field bend to the south to form an elongate platform about 1.6-km long (implying effusion rates up to ~4 m^3/s;

Walker 1973 [DIRS 178061], Figure 4), the central part of which is ~25 m above the surrounding desert floor. The overall geometry of the lava field suggests that it was fed by lavas that vented from the northeastern base of the cone. As lavas accumulated near the foot of the cone, they were successively diverted to the east until they were able to "catch" the gentle southward slope of the paleotopography. Then the bulk of lava emplacement was toward the south, probably following a shallow fluvial paleochannel. As the platform thickened and lengthened it also widened as lobes of lava broke out from the flow margin. Such lobes are preserved along the northern and eastern margins of the northeast lava field (Figure C-11), where they are typically ~10-m wide, ~10-m to 20-m long and have fronts ranging from 2-m to 5-m high. Many of the lobes have axial grooves (~1-m to 2-m wide) on their surfaces that may represent small collapsed lava tubes, and a few have ripply surface ridges. The common down-stepping, terrace-like nature of individual lobes (Figure C-12a) suggests that many of the lobes extended outward by successive breakouts from their toes (toothpaste lava; Rowland and Walker 1987 [DIRS 178122], p. 638; Rossi 1997 [DIRS 178141], p. 99).

NOTES: Lines show the eastern edge of the south lava field and the west edge of the northeast lava field (dashed where flow margins are not visible due to coverage by eolian sand). Dotted pattern indicates possible ripply surface ridges (largely obscured by eolian sands) along what might have been a main surface lava channel.

Figure C-11. Aerial View of Medial and Distal Parts of the Northeast Lava Field, Illustrating Lobate Nature of the Flow Margin

The lobe breakout mechanism described above suggests that lava tubes fed much of the lateral growth of the lava field. From this, it can be inferred that some portion of the thickness of the lava platform may result from inflation (see, for example, Luhr and Simkin 1993 [DIRS 144310], p. 86), but stacking of flows on the growing platform was also an important factor in its thickening. Features such as those shown in Figure C-12b clearly demonstrate stacking of flow units. It is common for successively higher flow units to have margins that are inboard of the underlying unit's edge. This reflects the occurrence of slight topographic highs near the edges of flows formed by swelling of the flow margin and squeeze-ups as it came to a stop. Thus as an overriding flow approached the outer margin of the earlier flow it began to move uphill, halting before reaching the edge of the earlier unit. This process helped produce a platform that is thickest along the axis of the lava field and steps down in a terrace-like manner towards its outer edges. Some stacked flow units, however, drape over and extend beyond the margin of underlying units (e.g., Figure C-12c). These may form relatively narrow (20-m to 40-m wide) channels where they flowed over the steep front of an underlying unit, and then fanned out to form a distributary set of lobes on the relatively flat desert floor. This is reminiscent, on a small scale, of observations at volcanoes such as Mt. Etna where lavas flowed through well-defined channels over steep slopes, and then feed broader lava fields at the break in slope (e.g., Duncan et al. 2004 [DIRS 178114], pp. 174 and 175).

The surface of most of the northeast lava field, where its platform is thickest, is obscured by eolian sand sheets and dunes, but some original emplacement features can be distinguished. One of these is a 40-m- to 60-m-wide, ~600-m-long zone along the lava field axis that has a vaguely defined, coarse (~10-m to 20-m wavelength) ripply surface texture (Figure C-11) caused by pressure ridges on the crust of an axial lava channel. Away from this axial channel there are small pressure ridges and lava terraces. The latter are typically arcuate in shape, 1-m to 2-m high and a few tens of meters long, and subparallel to the axial channel and lava field margins. Some of these terraces are likely the fronts of small overflows from the axial channel.

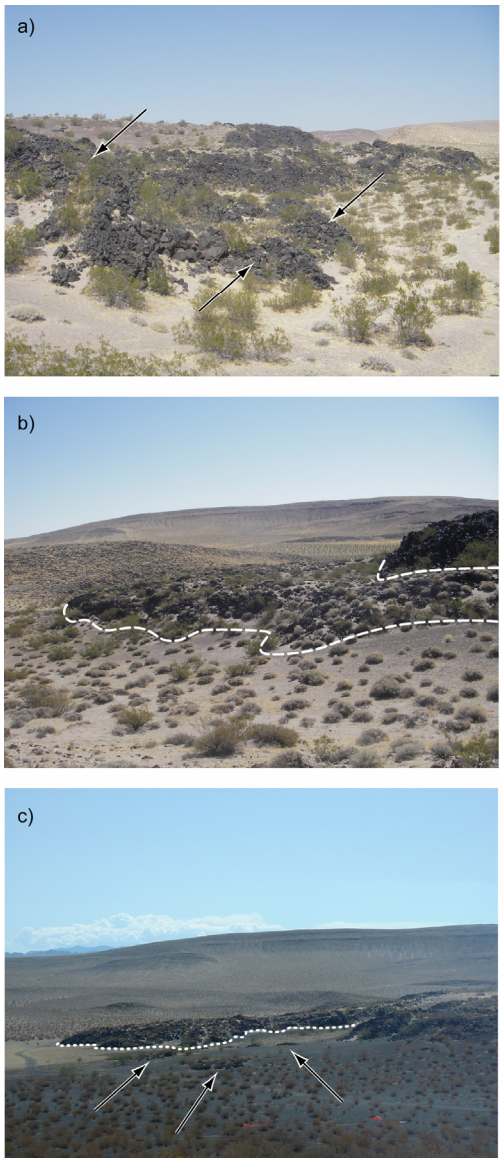

NOTES: (a) Down-stepping lobes (arrows) representing successive tube-fed breakouts of lava from the toes of lobes, along eastern margin of the lava field. Lowermost lobes are ~1-m high (original height cannot be determined due to partial burial by eolian sand ramps).

(b) Stacking of flow units. Dashed lines indicate outer margins of two flow units. The lower unit formed a ~100-m-wide, 3-m- to 5-m-high platform where lava abutted a hill of Miocene ignimbrite. Later lava lobes were emplaced on top of this platform, as shown by the upper flow front near the right side of the photograph.

(c) Low-lying flow units on the northern edge of the northeast lava field were partly buried by a combination of violent Strombolian fallout deposits, by sediment accumulation after the lavas temporarily dammed a drainage from the north, and by eolian sands. Arrows point to the tops of flow edges or squeeze-up features from these low-lying units that protrude above the pyroclastic and sedimentary deposits. Edges of flow units emplaced on top of the low-lying units are clearly visible. Unlike many stacked flow units, the longest of these, in the middle ground of the photograph (edge indicated by dotted line), did not stop inboard of the underlying flow's edge but flowed over it onto the desert floor. The total length of this unit, which has a central ripply channel that feeds four distributary lobes towards its northern (distal) end, is ~140 m.

Figure C-12. Features along Margins of the Northeast Lava Field

C.7 VOLUMES OF ERUPTIVE PRODUCTS, XENOLITH CONTENT, AND CONDUIT SIZE

Volumes of volcanic products of Lathrop Wells volcano were calculated by planimeter and using the thickness values mid-way between adjacent isopachs (Figure C-2c). The area covered by ≥1 cm of tephra is ~182 km^2. Volume of tephra fall enclosed by the 1-cm isopach is ~0.07 km^3 (DTN: LA0609DK831811.001). The total lava volume of 0.03 km^3 was obtained using a mean flow thickness of 15 m. The early (south) and later (northeast) flows were differentiated based on appearance, topographic expression, color aerial photography, and evaluation of recent aeromagnetic survey results (Perry et al. 2005 [DIRS 177379], Figure 1); the south lava flow has volume of 0.013 km^3 and the N flow volume is 0.016 km^3. Approximation of the cone as having a circular base with a mean radius of 700 m yields a cone volume of ~0.02 km^3 (this approximately corrects for cone volume that was removed by rafting; see Section C.6.1). Thus, the ratio of fallout to cone volumes is ~3.5. As with most prehistoric basaltic eruptions, a large uncertainty for Lathrop Wells is associated with the tephra fallout volume (Pyle 1995 [DIRS 162829]) caused by erosion or burial of much of its extent. The volumes reported here supersede those by Valentine et al. (2005 [DIRS 177782], p. 630) and Valentine and Perry (2006 [DIRS 177495]) and reflect a reassessment of the fallout volume.

Xenolith abundances were measured on eighteen 1-m^2 exposures of vertical quarry walls using the method of Valentine and Groves (1996 [DIRS 107052, pp. 79 and 80; DTN: LA0302GH831811.003 [DIRS 162865]). Xenolith types are dominated by light-colored, fine-grained Miocene tuffs, which reach ~335-m thickness beneath the volcano (Peterman and Spengler 1994 [DIRS 106499], p. 14). The xenoliths are present as loose clasts and in cored bombs. The abundance is greatest in the lower (early) violent Strombolian deposits in the cone and decreases one to two orders of magnitude in later scoria intervals (Figure C-13). The range of xenolith concentration values obtained at Lathrop Wells cone is consistent with that measured in deposits produced by magmatic fragmentation (predominantly Strombolian and Hawaiian mechanisms) at the Lucero volcanic field (New Mexico; Valentine and Groves 1996 [DIRS 107052], p. 77, Figure 5), and is significantly lower than values reported for hydrovolcanic eruption facies in the Lucero and Hopi Buttes (Arizona) fields (Valentine and Groves 1996 [DIRS 107052], pp. 77 and 78, Figure 5; White 1991 [DIRS 124930], pp. 247 and 248, Figure 3). Doubik and Hill (1999 [DIRS 115338, p. 60) used computer-assisted image analysis to derive an average abundance of 0.9 vol % for xenoliths > 1-mm diameter for the Lathrop Wells cone, about one order of magnitude larger than the average reported here of 9.8×10^{-4}. However, the common occurrence of secondary carbonate and/or silica coatings on lapilli surfaces is a possible reason why the Doubik and Hill (1999 [DIRS 115338, p. 60) xenolith concentration estimate is higher.

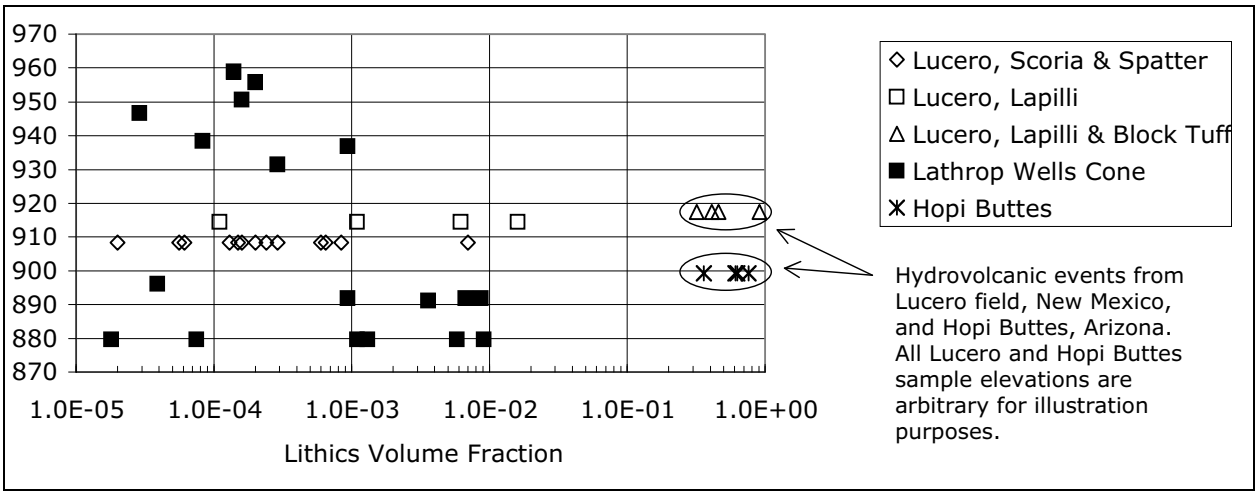

NOTES: Values for volcanoes of the Lucero Volcanic Field (New Mexico; Valentine and Groves 1996 [DIRS 107052]) and the Hopi Buttes Field (Arizona; White 1991 [DIRS 124930]) are shown for comparison. Lathrop Wells cone data from LA0302GH831811.003 [DIRS 162865].

Figure C-13. Xenolith Concentration (Volume Fraction) Plotted Against Elevation in the Lathrop Wells Cone

Combining the mean xenolith volume fraction of 9.8×10^{-4} with the cone volume from the preceding paragraph, and assuming a cylindrical conduit through the 335-m-thick Miocene tuff sequence, the average conduit diameter is ~16 m. Assuming fallout deposits and lavas have similar xenolith content (this is a conservative assumption because, as mentioned above, most fallout beds are virtually xenolith free and xenoliths are very sparse in the lavas), the added volume of xenoliths would imply a maximum average conduit diameter of about 21 m. In reality, the conduit is probably widest near the Earth's surface and narrows with depth (Section F, Figure F-9), but the lack of depth control of xenoliths within the 335-m Miocene interval does not allow an estimate of this shape.

No xenolith concentrations observed within the cone or fallout sheet indicate significant conduit-clearing activity. Doubik and Hill (1999 [DIRS 115338], p. 60) noted that distinctive, small clasts of basaltic breccia with up to 50 vol % angular xenoliths of heterogeneous Miocene tuffs are scattered around the lower flanks of the cone (none of this type have been observed within quarry walls). The clasts range up to 15-cm diameter, but average size is <5 cm. The occurrence is limited to the late (possibly last) deposits of the cone. The total volume of the breccia clasts is insignificant relative to the cone volume. The occurrence likely indicates some local, late-time disruption along the feeder dike or conduit boundaries within the thick ignimbrite host rock beneath the cone, possibly related to effects of waning magma flux below the vent.

C.8 POSTERUPTIVE FEATURES

C.8.1 Scoria Cone

The extent of erosion of the scoria cone has been a subject of debate, with arguments for little erosional modification of the cone centering on the lack of an erosional apron surrounding the base of the cone (Wells et al. 1990 [DIRS 107208], p. 551, Table 1), and upon the relatively low degree of rilling compared to parts of the fallout deposits beyond the cone that have been

completely stripped from some surfaces (discussed in Section C.8.2). Erosional features in the form of shallow rills (wavelengths of 10 m to 20 m and depths of 1 m to 2 m) are present on the upper 40 m to 60 m of the outer cone and inner crater slopes (Figure C-14). Well-developed garlands of coarser scoria clasts are abundant on the upper two-thirds of the cone slopes, an indication of creep processes. Trenching of the inner crater slopes and rim by Perry et al. (1998 [DIRS 144335], pp. 2-66 and 2-67) revealed that the uppermost primary tephra unit within the crater is a ~1-m-thick, black, primary scoria-fall deposit that overlies red oxidized scoria deposits with no evidence of any temporal break between the units. The black scoria unit does not extend to the crater rim but is truncated within the present inner crater wall by an erosional surface ~4 m vertically below the present rim. The contact between the black and the underlying red scoria deposit has a dip of 33°. Extrapolation of the basal contact of the black scoria would project ~7 m to 8 m above the present rim surface, assuming the contact maintained a constant 33° dip to the rim midpoint (Figure C-15). Analysis of digital elevation data from the cone and extrapolation of slopes also indicates that up to 9 m of rim material may have been removed. Thus, Perry et al. (1998 [DIRS 144335], pp. 2-66 and 2-67) estimate that the rim of the crater (on its west side) has been lowered by 5 m to 9 m by a combination of erosional rilling and creep.

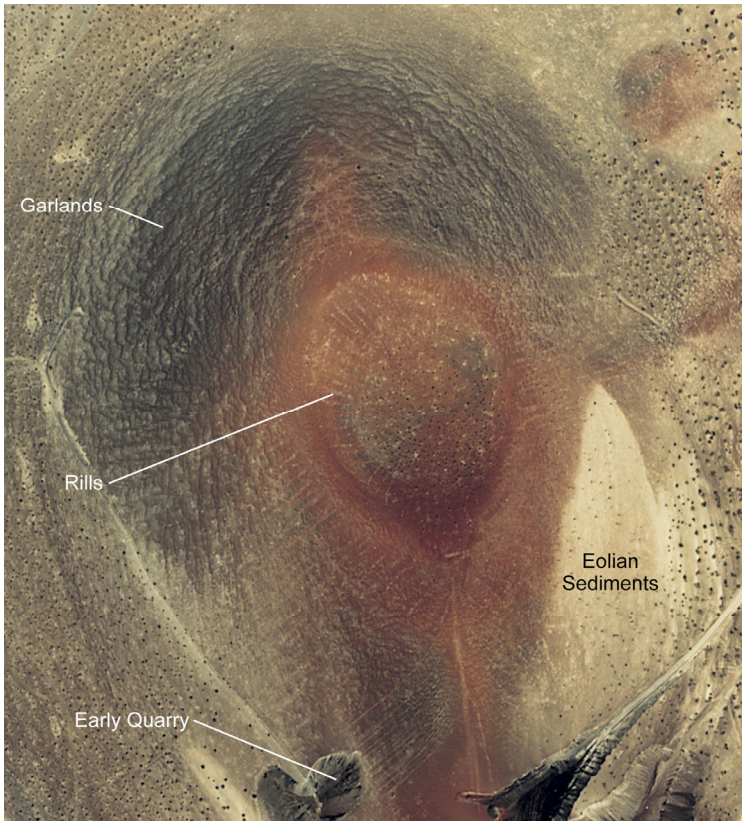

NOTES: Linear features extending both inward and outward from crater rim are erosional rills (especially visible on the southern half of the cone). Dark-colored arcuate features on outer cone slopes are garlands produced by creep of loose scoria deposits. Light-colored area on southeast slope of cone is caused by accumulation of eolian sand and silt at a rate that exceeds the rate at which the sediments can infiltrate into the underlying scoria (see also Valentine and Harrington 2006 [DIRS 177271], p. 535).

Figure C-14. Aerial View of Lathrop Wells Cone Taken in 1987 before Major Quarrying

The cone profile (Figure C-15a) departs from that of a symmetrical cone with slopes at the angle of repose (30° to 35°). Rounding of the rim is due to the erosional and creep processes described above. A subtle bulge on the western and northern slopes (between altitudes of 860 m to 930 m on the west slope profiled in Figure C-15a) represents scoria mass that has crept from the rim as well as a component that has washed down the rill system. The east flank of the cone rises at an angle of only 24° to a rim that is nearly 20 m lower than the opposing (western) rim, reflecting cone slumping and rafting during eruptions.

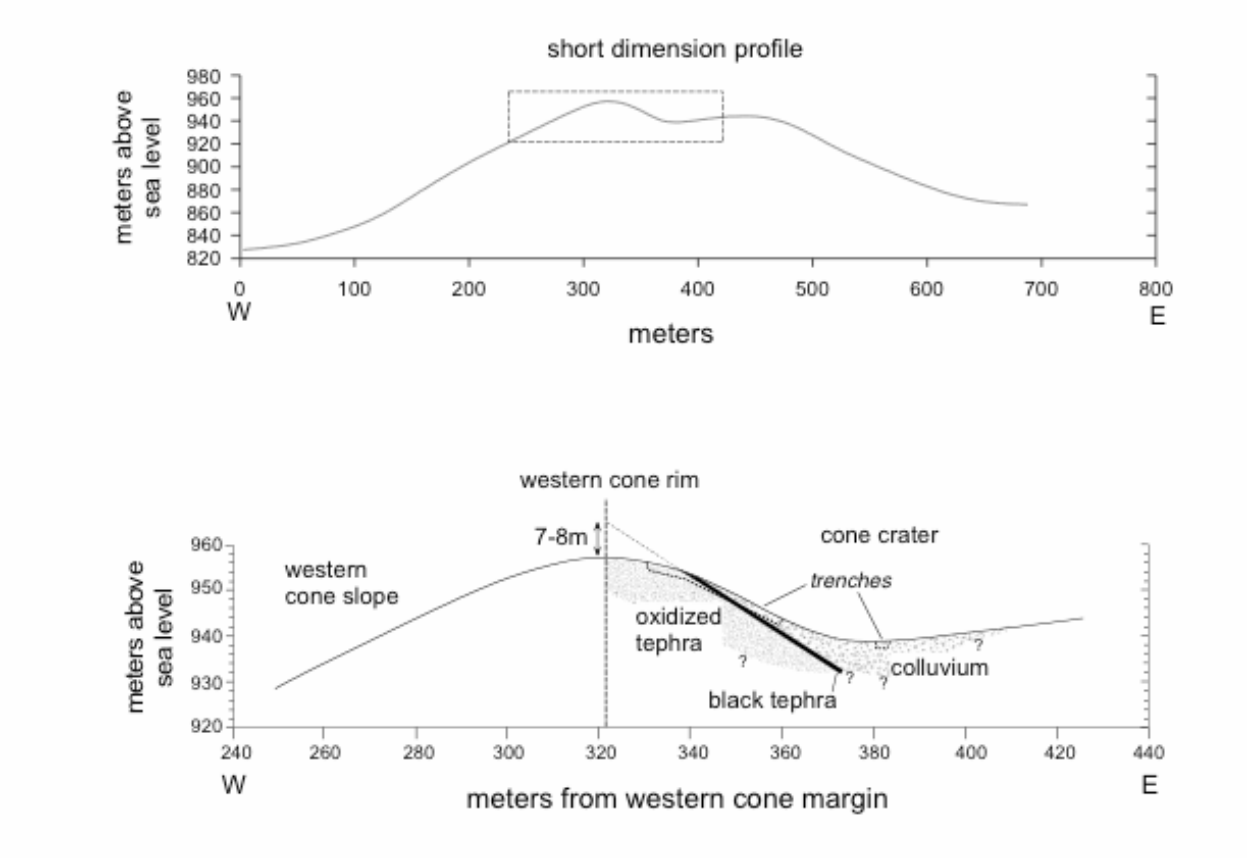

NOTES: (a) West-east profile of cone through the crater center. Dashed rectangle defines part of profile detailed in (b).

(b) Cross section through western crater rim, showing locations of trenches and depositional units (oxidized tephra, black tephra, and crater-filling colluvium) that constrain the degree of erosion of the rim (dashed line extrapolates basal contact of black tephra unit above modern rim).

Figure C-15. Cross Section to Illustrate Evidence for the Erosional History of the Lathrop Wells Cone

Wells et al. (1990 [DIRS 107208], p. 553) argued for a cone age of ~20 ka or less based upon the relatively low degree of rilling and absence of a cone apron, and comparison with relationships between cone morphology and age at other basaltic volcanoes in the Mojave Desert. The onset of degradation processes in this arid setting is delayed for cones that were dominated by violent Strombolian eruptions in their late stages of growth. The resulting cone slopes are composed initially of loose scoria blocks and lapilli. For some time after eruptions have ceased, rain will simply infiltrate into this loose, porous material and will not nucleate as runoff. As eolian sediments accumulate in the upper few decimeters (Section C.8.3) the porosity and permeability

of the surface, and thus the infiltration capacity, is reduced until runoff and resulting material transport can occur by facilitating formation of small debris flows that play an important role in cone degradation (Wells et al. 1990 [DIRS 107208], p. 550). Lathrop Wells cone is in the initial stages of this degradation. This lag time while eolian material accumulates contrasts with cones that have coarse, welded (relatively impermeable) material on their slopes. In these cases, runoff nucleates immediately after cone formation and degradation advances quickly. This dependence on initial surface textures on the Lathrop Wells cone may have complicated inferences about cone age (Wells et al. 1990 [DIRS 107208], p. 549). A topic of future research is to quantify this time lag and the implications for degradation-based age estimates (e.g., Wood 1980 [DIRS 162860], p. 137; Hooper and Sheridan 1998 [DIRS 178066], p. 241).

C.8.2 Fallout Deposits beyond the Cone

A discussion of surficial processes acting on fallout deposits beyond the cone is important for assessing geomorphic evolution of the Lathrop Wells tephra, as well as for insights into processes affecting erosion and redistribution of some future tephra fallout at Yucca Mountain. The fallout deposits have evolved in three different ways according to the types of surfaces upon which they were deposited. Where fallout accumulated within ~200 m of the immediate foot of the scoria cone, and on top of the lava fields (particularly the south lava field), the top surface is both above the level of active fluvial deposition and the surface slopes are low. The former means that the fallout deposits have not been buried by sediments in these locations, and the latter implies that the fallout surface (top of the deposit) has experienced relatively little surface runoff (rilling) and/or creep processes. In such locations, the dominant surficial process is that of accumulation of eolian sediment, infiltration of that sediment into pore spaces in the fallout deposits, and ongoing development of desert pavements (Valentine and Harrington 2006 [DIRS 177271], p. 535, Figure 3). This process is described in more detail in Section C.8.3.

The fallout has been buried in some places by fluvial sediments where it was deposited on the low, flat parts of the surrounding valley floors, but also locally eroded by fluvial channeling. This combination is most prevalent from ~300 m to 2 km immediately west and north of the Lathrop Wells cone. Depth of burial beneath coarse alluvial sediments (and finer playa-like deposits around the north edge of the northeast lava field; see below) typically amounts to ~20 cm to 50 cm.

Surficial processes have been more complex where fallout was deposited on slopes and ridges composed of Miocene tuff bedrock. In such settings much of the fallout has already been completely stripped, but in two more proximal locations the stripping process is still under way. One of these is the aforementioned hill immediately west and northwest of the cone. Here the fallout deposits have been eroded from the upper one-third of the slopes of the hill. The upper reaches of the remaining fallout are characterized by small, low-profile ridges of tephra that lap up onto bedrock and are partly littered with fragments of Miocene tuff that were transported from uphill locations by small debris flows. Currently, runoff nucleates in the notches between the ridges and has formed gullies that extend tens of meters downslope in a process that is very similar to that described on La Fossa (Vulcano Island, Italy) by Ferrucci et al. (2005 [DIRS 178115], pp. 177 and 178, Figure 5). As the slope shallows toward the base of the hill, the gullies transition into small, subdued alluvial fans. Typically, the primary fallout deposits beneath these gullies are overlain by decimeter-thick, massive debris flow deposits

(matrix-supported mixture of sand, scoria clasts, and angular fragments of Miocene tuff), which in turn are overlain by crudely laminated and cross-laminated deposits that exhibit cut-and-fill features, indicating transient, hyperconcentrated flows (similar to, but on a smaller scale than, deposits of localized hyperconcentrated flows documented by Valentine et al. 1998 [DIRS 177296], p. 630). Apparently the process of erosion of fallout deposits off slopes involves multiple stages of transport by debris and hyperconcentrated flows, formation of debris fans or small alluvial fans, and subsequent migration of runoff to the low points between these fans. As with remobilization of cone slope material (Section C.8.1), the accumulation of eolian sand and silt within the upper decimeters of fallout deposits plays an important role in reducing porosity and permeability to facilitate runoff, and in providing fines that facilitate transport via debris flows.

C.8.3 Lava Fields

Posteruptive surficial features have evolved differently on the two lava fields due to their different original surfaces, and provide an important snapshot at an earlier stage relative to similar, ~1-Ma lava surfaces in Crater Flat (Figure E-12). Because of a mantle of fallout deposits in addition to abundant rafted pyroclastic material on the south lava field, it has a more subdued surface than that of the northeast lava field. This difference in the original volcanic surfaces has also played an important role in the posteruptive geomorphic evolution of the lavas. Understanding the effects of initial conditions or textures on geomorphic processes is critical in attempting to determine relative ages of surfaces. For example, Bradshaw and Smith (1994 [DIRS 101996], p. 168) assumed that differences in surface morphology of lava fields at the ~1-Ma volcanoes in Crater Flat were evidence of significant age differences of eruptive units within individual small-volume volcanoes. Wells et al. (1990 [DIRS 107208], p. 551) came to a similar conclusion about the two lava fields at Lathrop Wells, stating, “Those flows along the southwestern edge of the cone appear to be the oldest, whereas flows along the northeastern part of the cone appear to be the youngest.” They concluded that the lava fields were produced by polycyclic eruptions separated by significant time (although not explicitly stated, the implication was thousands to tens of thousands of years; Perry et al. 1998 [DIRS 144335], pp. 2-2 and 2-3]) based upon the different lava field morphologies. In reality, the individual volcanoes both in Crater Flat and at Lathrop Wells are monogenetic (erupted over time frames of months to years) and the geomorphic differences were controlled by variations in initial conditions.

In more humid climates, soils form on volcanic deposits mainly by a combination of in situ weathering of the parent material and accumulation of organic material. In contrast, soil formation in the arid to semi-arid Mojave Desert is dominated by deposition of eolian sediment in the fine sand to silt size range (e.g., McFadden et al. 1987 [DIRS 105023], p. 505 and 507; 1998 [DIRS 176089], p. 110). The style of eolian sedimentation is in turn intimately linked with the development of desert pavement (a mosaic of lapilli-sized clasts on the surface of a desert soil). Valentine and Harrington (2006 [DIRS 177271], p. 535) described the development of soils and desert pavements on fallout lapilli deposits as a three stage process: (1) primary deposition of fallout lapilli beds; (2) deposition of eolian sediment on and around surface clasts and infiltration of the sediment into interclast pore spaces in the uppermost decimeters of the pyroclastic deposit (by a combination of mechanical movements associated with wetting, drying, freezing, and thawing, and by bioturbation); (3) aggradation of clean eolian sediment above the fallout deposit after pore space is completely clogged, and lifting of the surface layer of clasts as

a desert pavement. Subsequent geochemical processes cause additional zonation within the eolian soil (see McFadden et al. 1998 [DIRS 176089] for review). Based on field observations at Lathrop Wells volcano and at the nearby, ~1-Ma Red Cone volcano, Valentine and Harrington (2006 [DIRS 177271], pp. 533 and 536) determined that this process must occur over many tens of thousands of years if the parent material is well-sorted scoria lapilli.

A key element of the above sequence of processes is that the desert pavement serves to trap eolian sediments and stabilize them with respect to later remobilization by wind. On a surface initially covered with abundant lapilli, clasts are immediately available for formation of desert pavement. This is the case with the south lava flow field. Most of its surface is covered by a maturing desert pavement that is underlain by a 20-cm- to 40-cm-thick zone of mixed scoria and eolian sediment (the second stage discussed in the previous paragraph; Valentine and Harrington 2006 [DIRS 177271], Figure 3). If, on the other hand, such clasts are rare or absent (e.g., bare rock), pavement and resulting stabilization will be unable to develop until mechanical weathering of the surface has produced clasts from which a pavement can form; eolian sediment will be easily remobilized. This is the case with the northeast lava field, which is largely covered by an active dune field. Lava crags and other surface irregularities act as nuclei for dunes; abundant eolian sediment is trapped on the surface of the lava field but only temporarily, unlike that which is permanently trapped beneath desert pavements of the south lava field. Early stage formation of pavement material is actively taking place by mechanical weathering of lava highs (e.g., Figure C-16). Eventually this weathering process, combined with eolian accumulation in low spots, will result in a smooth, variably paved surface for the lava field (as described at the Cima volcanic field by Wells et al. 1985 [DIRS 178074], and at the ~1-Ma basaltic volcanoes of Crater Flat by Appendix E). The small portions of the northeast lava field with pyroclastic material (either directly deposited by fallout or rafted into place) have subdued topography and pavement similar to that of the south lava field (Valentine and Harrington 2006 [DIRS 177271], p. 534).

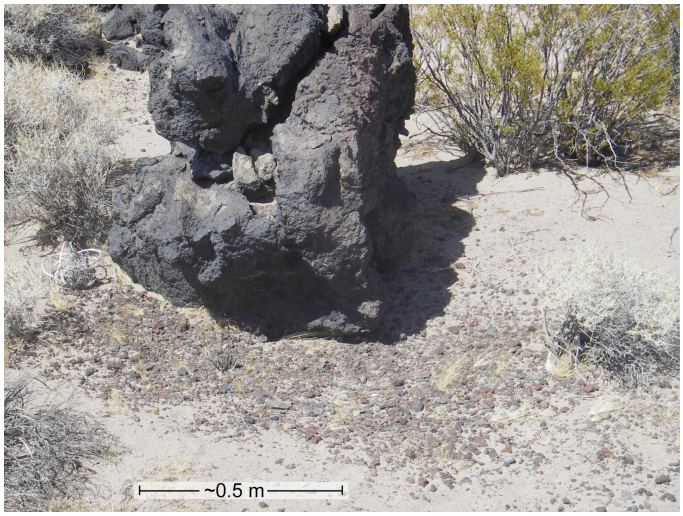

NOTES: Fragments of the crag are produced by freeze-thaw and thermal spalling of the lava, especially on the south (sunward) face of the crag (shown in the photograph). Where the clasts accumulate around the crag they begin to stabilize the eolian sediments and evolve towards a desert pavement.

Figure C-16. Mechanical Weathering of a Small Lava Crag on the Northeast Lava Field, Lathrop Wells Volcano

The effusion of the northeast lava field filled and raised the topography of the small fault-block-bounded valley occupied by the volcano and blocked a drainage from the north. Several meters of alluvial sediment accumulated just to the north of the lava field, which partly buried some low-lying flow lobes (Figure C-12c). It is likely that a lake (possibly ephemeral) formed in this area, as indicated by the presence of a small playa. As lake level rose, it overtopped the low point of the natural dam that was formed by the lavas and adjacent ridge (fault block) of Miocene ignimbrite, cutting a new channel through the ridge and around the eastern margin of the lava field.

C.9 SUMMARY AND CONCLUSIONS

The Lathrop Wells volcano, despite its relatively small volume, displays a wide range of eruptive processes (Figure C-17). These range from relatively weak Strombolian explosions of coarse, ballistic bombs to sustained eruption columns of well-fragmented, vesicular scoria lapilli. Pyroclastic facies range from coarse, variably welded agglutinate rich in fluidal clasts to well sorted fallout beds and localized surge or surge-like units. Lava effusion occurred during both Strombolian and violent Strombolian explosive activity (Valentine et al. 2005 [DIRS 177782], pp. 629 and 631). As with the nearby ~1-Ma volcanoes in Crater Flat (Appendix E), early lavas flowed southward down a gently sloping valley floor (although at Lathrop Wells, this was complicated by the presence of a low ridge of Miocene tuff that extended southward from the main vent area). The early lavas built a platform through a combination of inflation and flow-unit stacking; eventually this reversed the topography around the base of the cone such that later lavas were diverted northward and eastward until they encountered an unobstructed slope or a drainage channel down which they subsequently flowed. Early lavas were more likely to raft segments of the cone from its weaker down-slope (south) side, while later lavas rafted less material because of the buttressing effect of the sloping ground beneath the cone (Appendix E, p. E-9). Previous authors (summarized by Perry et al. 1998 [DIRS 144335], p. 2-41) inferred that the scoria mounds scattered across the lava fields are separate vents, which in turn implies multiple feeder dikes and conduits beneath the volcano's footprint. These mounds are rafted cone material and, as such, there was only one feeder dike/fissure and one main conduit from which all eruptive products emanated, with shallow (near the interface between cone and substrate), lateral breakouts from that conduit that fed lava flow fields.

Comparison of the Lathrop Wells cone height with the growth rates of historically observed scoria cones (Wood 1980 [DIRS 116536], p. 399, Figure 7) suggests that the cone could have been constructed over a period of 1 day to 100 days of explosive activity, most likely a time scale of a few weeks. The fallout deposits beyond the cone were deposited during the later (violent Strombolian) cone building activity. The south lava field would have required ~150 days to accumulate based upon a continuous effusion rate of about 1 m^3/s, while the northeast lava field would require ~45 days at a continuous effusion rate of 4 m^3/s (the effusion might have been pulsatory, as suggested by Appendix E, Section E6.1, which would extend the durations). These time scales, although very rough, indicate that the volcano might have been active for as little as approximately seven months, and that explosive cone-building activity occurred during only part of that time. Because much of the northeast lava field has little or no fallout scoria on its top, it seems likely that much of its emplacement continued after pyroclastic activity had ceased.

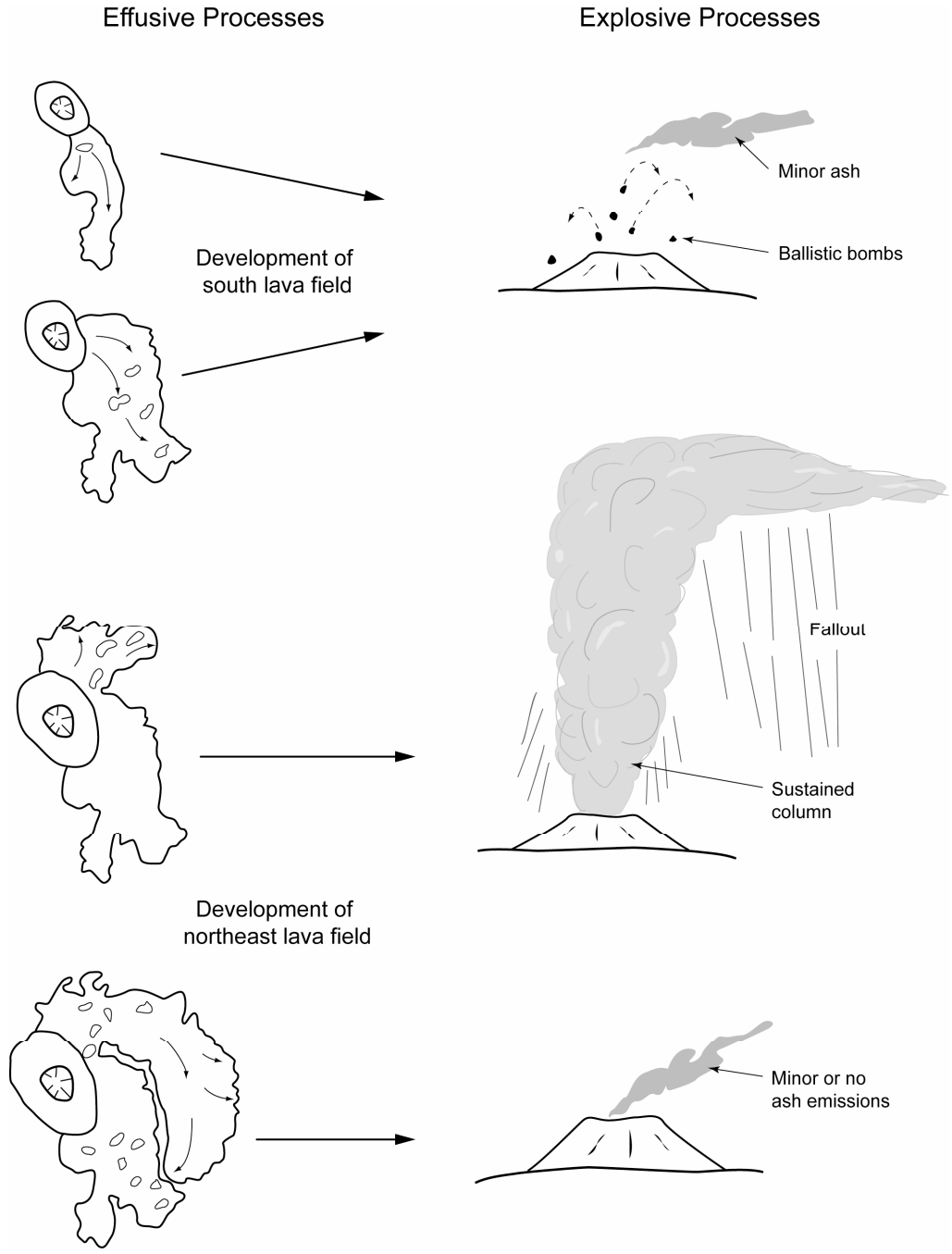

NOTES: Earliest (plagioclase phenocryst-bearing) lava flows to the southwest of the developing cone were contemporaneous with Strombolian explosions that ejected mainly coarse, ballistic bombs to form variably welded deposits. Strombolian cone building continued through the development of the remainder of the south lava field, and was counteracted to varying degrees by rafting of material atop the lavas. The south lava field increased in thickness in proximal areas, progressively diverting emerging lavas toward the north. Violent Strombolian activity produced multiple eruption column events and buried the south lava field and the early parts of the northeast lava field. Development of the remainder of the northeast lava field continued after violent Strombolian activity had waned, such that only remnants of ash and fine lapilli are present.

Figure C-17. Interpretation (Top to Bottom) of Effusive and Explosive Processes that Formed the Lathrop Wells Volcano

The complexity of the Lathrop Wells eruption, given that the major element composition changed very little throughout, indicates that fluid dynamic processes such as vesiculation and bubble coalescence, gas loss to country rocks, and varying degrees of separation in the two-phase eruptive mixture to produce simultaneous violent Strombolian columns and lava effusion, are of fundamental importance in determining eruption processes at scoria cone volcanoes.

The different volcanic surfaces left by the eruption that formed the Lathrop Wells volcano have been modified by a variety of geomorphic processes. As mentioned earlier, Lathrop Wells provides an earlier-time snapshot of these processes relative to those observed at the older volcanoes in Crater Flat (Figure E-12). The fact that such volcanoes initially produce a variety of surfaces, along with the fact that eruptions can be accurately dated by techniques such as $^{40}Ar/^{39}Ar$, suggests that the combination of quantitative physical volcanological and geomorphic characterization of successively older volcanoes can provide much insight into the rates of surficial processes as a function of initial condition in a given environmental setting (building, for example, on the work of Wells et al. 1985 [DIRS 178074]; McFadden et al. 1987 [DIRS 105023]; 1998 [DIRS 176089]; and Valentine and Harrington 2006 [DIRS 177271]).

If a future volcanic event occurs at Yucca Mountain and intersects the proposed repository (250-m to 350-m depth), based upon the phenomena that created the Lathrop Wells volcano, the following features are anticipated:

(1) The total volume of eruptive products will be ~0.1 km^3 and will be partitioned such that about one third of the volume is erupted as lavas and the rest is erupted as pyroclasts, most of which would be dispersed by eruption columns up to a few kilometers high.

(2) The event will be from one main feeder dike and conduit, up to ~20 m to 25 m in diameter at repository depth, with shallow lateral breakouts (as opposed to multiple feeder dikes and conduits) that feed lava flows.

(3) Based upon the violent Strombolian nature of much of the eruption, explosivity of the initial interaction with repository drifts and subsequent eruptive dispersal could be high if the basaltic magmas have significant volatiles (see Woods et al. 2002 [DIRS 163662] p. 19-3; Dartevelle and Valentine 2005 [DIRS 178142], Figures 2 and 3). Hydrovolcanic explosions might occur if shallow groundwater is available, but this would be relatively minor based upon the small fraction of products at Lathrop Wells that might be of hydrovolcanic origin and the near absence of evidence for such activity in other volcanoes of Crater Flat (Section E.6.1).

Fallout tephra, potentially contaminated by entrained radioactive waste, would be stripped from slopes (particularly bedrock slopes) and transported away by fluvial processes, with only thick proximal deposits remaining after tens of thousands of years, while fallout deposited on relatively flat surfaces may be buried and immobilized by an accumulation of eolian or fluvial sediments or locally incised by channels and transported downstream. Cone deposits might be relatively stable for several tens of thousands of years before degradation processes set in.

APPENDIX D

PHYSICAL VOLCANOLOGY OF THE LITTLE BLACK PEAK AND HIDDEN CONE VOLCANOES

APPENDIX D - ERUPTIVE STYLES AND INFERENCES ON PLUMBING SYSTEMS AT HIDDEN CONE AND LITTLE BLACK PEAK SCORIA CONE VOLCANOES (NEVADA, U.S.A.)

D.1 INTRODUCTION

Eruptive styles and the factors that control location of continental basaltic volcanoes and their vents are important from the perspective of predicting volcanic risk and for overall understanding of basaltic magmatism and volcanic field evolution. Sporadic basaltic volcanism in the Southwestern Nevada Volcanic Field (SNVF) (Figure D-1a) is of particular interest because of its potential impact on the proposed Yucca Mountain radioactive waste repository (depths of ~250 m to 350 m) over the 10^4 to 10^6 year time scales for which repository performance must be estimated. The eight Quaternary volcanoes in the SNVF are important analogues for potential future volcanic activity that might intersect the repository. Hidden Cone and Little Black Peak volcanoes (Figures D-1b and D-2) have $^{40}Ar/^{39}Ar$ ages between ~320 ka and 390 ka (Fleck et al. 1996 [DIRS 105337], p. 8,213; Perry et al. 1998 [DIRS 144335], p. 2-12). Perry et al. (1998 [DIRS 144335]) also reported one outlier age determination of 560 ± 10 ka. Compositionally they straddle the basalt to trachybasaltic fields on an alkali-silica plot (Fleck et al. 1996 [DIRS 105337], p. 8,218) and are relatively phenocryst-poor, with minor plagioclase and a few percent of olivine phenocrysts (mainly millimeter to submillimeter in size). This appendix discusses inferred eruption and emplacement processes of the volcanic products, in comparison with other Quaternary volcanoes in the SNVF, and shows that the locations of vents were controlled by preexisting faults. Implications of the relationships between volcano locations, faults, and topography with respect to the characteristic length scales of the deeper plumbing and magma source region are also discussed.

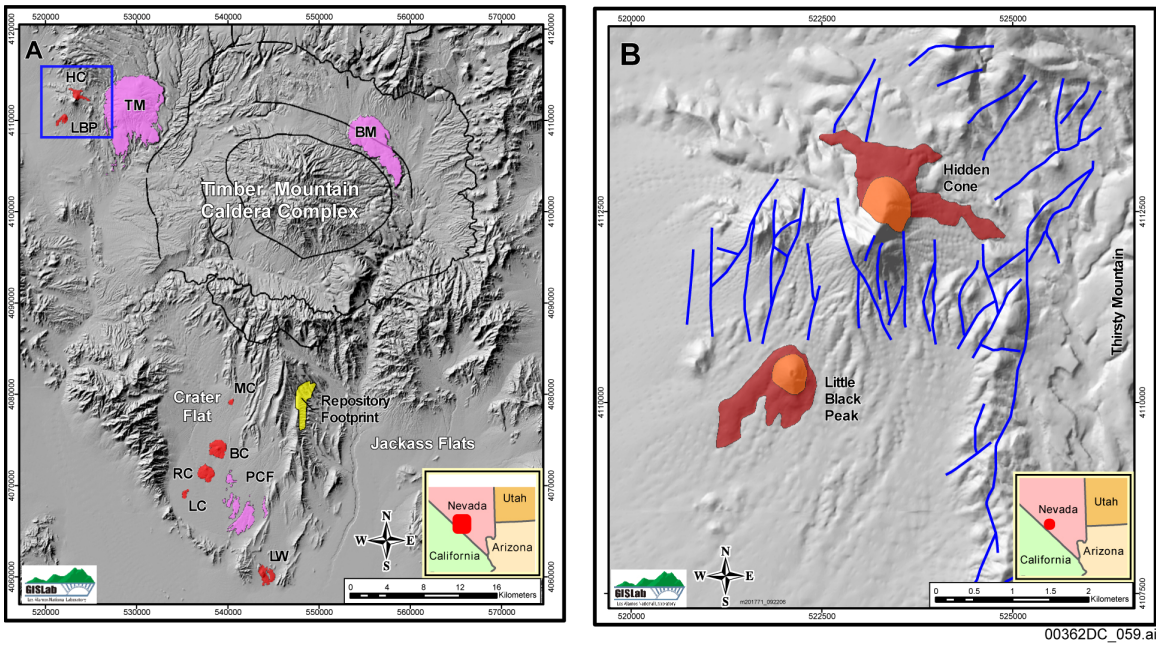

NOTES: (A) Digital elevation model (DEM) showing distribution of Pliocene-Pleistocene basaltic volcanoes in the Southwestern Nevada Volcanic Field (not including known or inferred buried volcanoes). Pliocene volcanoes (magenta) include Thirsty Mountain (TM), Pliocene Crater Flat (PCF), and Buckboard Mesa (BM). Pleistocene volcanoes (red) include Makani (MC), Black Cone (BC), Red Cone (RC), SW and NE Little Cones (both labeled together as LC), Little Black Peak (LBP), Hidden Cone (HC), and Lathrop Wells (LW). Area (footprint) of the proposed high-level radioactive waste repository is indicated in yellow. Solid lines represent margins of Miocene silicic calderas (Wahl et al. 1997 [DIRS 112289]). Crater Flat and Jackass Flats are major structural basins (note that most linear ridges and range fronts in the DEM coincide with normal faults). Inset shows location with respect to the southwestern United States. Blue box indicates location of Figure D-1b. Modified from Valentine and Perry (2006 [DIRS 177495]).
(B) Detail of study area, showing scoria cones (orange) and lava fields (red). Major faults (blue) are modified from Slate et al. (1999 [DIRS 150228]).

Figure D-1. Pliocene-Pleistocene Basaltic Volcanoes in the Southwestern Nevada Volcanic Field

D.2 HIDDEN CONE

Hidden Cone (Figure D-2a) is a scoria cone with two or three small lava fields, and an estimated total preserved volume of about 0.03 km^3. The scoria cone straddles the northeastern end of Sleeping Butte, a structural block of Miocene ignimbrite that rises ~230 m above the surroundings and has a summit ridge that is ~500-m-long with a north-northeast trend. Normal faults with oblique slip components extend across the east slopes of Sleeping Butte (Figure D-1b), displacing the ignimbrite successively downward to the east (Minor et al. 1998 [DIRS 178169]; Slate et al. 1999 [DIRS 150228], plate 1). The Hidden Cone deposits bury the northern extensions of the faults, and there is no visible displacement within those deposits, indicating that slip completely predates the volcano.

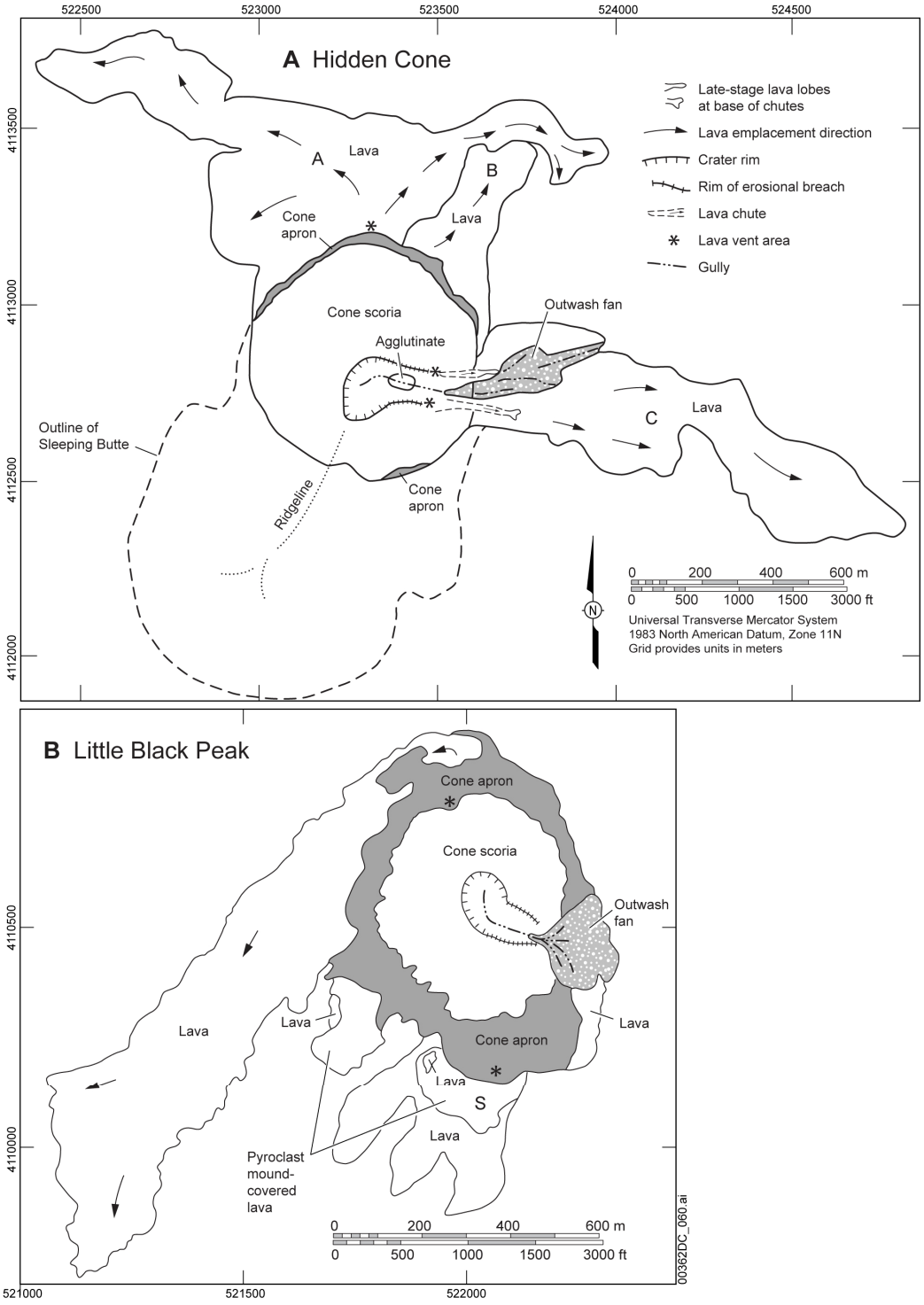

NOTES: (a) Geologic map of Hidden Cone. Cone scoria and agglutinate units correspond to upper and lower cone facies, respectively, as discussed in the text.
(b) Geologic map of Little Black Peak. Both maps use information from Crowe and Perry (1991 [DIRS 178143]), Fleck et al. (1996 [DIRS 105337]), Minor et al. (1998 [DIRS 178169]), and Slate et al. (1999 [DIRS 150228]), as well as observations from the current investigation.

Figure D-2. Geologic Maps of Hidden Cone and Little Black Peak

The cone has a small crater that is now breached on its east side by a gully that feeds a small outwash fan at the cone's base (Figure D-2a). The outer slopes of the cone are rilled, and a narrow zone of remobilized scoria, typically deposited in small fans, circles the base of the cone to form a cone apron. Most of the cone slopes, including the inner crater slopes near the top of the butte, are composed of loose, vesicular scoria lapilli with blocky to fluidal and irregular (e.g., small ribbons) shapes, forming the upper cone facies. The lapilli most commonly have millimeter or smaller-sized vesicles. These deposits are infiltrated with eolian sediment. The inner crater slopes have more-abundant fluidal bombs typically 10-cm to 30-cm long, and scattered chunks of agglutinate that formed close to the vent and were later reejected. Some rounded bombs are coated with scoria lapilli that are imbedded on the bomb surfaces, showing that still-molten bombs that landed on the crater walls commonly rolled back toward the vent and accreted smaller clasts. The only internal deposits visible in the cone are exposed in the gully between about 40 m to 50 m below the cone summit. These deposits form crude beds of variably welded spatter and bombs that dip back into the butte (westward) at 10º to 20º. Most clasts in this lower cone facies are bomb-size with ropy to ragged surfaces, and spindle and ribbon shapes are abundant; many of these are ~1-m long. In contrast to the upper cone facies, the lower cone deposits have more abundant coarse vesicles 2 mm or greater in diameter.

Lavas that extend from the northern base of the cone flowed both westward and eastward, mantling the north-trending ridge. The northern lava is subdivided into two main units, A and B (Figure D-2a), as done by Minor et al. (1998 [DIRS 178169]). The northern flows probably vented from a bocca near the base of the cone that was subsequently covered by loose scoria of the upper cone facies. The surfaces of the A unit lavas are subdued due to weathering and accumulation of eolian sediment, but still preserve some squeeze-ups and remnants of blocky texture. The lavas are composed of many stacked flow units, with upper (later) units commonly terminating inboard of the underlying unit, forming a surface that steps upward in a terrace-like manner toward the cone. Individual flow units range from about 2 m to 4 m in thickness. The B unit lava is poorly exposed but is higher standing than most of the A unit and appears to be a highly brecciated lava with rafted cone material on its top. There is some evidence that B partly overlaps onto, and was emplaced after, unit A.

The eastern lava field (unit C on Figure D-2a) is similar to unit A and extends 1.3 km from the base of the cone. The field can be traced to two vent areas or boccas about 70 m up the cone flank, on either side of the gully that drains the crater. The northern bocca is preserved as a prow-shaped (pointing uphill) body of lava, up to 6-m-wide and concentrically foliated, extending 10 m to 15 m down slope. Vertical contacts with the surrounding scoria are parallel to concentric layers (3-cm to 15-cm thick) within the lava and are marked by shear zones containing shark's-tooth texture. Near the down slope end of the bocca, the vertical contacts relax to dip steeply (70°) inward, toward the axis. The transition from outward directed flow from the bocca to down slope flow is marked by the attitude of the basal contact of the lava, which becomes concordant with underlying scoria about 15 m down slope of the top of the bocca. Below this transition, the lateral margins of the lava are less constrained, and the flow widens with increasingly jumbled jointing down slope. The southern bocca is not well preserved but its location is indicated by exposed outer margins of its channel that extend upslope into a subdued swale (~60-m wide) in the side of the cone. The channel is lined with alternating, decimeter-thick layers of lava and breccia that are inferred to record the passage of pulses of lava. Below the boccas, lavas flowed down channels or chutes to the base of the cone where

they fed the eastern lava field. A small, late-stage lava lobe extends from the base of the southern channel, possibly representing rheomorphic remobilization of channel-lining material.

D.3 LITTLE BLACK PEAK

Little Black Peak (Figure D-2b), although at a lower altitude than Hidden Cone, is located on the front of the Tolicha Peak range block, emplaced on a veneer of alluvial fan deposits, between ridges of Miocene Tuff of Sleeping Butte and the Middle Rhyolite of Quartz Mountain (Slate et al. 1999 [DIRS 150228]; Minor et al. 1998 [DIRS 178169], plate 1). Numerous normal faults are mapped in the nearby ridges (Figure D-1b), but none is observed to cut Quaternary fan deposits near the base of volcano. The total volume of preserved eruptive material at Little Black Peak is 0.014 km^3.

The scoria cone forming Little Black Peak is about 400 m in diameter, slightly elongated north-south, and 70-m to 100-m high. The cone is breached by an erosional gully to the east, forming a small outwash fan at the eastern base of the cone. Erosion of the cone surface has produced rills up to a meter deep and spaced ~10 m apart. The rills terminate downward in gullies between small, earlier-erosional-stage fans of the cone apron (intermediate stage of cone degradation illustrated in Appendix E). The summit crater is an irregular bowl about 10-m deep with gently sloping sides covered by loose scoria lapilli, blocks, and bombs. The rim of the crater is truncated by erosion to form a flat platform about 20-m wide, implying erosion of at least 5 m to 6 m of the original height of the cone (assuming original 30° slopes). Bedded, partially welded scoria lapilli, blocks, and bombs are exposed in the walls of the breach about 6 m below the base of the crater. These beds dip ~30° northwest, toward the crater. There is a marked difference in grain size of the loose pyroclasts between the south and north walls of the breach. On the south wall, red scoria lapilli blanket the walls of the gully, while on the north wall coarse lapilli to block- and bomb-size pyroclasts are dominant. The curving gully in the breach appears to follow this difference in grain size in the cone deposits.

Lavas erupted from the base of the cone in up to four locations; these lavas are similar to those at Hidden Cone. The western flow is the longest (1,500 m) and emanated from an inferred bocca in the northwest base of the cone (Figure D-2b; see also Crowe and Perry (1991 [DIRS 178143], p. 10)). A slight depression in the cone slope and a concentration of meter-size lava boulders with brecciated rinds marks the likely vent area. The flow thins away from this location to a 1-m- to 2-m-high flow front at the northern extent. The west margin of this flow is being eroded by an active wash, and several flow units produce a 10-m-high stack. The surface topography is subdued, with decimeter-scale terraces topped with tight pavements and underlying eolian silt that forms a desert soil with a vesicular A horizon. A small lobe of lava on the east side of the cone forms a low (5 m to 6 m) bench that is partially buried by the alluvial debris from the breach. This flow likely emanated from the eastern base of the cone. The south flank of the cone was the source of several other lava flows that formed three prominent benches at the cone base and thin tongues of lava on the desert floor, now partially covered by alluvium. These flows extend less than 400 m from the base of the cone. The lava and scoria platforms extend ~100 m from the base of the cone apron, with exposures of dense lava, lava breccia, and agglutinate around the margins (somewhat similar to lava unit B at Hidden Cone). A soil pit in the south platform (labeled S in Figure D-2b) exposes variably agglutinated scoria lapilli, blocks, and bombs to a depth of 1 m to 2 m. The abundance of ropy and spindle bombs, along with the

breccia and agglutinate exposures, indicates that the south platform, near the cone base, was a vent area for small lava flows. The coarse material might also be partly or wholly the result of rafting of cone material atop the lavas. The presence of the near-vent deposits on the south scoria platform in close proximity to the distinct package of fine-grained scoria lapilli on the upper southeast cone flank (exposed in the breach and contrasting with the coarser cone facies to the north) indicates that the southern sector of the cone may have been temporarily destroyed by rafting or vigorous lava effusion from the bocca related to south platform. Later stage, finer-grained eruptions from the main cone then healed the rafted sector and covered the lava vents with fallout deposits.

D.4 INTERPRETATION AND IMPLICATIONS

The inferred eruptive styles of Hidden Cone and Little Black Peak volcanoes are consistent with the styles inferred for most of the Quaternary volcanoes in the Southwestern Nevada Volcanic Field. Although the pyroclastic facies in the interiors of the two cones are not as well exposed as the deeply incised Red Cone and Black Cone volcanoes (Appendix E) or the actively quarried Lathrop Wells volcano (Appendix C), the facies appear to be similar. In particular, Hidden Cone appears to have had a similar sequence of explosive styles as the Lathrop Wells volcano, namely an early phase of Strombolian activity (low, short-lived bursts of coarse ejecta caused by bursting of bubbles through the top of a slow-rising magma column), reflected in the lower cone facies, followed by a more-energetic violent Strombolian phase that produced sustained eruption columns (hundreds of meters to a few kilometers high) of well-fragmented, finely vesicular lapilli and ash as represented by the upper cone facies.

Little Black Peak may have had a similar sequence of explosive styles, reflected in the contrasting deposit characteristics on either side of the erosional gully, although the relative timing of the styles is ambiguous. Unfortunately, the nature of any violent Strombolian tephra fallout deposits that might have extended beyond the immediate vicinities of the cones cannot be determined due to posteruptive erosion. Lava-flow styles are also similar to those at other Quaternary volcanoes in the SNVF, with most effusion from breakouts or boccas low on the cone flanks (as opposed to the central crater of the scoria cones) and relatively low effusion rates (less than ~3 m^3/s using the relationship between flow length and effusion rate used by Walker (1973 [DIRS 178061], p. 112).

The lava fields at Hidden Cone and Little Black Peak are generally thinner than other Quaternary lava fields in SNVF (Appendices C and E), but have similar flow morphologies (blocky surfaces, steep edges, squeeze-up structures, and stacked flow units). The relative thinness may simply be related to shorter effusion times, producing fewer stacked lava units and less inflation, for these smaller-volume volcanoes. The lava surfaces have evolved due to weathering, eolian sediment accumulation, and pedogenesis, to a stage (late Stage A described by Wells et al. (1985 [DIRS 178074], p. 1,525)) that is intermediate between those at Lathrop Wells and at Red and Black Cone volcanoes.

Crowe and Perry (1991 [DIRS 178143], p. 6) interpreted Hidden Cone to be polycyclic, with the latest eruption (corresponding to the upper cone facies) postdating the earlier (lower cone facies and lavas) eruptions by ~200 kyr to 300 kyr (perhaps as young as Holocene). Later interpretations by Perry et al. (1998 [DIRS 144335], pp. 2-36 to 2-38) allowed that Hidden Cone

was equally likely to represent a monogenetic or a polycyclic volcano. Crowe and Perry (1991 [DIRS 178143], p. 5) and Perry et al. (1998 [DIRS 144335], p. 2-37) cited a lack of, or weak, rilling on the cone slopes, in contrast with relatively advanced soil development on deposits around the base of the cone (cone apron deposits in Figure D-2a). Figure D-3a demonstrates that the cone slopes are indeed rilled. Furthermore, apron deposits at the base of the rilled slopes are composed of a remobilized mixture of primary scoria and eolian sediment that is continuously accreting on the cone slopes as well as on the apron deposits. This mixture, with its abundant fine sand and silt, results in more advanced soil development on the apron deposits compared to the cone slopes that are periodically eroded. In short, no evidence was observed in the current study that allows the possibility of Hidden Cone being polycyclic. The conclusion that the Silent Butte volcanoes are monogenetic is consistent with results of $^{40}Ar/^{39}Ar$ and paleomagnetic data reported by Fleck et al. (1996 [DIRS 105337], p. 8,223).

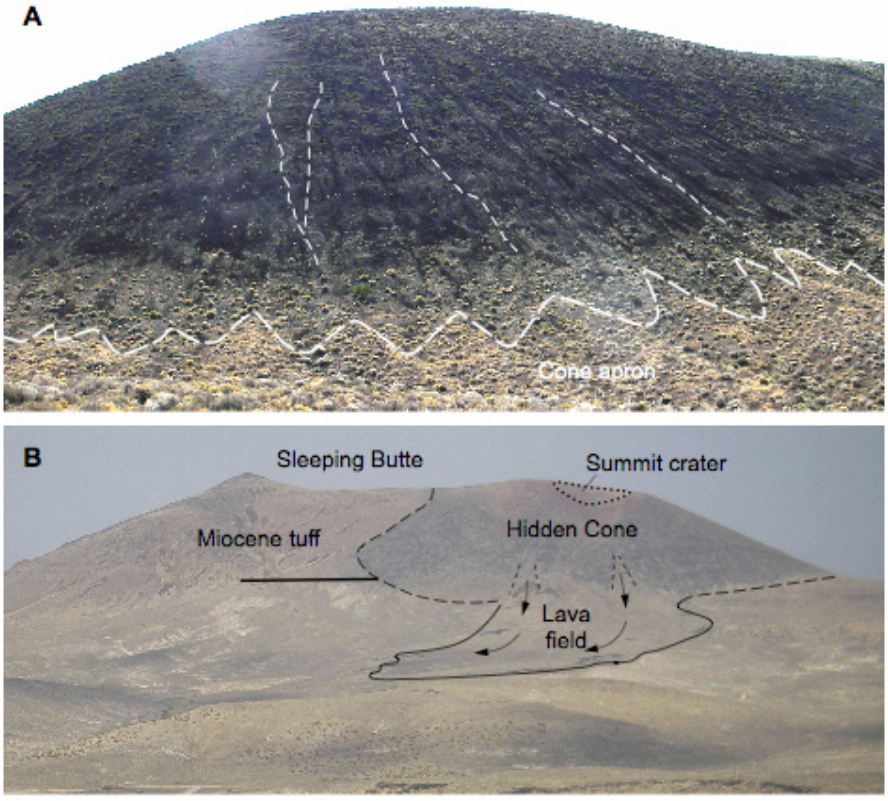

NOTES: (a) Photograph of the northwest side of Hidden Cone, showing rills (examples shown with short-dash lines) and cone apron deposits formed by coalescing debris fans (long-dash line) at base of cone slope.
(b) Photograph of east side of Sleeping Butte and Hidden Cone, viewed from the east. Summit crater (dotted line), cone base (long dash lines), eastern lava flow field (solid line), and lava breakouts/chutes (short dash lines) are highlighted. Arrows indicate main lava flow directions. Solid line shows approximate trace of a major normal fault in the lower part of the butte.

Figure D-3. Hidden Cone, Sleeping Butte, and Hidden Cone Rilled Cone Surfaces

Field relationships suggest that vents at the two volcanoes coincide with preexisting normal faults. The two boccas that fed the eastern lava field at Hidden Cone are roughly on trend with the projection of a north-striking, block-bounding fault along the east side of Sleeping Butte (Figures D-1b and D-3b). The inferred bocca that fed the northern lava field at Hidden Cone is approximately due north of the summit crater; if the two are connected at depth by a dike, the dike orientation would parallel much of the structural grain of the area. Fleck et al. (1996 [DIRS 105337], p. 8,225) reached a similar conclusion regarding fault control for Hidden Cone. The main apparent vent areas at Little Black Peak (summit crater, northern lava bocca, and south platform) also approximately form a north-south alignment that could be related to preexisting faults in underlying tuff bedrock, although the alluvial cover surrounding the cone precludes direct mapping of such faults into the cone. The north-south fault grain is inherited from an older stress field and is oblique to the modern (and presumed for the time the two volcanoes discussed here were emplaced) stress field that has a northwest-directed least principal stress (σ_3), such that young dikes that are unaffected by preexisting structures would have NE-trending strikes (BSC 2004 [DIRS 169989], p. 6-6). Older (Miocene) basaltic volcanoes in the region that erupted through similar structural blocks, and where the shallow feeder systems (dikes and conduits) are exposed by erosion, are reported by Valentine and Krogh (2006 [DIRS 177282], pp. 218 to 220; Appendix F). Vents within each of these volcanoes ubiquitously coincide with preexisting normal faults and, in some cases, were located on topographic highs. Hidden Cone and Little Black Peak appear to be younger examples of this phenomenon; however, it is not clear whether the eastern boccas at Hidden Cone represent discharge from a separate, fault-hosted dike, or from lateral dikes that propagated from the main conduit (beneath the pyroclastic vent) whose breakout location was influenced by the presence of a fault.

There are three fundamental controls on the location of individual monogenetic basaltic volcanoes in continental settings: (1) location and length scale of the mantle source region that is tapped to provide magma (magmatic footprint; Valentine and Perry (2006 [DIRS 177495], p. 4); (2) topographic variations within the magmatic footprint, which can cause an ascending dike to break the surface at a low point where conduit flow is subsequently focused (Gaffney and Damjanac 2006 [DIRS 178144], p. 3); and (3) preexisting structural weaknesses such as faults or joints that reside within the magmatic footprint. Hidden Cone and, to a lesser degree, Little Black Peak also demonstrate the relationships between volcano volume, dike length, and magmatic footprint. Features of the two volcanoes indicate that their dikes propagated mainly in a vertical (rather than lateral) direction, even though their feeder dikes are not exposed for direct observation. Both volcanoes erupted on relative topographic highs. This is most pronounced at Hidden Cone, which erupted through the topographic high of Sleeping Butte. If there had been a significant component of lateral magma flow in the feeder dikes, vents would have formed in surrounding topographic lows. Furthermore, Hidden Cone must have had a relatively short feeder dike(s), on the order of ~500 m along strike (note that no related dikes were observed in adjacent faults or bedrock extending beyond the volcanic construct). If the dike had been longer, it would have first vented in the immediately adjacent, lower-elevation topography and the main conduit would have formed there (Gaffney and Damjanac 2006 [DIRS 178144], p. 3), rather than on the side of Sleeping Butte.

The inferred dike length, which might increase by a factor of 2 to 3 at depth compared to its surface expression, is similar to the inferred characteristic length scale of the mantle source region that was tapped to feed the volcano. For example, this length scale might have been ~0.7

km to 1.8 km for a range of partial melting from 1% to 5% and allowing for a portion of nonerupted magma between 0 km^3 to 0.03 km^3 (the upper bound being equal to the erupted volume). This result is consistent with the notion proposed by Valentine and Perry (2006 [DIRS 177495], p. 4) that length scales of surface eruptive features are directly related to the length scales (magmatic footprints) of the magma source for each volcano in a basaltic field.

INTENTIONALLY LEFT BLANK

APPENDIX E

ERUPTIVE PRODUCTS AND PROCESSES, AND POSTERUPTIVE GEOMORPHIC EVOLUTION OF PLEISTOCENE VOLCANOES IN CRATER FLAT

APPENDIX E – ERUPTIVE PRODUCTS AND PROCESSES, AND POSTERUPTIVE GEOMORPHIC EVOLUTION OF PLEISTOCENE VOLCANOES IN CRATER FLAT

E.1 BACKGROUND

Crater Flat (Figure E-1) is an alluvial basin in the Basin-and-Range province of the western United States. It is bounded to the east by ridges of tilted Miocene ignimbrite (Yucca Mountain) and to the west by uplifted Paleozoic sedimentary strata (Bare Mountain). Basaltic volcanism within the basin has occurred in three cycles. The first cycle, between 11.5 Ma –and 10 Ma, produced widespread basalt flows that are now mostly buried by alluvium (Perry et al. 1998 [DIRS 144335], pp. 2-16 and 3-31). The second cycle occurred in the southeastern quadrant of the basin about 3.7 Ma (Fleck et al. 1996 [DIRS 105337], p. 8,220; Perry et al. 1998 [DIRS 144335], pp. 2-23 and 2-24). The third cycle produced a northeast-trending arc of five volcanoes that are the focus of this paper – SW and NE Little Cones, Red Cone, Black Cone, and Makani volcanoes (Figure E-1; Makani volcano is also referred to as "Makani Cone," "Northern Cone," and "Northernmost Cone" in the literature). Six independent potassium–argon and $^{40}Ar/^{39}Ar$ studies have been conducted since 1990 to determine the ages of these five volcanoes (Figure E-2) and the results are difficult to interpret. Age estimates for any one volcano typically have uncertainties of 100 ka to 200 ka and a large range of individual age determinations, leaving a detailed understanding of the age relationships between volcanoes uncertain as well as the possibility of a span of ages at individual volcanoes. Flows of all of the volcanoes have reversed magnetic polarity, indicating that, if all the volcanoes are close to the same age, they are either older than 1.07 Ma or younger than 0.99 Ma (Figure E-2); for simplicity, this appendix refers to the age of these volcanoes as ~1 Ma. The total volume of preserved eruptive products in the Pleistocene volcanic centers in Crater Flat is 0.15 km^3 (Table E-1). Red Cone and Black Cone volcanoes account for ~75% of this volume and receive the most attention in this report. Lathrop Wells volcano, located about 5 km outside the southeast margin of Crater Flat, erupted ~80 ka (Heizler et al. 1999 [DIRS 107255]); its volcanological and geomorphic characteristics are reported elsewhere (e.g., Crowe et al. 1983 [DIRS 100972]; Wells et al. 1990 [DIRS 107208]; Valentine et al. 2005 [DIRS 177782]; Valentine and Harrington 2006 [DIRS 177271]; Appendix C).

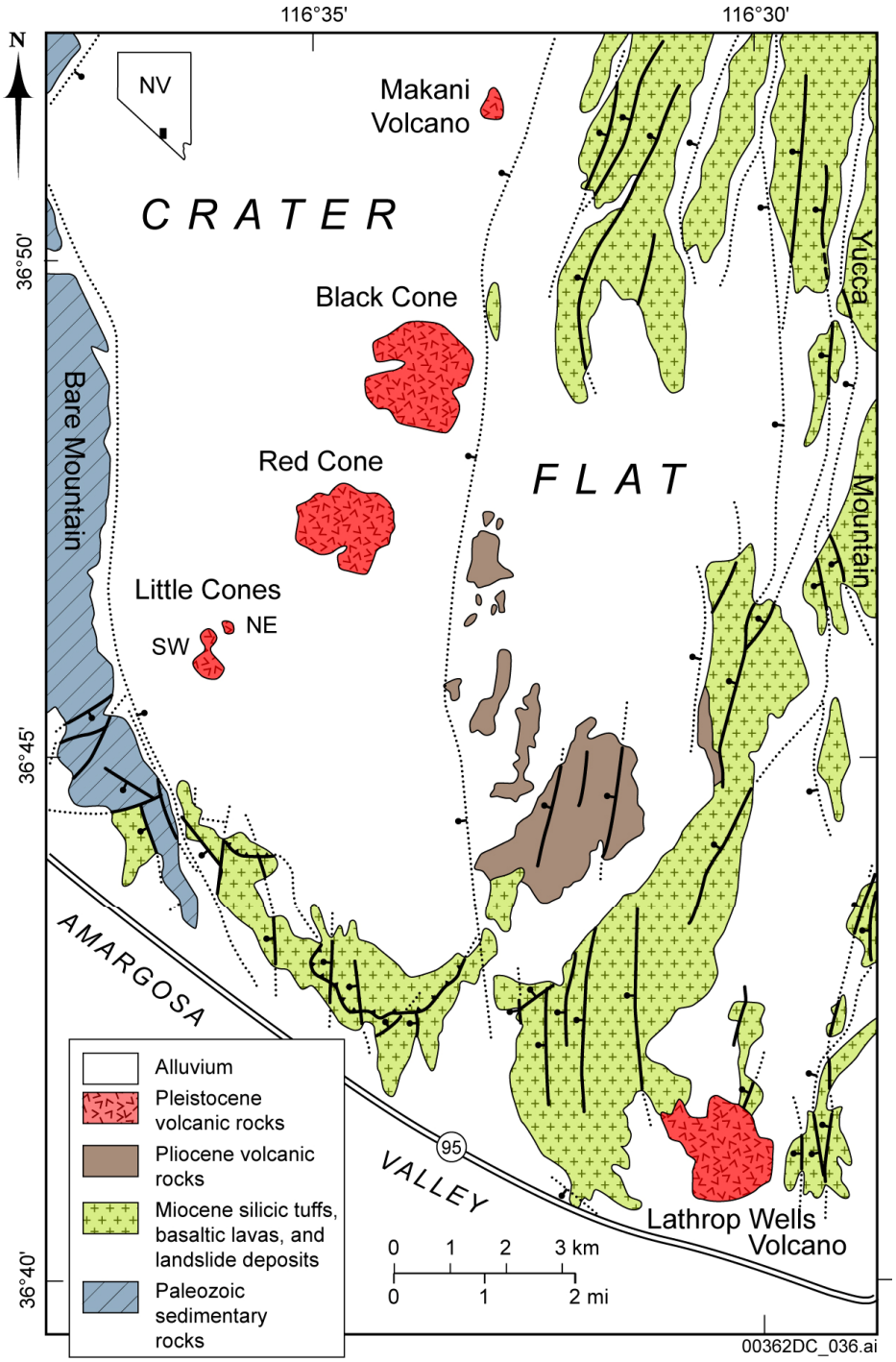

Source: Modified from Vaniman and Crowe 1981 [DIRS 101620], p. 7.

NOTES: Inset shows location of the study area within Nevada.

Figure E-1. Simplified Geologic Map of Crater Flat and its Immediate Surroundings

Table E-1. Estimated Volumes of Pleistocene Volcanic Centers in Crater Flat

Volcano Name	Volume (km^3)[†]	Description
Black Cone	0.061[‡]	Single cone with two lava flow fields
Red Cone	0.055	Single cone with two lava flow fields
Little Cones	0.03[§]	Two small cones, each with a lava flow field (mostly buried by alluvium) extending southward
Makani Cone	0.004[#]	Small lava field with minor pyroclastics

NOTES: [†]Volumes calculated by reconstructing a sloping planar paleosurface beneath each volcano (determined by elevation of points around the edge of each volcano, assuming that this is close to the contact between volcanic products and the paleosurface unless noted otherwise), and integrating the digital elevation data above that surface. The volume estimates do not account for distal fallout deposits that may have existed, but are now obscured or missing due to posteruptive surficial processes.

[‡]Bradshaw and Smith (1994 [DIRS 101996], p. 168) estimate the volume of Black Cone volcano to be 0.067 ± 0.015 km^3.

[§]Combined volume of SW and NE Little Cone volcanoes and their lava flow fields. Assumes each of the two lava fields is 10-m thick and buried by an average of 10 m of alluvium.

[#]Assumes 5-m partial burial of volcanic products, in addition to those exposed on the surface.

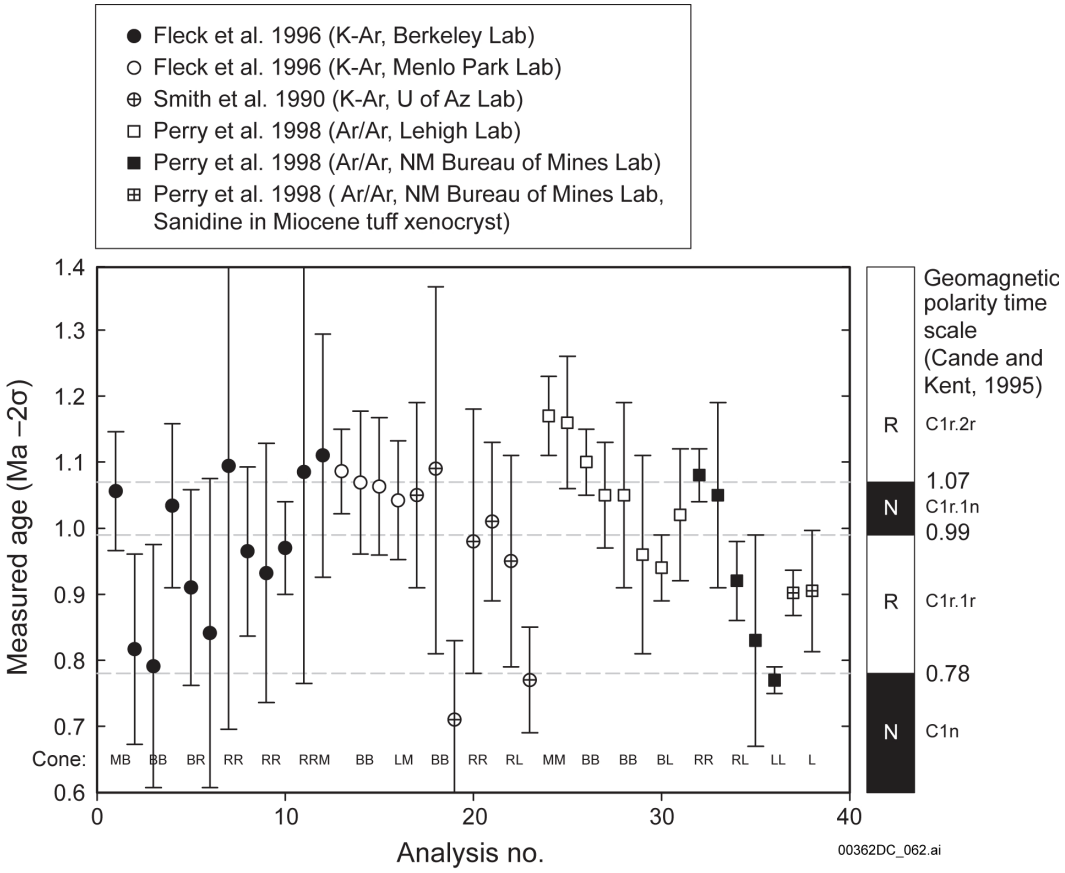

NOTES: Errors bars are ±2σ. Age determinations are grouped by laboratory. Labels M, B, R, L for "Cone" near the bottom of the figure indicate that the corresponding age determination was for Makani volcano, Black Cone, Red Cone, or Little Cones, respectively. For geometric time scale, R = reversed, N = normal polarity.

Figure E-2. Summary of K-Ar and $^{40}Ar/^{39}Ar$ Age Determinations for the Quaternary Basalts of Crater Flat

The eruptive products of the 1-Ma volcanic centers are sparsely porphyritic and are alkali basaltic to hawaiitic (trachybasaltic) in composition (Vaniman and Crowe 1981 [DIRS 101620], pp. 15 to 19; Vaniman et al. 1982 [DIRS 101031]; Bradshaw and Smith 1994 [DIRS 101996], p. 169; Fleck et al. 1996 [DIRS 105337], p. 8,218; and Perry et al. 1998 [DIRS 144335], pp. 4-12 and 4-13). Olivine is the principal phenocryst, with rare amphibole (mainly at Little Cones). Nicholis and Rutherford (2004 [DIRS 173945]) conducted experiments to determine phase equilibria and ascent rates for magma from SW Little Cone and Lathrop Wells volcanoes. They determined that SW Little Cone magma erupted at temperatures less than 975°C with a source pressure of at least 175 MPa (depth greater than ~7 km). Dissolved-water content at depth must have been at least 3 wt % for amphibole to crystallize. Melt inclusions analyzed by Nicholis and Rutherford (2004 [DIRS 173945], p. 490) yielded H_2O contents mainly in the range of 1.2 wt % to 1.7 wt % and as high as 3.5 wt % in one inclusion. Luhr and Housh (2002 [DIRS 178118]) reported values of 1.9 wt % to 4.6 wt % H_2O and CO_2 contents up to 930 ppm from Red Cone and Lathrop Wells volcanoes.

Vaniman and Crowe (1981 [DIRS 101620], pp. 15 to 19) and Bradshaw and Smith (1994 [DIRS 101996], pp. 168 and 169) describe the eruptive sequences of Red and Black Cone volcanoes. Both papers infer that mounds of pyroclasts scattered amongst the lava flows record the presence of multiple scattered vents, in addition to the main cone at each of the two volcanoes. However, the authors came to different conclusions with respect to timing of eruptive events. Vaniman and Crowe (1981 [DIRS 101620]) assume a monogenetic history (i.e., a single eruptive episode of weeks to years in duration, during which all the features of a volcano are formed). Bradshaw and Smith promote a polycyclic model with eruptive episodes separated by thousands or tens of thousands (or greater, but within the resolution of the age data show in Figure E-2) years. Bradshaw and Smith (1994 [DIRS 101996]) argued that differences in morphology of lava flows, some having rather subdued margins and gullied surfaces compared to others, are the result of significant age differences between the flows. These arguments, along with arguments related to primary volcanic features that Bradshaw and Smith interpreted to represent polycyclic eruptive episodes, are addressed throughout this appendix.

E.2 RED CONE VOLCANO

Red Cone volcano (Figure E-3) consists of three major features: (1) a cone remnant that rises 87 m above the floor of Crater Flat (combined debris apron, lapilli-and-block, and spatter units in Figure E-3b), (2) a lava flow field that extends to the south and southwest of the cone remnant (the southwest lava field), and (3) a lava flow field that extends to the south-southeast of the cone remnant (southeast lava field).

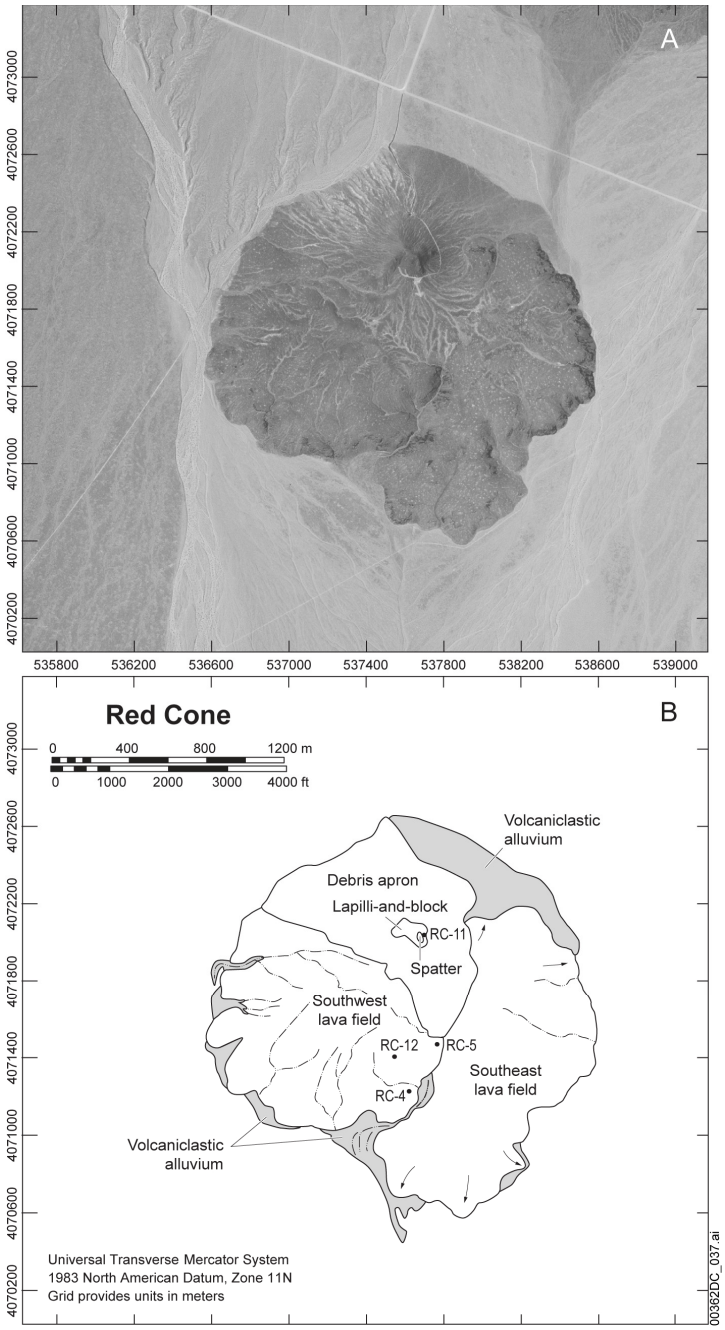

NOTE: Arrows represent inferred flow directions of lavas.

Figure E-3. Air Photo (A) and Geologic Map (B) of Red Cone Volcano

E.2.1 Cone Remnant

The topographically highest part of Red Cone volcano is a roughly horseshoe-shaped remnant of in situ cone deposits (Figure E-4a) that exposes two main pyroclastic facies. Xenoliths are extremely rare in both of these facies; only a few centimeter-sized xenoliths were observed, probably derived from basin-fill sediments, in the entire cone remnant. Deposits on the west and northern parts of the cone remnant are mainly lapilli and small blocks, are clast supported, form

crudely defined massive beds, and are partly welded – these deposits form the *lapilli-and-block facies*. Lapilli are poorly to moderately vesicular with mainly submillimeter vesicles and are blocky to subrounded in shape; many of these clasts likely are fragments of larger blocks or bombs that were recycled or churned due to avalanching of crater wall material into the vent and subsequent re-ejection (McGetchin et al. 1974 [DIRS 115469]; Heiken 1978 [DIRS 162817]). Blocks (and some bombs) are typically 20 cm to 30 cm in size and range from dense with blocky shapes to moderately vesicular clasts with fluidal shapes and cauliflower surface textures. Larger (up to ~50 cm) blocks and cauliflower bombs litter the surface where it is covered by colluvium but were not observed in place; these probably are a lag from eroded cone material.

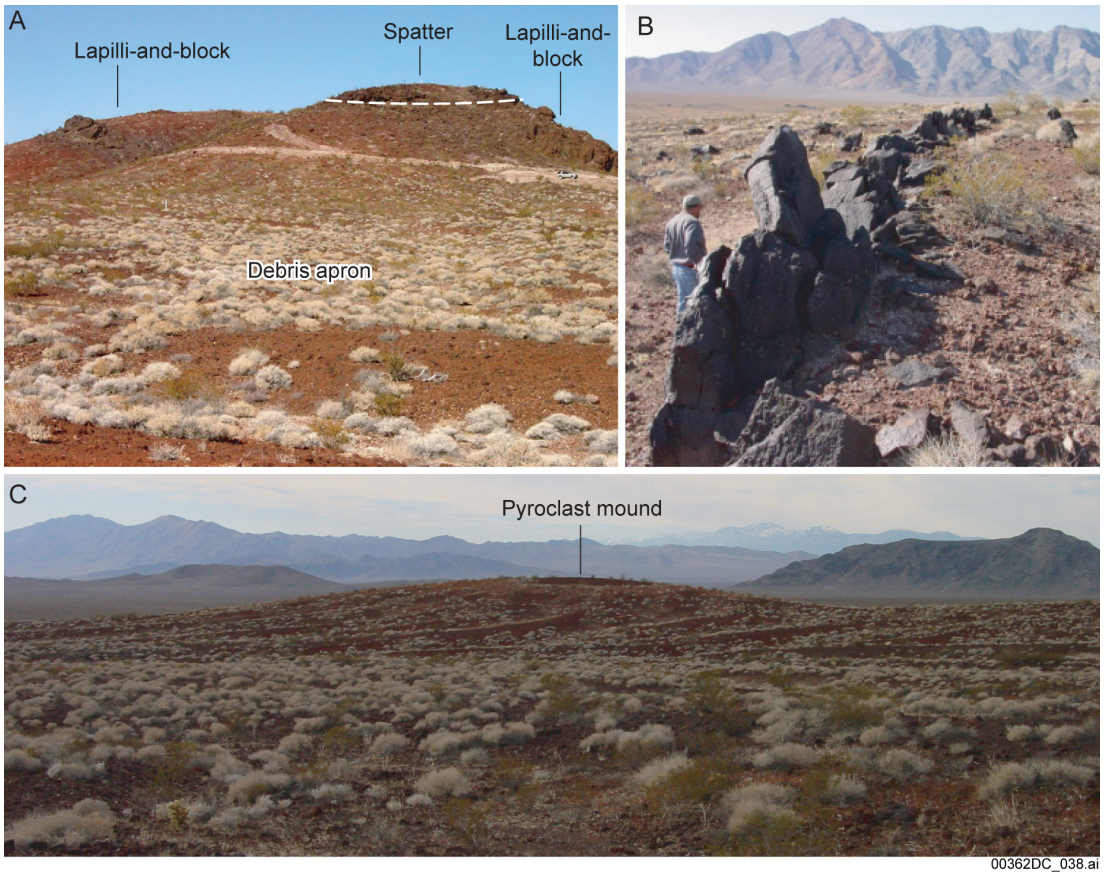

NOTES: (A) Cone remnant at Red Cone volcano, viewed from surface of cone apron looking northward.
(B) Lava ridge on down-flow flank of a large pyroclast mound (Station RC-12).
(C) Photograph taken from slopes of cone remnant looking to the south across the surface of the southwest lava field, showing large pyroclast mound in the middle ground.

Figure E-4. Red Cone Volcano

Bed attitudes in the lapilli-and-block facies on the western part of the cone remnant are irregular but typically dip steeply (50° to 60°) towards the center of the apparent crater. The deposits are locally faulted into small blocks on the order of a few meters wide that retain the original bedding internally, but that have undergone differing degrees of rotation. On the eastern side of the cone remnant, beds of this partly welded lapilli-and-block facies are nearly horizontal in attitude or dip shallowly back into the cone. These are broken into small fault or slump blocks. One small area on the east slope of the cone remnant (Station RC-11, Figure E-3B) exposes

primary, nonindurated scoria lapilli with faint bedding that dips about 32° eastward (away from the center of the cone remnant). This represents primary, in situ material at the angle of repose that was deposited on the outer flanks of the cone during its growth.

A sequence of several meters of coarse lapilli, spatter, and fluidal bombs that forms individual beds ~1-m thick overlies the lapilli-and-block facies on the eastern summit. The beds alternate between partly welded to completely welded where clasts have coalesced to form massive, lava-like beds. These beds, referred to as the *spatter facies*, dip about 45° toward the north (strike varies around ~N75°W). The characteristics of this facies require a period of pulsing fountain eruptions where the relatively coarse clasts had a short flight time (minimum cooling) and a rapid accumulation rate (allowing for coalescence and welding of clasts). Deposition was likely very close, within some tens of meters, of a vent (see Head and Wilson 1989 [DIRS 124674]; Sumner et al. 2005 [DIRS 178125]).

An apron of material eroded from the cone surrounds the cone remnant, and the apron is in turn deeply rilled (Figure E-3A). The apron partly covers the two lava flow fields to the south and east and merges with the Crater Flat valley floor to the west and north.

E.2.2 Lava Flow Fields

E.2.2.1 Southwest Lava Flow Field

The southwest lava flow field at Red Cone volcano fans out from the cone remnant to form a series of lava terraces that steps down toward the distal edge of the flows. The lavas flowed down the gentle (about 20 m/km) south-southeast slope of the Crater Flat valley floor. The length:width ratio of the lava field is ~1:1 (length measured southward from the cone, width measured along the widest east-west dimension). The four main surface features on the lava field are: (1) relatively flat areas, (2) flow fronts or margins, (3) lava ridges, and (4) pyroclast mounds. Flat areas have a desert pavement of scoria lapilli (commonly ~1 cm in size, depending upon distance from the cone remnant) with variable quantities of block-size clasts (ranging from surface mosaic types DP-1 to BG-1 as described on a 560-ka lava flow at the Cima volcanic field by Wood et al. 2002 [DIRS 178146], p. 311; Wood et al. 2005 [DIRS 178147], p. 207). The blocks are typically angular in shape and are poorly-to-moderately vesicular. Beneath the pavement is a zone (depth unknown, but probably variable) of eolian sand and silt forming a desert soil.

Flow fronts are partly obscured by alluvial deposits of reworked pyroclastic material that form relatively smoothly sloping surfaces to the surrounding valley floor, but where exposed the fronts are steep, lobate, and composed largely of lava blocks on the order of decimeters in size. The terrace-like nature of the lava field is especially apparent along its margins, where each flow front forms a step (typically a few m high) downward to the south and southwest.

Lava ridges are typically arcuate in shape (although some are roughly equant in map view, possibly representing tumuli), range from ~5 m to 50 m in length, are a few decimeters to ~2-m wide, and rise up to 2 m above the surrounding surface. Internal textures in these ridges are dominantly nonvesicular-to-moderately vesicular, massive to platy-jointed lava. Although the ridges occur in a scattered fashion throughout the lava field, they are most abundant near flow

margins where they appear to be squeeze-up ridges, roughly parallel to the flow margin, caused by pulses of lava behind a slowing flow front. This interpretation is supported by observations where gullies have exposed flow interiors within about 200 m of the southern margin of the southwest lava field. The flow interiors contain foliation patterns (due to vesicle concentrations or slide planes in the plastically flowing lavas) that range from horizontal to upward-sweeping; these record ramping and squeezing up of lava near flow margins that is expressed on the surface by the lava ridges. Depending upon the degree of erosion, the lava ridges can be similar in appearance to exposed dikes—in a sense they are "rootless" dikes as they are fed by the underlying lava flow rather than by a deeper magma reservoir. Two additional lava ridge features occur on the leading (southern) edges of pyroclast mounds (Figure E-4b). These are also arcuate, parallel the contours of their host mounds, and resemble dikes.

Several mounds of pyroclastic debris, ranging from a few tens to ~200 m in basal diameter, rise 5 m to 10 m above the southwest lava field surface (e.g., Figure E-4c). The mounds have subdued, rounded surfaces and are littered to varying degrees with scoria lapilli, blocks, and bombs with eolian sand between the pyroclasts. In most cases, the tops of the mounds have the coarsest clasts, probably representing lag deposits, while smaller lapilli have been moved down the shallow slopes by surficial processes. Coarse clasts have a wide range of vesicularity and a range of surface textures including ropy, fluidal textures (e.g., spindle bombs or bomb fragments) to blocky, although wind erosion has smoothed some features. Some large blocks are composed of agglutinate or basalt breccia. Bradshaw and Smith (1994 [DIRS 101996], p.168) state "cinder mounds typically occur at the tail-end of individual flows, and thus represent actual vent sites" at Red Cone volcano. However, because posteruptive surficial processes have obscured many original lava features, individual flows (in the sense of flow units) cannot be distinguished except perhaps as individual lobes at the distal margin of the lava field. Additionally, pyroclast mounds are observed out to the margin of the southwest lava flow field, along its eastern side, which were also mapped by Bradshaw and Smith (1994 [DIRS 101996], Figure 1). Bradshaw and Smith (1994 [DIRS 101996], Figure 1) mapped several features in the mounds as "intrusives" into the pyroclast mounds of the southwest lava field, supporting their hypothesis that the mounds are actual satellitic vents.

The abundance of large pyroclast mounds on the southwest lava field promoted development of gullies in the topographic lows between mounds, that now branch as rills onto the lower slopes of the mounds and have merged downstream with headward-eroding gullies that nucleated between marginal lava lobes. This drainage system supplies pyroclastic debris to the alluvial slopes that obscure some of the flow-margin features of the southwest lava field, and has locally incised the distal portions of the lava field to expose flow interiors, as mentioned above.

E.2.2.2 Southeast Lava Flow Field

The southeast lava field spreads from the eastern base of the cone and extends southward (Figure E-3) with a length:width ratio of ~2:1 (flow length is measured north to south, in the dominant direction of flow). It appears to overlap the southwest lava field where the two flows' margins come together at the apex of a small canyon that is the gap between the eastern and western margins of the two lava fields. The fact that the flows that fed the southeast lava field first flowed eastward is also consistent with the southwest lava field being emplaced first and forming a topographic high that diverted subsequent lavas. The top of the southeast lava field is

relatively flat compared to the southwest lava field and locally is covered with a pavement dominated by lapilli-sized scoria with some small blocks (similar to surface mosaic type DP-1 of Wood et al. 2002 [DIRS 178146], p. 311; Wood et al. 2005 [DIRS 178147], p. 207), and eolian material beneath the pavement. The few pyroclast mounds that occur on the southeast lava field rise only a few meters above the surroundings and tend to have flat tops that are armored with very mature desert pavements (Valentine and Harrington 2006 [DIRS 177271], pp. 534 and 535), although one or two small mounds, which are dominated by block-sized fragments of fluidal bombs, do have rounded tops.

The margins of the southeast lava field are lobate in form and very steep, descending 25 m to 30 m to the valley floor. Lobes have typical horizontal dimensions of about 40 m to 100 m and many have top surfaces that step down as terraces, each several meters high, toward their distal ends. The down-stepping terraces represent small lava breakouts from the toes of lobes (see also Pinkerton and Sparks 1976 [DIRS 178120], p. 178), each reaching successively farther onto the desert floor. Similar to the lava lobes described for the southwest lava field, the surfaces of those on the edge of the southeast lava field are characterized by decimeter-sized lava blocks; a feature that is shared by all of the Pleistocene lava flow fields in Crater Flat is the common occurrence of arcuate lava ridges, parallel to and just inboard from the flow margins.

Drainage networks are less strongly developed on the southeast compared to the southwest lava field. This is likely due to the lesser initial topographic variation and less abundant pyroclastic debris on the southeast lava field. Drainage development has been more restricted to headward erosion of gullies that nucleated between lava lobes at the margin of the lava field.

E.2.2.3 Interpretation and Summary of Red Cone Volcano

The two pyroclastic facies in the cone record two principal cone-building eruptive mechanisms. The lapilli-and-block facies represents accumulation of primarily solidified and well-fragmented clasts even in very proximal locations. While the clasts were hot enough to sinter and form an indurated deposit in the crater, they were sufficiently cool to retain their blocky shapes. It is possible that this facies formed during periods of violent Strombolian eruption that alternated with steam explosions that ejected little juvenile material but that re-ejected previously erupted clasts (and block/bomb fragments) that had slumped into the vent. Some of the internal faulting and rotation within the lapilli-and-block facies may be due to slumping of deposits as cone material was rafted away on top of lava flows (discussed below), in addition to a potential component of slumping during posteruptive cone degradation. The spatter facies records more-"classical" Strombolian eruptions (see e.g., Valentine and Groves 1996 [DIRS 107052], p. 78). Each densely welded zone in this facies formed during a peak in the clast accumulation rate for a given Strombolian burst. Lack of exposure prevents direct observation of cone facies that may underlie the lapilli-and-block facies, and it is unclear whether erosion might have removed deposits above the spatter facies. It is likely that during much of the eruptive history of Red Cone volcano the cone was horseshoe-shaped (open to the south) in map view.

Although Vaniman and Crowe (1981 [DIRS 101620], p. 15 to 19) and Bradshaw and Smith (1994 [DIRS 101996], pp. 168 and 169) inferred that pyroclast mounds scattered throughout the lava flow fields (particularly the southwest lava field at Red Cone volcano) are remnants of vents, an interpretation is favored here whereby these mounds are composed of proximal

pyroclastic material rafted from the main cone (see also descriptions of rafted cone material at other small volume basaltic volcanoes; Gutmann 1979 [DIRS 178116], pp. 449 and 450; Holm 1987 [DIRS 178117], pp. 322 to 324; Luhr and Simkin 1993 [DIRS 144310], pp. 80 to 86). Although interpretation of these features is complicated by the degree of posteruptive surface modification, this interpretation is consistent with several observations:

(1) The tops of the coarse pyroclast mounds are rounded and preserve no evidence of an eruptive vent or crater

(2) The mounds cannot be linked to individual lava flow units and occur out to the distal margins of lavas

(3) Features in the main cone suggest that its crater opened to the south and that deposits in the cone may have experienced syneruptive slumping as would happen if the cone was undermined as material rafted from its base,

(4) Lava ridges or dike-like features on the inferred leading edge of some scoria mounds are very similar to lava squeeze-ups at the front of rafted "mesoblocks" on the 1986 lavas at Izu-Oshima Volcano, Japan (Sumner 1998 [DIRS 178124], p. 206).

The squeeze-up features at Izu-Oshima resulted as lava from the fluid interior of the flow extruded through cracks in the chilled lava surface because of the weight of the rafted material and deceleration of lava behind a slowing flow front. An additional piece of evidence that occurs at Black Cone volcano (discussed below) is an exposure of the internal structure of a pyroclast mound showing that it consists of steeply tilted layers of scoria and spatter (similar to rafted cone material on lavas associated with the ~1ka Sunset Crater volcano, Arizona; Holm 1987 [DIRS 178117], pp. 322 and 323).

Sumner's (1998 [DIRS 178124]) description of squeeze-ups at Izu-Oshima, which also occur near flow margins, detailed how the tops of the features in some cases have an outward-flaring structure caused by the plastic behavior of the rapidly cooling lava as it protruded above the flow surface. Very similar squeeze up features are observed in lava lobes in the much younger, but compositionally similar, Lathrop Wells volcano, and Duncan et al. (2004 [DIRS 178114]) describe the active development of such squeeze ups at Mount Etna, Italy. Bradshaw and Smith (1994 [DIRS 101996], p. 168) interpreted such a feature where it occurs along the eastern margin of the southwest lava field as follows (at Station RC-5, see Figure E-2b): "Flow foliations and vesiculation in the top of one of the dike (*sic*) units suggests a mushroom-like shape that might be expected as a lava reaches the surface and initiates a new flow" (note – there is no evidence for a presumed flow that was fed by the dike). It seems likely that this feature is a lava squeeze-up (a rootless dike) from the core of the underlying flow, rather than a true dike related to a separate magmatic (polycyclic) event as argued by Bradshaw and Smith (1994 [DIRS 101996], p. 168). Gutmann (1979 [DIRS 178116], p. 449) described similar features where lava squeeze ups intruded overlying pyroclastic deposits produced later in the eruption sequence of the same vent in the Pinacate volcanic field.

As Red Cone grew, it was simultaneously cannibalized by lavas flowing from its southern perimeter that rafted away segments of cone material (similar to processes witnessed at Parícutin volcano, Mexico; see Luhr and Simkin 1993 [DIRS 144310], pp. 80 to 86, and 90). The rafted material was coarse-grained, rich in bombs and bomb fragments due to its origin close to the vent. Individual rafts may have retained their original bedding structures (Holm 1987 [DIRS 178117], pp. 322 and 323), particularly if there was any welding or agglutination, or in other cases may have been piles of unstructured, loose debris; however, subsequent surficial processes have obscured differences between these features. Lava squeeze-ups formed on the leading edges of at least two rafts, as well as intruding the bottoms of rafts that were transported to the flow margins. This early phase of lava flows produced the southwest lava field through a combination of stacking of flow units and inflation by successive injections of lava. Eventually the southwest lava field became thick enough to divert subsequent lavas such that they initially flowed eastward until they cleared the southwest lava platform, at which point they turned and flowed southward down the slope of the valley floor. These later flows accumulated to form the southeast lava field. The southeast lava field rafted much less material from the main cone, perhaps due to better stability or strength of the cone in the area of the southeast flow vent (discussed later), or because production of pyroclasts at the vent had waned or completely stopped during the southeast flows.

After eruptions ceased, surficial processes gradually began to degrade the main cone. Rilling and down-slope transport of cone deposits produced an apron of reworked scoria lapilli and blocks. The apron was in turn subject to rilling and a second generation of down-slope transport that is in process today. The cone-erosion processes were likely intimately tied to pedogenic processes that introduced eolian sand and silt and eventually calcium carbonate zones in the upper tens of centimeters of a volcanic deposit in this arid to semi-arid environment (Wells et al. 1985 [DIRS 178074]; McFadden et al. 1987 [DIRS 105023]; Valentine and Harrington 2006 [DIRS 177271], Figure 3). The erosional processes act to give the cone a concave-upward profile characteristic of highly degraded scoria cones (e.g., Wells et al. 1990 [DIRS 107208], p. 550; Hooper and Sheridan 1998 [DIRS 178066], pp. 257 and 265), although on its southern side the cone may have had an *initial* concave profile due to the large quantity of material rafted away on the southwest lava field.

The surfaces of the two lava fields evolved in somewhat different manners. The southwest lava field, with its abundance of pyroclast mounds, had a combination of relief and loose debris that promoted relatively faster and more extensive development of drainage networks and alluvial aprons or “fans” at the mouths of gullies. Where the southwest lava field did not have pyroclast mounds on its top, its surface evolution involved the gradual smoothing of the rough lava surface by eolian deposition in low spots and by weathering of high features (see Wells et al. 1985 [DIRS 178074], p. 1,525). The southeast lava field, on the other hand, had much less initial topographic variation and less loose debris on its surface, and simply has undergone gradual smoothing with associated soil and desert pavement development such that it now forms a relatively flat-topped platform. Both the southeast lava field and the flat parts of the southwest lava field are currently at Stage B in the surface modification scheme of Wells et al. (1985 [DIRS 178074], p. 1,525). Some drainage network development has occurred on the surface of the southeast lava field where there are three subdued mounds, but for the most part its erosion is dominated by very slow headward erosion of gullies between marginal lava lobes. Relatively little transport of loose debris from the central parts of the southeast lava field has resulted in

substantially less accumulation of alluvial fans or aprons that would obscure or smooth the edge of the lava field.

E.3 BLACK CONE VOLCANO

Black Cone volcano (Figure E-5) shares many of the characteristics of Red Cone, including the presence of a single main cone, rising 118 m above the surrounding desert floor, and two (possibly three) lava flow fields (see also Bradshaw and Smith 1994 [DIRS 101996], pp. 166 to 169), the first of which flowed south from the cone and has many pyroclast mounds, and the second of which spread around the northern base of the cone.

E.3.1 Cone Remnant

Although Black Cone proper at first glance appears to be relatively complete cone, nearly all the in situ primary pyroclastic deposits that crop out on the cone are inward dipping. This implies that a large volume of cone material that formed outward-dipping deposits has been removed by erosion. Most of the surface of the cone is covered with colluvium that has been indurated by pedogenic carbonate build-up, but exposures of primary volcanic deposits indicate that there are two main pyroclastic facies (Figure E-6). The predominant one, which occupies the lower ~80% of the cone, forms the *lapilli-and-bomb* facies (e.g., Station BC-1, Figure E-5b). Bedding in this facies ranges from massive, to crudely defined by bomb horizons, to lenticular and inversely graded grain avalanche beds; dips are typically 25° to 30° into the cone. Scoria lapilli are moderately vesicular and are predominantly blocky and angular in shape. The clast-supported framework of lapilli, which is nonwelded to slightly sintered, contains variable portions of larger bombs. The bombs are most commonly a few decimeters in length (parallel to crude bedding) and around one decimeter thick, although some ribbon bombs are as long as 1.4 m and rare ovoid bombs are over 2 m in diameter. Many bombs enclose blocky scoria lapilli (accretionary bombs; Heiken 1978 [DIRS 162817], pp. 2 and 3), likely caused as fluid bombs landed on the scoriaceous slopes and enfolded scoria as they rolled or slumped back into the vent to be re-ejected or simply as they rolled or slid into their final resting places. Dense blocks several decimeters in diameter also occur in this facies but are less common than bombs.

The upper ~20% of Black Cone is dominated by alternating zones of partly to densely welded spatter (e.g., Station BC-3, Figure E-5b), forming a spatter facies that is similar to that at the top of Red Cone. The transition from lapilli-and-bomb to spatter facies may be a lateral transition instead of, or in addition to, a vertical transition; stratigraphically lower deposits that were observed are also farther away from the central vent area due to the slopes of the cone remnant. Thicknesses of ledge-forming welded horizons range from one spatter clast thickness (~10 cm) to about 2 m. Thicker beds, which also have the densest welding, tend to grade laterally over distances of 20 m to 30 m to less-welded zones with poorly defined bedding. The gradation typically occurs as a gradual thinning of the densely welded middle zone of a

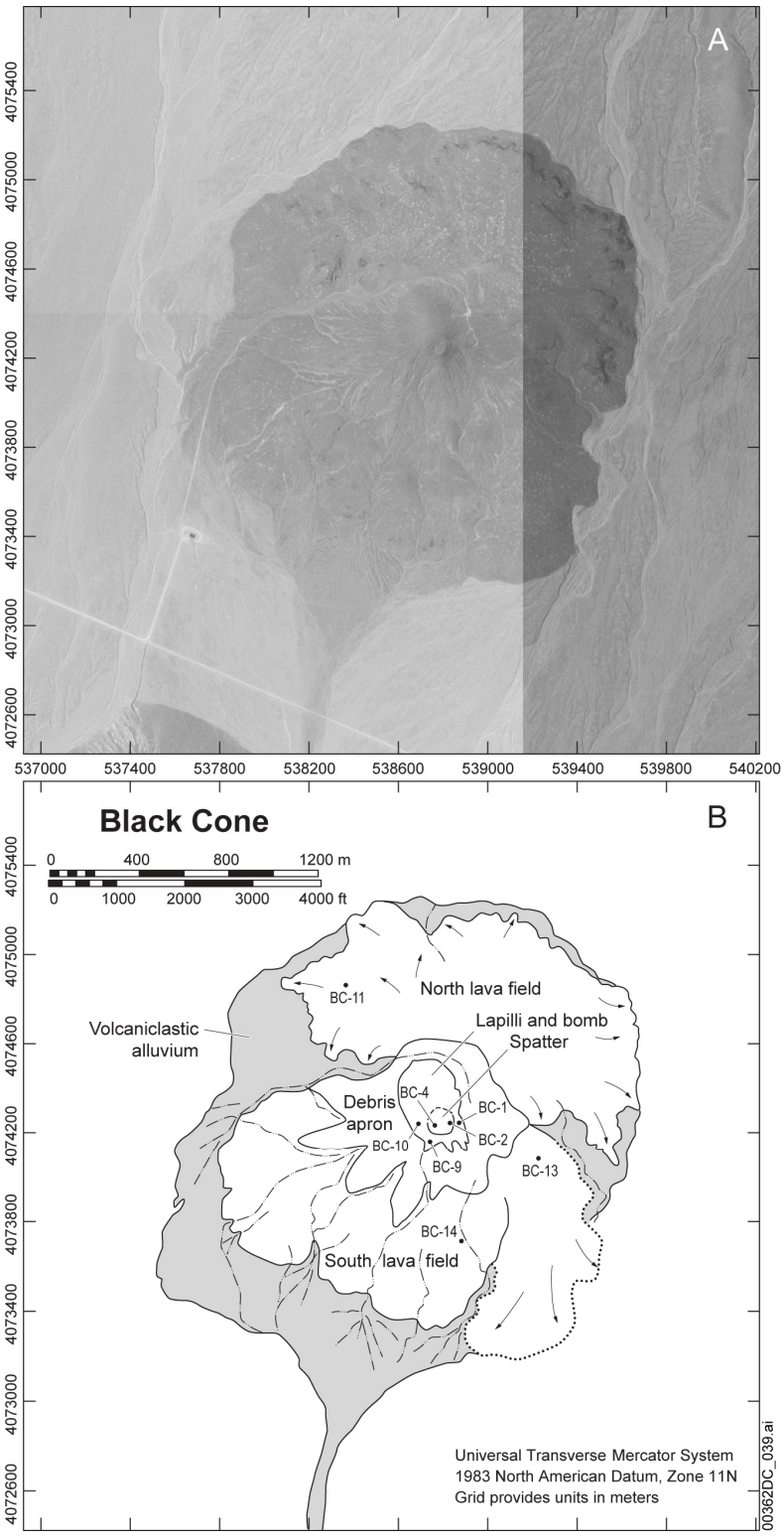

NOTE: Dotted line shows a lava field that is somewhat distinct because of its low profile, but is combined with the south lava flow field in the text.

Figure E-5. Air Photograph (A) and Geologic Map (B) of Black Cone Volcano

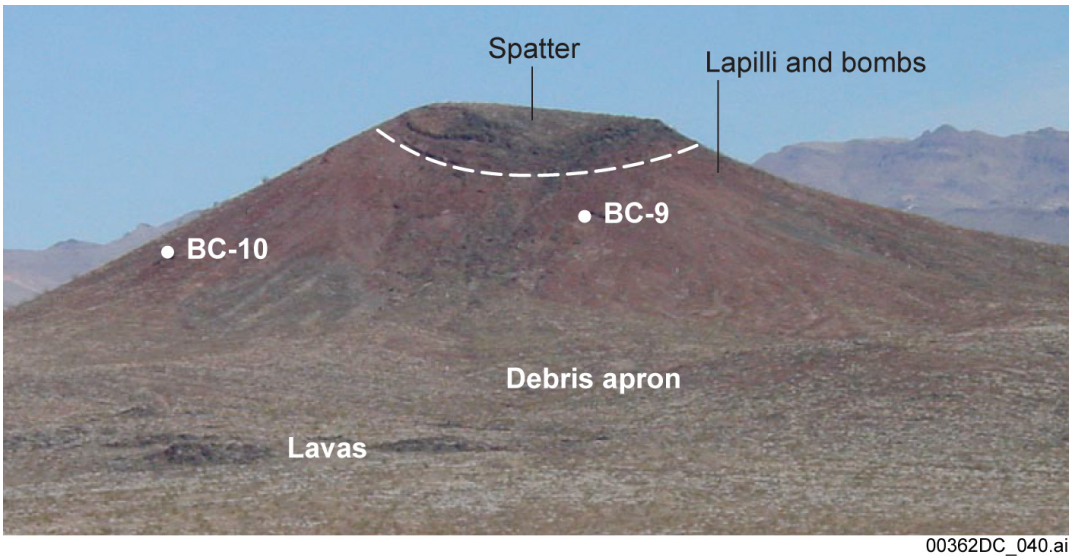

NOTES: This photograph shows the location of lapilli and bomb facies (lower cone), spatter facies (upper cone), upper reaches of debris apron, and location (BC-9, -10) of unconformities between outward- and inward-dipping beds (most exposures are of inward-dipping beds.

Figure E-6. Photograph of Black Cone (viewed from the south)

layer, increasing distinctness of clast outlines, and increasing abundance of lapilli relative to spatter and bombs. These features record deposition from asymmetric, short-lived spatter fountains. Locally, the thicker densely welded zones have swirling textures indicative of some rheomorphic flow (a.k.a. rootless or clastogenic lavas). The spatter facies bedding dips concentrically inward toward the center of a ~75-m diameter, bowl-shaped crater at the summit of Black Cone. Gullying on the southwest side of the crater has exposed deposits relatively close to its low point, and these are dominated by a 4-m-thick bed of densely welded spatter (Station BC-4, Figure E-5b) that grades laterally over 10 m to 20 m into a less-welded zone in a manner similar to that described above. Previous authors (Vaniman and Crowe 1981 [DIRS 101620], p. 18; Bradshaw and Smith 1994 [DIRS 101996], p. 169) have referred to this as a lava lake. However, a lava lake would normally be expected to have a bottom contact that conforms to the crater walls and floor, a flat top, and a relatively massive interior throughout its extent. This feature near the summit of Black Cone is simply another local, densely welded spatter zone rather than a true lava lake.

Crustal xenoliths are rare at Black Cone, but there is a horizon in the spatter facies that contains relatively abundant (estimated at a few percent by volume), white, vesiculated xenoliths with margins that indicate potential melting into the basalt host. These xenoliths are probably derived from the alluvial sediments that fill Crater Flat basin. Their presence in deposits that were produced by dominantly magmatic (Strombolian) eruptions (see below) underscores the observation that shallow crustal xenoliths do not necessarily record a locus of hydrovolcanic explosions in the volcanic feeder system (Valentine and Groves 1996 [DIRS 107052], pp. 84 to 87).

The angular unconformity that forms the contact between crater filling (inward dipping) and cone slope forming (outward dipping) deposits is exposed in two places (Stations BC-9and BC-10; Figure E-5b). These limited exposures and the patterns of bed orientations suggest that the cone may have had a crater that was open to the south-southeast during early phases, but that subsequently healed so that its final phases formed the relatively simple, circular crater that is indicated by the inward-dipping beds of the spatter facies at the summit of the cone remnant. Bradshaw and Smith (1994 [DIRS 101996], p. 168) argued that the presence of a purported caliche layer along one of the angular unconformities supported their polycyclic interpretation, but do not provide a location. The only feature in this study that resembles such a caliche layer is a layer of coarse ash along an unconformity that appears to have high calcium carbonate content (Station BC-9, Figures E-5b and E-6). However, this is due to pedogenic processes on the modern surface, where carbonate accumulation can vary as a function of the host material grain size. Larger scoria lapilli in the surrounding exposures are commonly coated with white carbonate, especially on their undersides, that is left after the evaporation of infiltrated rain water, while ash layers tend to hold water in the pores between clasts until the water evaporates, leaving carbonate material that is evenly distributed throughout the deposit. Thus, the "caliche layer" does not record a significant (polycyclic) time break. The angular unconformity is simply one that is so commonly associated with scoria cone construction, with inner and outer slopes, periods of slumping and healing, and changes in geometry (e.g., McGetchin et al. 1974 [DIRS 115469], pp. 3,261 to 3,264).

The cone remnant has a concave upward profile in most quadrants, is deeply rilled on its flanks and is surrounded by an apron of reworked pyroclastic debris that is also rilled. A gully system that cuts into the southwest flanks of the cone remnant exposes some scoria and bomb deposits near the base of the cone with poorly defined bedding that appears to dip shallowly (10° to 20°) away (southward) from the cone. These likely are exposed deposits of the debris apron rather than primary deposits.

E.3.2 Lava Flow Fields

E.3.2.1 South Lava Flow Field

The south lava field consists of a relatively low-lying, flat-topped area on its eastern part (possibly a separate lava field, but not further distinguished here; Figure E-5b) and a larger area that has several large pyroclast mounds. The length:width ratio is ~1:2. In general, the pyroclast mounds are similar to the mounds on the southwest lava field at Red Cone volcano. Most have shallow slopes and gently rounded tops that are littered with coarse (in some cases meter-sized) fluidal bomb fragments, scoria lapilli, and blocks. One mound has a beveled top that is littered with relatively dense lava blocks scattered among a "matrix" of large scoria lapilli – this mound may have originated as a high lava surface (e.g., a tumulus) that was covered with fallout scoria, rather than being a more easily modified mound of pyroclastic debris. A mound near the eastern part of the south lava flow field (Station BC-13, Figure E-5b) is littered with blocks and boulders of moderately welded agglutinate. Some of the larger blocks retain crude internal bedding, but there is no systematic orientation from one block to another. This is consistent with an origin by rafting of proximal pyroclastic facies from the main cone, and disintegration of the material as it was carried atop a lava flow, rather than the mound being a vent in which bedding orientations should vary systematically around the mound. In common with the southwest lava field at Red

Cone, the south lava field at Black Cone volcano flowed from the base of the cone southward along the gentle slope of Crater Flat.

Posteruptive surface features on the south lava field are also similar to the southwest lava field at Red Cone. Gullies formed in topographic lows between pyroclast mounds on the interior parts, and between flow lobes at the margin, of the lava field. In some places, the gullies have exposed interior features of pyroclast mounds. One excellent example (Station BC-14, Figures E-5B and E-7A) exposes steeply tilted (~80° northward toward the main cone) beds similar to those found in the main cone remnant, consistent with an origin of the mound by rafting of cone material where original bedding was preserved but rotated and tilted as it traveled atop a lava flow (e.g., Holm 1987 [DIRS 178117], pp. 322 and 323; Sumner 1998 [DIRS 178124], p. 206). Rills branch from the main gullies up onto the flanks of scoria mounds, and this drainage network in turn delivers pyroclastic debris from the interior of the lava field to its margins where it is actively accumulating as small alluvial fans or aprons that obscure the marginal features of the lava field.

E.3.2.2 North Lava Flow Field

The north lava field's length:width ratio is ~1:2, similar to that of the south lava field. A range of flow structures can be distinguished, even though the surface of the lavas has been modified. These include both arcuate lava ridges and circular or equant blisters or tumuli (e.g., Station BC-11 and vicinity, Figure E-5b) that appear to be due to squeeze-up processes in the active flows.

The north lava field forms a thicker platform than the south lava field and several features provide clues to its complex emplacement processes. Broad terraces - each a few meters high and with steep, arcuate margins covered with basalt blocks (flow edges) - on the top of the lava field may record stacking of lava flows along channel areas. Stacking can result if a time interval between lava pulses is sufficient to solidify channel-filling lava so that later pulses flow on top of it (e.g., Kilburn and Lopes 1991 [DIRS 178148], pp. 19,721 to 19,732), and by channel overflows (perhaps as described by Rossi (1997 [DIRS 178141], pp. 101 to 103)), as may occur if lava flux exceeds the local carrying capacity of a channel. In one location (~700 m to 800 m directly north of the summit of Black Cone) a patch of coarse pyroclastic debris inferred to have rafted from the cone is partly overridden by a lava flow unit, also recording stacking as an important mechanism for building up the lava platform.

Lava lobes along the outer margin are commonly 40-m to 100-m long and 20-m to 40-m wide. Top surfaces of most of these lobes step down as terraces to the valley floor (e.g., Figure E-7b) representing, as with the lavas at Red Cone volcano, successive breakouts from the toes of the lobes. The fact that these lobes protrude from the main, thick lava platform suggests that a significant portion of lava transport was through a tube network beneath the surface, with breakouts along the margins being an important mechanism by which the lava field widened and extended away from its vent area. This, in turn, implies that some of the thickness of the north lava field may be the result of inflation, as well as stacking of flows, as at Parícutin (Luhr and Simkin 1993 [DIRS 144310], pp. 10 to 26) and Etna (Duncan et al. 2004 [DIRS 178114], pp. 174 to 176). In one case a narrow (~10-15 m wide) tongue of lava, with preserved levees on either side of a narrow central channel, appears to extend about 60 m from a terrace on the top of

the lava platform toward the marginal lobes, partly overlapping and draping them. This also suggests a complex combination of subsurface transport within the lava field, breakout, and overlapping of lava flow units. It is inferred that these mechanisms worked in varying proportions in all the Pleistocene lava fields in Crater Flat, but the north lava field at Black Cone volcano better exhibits emplacement features because it is thicker and higher standing as a result of its lavas having advanced up slope on the valley floor.

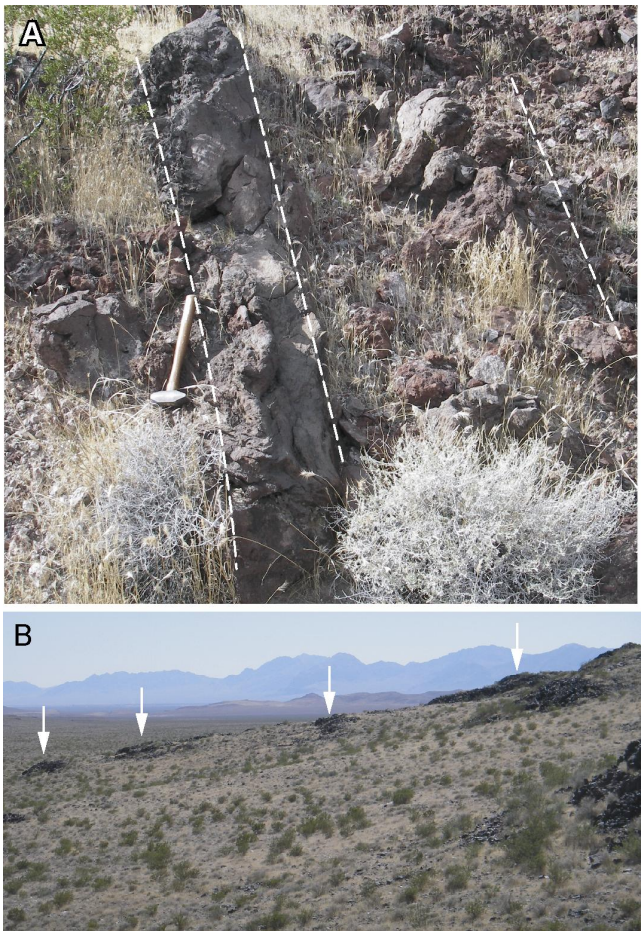

NOTES: (A) Interior of pyroclast mound exposed by deep gu lly along its eastern margin (Station BC-14), showing steeply tilted beds of densely welded spatter (next to hammer) and less-welded agglutinate beds.
(B) Terrace-like down-stepping of a lava lobe toward the valley floor due to successive breakouts (arrows) along eastern edge of north lava field.

Figure E-7. Features of Black Cone Lavas

Posteruptive geomorphic features at the north lava field are similar to those of the southeast lava field at Red Cone. Much of the top of the lava field is relatively flat as a result of original low spots having been filled with eolian sediment, and high spots having broken down by mechanical weathering (Stage B of Wells et al. 1985 [DIRS 178074], p. 1,525). Desert pavements of lapilli-size clasts are locally developed, but in many areas, the surface is dominated by angular (often somewhat smoothed by wind erosion) blocks of lava with eolian sediment and smaller lava clasts between. It is likely that these surfaces never had pyroclastic deposits on them, and the surface clasts are derived directly from lava surface rubble and weathered fragments of lava

crags (similar to surface mosaic type BG-1 studied by Wood et al. (2002 [DIRS 178146], p. 311; 2005 [DIRS 178147], p. 207)). Surfaces between lava terraces are smooth and variably paved, sloping gently downward toward the next lowest terrace. Although there is some drainage development between marginal lava lobes, most of the interior of the lava field is free of gullies or rills.

E.3.3 Interpretation and Summary of Black Cone Volcano

The overall eruptive sequence of Black Cone volcano is similar to that of Red Cone volcano. Pyroclastic facies in the cone remnant preserve an evolution from eruption of relatively well-fragmented material that was cool and brittle (except for large bombs) upon deposition even very near to the vent, forming the lapilli-and-bomb facies, to eruption of coarse spatter. The lapilli-and-bomb facies may have resulted from eruptions with sustained, high-standing columns approaching a violent Strombolian mechanism, although recycling and breaking-up of large clasts by avalanching in the vent area probably had an important role in producing this facies as well. The spatter facies represents a later phase of weak, asymmetric bursts or short-lived fountains of lava. The cone may have had an open horseshoe shape during part of its eruptive history that was filled in or healed by later pyroclastic activity that terminated with a bowl-shaped crater where the cone remnant's summit is now.

Early lavas emanated from the southern base of the cone and spread southward following the gentle slope of the valley floor and rafted significant quantities of cone material with them, probably simultaneously with explosive activity such that the lava field surface was partly covered with fallout lapilli. As the south lava field thickened and spread laterally (eastward and westward), it reversed the slope at the base of the cone such that the later north lava field flowed northward. The north lava field spread and thickened by a combination of stacking and overlapping of flow units and tongues, and inflation with marginal breakouts. This lava field rafted very little cone material and may have occurred after the most dispersive explosive activity (corresponding to the lapilli-and-block facies of the cone remnant) had ceased, as reflected in the lesser abundance of fallout lapilli on its surface. The spatter facies in the cone may have been contemporaneous with the north lava field.

The three main features of Black Cone volcano (cone remnant, south lava field, north lava field) each had different characteristics due to different eruption/emplacement processes, and have each undergone somewhat different posteruptive geomorphic evolution. The outward-dipping slopes of the cone have been removed, primarily through development of rills and runoff, to form a reworked apron around the cone remnant. This apron is in turn deeply rilled and its deposits are being gradually remobilized to lower elevations. The south lava flow, with its abundance of rafted cone fragments, had an initially hilly surface covered with loose pyroclastic debris. A combination of gully development in low spots between mounds, rilling of the sides of the mounds, and headward erosion of gullies that nucleated between marginal lava lobes produced an extensive drainage network and transported much pyroclastic debris to the margins of the lava field. This reworked debris is now accumulating as small alluvial fans and aprons that obscure the original lava margins. The north lava field was relatively flat to begin with. Combined accumulation of eolian sediment and mechanical weathering of crags and small highs have smoothed original lava surface roughness. Fluvial erosion and reworking is mainly limited

to gullies that nucleated between marginal flow lobes, and the paucity of easily remobilized pyroclastic debris has left the steep flow margins relatively clearly defined.

E.4 LITTLE CONES

E.4.1 Description

Little Cones consists of two cone remnants – the southwest and northeast cones - the summits of which are separated by ~380 m (Figure E-8). Because of their location at the southern end of Crater Flat, alluvial sediments have buried most of the two lava flow fields associated with these cones, but the extent of the lava fields is known from ground magnetic and aeromagnetic data (Figure E-8; Stamatakos et al. 1997 [DIRS 138819], pp. 326 to 328; Connor et al. 1997 [DIRS 102647], pp. 77 and 78; Perry et al. 2005 [DIRS 177379]).

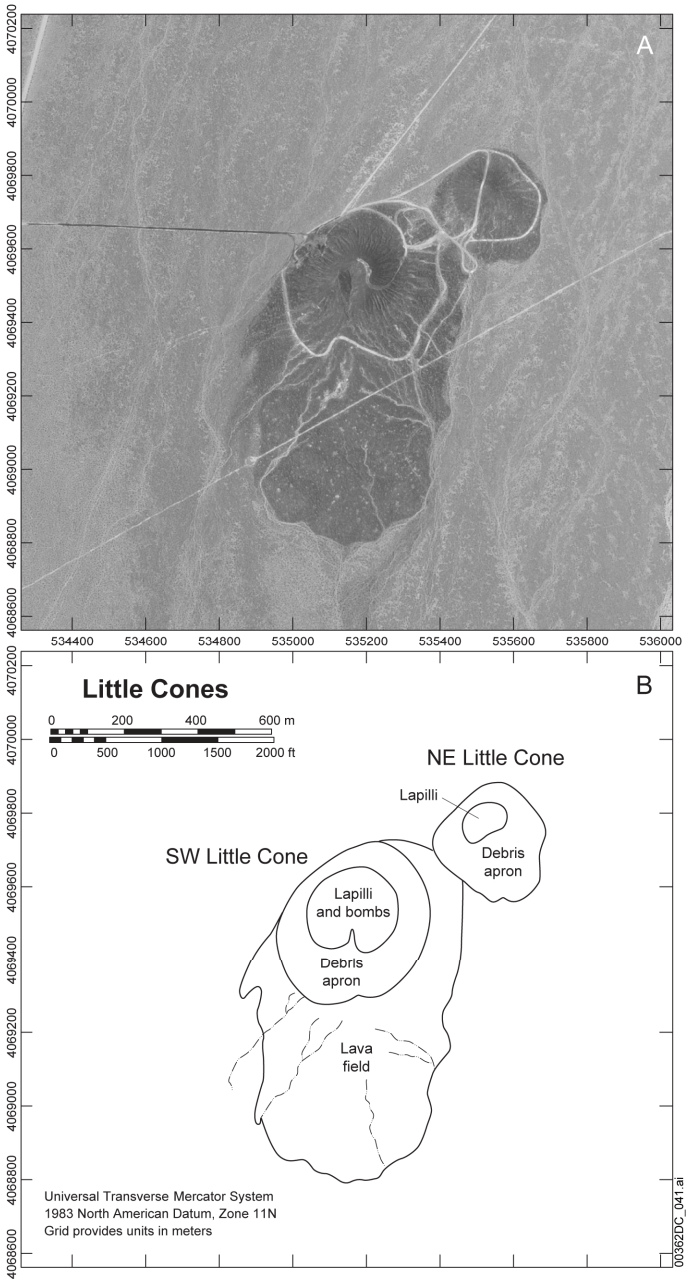

Figure E-8. Air Photograph (A) and Geologic Map (B) of Little Cone Volcanoes

The southwest cone remnant rises 24 m above the surrounding desert floor. A small quarry pit at the northwest base of the cone exposes clast-supported beds of highly vesicular, coarse, blocky scoria lapilli. The beds dip outward, away from the center of the cone remnant, at about 30°. Many of these beds are lenticular and inversely graded, and they show no evidence of welding. The most likely emplacement mechanism is a combination of fallout from sustained eruption columns with avalanching down the cone flanks. The higher flanks of the cone remnant are littered with scoria lapilli and bombs. Bombs are decimeters to ~1 m in size and commonly preserve some fluidal textures although some have cauliflower surface textures. The abundance of bombs on the surface could be due to a lag effect as smaller lapilli have been removed by

runoff. The cone remnant is deeply rilled and surrounded at its base by an apron of reworked pyroclastic material that is also rilled.

The southwest cone crater is open to the south and its lava field extends primarily in that direction; it is likely that the crater was open to the south during eruption with lavas erupting from the south and southwest base of the cone as indicated by aeromagnetic data (Figure E-9). Most of the lava flow field exposure is actually a surface with varying amounts of scoria lapilli and lava blocks, with eolian sand between the clasts. However, near its east edge, small lava ridges, probably representing squeeze-up structures as described above, do protrude above the surface, indicating that the top of the lavas is near the surface (Figure E-9). The length:width ratio of this lava field is ~1:1.

The northeast cone remnant is a 15-m-high hill with no crater. It is littered with scoria lapilli and is rilled. The buried lava flow field from NE Little Cone extends 2 km to the south (length:width ratio of ~2:1). It is possible that the lack of a crater remnant at NE Little Cone reflects advanced degradation of the cone by rafting of material on top of the lava flows, or simply by posteruptive erosion. However, since the surrounding alluvial surface is aggrading, and therefore base level for cone degradation is rising, it seems unlikely that posteruptive erosion at NE Little Cone would have been more rapid than at other Pleistocene volcanoes in the basin.

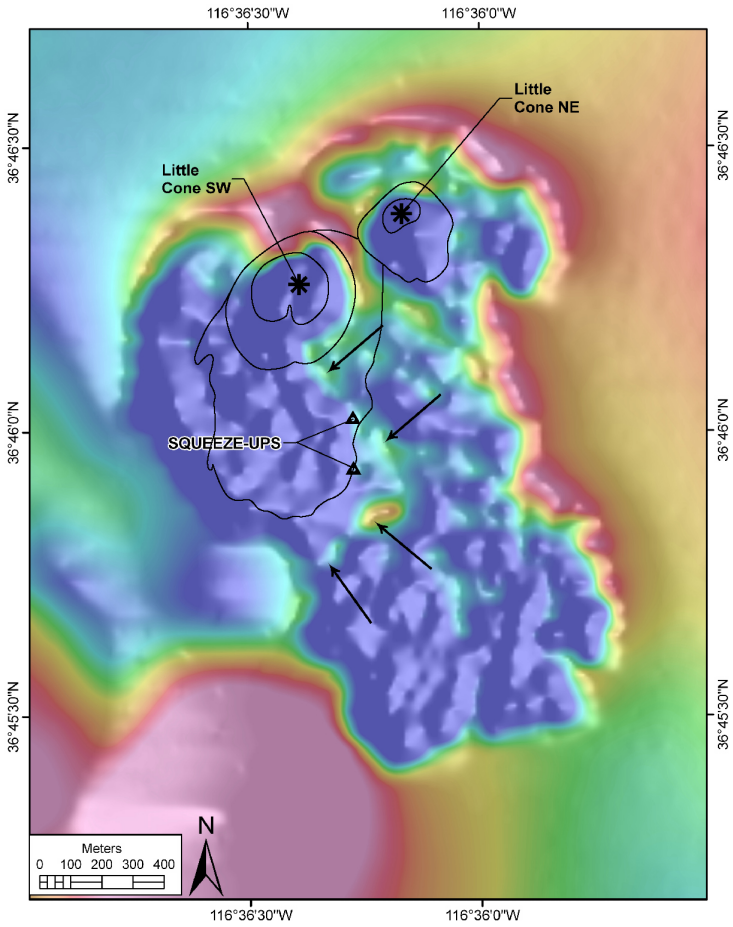

NOTES: Colors range from blue, representing strong reversed-polarity magnetization (including all lava flows), to red, which represents strong normal magnetization. Area characterized by high amplitude, small wavelength variations in magnetization are buried lava fields. One lava field spreads south to southwest of SW Little Cone, while another extends about 2 km directly south from NE Little Cone. Asterisks represent centers of cone remnants and triangles are location of lava squeeze-ups. Contacts from geologic map (Figure E-8b) are shown for comparison. Arrows point to eastern margin of the lava field associated with SW Little Cone.

Figure E-9. Aeromagnetic Anomaly Map of Little Cone Volcanoes

E.4.2 Interpretation and Summary of Little Cones

Little Cones appear to be similar to Red and Black Cone volcanoes in that they each have a cone that was likely built by a combination of Strombolian and violent Strombolian mechanisms, and lavas that extend southward down the valley slope. However, the Little Cones volcanoes appear to have one lava flow field each, rather than later ones that were diverted around early lavas. Incompatible trace-element compositions of bombs from the two cones differ significantly, consistent with an interpretation that each cone represents a separate eruptive episode. Strontium, thorium, and lanthanum, for example, have concentrations that are 45% to 70%

higher at SW Little Cone than at NE Little Cone (Perry et al. 1998 [DIRS 144335], pp. 4-8 to 4-13).

Aeromagnetic data, combined with the surface exposures south of SW Little Cones, allow a reasonable interpretation of the eruptive sequence of these two cones. The eastern lava flow field from NE Little Cone can be interpreted to represent the younger eruption, because it appears to have flowed around and past the western lava flow field from SW Little Cones (Figure E-9). The SW Little Cones lava flow field appears to have a top that is near the present surface, as suggested by the surface features described earlier. This implies that the western flow is thicker than the more completely buried eastern flow. Stamatakos et al. (1997 [DIRS 138819], pp. 326 and 327) used ground magnetic data to model the eastern flow as a 10-meter-thick flow buried by 15 m of alluvium. If this is correct, and if the base of both lava fields is at the same elevation, the thickness of the western flow (which nearly reaches the surface) is about 25 m.

E.5 MAKANI VOLCANO

E.5.1 Description

Makani volcano is a very small eruptive center that forms a subdued mesa with no cone structure. Its top is ~5 m above the surrounding terrain and the map-view diameter is ~500 m (Figure E-10). The eastern half is littered with scoria lapilli and fluidal bomb fragments and eolian sand and silt between clasts, has a slightly rounded top, and has some radiating rills in its surface that supply sediment to a narrow debris apron around the eastern part of the volcano. The western half has a relatively flat surface with lava blocks and eolian sediment between clasts, and a steep western margin of lava lobes.

E.5.2 Interpretation

Makani volcano is interpreted to have formed by eruption along a short (200 m to 300 m), roughly north-south-trending fissure located within the lapilli-and-bomb extent in Figure E-10b. Weak fountaining produced the bombs and scoria and possibly a low profile pyroclastic construct in the eastern part of the volcano, while lavas effused and flowed a short distance westward. Posteruptive surface processes were dominated by rilling and reworking of loose pyroclastic material on the eastern part of the volcano. The western part is a small lava platform in Stage B of surface evolution scheme used by Wells et al. (1985 [DIRS 178074], p. 1,525), and, like the southeast lava field at Red Cone and the north lava field at Black Cone volcanoes, has experienced little erosion except for gullies between marginal flow lobes.

E.6 DISCUSSION

E.6.1 Eruptive and Emplacement Processes

This study indicates that the lower exposures at Red and Black Cone volcanoes may record violent Strombolian mechanisms, while the upper deposits record later phases of explosive activity that were dominated by weak Strombolian bursts. Gutmann (1979 [DIRS 178116], p. 450) described cones in the Pinacate volcanic field that exhibit upward increases in abundance of coarse blocks and bombs, and capping sequences of welded agglutinate, that appear to be very similar to the described sequences. Gutmann (1979 [DIRS 178116]) attributed the variation to

the interplay between magma flux and bubble nucleation and growth processes. Previous authors referred to the upper spatter

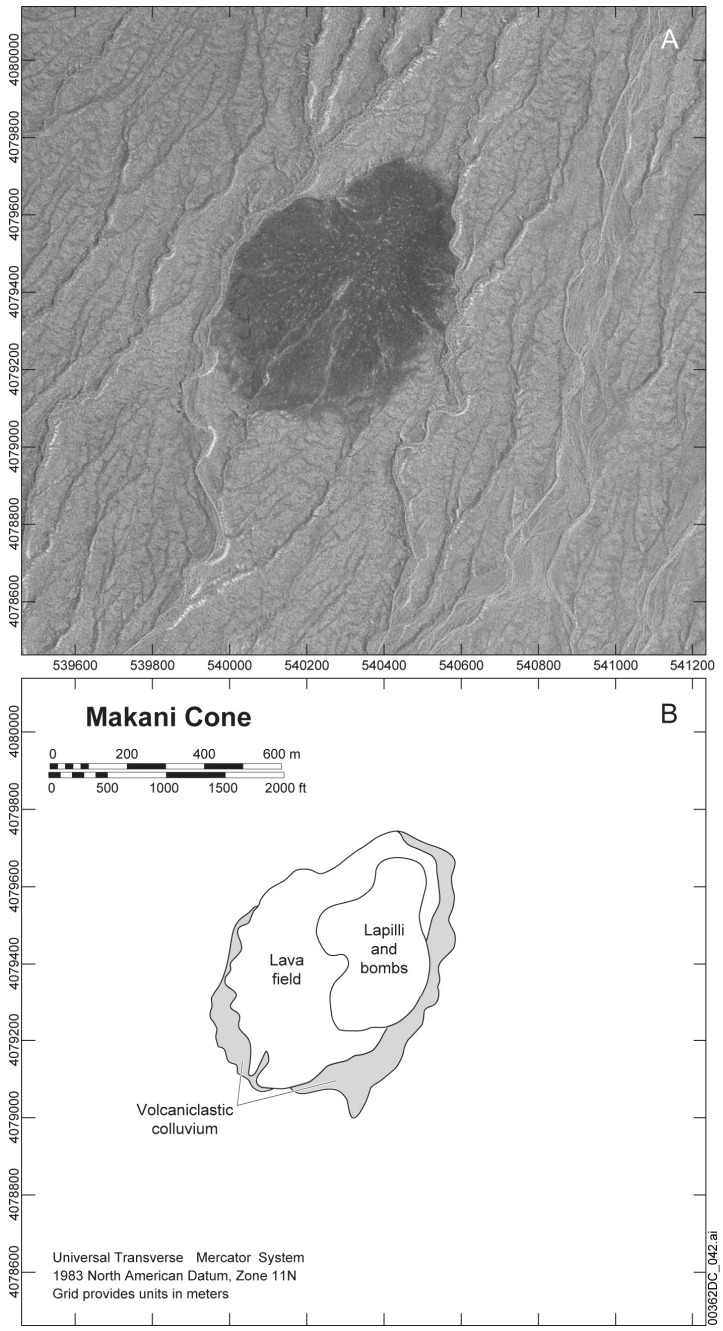

Figure E-10. Air Photograph (A), and Geologic Map (B) of Makani Volcano

facies at Red and Black Cone volcanoes as deposits of Hawaiian eruptions (e.g., Crowe et al. 1983 [DIRS 100972], p. 267; Bradshaw and Smith 1994 [DIRS 101996], pp. 168 and 169; Perry et al. 1998 [DIRS 144335], p. 6-11). However, the alternating degree of welding between beds and the limited lateral extent of densely welded deposits in very proximal locations indicate asymmetric, low, temporally discrete fountains more akin to Strombolian eruptions than to

Hawaiian eruptions, which produce sustained lava fountains (e.g., Parfitt 2004 [DIRS 170145], pp. 78 to 80) and more extensive welded facies. The presence of cauliflower surface textures on bombs in the lapilli-and-block facies at Red Cone, along with a relatively higher abundance of rounded (recycled) clasts, may reflect a component of magma-water interaction and steam explosions in the vent. Other than this, and a few cauliflower bombs at SW Little Cone, there is no evidence of any substantial hydrovolcanic activity in the 1-Ma centers.

All of the volcanoes discussed here, except for Makani volcano, produced lava flows that first erupted from the southern bases of the main cones, and spread south-southwestward down the shallow slope of the Crater Flat valley floor (the estimated southward topographic gradient varies from 25 m/km beneath Black Cone, 20 m/km beneath Red Cone, and 16 m/km beneath the two Little Cone volcanoes). The resulting lava fields at Red Cone, Black Cone, and SW Little Cone volcanoes extend 600 m to 800 m away from their vents, while the lava field at NE Little Cone extends ~2 km. The NE Little Cone lava field length must reflect a relatively higher effusion rate (~1 m^3/s to 3 m^3/s) compared to the other volcanoes (< 1 m^3/s, Walker 1973 [DIRS 178061], p. 112). With these rates the southwest and south lava fields at Red and Black Cone volcanoes, respectively, would have been emplaced over periods of 9 months to a year.

In detail, the flux may have been variable; it may be that for these small lava fields the effusion occurred as discrete pulses that achieved higher effusion rates but for short time periods. The small length:width ratios for the early lava fields at Red and Black Cones could be explained by the following model (Figure E-11). Discrete pulses of lava first flowed directly down hill. These flows solidified during a non- or weakly effusive period, forming a small platform (perhaps a few meters high) that was sufficient, given the gentle paleoslope, to divert the subsequent batch of flows to the side so that over time the field spread laterally as a fan around the south side of a given cone. Lava pulses that were separated by insufficient time for the previous flows to solidify might have inflated those flows, or pushed new extrusions of lava from the toes of marginal lobes. Pulses that were separated by enough time for previous flows to solidify, but that had low effusion rates, may have traveled across the top of the previously built flows for short distances after which they solidified to form a terrace on the top of the growing platform. Thus, a lava field was built in a fan-like manner where the radial distance from the vent to the margin was determined by peak effusion rates and durations of lava pulses, The circumferential spread was determined by some minimum period between pulses (sufficient to allow solidification of the just-previous pulse) and the thickness of flow units relative to the slope of the depositional surface. Once the footprint of such a lava fan was covered with flows, stacking and inflation might have continued to thicken the lava field until its top was sufficiently high to essentially reverse the slope around the base of the cone (which was likely to have been growing as all the above was taking place). At this stage, if effusive activity continued, lava broke out from some new location around the base of the cone to form a new lava field (the southeast and north lava fields at Red and Black Cone volcanoes, respectively). If effusive activity ceased before this stage, the volcano had only one lava field that extended from its downhill side.

The later lava fields at Red and Black Cones grew in different manners. At Red Cone volcano, the southeast lava field appears to have welled out of the southeastern base of the cone. After growing a short distance (~400 m) eastward across the valley floor it was able to catch the southward paleoslope and grow mainly in that direction for a distance of 1.6 km with a lesser

degree of lateral spreading, compared to the earlier southwest lava field, such that its length:width ratio is about 2:1. In contrast, the north lava field at Black Cone appears to have vented from the northern base of the cone. Because its lavas were flowing northward against the paleoslope, individual pulses or flow units were easily diverted laterally and the resulting length:width ratio is ~1:2. It can also be inferred that a significant component of the north lava field thickness is due to inflation as lavas were intruded into the interior of the platform as it thickened due to the limited uphill flow capability of the lavas.

Pyroclastic mounds observed in association with lavas in Crater Flat are not separate vents, but rather are masses of material rafted from the main cones. A final point focuses on the fact that these mounds are most abundant on the early lava fields at Red and Black Cone volcanoes, compared to the later lava fields. In the discussion of Red Cone, it was speculated that the later (southeast) lava field vented from a stronger part of the cone, or that production of pyroclasts at the vent had waned or completely stopped during emplacement of the southeast lava field. The first possibility is related to the observation that the cones were built upon a sloping surface (see schematic cross section views in Figure E-11). The downhill (south-southwest) flanks of the cones would be weaker (perhaps in a state of relative tension) than the uphill sides, which were in effect buttressed by the paleosurface. Although the elevation difference between the base of the cones on their uphill and downhill sides would have only been on the order of 10 m to 20 m, this may have been sufficient to promote cone failure and rafting on lavas emanating from the downhill cone bases. Lava flow speeds might have been faster when emanating from the downhill side, also promoting rafting. The Lathrop Wells volcano was also formed on a southward-sloping surface and exhibits the same relationships of preferential rafting with its early, southward-emplaced, lava field (Valentine et al. 2005 [DIRS 177782], pp. 630 and 631). Gutmann (2002 [DIRS 178149], p. 347) pointed out that a large number of scoria cones in the Pinacate volcanic field that were built upon a sloping paleosurface are breached on their downhill sides by lavas that carried away significant quantities of cone material as rafts. This suggests that the process of cone deconstruction by rafting is an important, general process on the development of small basaltic volcanoes that are emplaced upon sloping surfaces.

An issue that cannot be resolved about the Pleistocene Crater Flat volcanoes is whether significant fallout tephra deposits extended beyond the immediate vicinities of the pyroclastic cones. The volumes of lava and cone material at Red Cone and Black Cone volcanoes are very similar to the lava and cone volume at the ~80 ka Lathrop Wells volcano (0.05 km^3; Appendix C). Red and Black Cones expose pyroclastic sequences that potentially evolved from early violent Strombolian to late-stage, weak Strombolian eruptions; this is typical of many scoria cones around the world (Wood 1980 [DIRS 116536], p. 389; Gutmann 1979 [DIRS 178116], p. 450), but is an opposite trend to that at Lathrop Wells volcano (Valentine et al. 2005 [DIRS 177782]). However, because other features of the three volcanoes are very similar, it seems reasonable to postulate that Red and Black Cone volcanoes may have originally had laterally extensive fallout deposits similar to those associated with Lathrop Wells (~0.04 km^3; Valentine et al 2005 [DIRS 177782], p. 629). Similarly, the two Little Cones volcanoes may have had laterally extensive fallout deposits, though probably not as large as Red and Black Cone volcanoes, assuming that the fallout volume was proportional to cone and lava volumes.

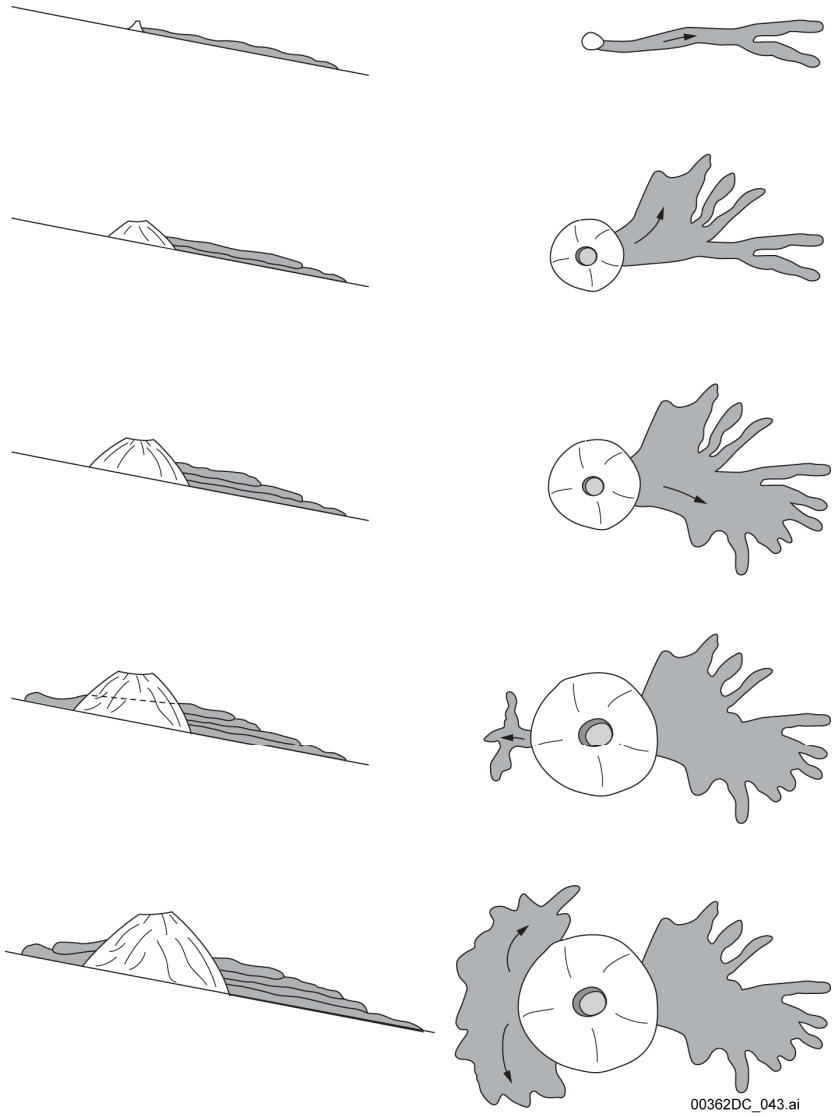

NOTES: Left column shows cross-section view and right colum n shows map view at corresponding stages. The beginning of the sequence is shown at the top with initial lava flow from a small cone. Subsequent pulses of lava build a fan-shaped lava field. When the thickness of the lava field is sufficient, subsequent lava effusion is diverted to a different location along the cone base (bottom figures).

Figure E-11. Sequence of Events for Developing Fan-Shaped Lava Flow Fields Simultaneously with Cone Growth on a Gently Sloping Surface

E.6.2 Posteruptive Surficial Processes

Different eruptive and emplacement processes at the Pleistocene centers in Crater Flat produced three major surface types: (1) main pyroclastic cone, (2) lava flow fields with abundant rafted cone material, and (3) lava flow fields with little pyroclastic surface material. These three surfaces provided different initial conditions for subsequent geomorphic evolution as summarized in Figure E-12, and add a level of complexity to the landscape evolution scheme of Wells et al. (1985 [DIRS 178074]).

Posteruptive degradation of the main cones (Figure E-12a) begins with development of rills on cone slopes. Initiation of rilling requires low-permeability areas on the cone surface that enable runoff of rainwaters rather than simple infiltration into loose scoria. At cones that are characterized by closing stages of violent Strombolian activity, such as Lathrop Wells volcano, a significant period of time, perhaps many tens of thousands of years, may be required as eolian sediment and carbonate clogs pore spaces in loose surface scoria, finally reducing its permeability sufficiently to stop rain infiltration. At the Pleistocene Crater Flat volcanoes, however, the presence of large bombs and densely welded spatter facies from closing pyroclastic eruptions may have provided impermeable surfaces such that runoff and rilling began relatively quickly. Formation and down-cutting of rills transports pyroclastic material to a growing apron around the base of the cone. As pedogenic processes clog the upper horizon of the reworked apron, it in turn becomes relatively impermeable to rain water such that runoff nucleates and forms rills in the apron, transporting pyroclasts farther away from the cone. This multi-stage process presumably continues until the cone topography is quite subdued.

Lava fields with abundant mounds of pyroclastic material (Figure E-12b) develop drainage networks by a combination of headward erosion of gullies that initially nucleate between marginal lava lobes, and development of rills on mound slopes that converge to form gullies in low areas between mounds. The resulting networks transport pyroclastic debris to the distal edges of the lava field, where it accumulates as small alluvial fans and aprons. These aggradational features obscure the primary features of the lava margins (e.g., flow lobes, steep flow fronts). This contrasts with a lava field that has few or no pyroclast mounds and little or no fallout lapilli on its surface (Figure E-12c), which undergoes processes of smoothing on the top of the platform and gullying that begins only between flow lobes at its margin with slow headward erosion. Such a lava field may retain its steep flow fronts and other lava structures much longer than a pyroclast mound-rich lava field. This points out the importance of accounting for different initial conditions of surfaces when determining relative ages based on modern morphology. Bradshaw and Smith (1994 [DIRS 101996], p. 168) inferred that the different morphologies of the two lava fields each at Red Cone and Black Cone volcanoes represented significant gaps in time between emplacement of the lavas (although not specified by Bradshaw and Smith 1994 [DIRS 101996], p. 168, such differences would imply time gaps of many tens to hundreds of thousands of years), but the differences primarily reflect different initial characteristics of the lava fields.

Posteruptive surficial processes also provide an explanation for the morphology of pyroclast mounds, most of which have subdued, rounded shapes and abundant coarse pyroclastic material on their tops. There are probably many different types of rafts (e.g., see Holm 1987 [DIRS 178117], pp. 322 to 324; Luhr and Simkin 1993 [DIRS 144310], pp. 80 to 95); Figure E-13 shows postemplacement evolution of three different types: (1) raft with intact cone bedding (e.g., Holm 1987 [DIRS 178117], pp. 322 to 324), (2) raft of agglutinate deposits that have partly disintegrated during transport on top of a lava, and (3) raft of initially unconsolidated, loose pyroclastic debris blanketed by scoria fallout. These different types of rafts can evolve to mounds with similar appearances that do not on the surface show much of their original character, due to mechanical weathering and accumulation of eolian sediment.

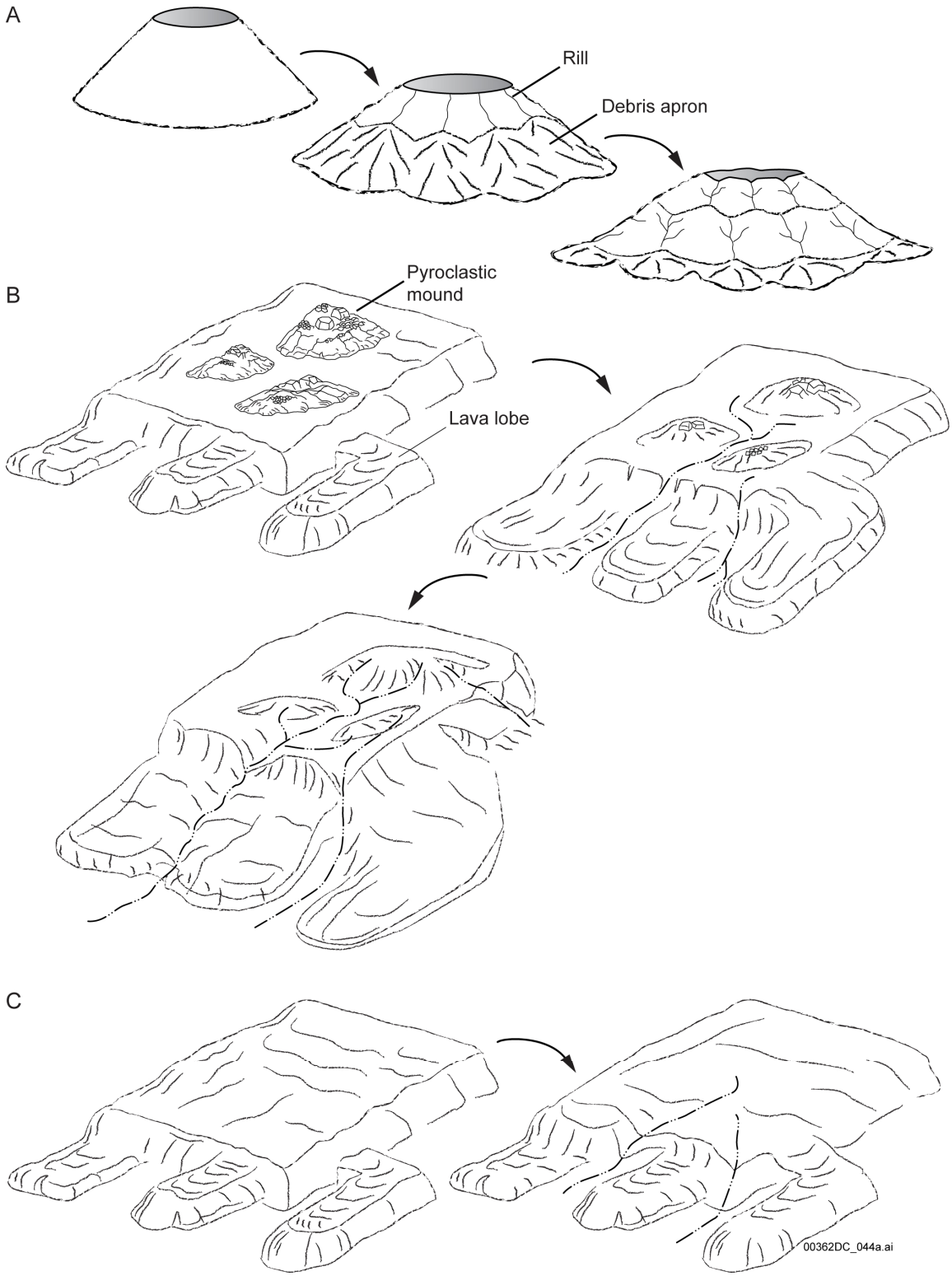

Figure E-12. Schematic Illustration of Geomorphic Evolution of Pyroclastic Cone (A), Lava Field with Abundant Pyroclastic Mounds (B), and Relatively Pyroclast-Free Lava Field (C).

E.7 CONCLUSIONS

The Pleistocene volcanoes in Crater Flat formed by a range of explosive processes including Strombolian and, potentially, violent Strombolian explosive activity. These were accompanied by development of lava fields that thickened through a combination of flow unit stacking and

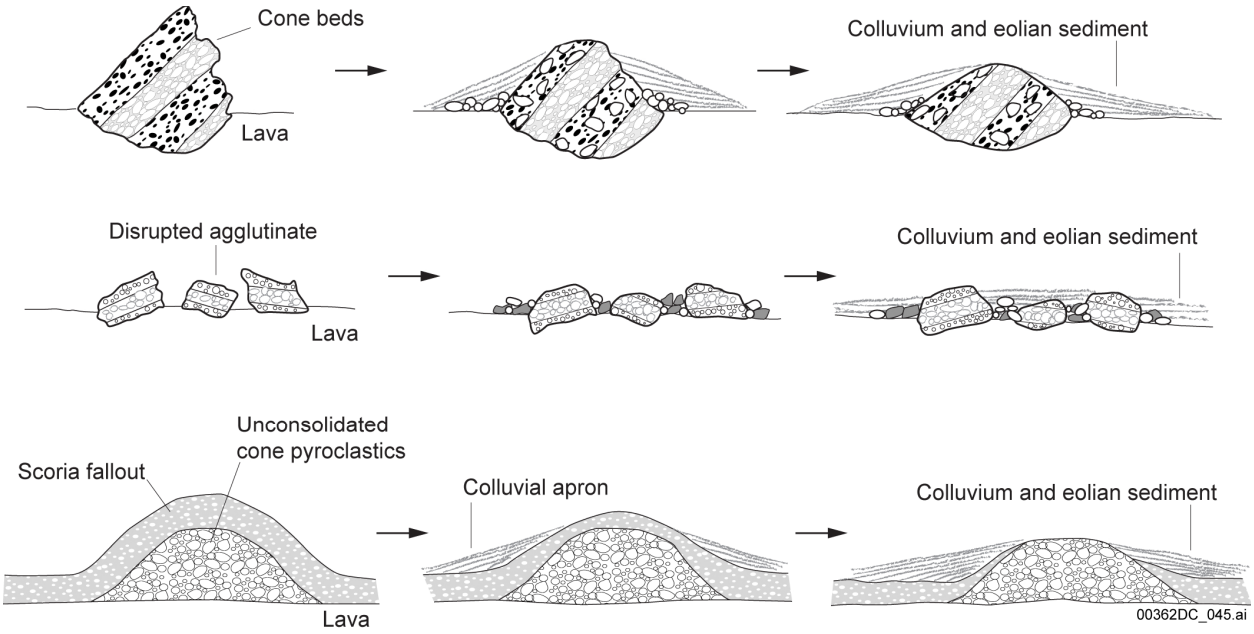

NOTES: (Top row) Raft emplaced with cone bedding still intact. Gully exposure of tilted beds shown in Figure E-7A is an example of this type of mound.
(Middle row) Raft of partly welded agglutinate that disintegrated into large blocks during emplacement. Station BC-13 on Figure E-5b is an example of this type of mound.
(Bottom row) Raft emplaced as loose, coarse pyroclastic material subsequently covered with fallout lapilli. Note that the top and middle raft types could also be mantled (except on initially steep faces) with fallout lapilli, which would modify their geomorphic evolution somewhat. As time progresses the initially different types of pyroclastic mounds grow increasingly similar in appearance due to surficial processes.

Figure E-13. Postemplacement Evolution of Pyroclastic Mounds that Originate as Rafted Cone Material

inflation, expanding laterally in a manner determined by the interplay between effusion rates and paleotopography. Cone growth, cone deconstruction by failure of cone segments and rafting atop lava flows, and cone healing were intimately linked and resulted in complex histories preserved in cone remnant deposits. The volcanoes are monogenetic and geochemical variations within individual volcanoes (Bradshaw and Smith 1994 [DIRS 101996]) should be interpreted within that framework (e.g., Strong and Wolff 2003 [DIRS 178150]) rather than invoking long time gaps. Posteruptive geomorphic evolution in this arid to semi-arid region was strongly influenced by the characteristics of the original volcanic surfaces, thus complicating any relative age determinations based upon erosional characteristics of different volcanic features.

If a potential volcanic eruption at the proposed Yucca Mountain repository is similar to the Pleistocene Crater Flat volcanoes and to the Lathrop Wells volcano, the results presented here indicate that the event would consist of one main feeder conduit forming a main cone with shallow lava breakouts (boccas) around the base of that cone, and a duration of ~1 yr to 3 yrs based upon estimated effusion rates. This contrasts with previous interpretations (Vaniman and

Crowe 1981 [DIRS 101620], pp. 15 to 19; Bradshaw and Smith 1994 [DIRS 101996], pp. 168 and 169) that imply multiple feeder conduits (based upon their inferences that pyroclast mounds each represent separate vents) and long gaps in time between polycyclic eruptions.

INTENTIONALLY LEFT BLANK

APPENDIX F
SHALLOW PLUMBING OF BASALTIC VOLCANOES IN THE YUCCA MOUNTAIN REGION

APPENDIX F – SHALLOW PLUMBING OF BASALTIC VOLCANOES IN THE YUCCA MOUNTAIN REGION

F.1 INTRODUCTION

Small-volume basaltic volcanoes (volumes on the order of ~1 km^3 or less) characterized by pyroclastic (also known as scoria or cinder) cones, fall deposits, and lava fields are the most common subaerial volcanic landform on Earth (Wood 1980 [DIRS 116536], p. 388). Despite its abundance, this type of volcano has received significantly less attention in the literature, compared to more silicic systems, regarding its range of eruption styles and the nature of its shallow plumbing system. This appendix describes direct observations of field characteristics of shallow dikes and conduits that feed such eruptions and the relationship between field data and corroborative theoretical models of conduit flow. The immediate application of this research lies in constraining the consequences of a potential volcanic eruption at the proposed underground Yucca Mountain radioactive waste repository (e.g., Crowe et al. 1983 [DIRS 100972]; Doubik and Hill 1999 [DIRS 115338]; Woods et al. 2002 [DIRS 163662]; Dartevelle and Valentine 2005 [DIRS 178142]; Appendix E, this report). In addition, the improved understanding of this common type of volcano has broader implications for models of basaltic volcano dynamics on Earth and other planets and for risk assessment and management in basaltic volcanic fields, in that this work demonstrates the appropriateness of assuming conduit geometry is determined by local lithostatic pressure in conduit flow models (validating arguments of Wilson and Head 1981 [DIRS 101034], pp. 2,980 and 2,981). The focus is on the plumbing of volcanoes dominated by eruptions that were driven by magmatic volatiles (e.g., Strombolian, violent Strombolian, and effusive eruption styles), rather than by explosive magma-water interaction (e.g., Lorenz 1986 [DIRS 178152]; Mastin 1991 [DIRS 124749]).

A starting conceptual model for the evolution of small basaltic volcanoes and their shallow (uppermost hundreds of meters) feeder systems has three stages (Figure F-1). Basaltic magma rises through the crust in dikes that, in the study areas, are typically a few meters wide and have strike lengths of a few kilometers (Figure F-1a). The dikes commonly occur in several-hundred meter-wide sets of ~2 to 6 subparallel dikes. At the paleosurface, one of these dikes, typically the widest, is the "master" dike that feeds eruptive vents. Each dike may consist of many en echelon segments along its strike, but in general each maintains its identity as a single dike along much of its length. Where the master dike intersects the Earth's surface it may initially feed eruptions from linear fissure vents (Figure F-1b), but eruptive flow becomes progressively focused into one or more main vents that form pyroclastic cones (Figure F-1c). Such transitions have been observed in historical eruptions (e.g., Richter et al. 1970 [DIRS 178153], p. E9; Thorarinsson et al. 1973 [DIRS 178151], pp. 372 and 373). In some cases the initial fissure may not feed significant eruptions, which instead are quickly (hours) focused into a central vent area that rapidly builds a pyroclastic cone (an example being Paricutin; Luhr and Simkin 1993 [DIRS 144310], p. 62). Valentine and Perry (2006 [DIRS 177495], p. 4) showed that there is a strong correlation between total erupted volume, eruptive fissure length, and effusion rate for Plio-Pleistocene basaltic volcanoes in the Crater Flat Volcanic Zone of southern Nevada (Crowe and Perry 1990 [DIRS 100973], p. 328).

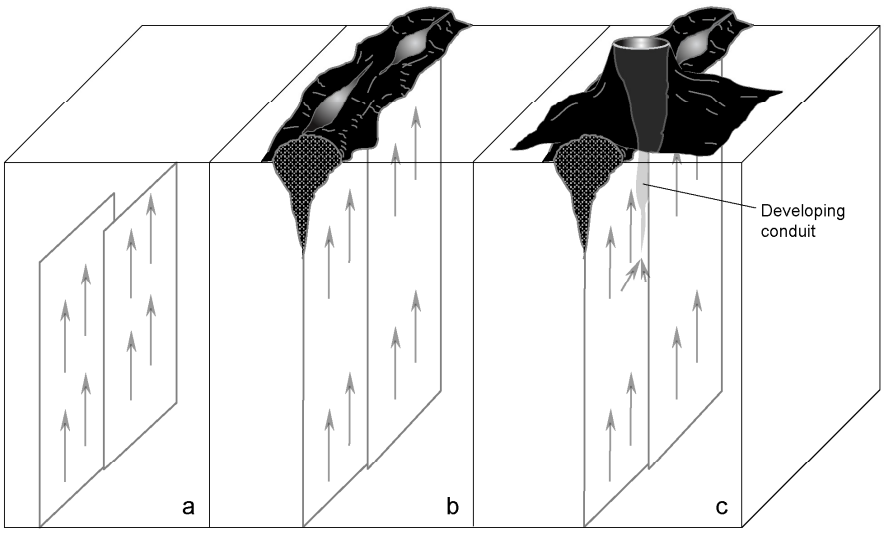

NOTES: In the panel a), a pair of en echelon dikes approach the surface. One or both of these dikes reaches the surface in a fissure eruption, forming spatter ramparts and areas of localized magma flow (b). Within hours to days, the fissure eruption localizes into a single vent, an enlarged conduit forms in the upper ~100 m, and an edifice (cone) is constructed above (c).

Figure F-1. Schematic Diagram of Three Stages of Development of a Dike into a Small-Volume Basaltic Volcano

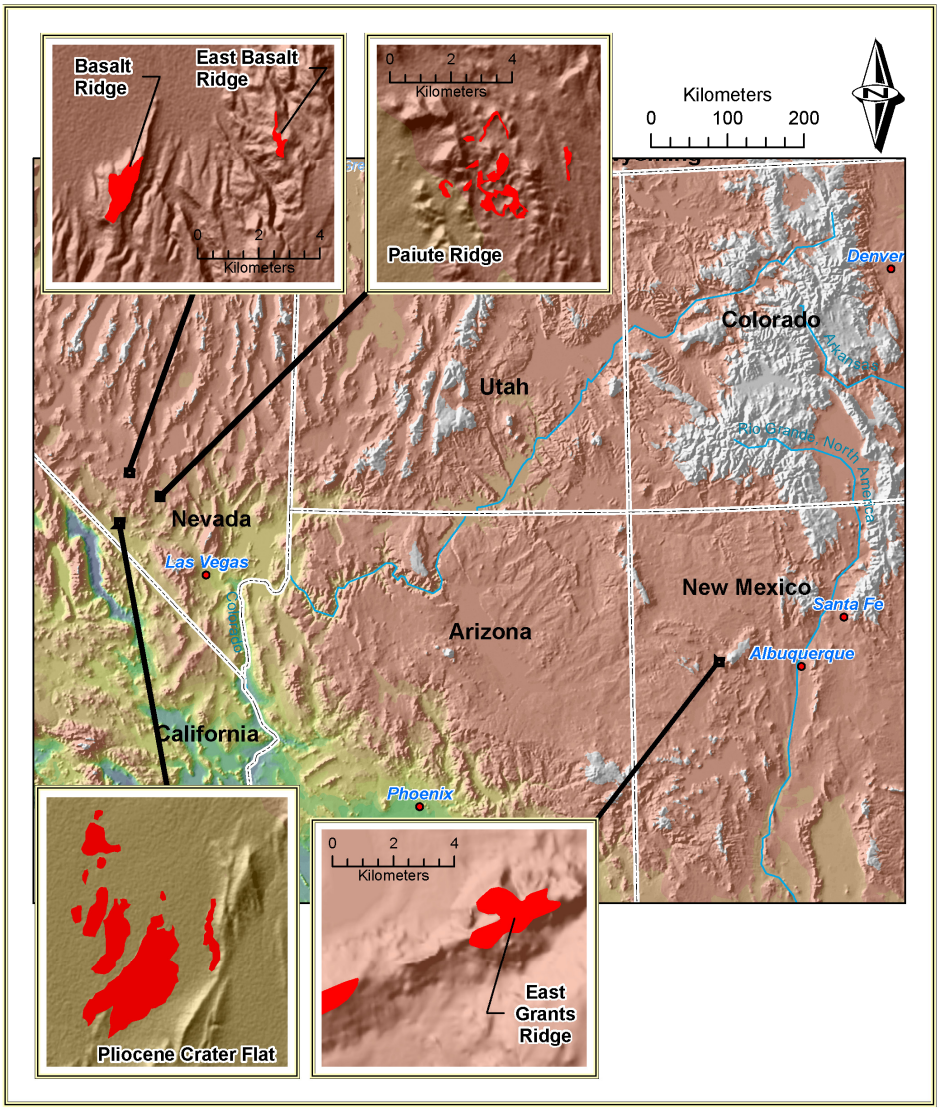

NOTE: Basalts in each study area inset shown in red.

Figure F-2. Regional Locator Map for Field Areas Described

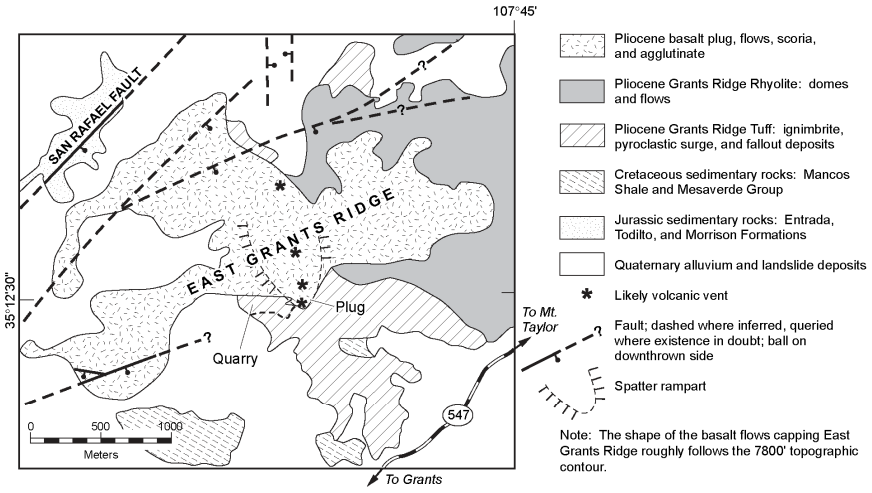

NOTES: The prominent basalt plug is located at the south en d of a series of probable eruptive vents, the locations of which are interpreted from eroded remnants within the elongate spatter rampart.

Figure F-3. Generalized Geologic Map of East Grants Ridge, New Mexico

As basaltic volcanic eruptions progress, it is thought that their vents and shallow feeder dikes/conduits widen. Such widening is most intense near the surface and can produce a flaring vent shape that plays a key role in eruptive dynamics (Wilson and Head 1981 [DIRS 101034], pp. 2,980 and 2,981; Mitchell 2005 [DIRS 178154], p. 200). Valentine and Groves (1996 [DIRS 107052], p. 85) summarized the processes that can contribute to dike/conduit wall erosion:

- Erosion from shear stress of flowing magma (below fragmentation level; Dobran 2001 [DIRS 162802], p. 481)
- Erosion from particle collision (above fragmentation level; Macedonio et al. 1994, [DIRS 178155], p. 141; Dobran 2001 [DIRS 162802], p. 481)
- Thermoelastic stressing of wall rock (McBirney 1959 [DIRS 162826], p. 443)
- Conduit wall collapse due to variations in magmatic pressure as a result of conduit processes (variations in magma pressure, shock/rarefaction waves; Wilson and Head 1981 [DIRS 101034], p. 2,980; Macedonio et al. 1994 [DIRS 178155], p. 139; Dobran 2001 [DIRS 162802], pp. 480 to 484)
- Hydromagmatic processes: interaction of magma with groundwater or saturated sediments (McBirney 1959 [DIRS 162826], pp. 443 to 445; Lorenz 1986 [DIRS 178152], p. 266; White 1991 [DIRS 124930], p. 239)
- Inclusion of wall-rock blocks where offshoot dikes rejoin the master dike

- Pore pressure buildup (McBirney 1959 [DIRS 162826], p. 443; Delaney 1982 [DIRS 162799], p. 7,753)

- Brecciation and erosion of dike wall rocks, local enlargement (Delaney and Pollard 1978 [DIRS 162800], p. 1,212; Delaney and Pollard 1981 [DIRS 162801], pp. 17 and 18; Delaney and Gartner 1997 [DIRS 145370] p. 1,178)

- Progressive melting of the host rocks, enhancing localized flow (Bruce and Huppert 1989 [DIRS 178156], pp. 666 and667; Quareni et al. 2001 [DIRS 162830], p. 218)

- Magma viscosity variations induced by solidification of magma at dike margins (Wylie et al. 1999 [DIRS 162861], p. 438).

From a continuum mechanics view, a planar dike is the preferred form for propagation of mafic magma through brittle and elastic host rock, whereas a cylindrical conduit is the preferred form for magma flow and delivery to the surface (Delaney and Pollard 1978 [DIRS 162801], p. 1). Most theoretical models for shallow magma ascent assume either flow through a dike or flow through a cylinder as end-members (e.g., Wilson and Head 1981 [DIRS 101034], p. 2973; Papale et al. 1998 [DIRS 178157], p. 77; Mastin and Ghiorso 2000 [DIRS 170144], p. 6; Mitchell 2005 [DIRS 178154], pp. 187 and 188). The last three mechanisms in the above list, in particular, address the transition from magma flow in a subplanar dike to flow in a cylindrical conduit. This transition is critical in defining the fluid dynamical processes of basaltic eruptions and remains poorly constrained.

From a field perspective there are several difficulties in constraining the dike-conduit transition and conduit geometry. In most locations where basaltic dikes and circular intrusive bodies that might be conduits are exposed, the eruptive products have been stripped by erosion (e.g., Delaney and Pollard 1978 [DIRS 162801], p. 1,212; Delaney and Gartner 1997 [DIRS 145370], p. 1,177; Diez et al. 2005 [DIRS 178158]), making it impossible to definitively tie the intrusive features to specific eruption styles. Additionally, intrusions record the integrated effects of an entire volcanic event that might extend for months or years (e.g., Luhr and Simkin 1993 [DIRS 144310], pp. 10 to 26; Appendix E, this report) and, therefore, do not, in most cases, provide direct information on geometry during a specific eruptive event with a specific volume flux, for example. Conversely, lack of erosion in young volcanic fields preserves information related to eruptive styles, but reveals only indirect information on the geometries and textures of feeder intrusions based, for example, on abundances of xenoliths from various depths (Valentine and Groves 1996 [DIRS 107052], Table 1; Doubik and Hill 1999 [DIRS 115338], p. 59).

This appendix reports data from five sites with intermediate erosional levels, where remnants of the volcanic constructs allow some definition of eruptive styles, and subsurface plumbing is partially exposed (East Grants Ridge, Paiute Ridge, Basalt Ridge, East Basalt Ridge, and Pliocene Crater Flat; Figure F-2, Table F-1). Several of the intrusive features can be observed to depths of about 250 m below the paleosurface, building upon observations such as those of Nemeth and White (2003 [DIRS 178160]). A weakness in these studies is that for two of the sites where eruptive products are still partially preserved (Basalt Ridge and East Basalt Ridge), the plumbing is not exposed directly beneath the vents but only at some lateral distance away. The combination of these field observations with theoretical models of magma ascent allows us

to draw general conclusions about geometry and conduit processes in shallow basaltic conduits and to discuss implications for future research.

F.2 FIELD DATA

F.2.1 East Grants Ridge, New Mexico

East Grants Ridge (Figures 2 and 3) is an erosional remnant of an alkali basaltic volcano, 2.573 ± 0.130 Ma in age (Laughlin et al. 1993 [DIRS 174240], Table 3), that is part of the Mount Taylor volcanic field in New Mexico (Perry et al. 1990 [DIRS 173994], Figure 1; Keating and Valentine 1998 [DIRS 111236], Figure 1; WoldeGabriel et al. 1999 [DIRS 110071], p. 390). Lavas of Grants Ridge erupted from an approximately N20°W-trending chain of vents on East Grants Ridge and flowed mainly westward and now form a series of prominent mesas. The preserved erupted volume is about 0.1 km^3 (Table F-1), and the original volume was probably somewhat greater. The south side of East Grants Ridge exposes a plug-like body of vertically jointed, massive alkali basalt that intruded older rhyolitic tuffs (about 3.3 Ma; Laughlin et al. 1993 [DIRS 174240], Table 1) and volcaniclastic deposits (Figure F-4) (Keating and Valentine 1998 [DIRS 111236], pp. 39 and 41; WoldeGabriel et al. 1999 [DIRS 110071], pp. 390 to 393). These deposits are capped by beds of variably welded scoria and spatter that dip symmetrically away from the approximately 125-m-wide plug. Based on the orientation of a prominent rampart of welded spatter extending northeast from the main plug (Figures F-3 and F-4), as well as similar exposures on the top of the ridge, the southern cliff exposure is interpreted to be the southern extent of a system of aligned vents along an eruptive fissure. Vent locations on East Grants Ridge are indicated by inward-dipping beds of welded scoria and spatter, the remnants of pyroclastic ramparts or cones that formed around the vents. These features indicate that there were from 2 to 4 vents and that the chain of vents was between 1 km and 1.5 km long. Vent spacing is approximately 125 m, 325 m, and 800 m, respectively. The dense basalt plug represents late-stage magma that filled one locus of eruption at the southern end of the fissure near the end of its final eruptive phase. This interpretation differs from that of Crumpler (2003 [DIRS 174074], pp. 161 and 163), who inferred that the plug is a lava lake within a single, circular scoria cone and did not consider the evidence for a fissure system that extends northward. Based on the remnants of spatter ramparts, the eruptive style was likely Hawaiian, beginning as a continuous fissure eruption and focusing to about four loci of eruption (discrete vents) within hours (e.g., Kilauea Iki; Richter et al. 1970 [DIRS 178153], p. E9). The lava flows associated with these vents may have emanated from the vents effusively or coalesced in part from spatter ramparts, forming clastogenic flows that flowed west-southwest, confined to a paleochannel for several kilometers until reaching a broad valley where the flow spread out in a fan-like fashion (Thaden et al. 1967 [DIRS 174076], plate 1).

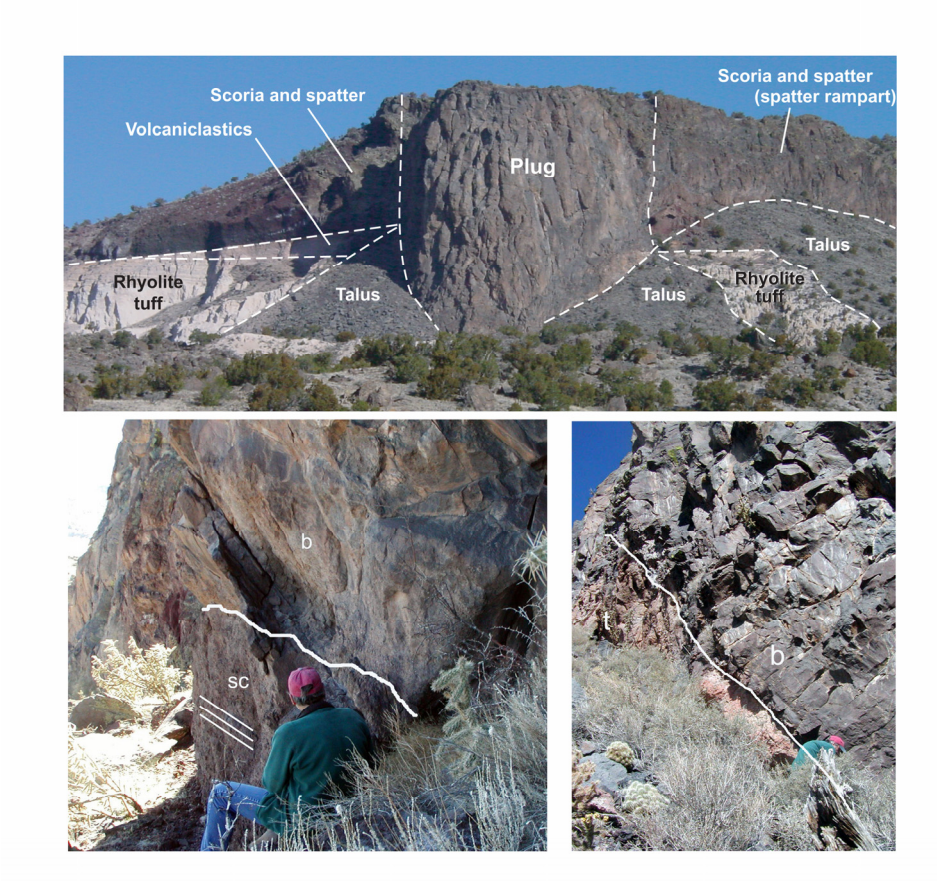

NOTES: Top: photograph of the south side of East Grants Ridge, showing rhyolitic tuffs and volcaniclastic host rocks, alkali basalt plug, and basaltic pyroclastic deposits. Bottom left: photo looking southwest along base of the spatter rampart ~100 m east of the plug; west-dipping bedded scoria (sc) is truncated at a high angle by dense basalt (b) that forms the core of the spatter rampart (east fissure boundary). South face of the plug is in the background left. Bottom right: photo looking north along the western contact of the plug basalt (b) with the host rhyolite tuff (t). The contact dips at about 80° east in this area. Note pale orange, contact-welded tuff adhering to the dense basalt of the plug.

Figure F-4. East Grants Ridge Layout and Structure

Table F-1. Summary of Dimensions of Basaltic Volcanic and Subvolcanic Features at the Study Areas

Location	Age (Ma)	Volume (km^3)	Intrusion Geometry	Intrusion Width[a] (*at Depth*) (m)	Nature of Host-Rock Impact (Comments)	Length of Dike, *Eruptive Fissure* (km)	Number of Major (Minor) Vents	Spacing for Major (Minor) Vents (m)	Location of Major Vents along Dike/Fissure
Basalt Ridge, Nevada	9.1±0.7[e]	≥0.07[f]	Dike, flaring to conduits	10 (*30*) 4 (*150*)	Sharp contacts, branching dikes, sills (Dike/conduit measured distal to conduit)	4.5 *2.5*	2 (1)	1,000 (650)	Center
East Basalt Ridge, Nevada	8.8±0.1[e]	≥0.003[g]	Dike, flaring to conduits; dikes between focused vents along fissure	100 *(0)* 45 *(25)* 40 *(35)* 30 *(48)* 25 *(50 to 90)* 15 *(90)* 10 to 12 *(120 to 240)* 15 (*250)* ------ 40 (*0*) 7 (*25*)	Sharp contacts with vitrophyre at 50 m to 250 m; branching dikes, brecciation of host rock <50 m depth (Dike/conduit widening at depth of ~<90 m; pronounced conduit flare at depths ~25 m; two separately measured conduit profiles reported here)	4.3 *1.5*	3	500 to 600	Center
Paiute Ridge, Nevada	8.6±0.07[c]	≤1	Dikes; intersection of dikes forms conduit	Dense basalt: 65 × 110 (elliptical) Total: 110 × 220 (*30 to 70*)	Significant; range from sharp contact with vitrophyre to 20-m-wide zone of diking, brecciation, mixing	0.5 to 5 *?*	1 (2 to 3)	500 to 2,000	End
Southeast Crater Flat, Nevada	3.73±0.02[d]	0.6[g]	Elongate fissure	15 *(0)* 75 (*25 above surface*)	Unknown	3.5 *3.5*	3 (10)	1,000 to 1,500 (20 to 300)	Center, End

Table F-1. Summary of Dimensions of Basaltic Volcanic and Subvolcanic Features at the Study Areas (Continued)

Location	Age (Ma)	Volume (km^3)	Intrusion Geometry	Intrusion Width[a] (*at Depth*) (m)	Nature of Host-Rock Impact (Comments)	Length of Dike, *Eruptive Fissure* (km)	Number of Major (Minor) Vents	Spacing for Major (Minor) Vents (m)	Location of Major Vents along Dike/Fissure
East Grants Ridge, New Mexico	2.57±0.13[b]	≤0.1[g]	Equant plug; end of elongate fissure	125 (*60 to +60*)	Minor; sharp contact with vitrophyre and minor intrusion, stoping	1.0 to 1.5 *1.0 to 1.5*	2 to 4	125 to 800	Center, End

NOTES: "Intrusion width" encompasses the size of the subvolcanic feature below the paleosurface: dike, conduit, plug, or neck.

[b] Laughlin et al. 1993 [DIRS 174240], Table 1.

[c] Ratcliff et al. 1994 [DIRS 106634], p. 415.

[d] Weighted mean values from Fleck et al. 1996 [DIRS 105337], Table 2.

[e] Perry et al. 1998 [DIRS 144335], p. 2-18.

[f] Based on outcrop area of 1.25 km^2.

[g] Volumes calculated using GIS. Southeast Crater Flat: assumed 15-m flow thickness and extent of buried flows delineated in 2004 aeromagnetic survey (Perry et al. 2005 [DIRS 177379]). Grants Ridge: combined digitized basalt contacts from Thaden et al. (1967 [DIRS 174076]), 10-m U.S.G.S. DEM, and field observations. East Basalt Ridge: combined 10-m U.S.G.S. DEM and field mapping. All volume values produced in this way are minimum estimates that do not account for loss due to erosion.

The plug is remarkably constant in width (~125 m) as it extends downward into underlying rhyolite tuff to the lowest depth of exposure (~60 m beneath the prebasalt paleosurface). The geometry of the plug as it extends laterally beneath East Grants Ridge is not known, but it could resemble elongated plugs or wide dikes exposed elsewhere around the Mount Taylor volcanic field, which have experienced deeper levels of erosion since the period of active basaltic volcanism (e.g., Cerro Cuate; Hallett 1992 [DIRS 124671], pp. 140 to 141).

The contact-metamorphosed zone in the rhyolite tuff host rocks is remarkably limited, considering the large size of the plug (WoldeGabriel et al. 1999 [DIRS 110071], pp. 404 to 409; Figure F-4, Table F-1). The tuff-basalt contact is exposed and accessible over about 60 vertical meters on the west, east, and south sides. Local peperitic textures indicate some mechanical mixing of alkali basalt and tuff host rock within distances of several decimeters from the contact, and the fused nature of the host tuff within ~1 m of the contact provides evidence of thermal interaction with the wall rock (WoldeGabriel et al. 1999 [DIRS 110071], pp. 396 and 398). Orientations of the contact vary locally, with dips ranging from as low as 12° (basalt over tuff) to as much as 80° to 90° (typical), but the overall orientation is vertical (Figure F-4). In detail, the contact between the host tuff and the basaltic lava plug undulates on the scale of meters, ranging from gentle low-amplitude (~1-m) scallops into the tuff, to angular blocks (protrusions) of tuff surrounded on three sides by basalt, to short spur-like dikes. Most of these dikes extend less than 2 m into the tuff, although one vertical dike, exposed in a quarry wall, extends about 50 m into the tuff; this dike is up to ~1-m thick near the plug. Short sill-like protrusions extend into the tuff; these are on the order of 1-m thick, but their original lateral extent is unknown due to erosion of the cliff walls. Likewise small blocky protrusions of tuff extend into the basalt mass to produce local occurrences of host rhyolitic tuff over basalt. Crumpler (2003 [DIRS 174074], p. 159) argued that the plug narrows dramatically near the base of the exposure (resembling a wineglass), merging to a ~2-m-wide feeder dike, but field evidence of this was not observed.

The relationship of the eruptive fissure system to regional structure is not clear, but several mapped regional structures indicate that it may have been aligned perpendicular to the direction of least principle stress during a phase of deformation in the region. While the vents are aligned approximately orthogonal to vent alignments associated with the Mount Taylor volcanic field (Crumpler 1980 [DIRS 173900], p. 254), a north-south graben and single normal faults, with limited exposures in Jurassic sedimentary rocks (Thaden et al. 1967 [DIRS 174076], Plate 1; Figure F-3), are located about 1.5 km north and south of the plug and project into the aligned vents; however, the relation to vent alignment is equivocal. Similarly, 5 km south of the ridge, the locations of two Pliocene basaltic vents in alignment with East Grants Ridge vents suggest possible structural control, but any direct evidence would be buried beneath lavas and younger talus. Stratigraphic displacement between the top of the host silicic tuff and volcaniclastics on the west side of the plug, relative to the east side, indicate that the aligned vents might occupy a fault, and vent alignment suggests a north-south orientation.

F.2.2 Paiute Ridge, Nevada

Magma of alkali basaltic composition intruded into Paleozoic carbonates and shales and middle Miocene silicic tuffs at Paiute Ridge, located on the east side of the Nevada Test Site (Figures 2 and 5). The volcanic complex is composed of Miocene (8.58 ± 0.07 Ma; Ratcliff et al. 1994 [DIRS 106634], p. 416) dikes, sills, scoria cone remnants, and lava flows that are well exposed

within uplifted and eroded structural blocks (Table F-1). Petrologic, paleomagnetic, and field relations are consistent with a single, brief magmatic pulse of alkali basalt (Ratcliff et al. 1994 [DIRS 106634], p. 415; Perry et al. 1998 [DIRS 144335], p. 5-29; Keating et al. 2002 [DIRS 174077], p. 430; Valentine and Krogh 2006 [DIRS 177282], p. 218). Although highly eroded, the complex is thought to have had a total volume of less than a cubic kilometer (Valentine and Krogh 2006 [DIRS 177282], p. 218). The dikes and sills were intruded into a small preexisting, NNW-trending horst and graben system; topographic reconstruction shows that the current exposures are at a depth of 0 m to 250 m beneath the paleosurface at the time of intrusion (Crowe et al. 1983 [DIRS 100972] p. 266; Valentine and Krogh 2006 [DIRS 177282], pp. 227 and 229).

Most dikes in the Paiute Ridge complex occupy normal faults within the graben, indicating that the planes of weakness presented by the faults captured the dikes as they ascended through the upper several hundred meters of crust (Crowe et al. 1983 [DIRS 100972], p. 265; Valentine and Krogh 2006 [DIRS 177282], pp. 221 and 225). The dikes range up to 5 km in length and from 1 m to 10 m (locally more) in width, and they occur singly and in swarms of up to four. Fault-occupying dikes are typically composed of several segments between 4-m and 100-m long; in one case (“PR” dike, Figure F-5), the upper tip of the dike visibly occupies a fault plane that continues upward to offset the surface of a mesa (Valentine and Krogh 2006 [DIRS 177282], p. 221). The dikes and sills produced contact metamorphic vitrophyre and mineralogic alteration in the surrounding tuff up to 3 m from the contact (Keating et al. 2002 [DIRS 174077], p. 432).

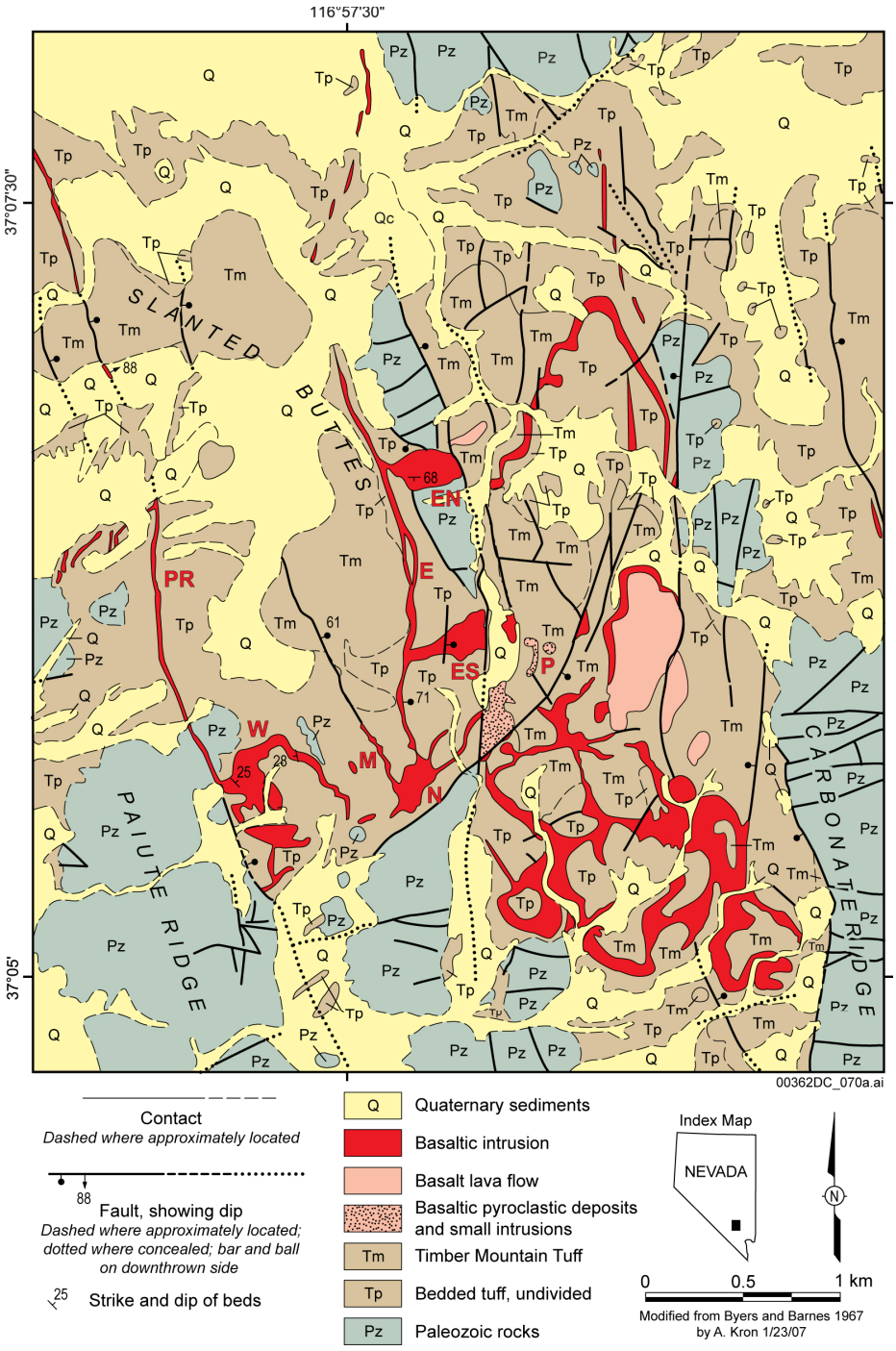

Source: Modified from Byers and Barnes 1967 [DIRS 101859].

NOTES: Pz – undivided Paleozoic basement rocks (mainly carbonates and shales); Tp – undivided bedded and massive Tertiary tuffs including units belonging to Tunnel Formation, Indian Trail Formation, and Paintbrush group (composed of fallout deposits, ignimbrites, and reworked non-welded tuffs with varying degrees of zeolitic alteration). Tm – Timber Mountain Tuffs (mainly ignimbrites of the Rainier Mesa and Ammonia Tanks members); Q– Quaternary alluvium and colluvium. PR – Paiute Ridge fault and dike; W – W sill; M – M dike and fault; E – E dike and fault; ES – ES sill along E dike near volcanic neck N; EN – EN sill along E dike; P -- plug-like bodies with roughly circular shapes within the basaltic pyroclastic deposits.

Figure F-5. Simplified Geologic Map of the Paiute Ridge, Nevada, Area, Emphasizing Basaltic Rocks

Reconstruction of eruptive styles is limited at Paiute Ridge because post-volcanic erosion and faulting have removed most in situ deposits. A small area roughly 500 m to the northwest of the neck (described below) has characteristics consistent with an origin as proximal scoria cone facies (basaltic pyroclastic deposits and small intrusions; "P" on Figure F-5). These characteristics include areas of poorly sorted scoria (coarse ash to coarse lapilli) containing fluidal spatter clasts up to 1-m long. These deposits are dominantly massive, with local zones of crude bedding defined by long axes of coarse spatter clasts. The pyroclastic deposits host small, irregular bodies (up to several meters in dimension) of massive to jointed lava. The northeastern part of this area contains plug-like bodies with roughly circular shapes ("P" on Figure F-5). The largest of these is about 20 m in diameter and consists of massive basalt; about 50 m from this massive plug-like body is an outcrop of breccia composed of angular, coarse ash- to block-size dense basalt fragments, some of which are cored by xenoliths of Miocene tuff bedrock. This breccia outcrop has crude bedding that dips steeply (~65°N) toward the basalt plug, suggesting that the plug represents a small vent and the breccia beds filled a small crater around it. Other smaller (~5-m diameter) plug-like bodies of basalt breccia are exposed in the area, and together may represent the lower extent of pipes feeding overlying bocas. The deposits in this area are interpreted to have formed in very proximal areas within a scoria cone or cluster of small cones, with some of the plug-like bodies representing subsidiary vents or lava breakouts (all subordinate to the main volcanic neck nearby). A remnant of a related lava flow ~1 km to the northeast is underlain by 6 m of planar bedded, well sorted scoria lapilli that mantle the underlying paleotopography, indicative of deposition by fallout. These features suggest that the Paiute Ridge complex erupted to form a volcano very similar to younger basaltic volcanoes in the region characterized by a single scoria cone, fallout deposits, and one or two small lava fields that emanated from breakouts, or bocas, around the bases of the cones (Valentine et al. 2005 [DIRS 177782]; Appendix E, this report).

A basalt pinnacle located in the south-central part of the complex is interpreted as a neck and the main conduit that fed volcanic activity (Figures F-5, F-6, and F-7; Table F-1). The top of the edifice is lower than the base of the mapped subaerial basalt flows on a nearby ridge (Byers and Barnes 1967 [DIRS 101859]), but the precise relationship is ambiguous due to erosion and faulting in the intervening canyon. Approximately 40 vertical meters of neck are exposed, interpreted to represent 30 m to 70 m in depth below the paleosurface. The elongate geometry of the neck reflects a complex coalescence of about eight mapped dikes (Figure F-6). Four prominent dikes (1-m to 3-m wide) merge at the northern end of the neck and, together with the intervening thermally altered rhyolite tuff country rock, form a rough ridgeline. The largest of these dikes (dike #1 in Figure F-6) is continuous with the main, dense basalt mass of the neck. Three additional dikes (1-m to 2-m wide) adjoin the neck on the east side, and one merges tangentially on the southwest edge.

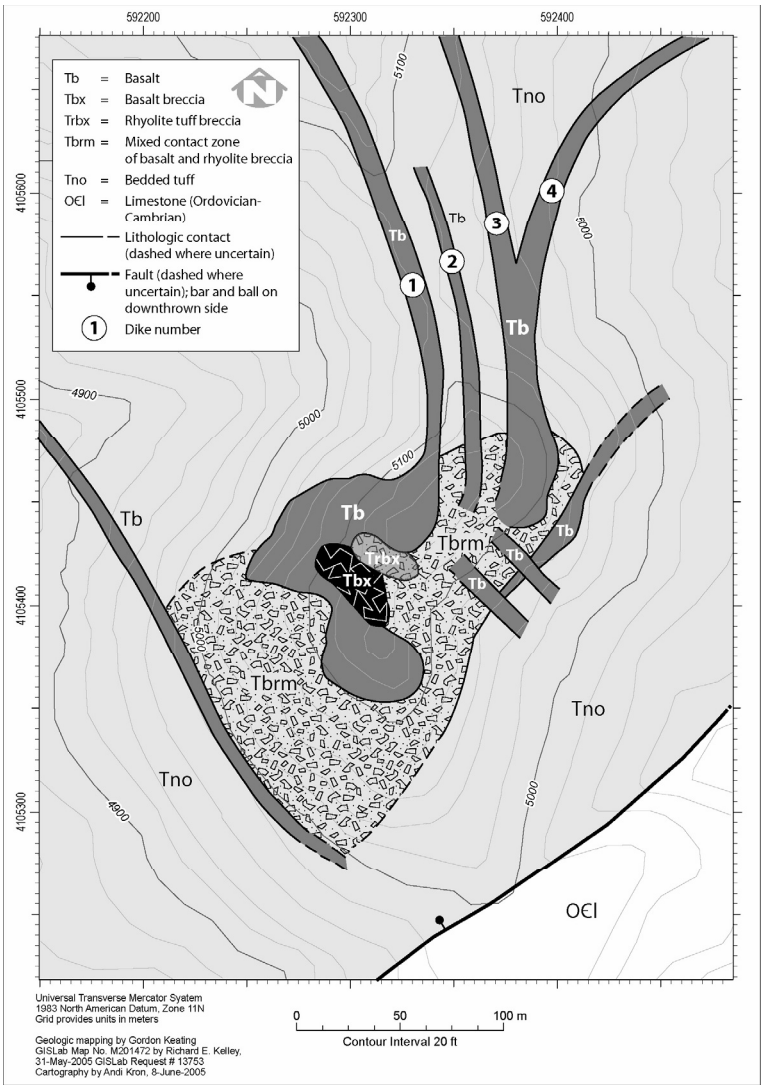

NOTES: The core of the neck is composed of dense basalt and breccia bodies (basalt- and rhyolite tuff-hosted). Four major dikes coalesce at the north end of the neck. Additional radial and tangential dikes intersect the neck on the east and southwest. The zone of host-rock impact due to the development of the neck is variable in width, from a 1-m-wide vitrophyre on the west to a 50-m-wide zone of brecciation on the southwest.

Figure F-6. Map of Volcanic Neck at Paiute Ridge

The neck is interpreted as a zone of intersection of several dikes that formed a central conduit and a surrounding zone of disturbed host rock. The convergence of the dikes was at least partially controlled by local structures, as indicated by the colocation of dikes and faults and the orientation of intrusions mostly parallel to the trend of the local graben (Valentine and Krogh 2006 [DIRS 177282], pp. 218 to 220). The central, dense basalt body is irregular in shape, approximately 100 m north-south by 50 m to 70 m east-west. It contains zones of basalt-dominated and rhyolite-dominated breccia near its center (Figures F-6 and F-7). In some areas (e.g., the western flank; Figures F-6 and F-7) the contact between the dense basalt (or basalt breccia) and the bedded rhyolite tuff country rock is sharp, formed by a near-vertical, 1-m-thick zone of tuff vitrophyre, beyond which is undeformed, horizontally bedded host tuff.

On the southwestern flank of the neck, the contact zone widens to several tens of meters from the contact with the dense basalt (Figure F-7). In this area, the transition from basalt to host tuff is gradual, beginning with 1-m- to 2-m-wide stringers of remobilized (melted) tuff within the basalt and grading outward into tuff-hosted breccia containing angular basalt clasts and blocks (Figure F-8). The breccia is composed of a flow-banded, frothy rhyolite tuff matrix containing angular to rounded basalt clasts with quenched rinds. Ledges of basalt (1-m to 2-m thick and dipping steeply inward) occur throughout this zone and are interpreted as discontinuous, roughly concentric dikes (or cone sheets) related to the central dense basalt body (Figure F-9). Radial dikes were also observed on the southwestern and eastern flanks. The overall dimensions of the contact-mixing zone (including the dense basalt core) are approximately 220 m north-south by 110 m east-west, or about twice the size of the body of dense basalt (Figure F-6).

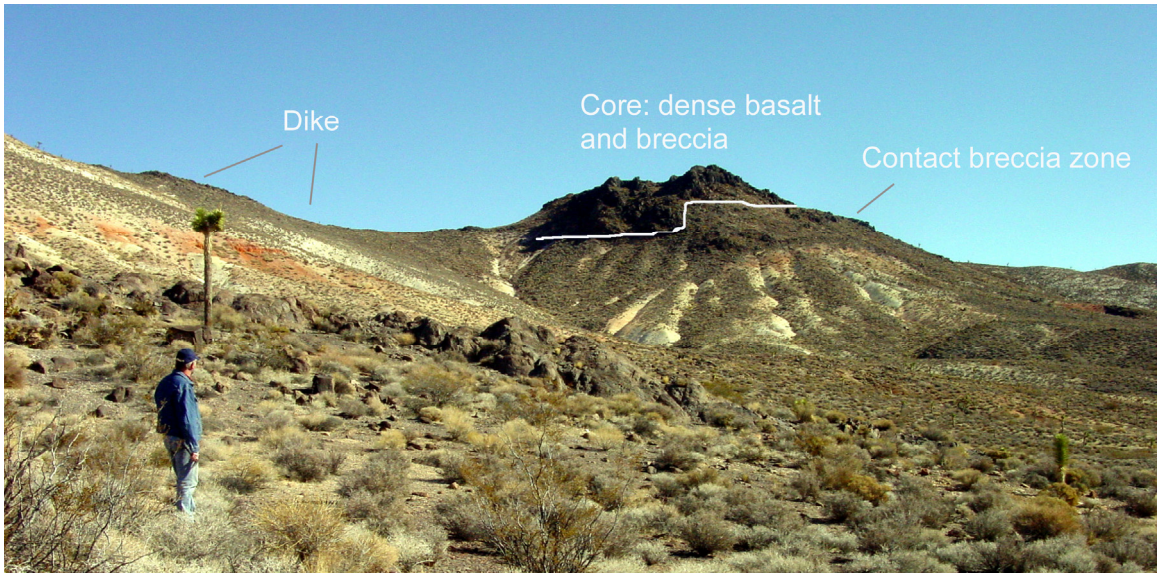

NOTES: The contact zone varies from a 1-m-wide vitrophyre at the lower left of the core to a 50-m-wide zone of brecciation and dike intrusion (contact breccia zone) on the lower right. The summit skyline is composed of dense basalt and bodies of basalt- and rhyolite-tuff-hosted breccia. Dike #1 forms ridgeline in the upper left and joins the dense core of the neck (Figure F-6).

Figure F-7. The Volcanic Neck in the Paiute Ridge Intrusive Complex, Nevada, from the West

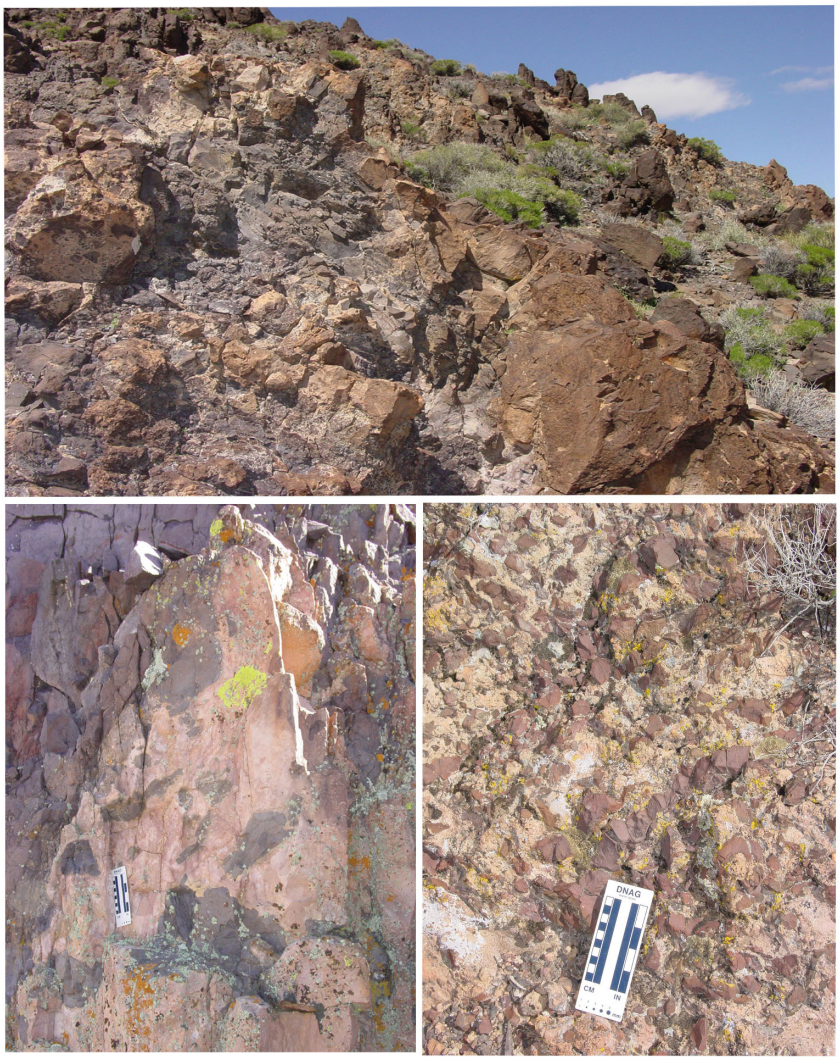

NOTES: Top: transition from basalt-dominated region containing melted tuff stringers (left) to tuff host-rock dominated region containing angular basalt clasts. Tuff boulder in lower right-hand corner is approximately 1-m across. Lower left: exposure near the contact displaying brecciated basalt on the left and melted, light-colored tuff with fluidal textures to the right. Left side of scale bar is divided into cm increments. Lower right: rhyolite tuff-hosted breccia containing reddish, dense to vesicular, cm-scale basalt clasts. This exposure is located ~5 m from the contact with the dense basalt body.

Figure F-8. Breccia Zone on the Southwest Flank of the Neck at Paiute Ridge, Nevada

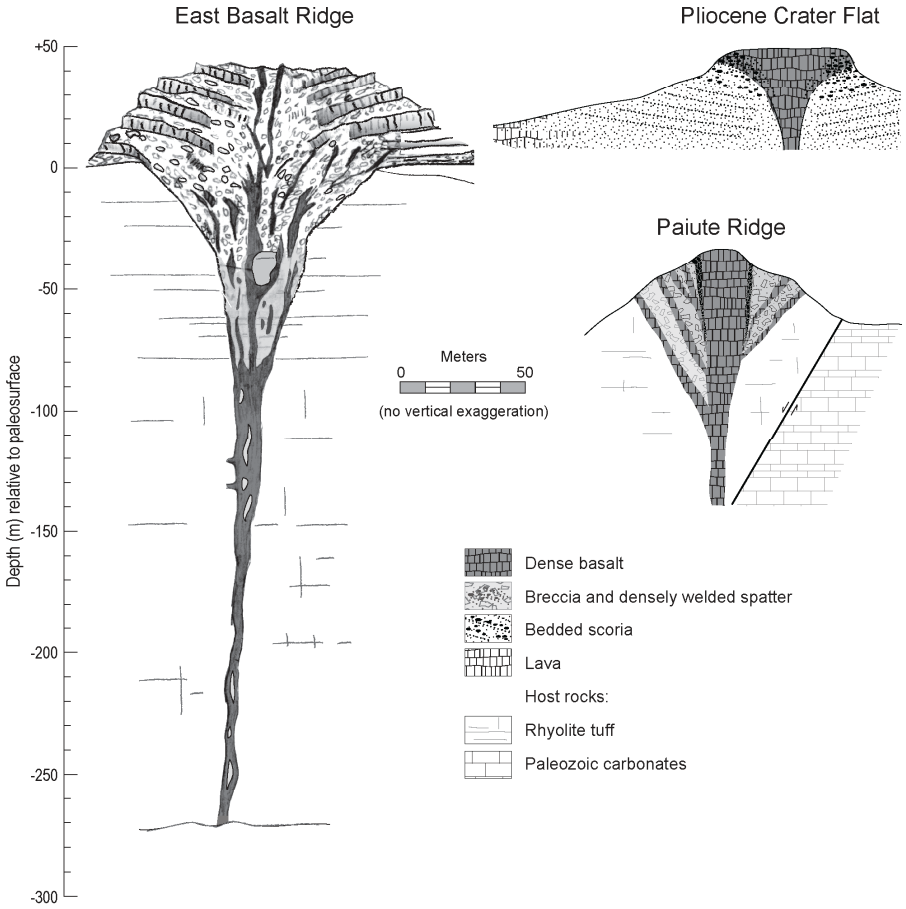

NOTES: East Basalt Ridge, Paiute Ridge, and South east Crater Flat. Horizontal and vertical scales are approximately equal throughout. The sketches of the Paiute Ridge neck and the fissure deposits at Pliocene Crater Flat have been placed in relative vertical position with respect to the vertical axis on the left. East Basalt Ridge (left): the view is along the plane of the dike set. The eruptive pile contains welded scoria and densely welded agglutinates dipping inward toward the fissure eruption marked by the location of the dikes. The dike is about 4-m to 10-m wide at the lowest exposures (250-m depth) and widens strongly above 90 m, forming a 100-m-wide crater. The flaring above 90 m is accomplished through dike splays, host-rock incorporation, and brecciation. Pliocene Crater Flat (top right): schematic west-east cross-section of Shirtcollar Butte above paleosurface (0-m depth on vertical scale); inward-dipping scoria beds exhibit increasing degree of agglutination up-section, grading into densely welded spatter and vent-filling basalt. The width of the fissure-filling dense basalt near the paleosurface is interpreted from other exposures at the field site. Paiute Ridge (lower right): dense basalt and breccia (basalt- and rhyolite tuff-hosted) form the core of the exposed neck, interpreted to represent paleodepths of 30 m to 70 m. Dense basalt dikes cut the contact breccia zone in both radial and cone-sheet geometry

Figure F-9. Comparison of Sketches of Three Conduit Systems

F2.3 Basalt Ridge and East Basalt Ridge, Nevada

Basaltic volcanic rocks of Miocene age erupted during silicic volcanic activity associated with the Black Mountain caldera complex of the Southwestern Nevada Volcanic Field (Byers et al. 1976 [DIRS 104639]; Christiansen et al. 1977 [DIRS 157236], pp. 953 and 954; Crowe et al. 1983 [DIRS 100972]; Sawyer et al. 1994 [DIRS 100075], pp. 1,311 and 1,314; Slate et al. 1999 [DIRS 150228]). Two sites of such basalt eruptions, Basalt Ridge and a nearby ridge (informally called East Basalt Ridge), are located on northern Pahute Mesa at the northern boundary of the Nevada Test Site and produced what has been called Basalt of Black Mountain (Orkild et al. 1969 [DIRS 106460], Plate1) or Basalts of Pahute Mesa (Perry et al. 1998 [DIRS 144335] p. 2-18; Figures 2 and 10). The ridge-capping alkali basalts have radiometric ages of 9.1 ± 0.7 Ma (Basalt Ridge) and 8.8 ± 0.1 Ma (East Basalt Ridge; Perry et al. 1998 [DIRS 144335], p. 2 18; Table F-1). The two ridges are underlain by linear dike sets, welded agglutinate and scoria, and lava flow remnants, and they represent eroded subvolcanic and surface deposits associated with ascending basalt dikes and eruptive equivalents, with paleosurfaces and host rocks exposed in adjacent canyons (Table F-1).

F.2.4 Basalt Ridge

Basalt Ridge is an eroded remnant of a 2,500-m-long chain of basalt vents. Feeder dikes, exposed in the walls of the ridge, extend to the south and north of the volcanic deposits (Figure F-10). Based on the outcrop area of about 1.25 km^2, the minimum volume of these eroded basalt deposits is 0.07 km^3 (Table F-1) but nearly all loose pyroclastic material has been removed by erosion. Basaltic volcanic rocks were emplaced on the relatively flat, gently northward-dipping surface of older Miocene ignimbrites. Eruptive deposits up to 70 m total thickness are dominated by sequences of alternating poorly welded and densely welded basaltic pyroclastic beds. Individual beds are massive, typically several decimeters to ~ 2-m thick, and composed of coarse ash to blocks and fluidal bombs. Most of the deposits dip inward toward the centerline of the ridge and are interpreted as having been emplaced on the inner slopes of vent craters. Dip angles of stratigraphically lower beds tend to be relatively shallow, but increase upward in the section to dips as high as 57°, recording cone building (e.g., McGetchin et al. 1974 [DIRS 115469], p. 3,268). Bed orientations suggest at least three elongate cone structures along the fissure system, representing development of focused eruptions from the subsurface feeder system. Uppermost beds are completely welded and merge into clastogenic lavas. At least one dike segment— ~30-m long, 1-m thick, and trending N20°E — is exposed along the southern ridgeline, probably representing a late stage extension of the feeder intrusions into the volcanic edifice. Only one small remnant of outward-dipping, outer cone-slope deposits was observed, and this was capped by a layer of densely welded spatter. The above relationships are consistent with deposition from pulsing fountains of coarse, fluid pyroclasts along a fissure system and accumulation of spatter cones and ramparts around focused vent areas spaced ~300 m to 500 m apart. Lava remnants are relatively sparse on Basalt Ridge so it is not possible to estimate whether there originally was a significant volume of flows.

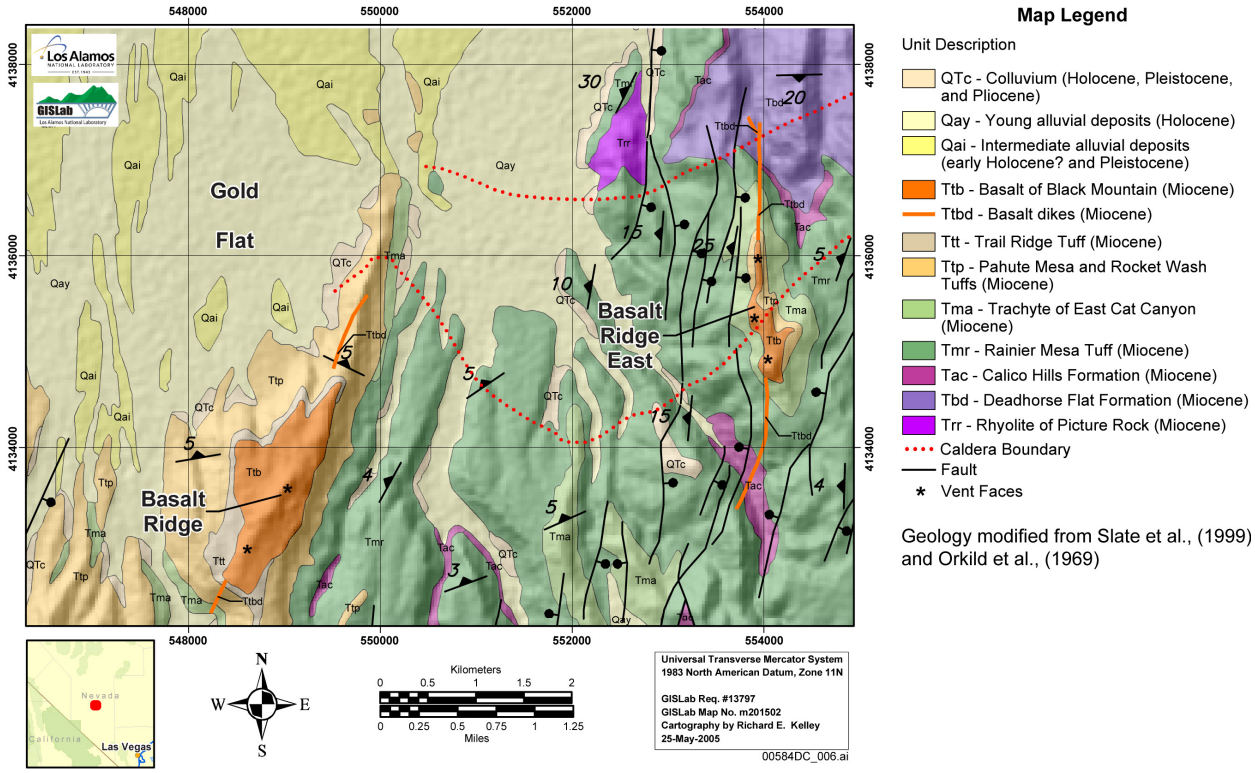

NOTE: Modified from Slate et al. (1999 [DIRS 150228]) and Orkild et al. (1969 [DIRS 106460]).

Figure F-10. Location Map for Basalt Ridge and East Basalt Ridge, Pahute Mesa, Nevada

The feeder dike is well exposed over about 150 m of vertical relief and a horizontal distance of 300 m on the southwest edge of Basalt Ridge. At its deepest exposed level (~150 m), the dike is composed of a single vertical tabular mass up to ~4-m thick. Vesicle development is poor at this depth beneath the paleosurface, but breccias occasionally mark the dike margins.

At 30 m to 35 m below the paleosurface, the single dike gradually widens up-section as it nears the contact in the host rock between a weak, Plinian fallout deposit and overlying welded ignimbrite; here the dike is locally brecciated and includes altered fragments of rhyolite tuff ripped from levels below this exposure. A small sill extends laterally ~30 m to one side of the dike along the top of the fallout deposits. Sill thickness varies from about 3 m (thickness of the fallout deposits) near the dike to a blunt, rounded terminus. Within the sill, trains of fine vesicles are folded on a submeter scale and are crosscut by similar trains, and there are multiple quenched margins, indicating successive lateral injections of basalt. Commingling of basalt and melted host tuff is visible on centimeter- to meter-scales, including swirled masses, stretched clasts of rhyolitic vitrophyre, basalt stringers enclosed in vitrophyre, rare drip textures, and bulbous basalt masses with pillow-lava morphology. Magmatic heat and compression during intrusion into the weak, porous Plinian fall material produced an aureole of dense, black vitrophyre that extends 2.0 m to 3.5 m beyond the end of the sill, and about 1 m from the top and bottom of the sill margin. Above the sill near the paleosurface, two thin (<1-m) dikes adjacent to the main dike clearly follow preexisting cooling joints in the welded tuff, terminating with blunt dike tips that have textures ranging from nonvesicular to brecciated and vesicular within 10 m of the paleosurface. At this shallowest level of exposure, the master dike is 1.6-m wide. These features

all indicate the important role of pre-existing structures (joints, faults, bedding planes) on shallow intrusion mechanisms, consistent with, but on a smaller scale than, processes described by Valentine and Krogh (2006 [DIRS 177282]).

F.2.5 East Basalt Ridge

Basalt breccias, welded agglutinate, and clastogenic lavas with a minimum volume of 0.003 km^3 (Table F-1) cap East Basalt Ridge for ~1,600 m (Figures 10 and 11), and outcrops of the feeder dike extend 1200 m north and 1500 m south of the eruptive cap, respectively, occupying a normal fault. The dike system is oriented ~N5°W, subparallel to the trend of regional faults and is exposed in steep canyons on the south and north edges of the ridge. The exposed paleosurface for the eruption slopes ~ 4ºN at the southern and ~20º west-northwest near the center of the eruptive fissure. Eruptive facies at East Basalt Ridge are similar to those described for Basalt Ridge.

Below 100 m, the feeder dike maintains relatively consistent width, with little evidence of interaction with the host tuff. At a depth of about 250 m (Figure F-9, Table F-1), the feeder dike is approximately 15-m wide, massive and blocky-jointed at the center, and poorly vesicular with flattened vesicles in trains and pockets within 2 m of the lateral contacts. The dike has sharp, smooth contacts oriented about N15°E and dipping 85°E, without breccia zones, splays, or included wall rock.

Above 100 m depth there is evidence of increasing interaction between the intruding basalt and host tuff and the transition from a parallel-walled dike to a more complex conduit (Figure F-9). The dike width increases to 15 m at 90 m depth below the paleosurface, with 1-m-wide splays and large breccia bodies forming a complex zone. At depths of 90 m to 52 m, the dike branches into five or six dikes, from 0.5-m to 2.8-m wide, and extending over a 25-m zone. The feeder zone comprises three to four dikes in a zone 28 to 30 m wide at 48 m depth, separated by lenses of rhyolitic tuff. At this point the dike zone can be continuously mapped, traversing ~300 m of gently rising terrain to the next vertical exposures. At 35 m depth, the conduit is 40-m wide, mostly massive basalt but including partially fused zones of angular breccia, particularly at the contact with tuff. At 35-m depth, a mass of light gray tuff about 15 m across is caught up in the basalt dike material and might be intact host rock separating branching dikes and breccias, or may be completely detached within the dike material. Finally, just 20 m to 25 m below the eruptive surface, the conduit boundaries flare outward at roughly 45° and form the vent. The elevation of the hinge for the flaring on the east side is 10 m to 12 m higher than on the west. At the paleosurface, the pyroclastic vent is 80-m to 100-m wide. Above this level, inward dipping, alternating agglutinate and spatter merge upward into densely welded spatter and lavas with occasional exposures of the feeder dike, creating resistant piles of dense basalt vent facies that form the linear ridge.

Black rhyolite vitrophyre marks the contact zone of the basalt dikes with the host ignimbrites. The host tuff varies between massive ignimbrite and bedded fallout deposits and is fused to a black to dark red vitrophyre adjacent to the dike, grading outward to a 1-m to 1.5-m zone of slight to moderate welding. Contact-parallel fiamme in the vitrophyre are typically formed at high angles to the subhorizontal primary bedding in the tuff. At lower elevations in the section where the dike zone is thinner (10 m to 12 m), the vitrophyric rind is 10-cm to 30-cm thick.

High in the section, 12 m below the flaring of the dike, the vitrophyre is about 3-m thick. Near the paleosurface, the contact grades laterally from a breccia of intensely commingled basalt and remelted chunks of tuff with well-developed vitrophyric textures in the first meter, to nonbrecciated black vitrophyre, and to the original unaltered tuff. The unaltered parent tuff (vitric, highly pumiceous, nonwelded tuff) is exposed within 10 m of the dike material. These features indicate that the processes controlling the evolution of feeder dike width include components due to inelastic (contact welding) deformation (Valentine and Krogh 2006 [DIRS 177282], pp. 224 to 225) with mechanical erosion of wall rocks becoming predominant very near the surface.

Near the center of the long eruptive fissure, the feeder system linking two vent areas flares from a 7-m-wide dike at 25-m depth to a 40-m-wide complex of dikes and pyroclastic material at the paleosurface, here marked by the accumulation of basal scoria and agglutinate on the sloping tuff bedrock. In this location, there is no evidence of brecciation of the host rock, and the smooth contacts of the feeder dike continue upward to meet the paleosurface. The central mass of basalt within the dike grades upward from massive basalt in the dike to vesicular vent facies with subvertical (flaring) joints (Figure F-12).

The three vent locations at East Basalt Ridge (Figure F-11) are spaced 500 m and 600 m apart, respectively. The axis of the eroded vents is located about 50 m to 100 m west of the centerline of the mesa, near its edge, producing an asymmetrical basalt edifice. Bedded scoria and clastogenic lava flows ponded against tuff highs to the east of the fissure, while the west side of the eruptive deposits falls away precipitously to the canyon on the west. Proximal to the eruptive fissure, basal bedded scoria, agglutinate, and lava dip 20° to 40° W, mantling the slope of the tuff bedrock.

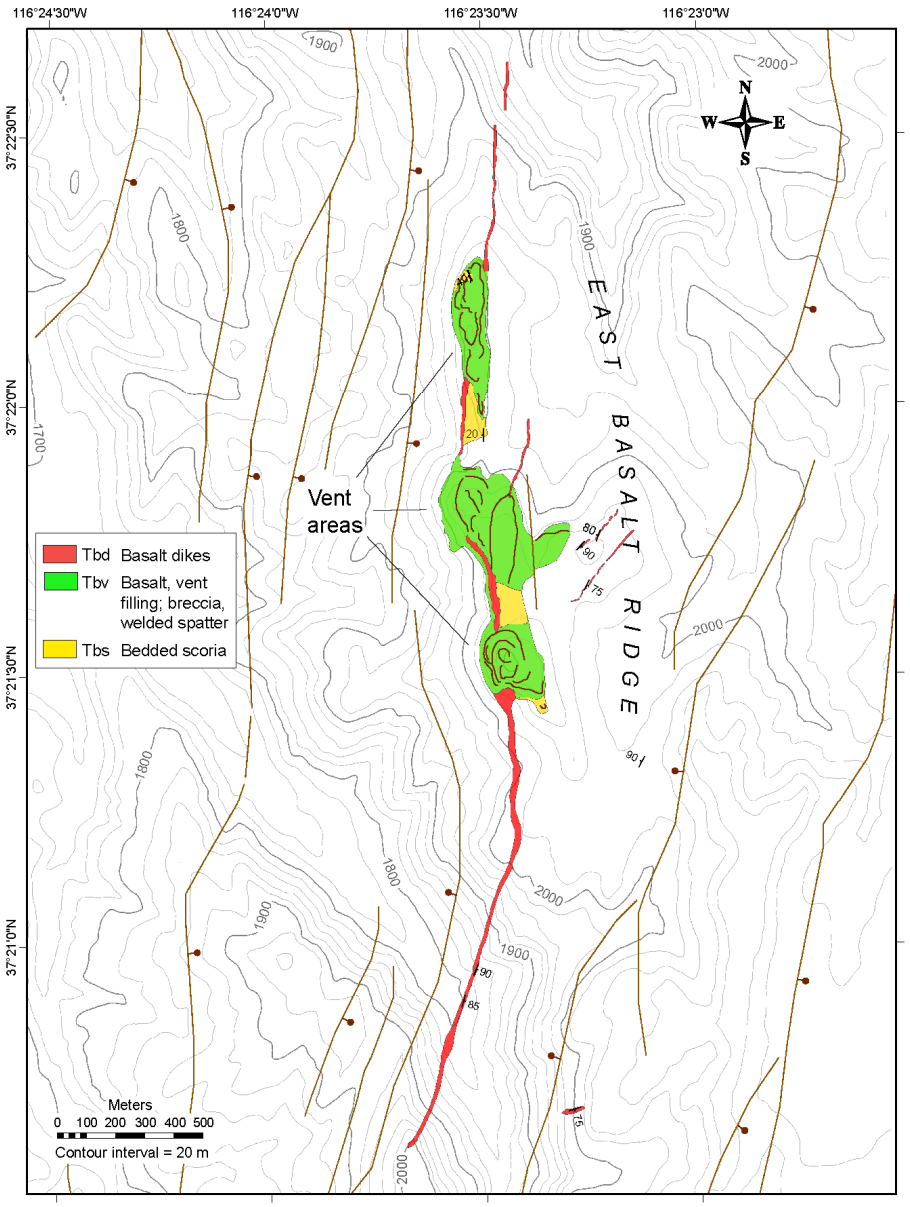

NOTE: Overall congruence of the dike-fissure geometry with the regional normal faults (brown lines, ball and bar on downthrown side; Slate et al. 1999 [DIRS 150228]). White areas are pre-basalt, rhyolite tuff. Map coordinate system is Universal Transverse Mercator, zone 11, NAD 83 datum.

Figure F-11. Geologic Map of the East Basalt Ridge Basaltic Fissure System

F.2.6 Southeast (Pliocene) Crater Flat

The Pliocene alkali basalt flows of southeast Crater Flat (PCF), Nevada, are exposed as low-relief platforms of basalt flows and scoria within the alluvial sediments of the basin (Figures F-2 and F-13). The Crater Flat basin is bounded on the east by a series of north-trending Basin and Range normal faults within Yucca Mountain and on the west by the regional Bare Mountain normal fault (Carr 1982 [DIRS 101519], p. 6, Figure 2; Brocher et al. 1998 [DIRS 100022], p. 949). A recent aeromagnetic study (Perry et al. 2005 [DIRS 177379]) confirmed the extent of

the basalt flows buried by alluvium, originally suggested by seismic profiling (Brocher et al. 1998 [DIRS 100022], p. 959). The volume for the flow field has been estimated at 0.6 km^3 (Table F-1) based on the thickness of exposed flows and in boreholes. After they erupted about 3.7 Ma (Fleck et al. 1996 [DIRS 105337], Table 2), the PCF basalts were faulted into four or five gently westward-dipping blocks along eastward-dipping normal faults that follow the regional north-south trend in Crater Flat or that of the NNE-trending Windy Wash fault zone (Brocher et al. 1998 [DIRS 100022], pp. 961 to 962; Potter et al. 2002 [DIRS 160060]). The north-south grain of the normal faults through Crater Flat probably controlled the ascent of magma feeding the PCF eruptions, as well as the orientation of the exposed remnants of the fissure system (Carr 1982 [DIRS 101519], p. 7; Brocher et al. 1998 [DIRS 100022], p. 967).

An axis of en echelon, eroded pyroclastic deposits provides evidence for the origin of the PCF flow field as a fissure eruption. These near-vent deposits are preserved as resistant buttes composed of a central core of dense basalt and welded spatter (20-m to 75-m wide, 20-m to 40-m high) flanked by inward-dipping sequences of partially to highly agglutinated scoria, breccia, and spatter (Figures F-9 and F-13). The eruptive centers typically narrow abruptly on one or both ends, transitioning into elongate fissure vents characterized by central, dense basalt dikes surrounded by inward-dipping beds of variably agglutinated scoria. This area provides a younger, less-eroded analog to the exposures at Basalt Ridge and East Basalt Ridge and illustrates the geometry of an eruptive conduit system above the paleosurface, within the fissure edifice.

This 3.5-km-long fissure system is divided into three en echelon segments, each dominated by a prominent butte (Figure F-13). The system is interpreted as having vented in fire fountains in the early stages of the eruption, localized rapidly (hours) into three to five subordinate vents on each fissure segment, and finally focused into one main vent per segment (hours to days). Evidence of outer flank remnants of scoria cones built on the fissure segments indicate that the overall basal diameter of the cones (e.g., centered on Shirtcollar Butte and North Butte) was on the order of 200 m. While individual vents for the surrounding lava flows are not recognized, bocas identified near the base of the scoria cones built on these vents would have allowed for the effusion of lava.

The geometry of the central conduit(s) feeding the eruptions has been interpreted based on eroded exposures (Table F-1), although the base of the lava flows and pyroclastic deposits is not exposed. Foci of eruption (major and minor vents) are connected by dikes exposed in narrow segments of the fissures. These dikes, typically 1-m –to 3-m wide, occur singly and in swarms up to 75-m wide (e.g., the exposures near Stagecoach Road, Figure F-13). The trend of the dikes is observed to curve around and merge with the wider areas of focused eruption. The lack of clear contact relationships between these dikes and the host bedded scoria deposits makes it unclear whether these narrow dikes erupted. The width of the core of the eruptive fissure near the paleosurface is determined from the southern tip of North Butte, where the dense basalt core is exposed in sharp contact with surrounding inward-dipping, bedded scoria at the desert floor. At this location, the dense core of the fissure is 15-m wide. The other end of this ridge exposes the core of a major vent edifice approximately 75-m across and composed of a 40-m-thick sequence of variably welded scoria, agglutinate, and breccia, which wraps around the northern end of the fissure segment with consistent inward dip. Intermediate to these extremes is the 40-m-wide dense basalt core of Shirtcollar Butte on the central fissure segment and the

20-m-wide core of Stagecoach Hill on the south fissure segment. The nature of the feeder dike at depth is uncertain, but a 0.5-m basalt dike was encountered, possibly obliquely, at a depth of 353 m in drillhole VH-1, located near the northernmost exposures of the PCF basalts (Carr 1982 [DIRS 101519], Table 2), possibly indicating that the feeder dike was quite narrow at that depth and 1 km to 1.5 km north of the eruptive vents.

F.3 DISCUSSION

Each study area preserves a record of various aspects of the development of the plumbing system for a small-volume basaltic volcano and provides information about the size and geometry of the conduit at that location. Basalt Ridge and East Basalt Ridge represent the simplest cases in which relatively straight-walled, fault-occupying feeder dikes flare out within the upper tens of meters beneath vent areas. Bedding of rhyolitic tuff country rock, with inferred contrasts in mechanical properties between welded and nonwelded zones, exerts little influence on the path of the intrusion except at very shallow depths. In the case of East Basalt Ridge (south end), the feeder dike maintains a relatively constant 10-m to 12-m width from about 250-m to 90-m depth (Figure F-14a), at which depth the magma-country rock interface becomes more complex as small (<1-m wide) dikes splay off and large (2 m to 3 m) bodies of country rock breccia are contained within the conduit. Above ~90 m below paleosurface, heterogeneities in the country rock form preferential pathways for small sills and splays. Above 40 m, the boundaries of the dike system flare outward, enclosing massive eruptive breccia and dense basalt.

Near the center of the East Basalt Ridge eruptive fissure, a gap in the eruptive deposits exposes the narrow (7 m) feeder dike penetrating the rhyolite tuff paleosurface and connecting one eruptive vent with the next (Figure F-12). Although the eruptive flux apparently focused into three main vent areas, the dike between them did not enlarge appreciably compared to the same dike exposed up to a kilometer north and south of the eruptive centers, consistent with observations of the size of the fissure core at Pliocene Crater Flat. Bedded scoria drapes the moderately (20º) west-dipping paleosurface, and the base of the welded spatter and clastogenic lava flows also conforms to this dip. The axis of the fissure was apparently situated on the edge of a tuff ridge or mesa; the east flank of the fissure was built up by scoria, spatter, and lava that accumulated against local bedrock highs, while the west flank of the fissure rampart fell away sharply toward the canyon to the west (enhanced by subsequent erosion).

NOTES: Top: the center vent area of the East Basalt Ridge fissure system, looking south from the northernmost vent area (Figure F-11). The feeder dike or conduit is about 7-m wide where it is exposed at the base of the ravine, about 25 m below the paleosurface (defined by the horizontal contact between tuff bedrock and variably welded scoria). Bottom: view north from the center vent area towards the north vent area, across the same ravine shown in the photo above. Note the dark feeder dike crossing the middleground on the left side of the photo, continuing from the 7-m-wide ravine exposure shown in the top photo. The reddish material dipping off to the left (west) near the base of the dark, dense rock at the top of the ridge is poorly welded scoria resting conformably (dip 20º west) on the underlying rhyolite tuff bedrock.

Figure F-12. East Basalt Ridge Fissure System

The neck at Paiute Ridge represents part of a complex subvolcanic system affected by depositional discontinuities in the country rock, significant offsets across normal faults that host dikes, and perhaps unsteady magma flow that produced marked brecciation of the host rock, intrusion of cone sheets, and radial dikes. The position of the neck near the end of a set of dikes underscores the possible controlling effect of discontinuities in the shallow subsurface (<250 m) on magma transport; unconformities between Paleozoic carbonate paleohills and infilling Miocene ignimbrites have been demonstrated to contribute to local rotation of principle stress directions and development of shallow sills in this intrusive complex (Valentine and Krogh 2006 [DIRS 177282], pp. 227 to 228). In the case of the neck, a nearby unconformity (possibly due to faulting) between Paleozoic carbonate and Miocene tuff may have helped guide the convergence of approximately 8 dikes, where they enlarged to form the eruptive conduit. Extensive country-rock brecciation and multiple crosscutting basaltic intrusions in the core of the neck provide evidence for unsteady flow in the conduit. In this type of basaltic conduit, the convergence of several major dikes creates a wide zone of brecciation, melting, and remobilization of the country rock. No evidence for conduit flaring is preserved in the limited vertical exposure. While the size of the actual conduit for magma flow to the surface (50 m by 100 m) is similar to those measured in the shallow subsurface at the other study areas (e.g., East Basalt Ridge), the large zone of host rock brecciation, melting, and dike intrusion has not been observed in other sites (Table F-1) and may reflect syn-intrusive fault motion proposed at Paiute Ridge by Valentine and Krogh (2006 [DIRS 177282], p. 225). A large zone of brecciation is observed near the vent area at Basalt Ridge and East Basalt Ridge, but only very high in the section.

The Pliocene basalts of Crater Flat provide a view of the geometry of the conduit within the scoria cones and ramparts associated with a small-volume fissure eruption. The size of fissure structures near the paleosurface and upward about 40 m into the overlying edifice ranges from 1-m dikes to 75-m vents, with 15 m as the approximate functional minimum for an erupting fissure near the paleosurface. This size range is consistent with the dimensions of feeder dikes exposed at East Basalt Ridge, which likely also vented as a fissure eruption. The dense, fissure-filling core basalt typically merges outward into bedded agglutinate, indicating that the core is composed of late-stage, recycled spatter. The contact zone between the dense core and the surrounding bedded pyroclastics occurs over the distance of about 1 m, preserving the steep-walled vent geometry within the edifice. These inward-dipping pyroclastics that border the fissure core provide a means to define the longitudinal extent of the fissure segments as their inward dips wrap entirely around the dense core in some places; preserved fissure segments are 275-m, 925-m, and 1,075-m long (Figure F-13).

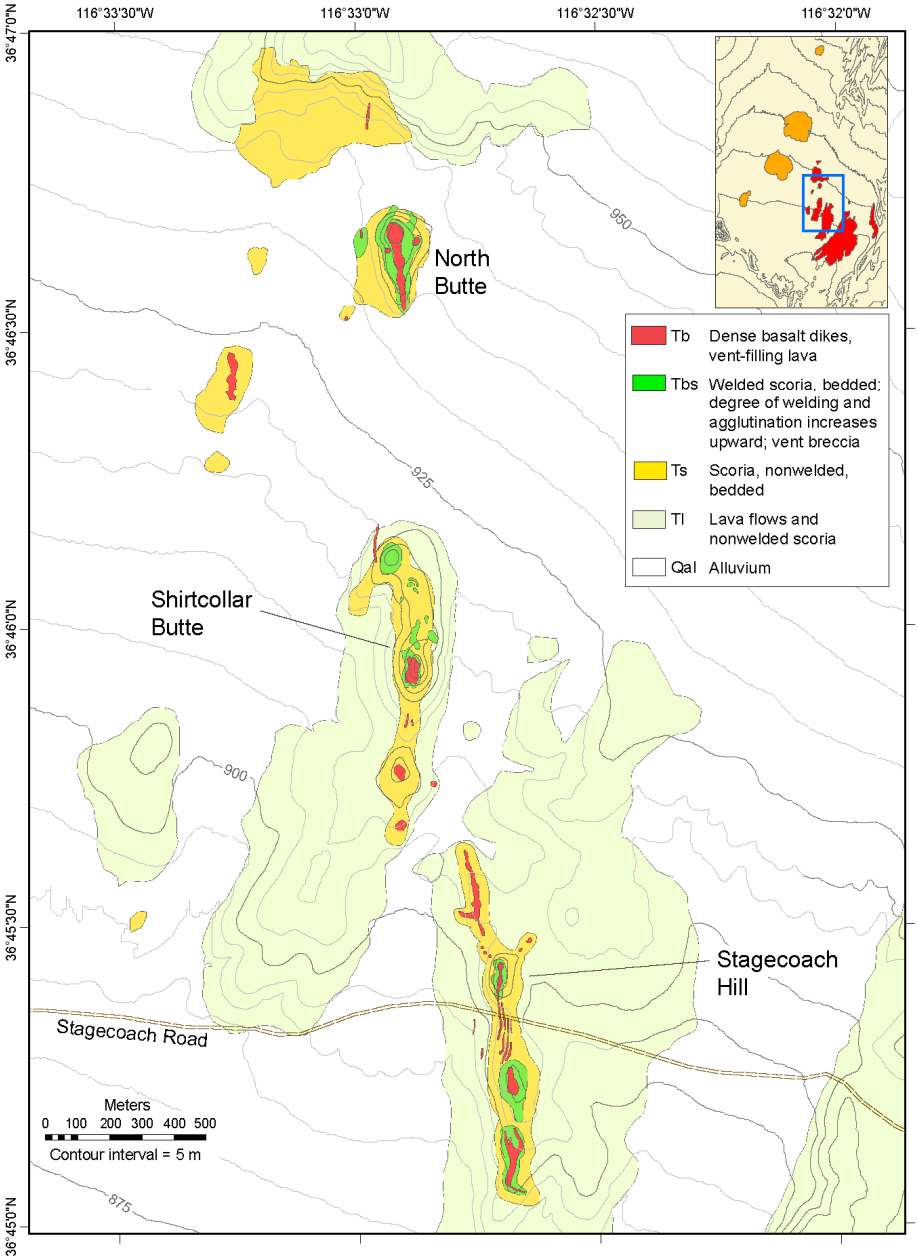

NOTES: Inset map shows the position of the entire southeast Crater Flat basalt field (red) in relation to the alignment of Pleistocene basaltic cones (orange) within Crater Flat. Main map: Erosional remnants of basaltic fissure system remain as topographic highs on a partially buried field of basalt flows. The core of the fissure system is composed of dense basalt (including densely welded spatter), ringed by inward-dipping beds of scoria that exhibits increasing degree of agglutination upwards and toward the axis of the fissure. Three main fissure segments are identified, each dominated by a major vent area (north to south): North Butte, Shirtcollar Butte, and Stagecoach Hill. The north-south orientation of this set of fissures parallels the grain of regional normal faulting in Crater Flat. Map coordinate system is Universal Transverse Mercator, zone 11, NAD 83 datum.

Figure F-13. Geologic Map of the Fissure Vent System of the Southeast (Pliocene) Crater Flat, Nevada, Basalts

Grants Ridge represents an outlier in the group. The mass of dense basalt preserved in the core of the eruptive center appears to maintain a consistent 125-m width from 60 m above the paleosurface to ≥60 m below it. Although there are small excursions of basalt into the rhyolitic tuff country rock, the contact is relatively smooth, without evidence of energetic conduit-widening or cratering explosions. This implies a different conduit-formation process; perhaps the formation of a lava lake by meltback during long-term lava effusion from a persistent fissure system. As an alternative, simple mechanical erosion of a volume of country rock equivalent to the exposed plug (as a cylinder – 7.4×10^5 m^3) and dispersal as xenoliths within the eruption products (volume ~ 10^8 m^3) results in a volume fraction of 7×10^{-3}, which is similar to or slightly greater than country-rock xenolith volume fractions calculated for magmatic eruptions at Alkali Buttes, New Mexico (Valentine and Groves 1996 [DIRS 107052], Table 1) and Lathrop Wells volcano (Appendix E). Although wallrock xenolith data are not available for the Grants Ridge basalts, this hypothetical process could be tested by field studies, particularly in the ~10-km-long lava flows.

Other wide lava-filled craters have been described beneath basaltic volcanoes, for example, Crater Hill, New Zealand. Houghton et al. (1999 [DIRS 178161], p. 117) conclude that magma degassing, fragmentation, and interaction with groundwater occurred at shallow depths (80 m to 120 m) below Crater Hill, a monogenetic basaltic center, based on lithologies of wall-rock xenoliths and interpretation of geophysical studies (Raut et al. 1993 [DIRS 178162]). The geophysical study of Raut et al. (1993 [DIRS 178162], pp. 75 to 78) suggests that early hydromagmatic explosions at Crater Hill excavated a 110-m-deep, wineglass-shaped crater that was about 75-m wide at its lower tip and widened sharply to a 350-m-wide crater that subsequently filled with dense basalt. However, the analogy of Crater Hill to East Grants Ridge is hampered by the lack of observed hydromagmatic deposits at the latter; the mechanism for the creation of the wide basalt plug at East Grants Ridge remains unexplained.

The direct and indirect evidence of the geometry and dimensions of feeder systems for small-volume basaltic volcanoes can be better interpreted in the context of theoretical considerations of conduit flow processes. Mitchell (2005 [DIRS 178154], pp. 187 to188, and 201) summarizes historical developments from assumptions of either: 1) fixed, parallel (vertical)-walled conduits with atmospheric-pressure vent boundary conditions; 2) lithostatic-pressure-balanced conduit flow conditions in which the conduit radius varies with depth; or 3) various combinations of the two that involve complex initial conduit shapes and velocity structures. While each of these approaches seems to provide a good fit to certain features and conditions during an eruption, Mitchell (2005 [DIRS 178154], pp. 196, and 198 to 200) points out that the conditions within a basaltic eruption conduit likely begin as a parallel-walled pipe and rapidly evolve into a flaring geometry that accommodates lithostatic-pressure-balanced flow at subsonic conditions and even more complex geometries as the fragmentation and choked flow points migrate downward and the flow transitions to supersonic regimes.

Simple corroborative conduit flow modeling based on the first two cases described above provides the context for characterizing the conduit flow conditions during the eruptions at the study areas. Field observations are compared with theoretical results in a corroborative fashion using the open-source flow code, *Conflow*, developed by Mastin and Ghiorso (2000 [DIRS 170144]) and further discussed by Mastin (2002 [DIRS 178163]), functioning in the pressure-balanced (variable conduit width) mode (Figure F-14). The model runs produced a

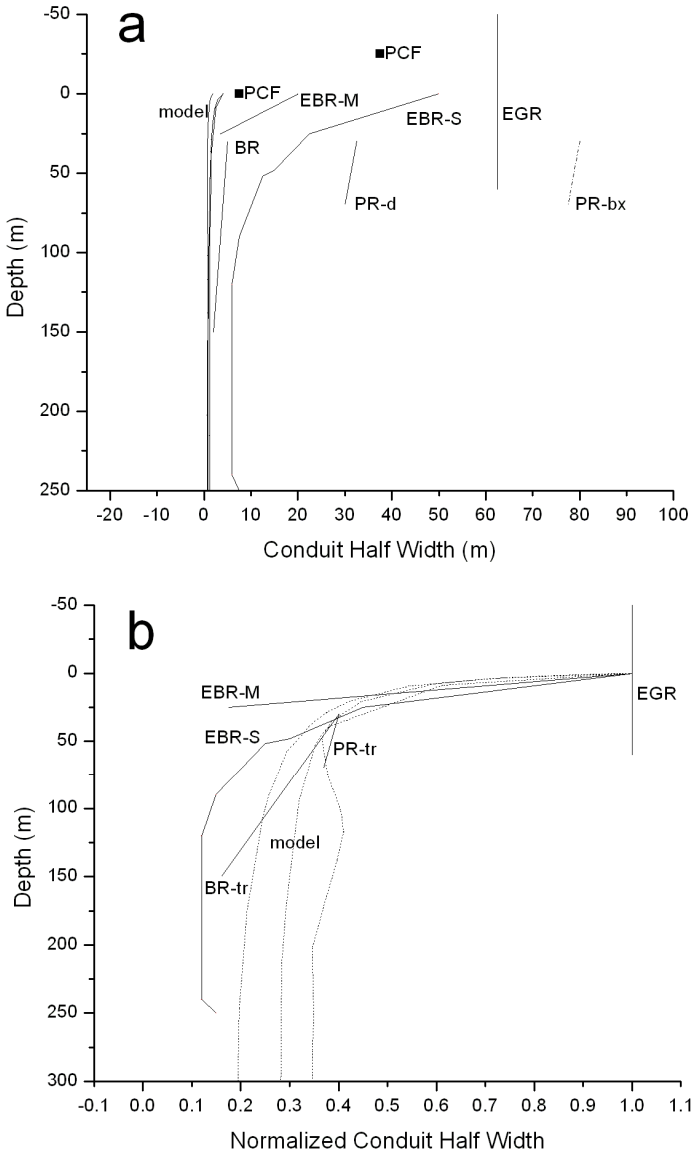

NOTES: BR is Basalt Ridge; EBR-M is East Basalt Ridge – middle vent area; EBR-S is East Basalt Ridge – south vent area; PR is Paiute Ridge (dense basalt of neck core in solid line, PR-d; extent of neck breccia in dash-dot line, PR-bx); EGR is East Grants Ridge; PCF is Pliocene Crater Flat (squares correspond to measured fissure widths above the paleosurface). Note horizontal exaggeration for clarity. *Conflow* model results were obtained using the built-in petrologic parameter set for the alkali basalt of Ukinrek Maars (with 1 wt % to 4 wt % dissolved H_2O and 2 vol % to 24 vol % crystals), setting a 4-m- to 10-m-wide conduit at 1-km depth and 3-MPa driving pressure. a) The main control on the modeled conduit radius in the upper 250 m was the value of initial conduit radius at 1 km: wider initial conduits provided greater mass flux and resulted in a near-linear increase in vent widening. There was no significant change in the results by adopting the Kilauean basalt parameter set. b) Normalized conduit half-width profiles. Because the profiles for Basalt Ridge (BR-tr) and Paiute Ridge (PR-tr) do not extend completely to the paleosurface, the widest point of each of these conduits has been translated to the normalized half-width value on the middle modeled profile for comparison. The Paiute Ridge line corresponds to the normalized half width of the dense basalt in the core of the neck.

Figure F-14. Summary of Conduit Profiles from Eroded Study Areas and *Conflow* Modeling

steady-state mass flux of 3×10^4 to 2×10^5 kg/sec (appropriate for an Hawaiian or Strombolian eruption, e.g., Lonquimay, Pyle 2000 [DIRS 178165], Table iii; Etna, Scandone 1979 [DIRS 178164], Figure 2), an eventual 95-m-deep fragmentation depth, and a conduit about 2 m in width at 900-m depth and flaring out to about 8 m over the uppermost 40 m. It is difficult to induce a conduit flare wider than about 10 meters in these model cases, based simply on variations in magmatic pressure balance (1 km versus surface), initial dike size at 1-km depth, magmatic water content, or the overpressure. While the model generally predicts some flaring within the upper 30 m to 40 m, the flare is typically on the order of 2 m to 4 m widening to 5 m to 8 m at the surface.

A plot of conduit half-widths demonstrates a marked difference between the observed and modeled conduit sizes (Figure F-14a). For magmatic eruptions that do not involve significant hydromagmatic component, the difference from the modeled conduit size is up to factor of 10 greater at the vent and a factor of 2 to 4 greater at 200-m to 500-m depth. Despite the differences in overall size, the shape of the observed conduits is similar to the model; when normalized to the widest point at the vent (Figure F-14b), there is a striking consistency in the depth of the flare hinge in the upper 50 m to 100 m of the feeder systems. This shape is consistent with the multiphase flow modeling of Mitchell (2005 [DIRS 178154], p. 196), who concluded that deep wall stresses are low enough to preclude wall failure, the initial deep dike shape is likely to be preserved during eruption, and that high stresses near the surface produce the shallow flaring vent shape.

Three factors contribute to the difference between the magnitude of the observed conduit widening and the theoretical values (Figure F-14a). First, there is a great deal of complexity in the interaction of magma and host rock. Heterogeneities in host rock (e.g., bedding, lithologic contacts, joints, unconformities) and regional structure (faults and faulted terrane) exert a strong influence on dike propagation and magma flow in the shallow subsurface (e.g., Valentine and Krogh 2006 [DIRS 177282]). Multiple small dike splays near the surface provide larger effective flow cross-section (hence, heat transfer) and induce brecciation, stoping, and dead-end lateral intrusions. The flaring conduit zones, particularly the margins, observed in the study areas are generally composed of a mixture of bifurcating dikes, incorporated blocks of country rock, and breccia zones rather than a pure flaring pipe as modeled. The overall width of the flared zone observed in the field may not be equivalent to the cross-section of the active conduit associated with a single eruptive flow event; evidence of annular flow, small local zones of flow, and multiple pulses of magma defining individual paths have been observed in other necks (e.g., Cerro Chafo, New Mexico, Hallett 1992 [DIRS 124671], pp. 21 to 22; San Rafael, Utah; Diez et al. 2005 [DIRS 178158]). At depth (<200 m), the processes that form the feeder dike include irrecoverable inelastic deformation of host rock and loss of country rock volume via development of contact-welded vitrophyre, both processes that are not included in the model. Thus it is important to think in terms of "effective flow diameter" within these hypabyssal zones; the widening process that happens by steady abrasion in the model is actually a nonuniform process, especially in the presence of unsteady flow and inhomogeneous thermo-mechanical response. As demonstrated in Figure F-14a, the zone of effect caused by this complex region of multiple intrusion, abrasion, brecciation, and stoping, may be an order of magnitude wider than is required by simple conduit flow calculations.

Second, the conduit geometries deduced from eroded systems represent time-integrated composite views of the eruptive plumbing systems, rather than the optimal flow geometry established by steady-state flow in a single eruption phase. Unsteady flow during individual eruptive phases (pressure transients translated within a dike–conduit system) can lead to brecciation and local conduit widening (e.g., Paiute Ridge). Multiple phases of eruptive activity over months to years may include the arrival of several batches of magma, pressure transients, and associated variation in eruption dynamics (Wood 1980 [DIRS 116536], pp. 396 and 397). The entire cross-sectional area of a conduit may be actively transferring magma to the vent (e.g., WoldeGabriel et al. 1999 [DIRS 110071], p. 403) or, at any given time, only a small fraction of its cross-sectional area may be active (e.g., due to variations in flow velocity or viscosity as a function of composition and temperature) to produce localized flow in a subsection of the conduit or in an annulus. These flow complexities are observed as subtle crosscutting relationships within breccia bodies, dikes, and dense plugs (e.g., Hallett 1992 [DIRS 124671], pp. 21 to 22). The preserved deposits represent a picture of the final form of the eruptive center after deposition, explosive excavation, late-stage lava ponding, and erosion.

Third, the conduit flow models themselves represent simplified systems based on certain assumptions (lithostatic-pressure balance, parallel pipe, etc.) that do not capture the complexities of natural systems. Complexities in shallow conduit shape are implied in the work of Mitchell (2005 [DIRS 178154], pp. 198 to 200), who describes the downward migration of the choke point, above which the transition to supersonic conditions near the vent may continue to widen the conduit. Complex eruptive dynamics may include a mixture of magmatic and hydromagmatic mechanisms that will contribute to additional disruption of the near-surface country rock. Although some models account for the evolution of the conduit via uniform erosion processes that are slow compared to the sound speed in the conduit (Macedonio et al. 1994 [DIRS 178155], p. 140; Mitchell 2005 [DIRS 178154], p. 189), the complex or catastrophic processes of vent widening (annular flow, multiple intrusion, pulsing, brecciation, slumping) are not explicitly considered (Mitchell 2005 [DIRS 178154], pp. 195 to 197). Likewise most modeling studies have assumed time-invariant boundary conditions: either the parallel plate (with or without atmospheric vent pressure) or the lithostatic-pressure balanced, flaring conduit conditions (or more complex variants of the two) that do not evolve during the modeled eruption (Wilson and Head 1981 [DIRS 101034], p. 2,973; Macedonio et al. 1994 [DIRS 178155], pp. 139 and 140; Morrissey and Chouet 1997 [DIRS 178166], p. 7,969). In spite of these limitations, the models are useful in interpreting the observed flaring shape and the depth scale as consistent with conduit widening processes due to expansion, fragmentation, and acceleration of gas-rich magma.

F.4 CONCLUSIONS

Field observations provide a composite view of the shallow plumbing system for small-volume basaltic volcanoes undergoing eruptions driven primarily by magmatic volatiles. Feeder dikes at depths of about 250 m to 100 m have widths of 4 m to 12 m, with relatively smooth contacts with host-rock (rhyolite tuff in the areas studied). At depths shallower than 100 m, heterogeneities in the host rock may form preferential pathways for small dike splays and sills, gradually widening the zone of effect of the feeder dike to about 30 m by depths of 50 m. At two locations, a marked flare in the feeder dike above 50 m depth was observed, characterized by bifurcating feeder dikes and brecciation and stoping of the country rock that indicate the

development of a conduit, resulting in a vent width on the order of 100 m. The width of the zone of effect (dense basalt and surrounding brecciated host rock) in the shallow (<50 m) zone may range up to 110 m (220 m elongated along the feeder dike).

The flaring shape of the observed feeder dike-conduit systems is similar to theoretical conduits modeled using lithostatic pressure-balanced flow conditions. This result validates the conclusions of Wilson and Head (1981 [DIRS 101034], pp. 2,980 to 2,981), who argued that the conduit shape always approaches the pressure-balanced solution due to wallrock failure. The absolute size differs from the modeled dimensions by up to a factor of 10 in the shallow (<50 m) subsurface, but below depths of about 100 m the difference is on the order of a factor of two to four. The difference in size between the observed and modeled feeder dike-conduits is due in large part to the fact that conduits for observed eroded volcanoes record the time-integrated effects of multiple eruptive events while the theoretical model represents the dimensions necessary for a single, steady eruption phase. The complex details of the magma-host rock interactions described at each of the study areas (contact welding, brecciation, bifurcating dikes and sills, and stoping) represent the mechanisms by which the lithostatic pressure-balanced geometry is attained, rather than simple abrasive erosion in the theoretical model. The similarity in the normalized shapes of theoretical and observed conduits (over a range in erupted volumes of 0.1 km^3 to 0.5 km^3) demonstrates the appropriateness of the pressure-balanced modeling approach.

The nature of feeder dikes below 250-m depth was not observed, but based on the comparisons with modeled dike size necessary to deliver an appropriate eruptive flux, it is expected that dike width would decrease to about one to two meters below roughly 500 m. Variations in host-rock strength and the magnitude of elastic and inelastic deformation (e.g., contact welding) result in a range of likely feeder dike widths from 1 m to 10 m in the 500-m to 250-m depth range.

The transition from a tabular feeder dike to a roughly cylindrical conduit is gradual, and it appears to begin above 100 meters, with most of the flaring occurring in the upper 50 m. These dimensions and depth ranges will vary with the volume and duration of eruption at a given volcano, as well as the nature of the host rock, but the normalized geometry of the conduit is expected to follow the pressure-balanced shape for basaltic eruptions driven primarily by magmatic volatiles.